Degradation of therapeutic proteins: Screening methods and identification of epimerized amino acids and local conformational changes in light exposed proteins

By

Rupesh Bommana

Submitted to the graduate degree program in Pharmaceutical Chemistry and the Graduate Faculty of the University of Kansas in partial fulfillment of the requirements for the degree of Doctor of Philosophy.

_____

Chairperson - Christian Schöneich

_____

David B. Volkin

_____

Zhou (Michael) Wang

_____

Thomas J. Tolbert

_____

Eric Deeds

Date Defended: September 21, 2017

The Dissertation Committee for Rupesh Bommana

certifies that this is the approved version of the following dissertation:

Degradation of therapeutic proteins: Screening methods and identification of epimerized amino acids and local conformational changes in light exposed proteins

_____

Chairperson - Christian Schöneich

Date approved: September 21, 2017

Abstract

Protein-based pharmaceuticals are a fast growing class of therapeutics, which are widely used in the treatment of various diseases such as cancers and autoimmune diseases. Proteins are susceptible to multiple degradation pathways including oxidation, deamidation and photodegradation. Over the past decade, the pharmaceutical industry has become increasingly cognizant of the sensitivity of proteins towards light. The exposure of proteins to light during their development and patient administration is inevitable, and may result in protein degradation. In the recent past there have been multiple reports indicating formation of aggregates, discoloration, oxidation, covalent crosslinking and fragmentation on exposure of protein pharmaceuticals to light. These degradation pathways could enhance immunogenicity or cause inactivation. Therefore, to increase the stability of these proteins, an understanding of their degradation is necessary. The research covered in this dissertation focused on two major degradation mechanisms for an IgG monoclonal antibody (mAb): chemical and physical degradation by photo irradiation. First, this dissertation explored the effects of certain pharmaceutical excipients on the extent and site-specificity of epimerization in UV irradiated mAb formulations. Amino acid analysis of UV irradiated mAb revealed formation of D-Ala, D-Glu, and D-Val in mAb formulations. Secondly, the underlying mechanism behind the increased aggregation propensity of a photo irradiated IgG1 mAb was investigated using hydrogen deuterium exchange mass spectrometry and biophysical characterization. Specific correlations were established between changes in dynamics of distinct segments in the C_H2 domain of the IgG1 mAb and decreased thermal stability as well as increase in aggregation propensity of the IgG1 mAb on light exposure.

This dissertation also describes development of a rapid screening methodology to identify protein oxidation by monitoring Tyr and Phe oxidation using fluorogenic derivatization. The Fluorogenic derivatization technique was adapted to a 96-well plate, in which several protein formulations can be screened in a short time. In addition, this dissertation also outlines the capability of an extreme ultra pressure liquid chromatography system in investigating complex chemical degradation problems.

Dedicated to:

My

Mom

(Sujatha Reddy Bommana)

Dad

(Peddi Reddy Bommana)

Wife

(Sindhu Reddy Bommana)

and

Brother

(Rakesh Reddy Bommana)

Acknowledgements

Many people were instrumental directly or indirectly in helping me in being where I am today. It would have been not possible for me to succeed in my doctoral work without the irreplaceable support of these folks and here is a small tribute to all these people.

First of all, I take this opportunity to thank my research advisor, Dr. Christian Schöneich, for his guidance and encouragement throughout my time in Pharmaceutical Chemistry graduate program at The University of Kansas. I will forever be grateful for his time and effort in contributing for my scientific upbringing. I have learnt a lot over the years from our interactions during the group meetings, regular conversations and I treasure his enthusiasm for science and attention to details in research and presentations. I also greatly admire his ability to balance research interests and personal pursuits. I also thank Dr. Christian Schöneich for acknowledging my research strengths and patiently encouraging me to improve in my weaker areas.

I would also like to thank the other members of my dissertation committee: Dr. David Volkin, Dr. Michael Wang, Dr. Thomas Tolbert, and Dr. Eric Deeds. Thank you very much for spending time to evaluate my thesis. Your comments and suggestions helped me in the experimental and writing process.

I would like to thank all the faculty in the department of Pharmaceutical Chemistry for providing me with a wealth of knowledge through a great coursework which helped me to acquire basic scientific principles which I could later use in my research work. I would specially like to thank Dr. John Stobaugh for providing me an opportunity to work with novel analytical systems. I have learned a lot from him about research and tackling problems.

I was very fortunate to work with amazing colleagues in Dr. Schöneich's laboratory and I thank each one of them for their help and friendship. First, I owe my deepest gratitude to Dr. Olivier Mozziconacci for his encouragement, scientific inputs, and continuous optimism. He was always there to provide me a helping hand in solving scientific problems. At several points during my research, he put my interests as student ahead of his own. His strong support of my ideas and confidence in my abilities were very beneficial during initial years of my graduate work. I will always treasure all the late evenings we spent repairing the instruments and solving research problems. Graduate school at times can be difficult and draining experience, but having great colleagues around you in the lab will make it intellectually fun and exciting. Thanks to Dr. Jessica Bane, Dr. Asha Hewarathna and Dr. Daniel Steinmann for all their help with the experiments and scientific training, above all for welcoming me to the lab with open arms. A special thanks to Indira Prajapati and Hasitha Rathnayaka for their encouragement and friendship. To Natalia Subelzu and Huan Kang, many thanks for sharing the work space, great company and proof-reading my thesis. I greatly look forward to having all of you as colleagues in the years ahead. I would also like to thank the present and past members of the Dr. Schöneich's group for their support: Dr. Björn Hendrik Peters, Dr. Maria Feeney, Dr. Elena Dremina, Dr. Lin Zhang and Dr. Christopher Asmus.

I was fortunate enough to get in to Eli Lilly and Company for a 6-month internship program which convinced me to pursue my career in pharmaceutical industry. First and foremost, I would like to thank Dr. Ranajoy Majumdar for mentoring me during my internship and convincing the company to allow my internship work to be published. I would also like to thank wonderful scientists with whom I worked while I was at Eli Lilly and Company: Dr. William F Weiss, Dr.

Qing Chai, Wesley Clinton Jackson, Ronald Lee Kowle, Charles E Mitchell, Frank Snelwar, Dr. Ning Wang and Dr. Lihua Huang.

I would also like to thank Pharmaceutical Chemistry staff: Nancy Helm, Andre Faucher, Ann Heptig, Karen Hall and Nicole Brooks.

I cannot forget my friends who cheered me up during my tough times and celebrating each accomplishment: Sriram Koppaka, Rakesh Alluri, Dr. Aravind Gade, Indraneel Varma, Yakub Reddy, Sivakrishna Angalakurthi, Varun Kambam, and Venugopal Reddy Bommu.

I want to thank my family for being the source of inspiration, courage, love and helping me to pursue doctoral research. I would like to thank my parents for allowing me to realize my own potential. Thanks for providing me with all the support through ups and downs over the years, and I believe that's the greatest gift that anyone has ever given me. I really cannot express in words how much I admire and love you. I share strong love and friendship with my brother who was always there for me. I would also like to thank my grandmother and grandfather for their love and affection. I would also like to thank my father-in-law and mother-in-law for their support.

Finally, and most importantly, I would like to thank my wife, Sindhu. Her support, encouragement and unwavering love were undoubtedly the foundation on which the last eleven years of my life have been built. Her patience during my occasional frustrations is a proof of her unyielding affection and love. Thanks for being a best friend, great companion, who encouraged, entertained, and helped me to get through tough times. Thanks for believing in me, I love you.

Table of contents

List of Abbreviations

AAPH	2, 2’-azobis (2-methylpropionamidine) dihydrochloride
ABS	4-(aminomethyl) benzenesulfonic acid
BMS	bis (2-mercaptoethyl) sulfone
BSA	bovine serum albumin
CD	circular dichroism
DOCH	2-amino-3-(3, 4-dioxocyclohexa-1, 5-dien-1-yl) propanoic acid
DOPA	3, 4-dihydroxyphenylalanine
DSC	differential scanning calorimetry
DTT	dithiothreitol
EDTA	ethylenediaminetetraacetic acid
ESI	electron spray ionization
FDA	Food and Drug Administration
HC	heavy chain of an IgG1 mAb
hGH	human growth hormone
HPLC	high pressure liquid chromatography
IAA	iodoacetamide
IgG	immunoglobulin G

$K_3Fe(CN)_6$	potassium ferricyanide
LC	light chain of an IgG1 mAb
LTQ-FT	linear ion trap quadrupole-Fourier transform
MALS	multi-angle light scattering
mAb	monoclonal antibody
MCO	metal catalyzed oxidation
MetSO	methionine sulfoxide
MS	mass spectrometry
Q-TOF	quadrupole time-of-flight
RPLC	reverse phase liquid chromatography
RGH	rat growth hormone
SAP	spatial aggregation propensity
SASA	solvent accessible surface area
SEC	size exclusion chromatography
SDS-PAGE	sodium dodecyl sulfate-polyacrylamide gel electrophoresis
UPLC-MS	ultra-pressure liquid chromatography- mass spectrometry
UV	ultraviolet
XUPLC	extreme ultra pressure liquid chromatography

Chapter 1. Introduction to protein photodegradation

1.1 Therapeutic proteins

In the last 30 years, proteins have emerged as a major class of pharmaceuticals with approximately 250 products in the market which are primarily used as therapeutics with a limited number as diagnostics.[1,2] Protein therapeutics have multiple advantages over small-molecule drugs. First, proteins are highly specific in their mode of action, hence less likely to cause side effects. Second, proteins are often well tolerated because the body inherently manufactures most of the current protein therapeutics. Third, as proteins are distinctive in configuration and operation, pharmaceutical companies are capable of obtaining comprehensive patent protection for protein therapeutics. The final advantage makes proteins economically appealing compared to small-molecule drugs.[1-5]

Protein therapeutics can be classified based on their function and therapeutic activity as drugs that: 1) substitute a deficient or abnormal protein, 2) enrich an existing pathway, 3) block a molecule or organism, 4) provide a unique function or activity, or 5) deliver a cytotoxic drug as a payload.[2] In addition, protein therapeutics can be grouped into different molecular types that include: anticoagulants, blood factors, enzymes, engineered protein scaffolds, thrombolytics, Fc fusion proteins, hormones, interferons, interleukins, growth factors, and antibody-based drugs.[6,7]

1.2 Rapid growth of monoclonal antibody market

In the last six years, the U.S Food and Drug Administration (FDA) and the Center for Biologics Evaluation and Review (CBER) combined have approved 62 therapeutic proteins, of which 11% were enzyme replacement approvals, 19% were coagulation factors, 22% comprised fusion proteins, hormones, growth factors, and plasma proteins, and the remaining 48% approvals were for monoclonal antibodies (including antibody-drug conjugates and antibody fragments).[8]

Monoclonal antibody (mAb) drugs are the fastest and largest growing class of protein therapeutics. At the current approval rate of four new products per year, approximately 70 mAb products will be on the market by the year 2020, with combined worldwide sales estimated to reach $125 billion.[9]

The increased interest in antibody drug development is because these products are receptive to cost-effective platform-based approaches and predominantly well-tolerated and highly specific.[9-12] The chances of the unexpected safety issues during human clinical trials of mAb products are relatively small compared to other therapeutic products. Consequently, for many novel disease targets, mAb products are frequently the first line of products advancing to clinical development.[9] As the patents of many high-profile blockbuster mAb products is expiring, there is growing interest in the development of biosimilars, which further could increase the influx of mAb products into the market.[9-13]

1.3 Antibody structure and instability

Antibodies are roughly Y-shaped glycoproteins belonging to the immunoglobulin (Ig) family which are secreted by B-cells to spot and neutralize antigens or nonnative organisms. Antibodies are composed of two identical heavy chains (H, ca. 50 kDa), and two identical light chains (L, ca. 25 kDa) with a total molecular weight approximately at 150 kDa.[13-15] Antibodies are grouped into separate isotypes based on the type of heavy chain they contain. Therapeutic mAbs are generally of the γ-immunoglobulin G (IgG) isotype. The amino-terminal variable (V) domains of the heavy and light chain (V_H and V_L, respectively) combine to form an antigen binding domain (F_{ab}), while the constant domains (C) form the fragment crystallizable (F_c) domain which is responsible for the effector function.[13,14] The H and L chains are linked through intra-chain and

inter-chain disulfide bonds. Most IgGs have four inter-chain disulfide bonds: two connecting the two heavy chains to light chains and the other two connecting heavy chains at the hinge region. Each IgG molecule contains a total of 12 intra-chain disulfide bonds; each disulfide bond is associated with an individual domain.[14, 16] Like other proteins, antibodies are susceptible to a variety of physical and chemical degradation pathways.[14, 17, 18]

In general, degradation pathways can be categorized into two major groups: chemical and physical degrdation.[17,18] Chemical degradation involves the formation of new covalent bonds or the breakage of existing covalent bonds, yielding new chemical species,[18-22] whereas physical degradation refers to changes in the higher order structure (secondary, tertiary, and quaternary structures) of the protein, aggregation, precipitation and particle formation.[14,18] However, chemical degradation can lead to physical degradation and vice versa. Oxidation, deamidation, racemization, proteolysis, hydrolysis, β-elimination, disulfide exchange are some of the major forms of chemical degradation reported for therapeutic proteins.[17,18] Physical degradation includes denaturation, aggregation, precipitation and surface absorption.[17] These instabilities can lead to loss of activity and, in some cases, can cause unwanted immunogenic responses.[22,23] Both physical and chemical instability can be initiated by multiple factors, such as reactive oxygen species (ROS), temperature, shaking, pH, light exposure, etc.[18,19,22,24]

1.4 Sources of light exposure in biopharmaceutical industry

The protein molecules are normally processed under ambient light conditions provided by fluorescent, LED and/or metal halide lamps.[25] They are exposed to light during various stages of their developmental process.[24-26] Proteins purified using chromatographic analysis are often detected using UV (214 nm, 280 nm or 254 nm) absorbance, which can induce degradation in

proteins.[24] Light exposure can also occur during the production process.[25] For example, Mallaney et al. have identified an increase in charge variants during small-scale production of mAbs in 2 L bioreactors.[25] As the bioreactors were made of clear transparent glass the ambient light in the laboratory induced photodegradation in mAb leading to formation of various acidic variants. Other potential sources of light exposure occur during fill and finish processes, visual inspections, packaging, storage or during drug administration to the patients, e.g. using clear IV bags.[24,26] The photosensitivity of a protein could be enhanced through the accumulation of oxidation products of Trp such as N-Formylkynurenine (λ_{max} = 318 nm), which can function as a photosensitizer.[24-26] To guarantee that ambient light exposure under good management practice (GMP) settings does not alter protein pharmaceuticals to unacceptable levels, regulatory agencies have introduced photostability testing.[25,26] Photostability testing has become an integral part of stress testing for a drug molecule during its submission to the FDA under The International Conference on Harmonization (ICH) guideline.[27] As indicated in the ICH Q1B guidelines, photostability testing under ICH conditions is usually carried out using no less than 1.2 x 10^6 lux-hours of visible light and no less than 200 W h/m^2 of UV light.[26,27]

1.5 Mechanisms of photodegradation in proteins

Photodegradation can result in altered physical [28] (e.g. conformational changes) and chemical [29-31] (e.g. oxidation) protein properties, aggregation,[28,31] loss of bioactivity[30], fragmentation,[31] and increase in immunogenic potential of the light exposed protein sample.[32]

As shown in Figure 1, the indole side-chain of tryptophan (Trp) is the strongest chromophore with an absorption maximum at λ_{max} = 280 nm, where the absorbance band extends in to the UVB (290 nm-320 nm) range of UV light. Absorption band of Trp in proteins depends on the

location of the residue in the three-dimensional structure of proteins (solvent exposure).[33-35] Previously, Pigault et al.[33] have studied the photo degradation in four different proteins, each with single Trp residues with different solvent accessibility. The degree of Trp photodegradation was dependent on solvent exposure indicating the effect of Trp location on its light absorption ability.[33] Additionally, Rao et al.[34] have studied the photodegradation of Trp in native and random coil forms of melittin and β-lactoglobulin. The results from this study further confirmed the effect of protein conformation on the light absorption of Trp.[34] Tyrosine (Tyr) absorbs light at a much lower intensity when compared to Trp, with its absorption maximum at λ_{max} = 275 nm, however there is minimal or no absorbance beyond λ = 290 nm.[24] Both phenylalanine (Phe) and the disulfide bond absorb light to a similar extent with absorption maxima at 260 nm and 254 nm, respectively.[24,36,37] Absorption spectrum of the disulfide bond is determined by its molecular geometry.[36] As a result of repulsion between 3pπ orbitals of the sulfur atom, the disulfide bond has a dihedral angle of 90º (for C-S-S-C bond) in the unstrained conditions.[36,37] Absorption spectra of disulfide bond is dependent upon the specific value of the dihedral angle. Large alterations from 90º result in absorption at longer wavelengths and a significant decrease in absorption.[37]

1.5.1 Photo-oxidation

Photo-induced damage to proteins can occur through two major pathways. The type I pathway involves absorption of light (predominately UVB light, λ = 280-320 nm) by specific amino acid residues (Trp, Tyr, Phe), cysteine (Cys) and disulfide bonds resulting in excitation of electron to higher energy singlet states. The excitation to higher energy state is followed by one of a number of processes such as, relaxation to the ground state, formation of a triplet state, reaction with oxygen to form peroxy radicals, and photoionization resulting in formation of aqueous electron

(e^-_{aq}) and a radical cation.[24,38,39] The Type II pathway involves energy transfer from the triplet excited state to ground state triplet oxygen ($^3O_2$), forming singlet oxygen ($^1O_2$) which can react with other amino acids in the protein.[38,39] The amino acids Trp, Tyr, Phe, His, Cys and methionine (Met) have been shown to be predominantly susceptible to photo-oxidation.

The formation of photo-oxidation products is not without consequences for proteins. Photo-oxidation of proteins can result in an increased extent or susceptibility to unfolding,[40] aggregation,[41-45] and fragmentation.[45] Photo-induced aggregation (formation of dimers and higher molecular weight species) is a well-documented consequence of protein photo-oxidation.[38-45] Aggregates can arise through radical termination reactions, such as reaction of Tyr-derived phenoxyl radicals to give di-tyrosine [41,42] or through addition reaction of carbonyl groups of the His oxidation products with nucleophilic Lys, Arg and Cys side chains yielding covalent cross-links.[43,44]

1.5.2 Photodegradation of disulfide bonds

Chemical degradation of disulfide bonds under neutral or basic conditions can proceed through three major pathways: 1) direct attack of sulfur atom by the hydroxyl anion resulting in breakage of the disulfide bond, forming sulfenic acid/thiolate anion; 2) the α-elimination caused by the hydroxyl ion attacking the β-proton of the Cys residue to yield thiolate/thioaldehyde moieties, 3) a β-elimination by abstraction of acidic α-proton of the Cys residue by hydroxyl anion yielding dehydroalanine/persulfide.[46] But, upon light exposure (UVC, λ = 254 nm) the disulfide bond can undergo homolytic dissociation, yielding a pair of thiyl radicals ($CysS^\bullet$) (Fig.2). During photoionization of protein, Trp (or Tyr) residues generates electrons, which can reduce nearby disulfide bonds also yielding $CysS^\bullet$ and Trp radical cation. The $CysS^\bullet$ radical pair can undergo

disproportionation yielding a thiol and thioaldehyde, or participate in reversible hydrogen atom transfer reactions with C-H bonds of adjacent amino acids, leading to the formation of carbon centered radicals ($C^{\bullet}$).[47-50] The reversible hydrogen atom transfer can be followed by covalent deuterium incorporation of deuterium when photolysis of disulfide bonds is achieved in deuterium oxide (D_2O).[47,49] When such intramolecular hydrogen atom transfer occurs between $CysS^{\bullet}$ and C-H of a chiral carbon, the resulting $C^{\bullet}$ exhibits two prochiral faces, where the subsequent reversible hydrogen atom transfer yielding either L or D amino acids.[52]

1.6 Overview of various novel photodegradation products identified in therapeutic proteins

In recent years, the biopharmaceutical industry has become more aware of the marked sensitivity of therapeutic proteins to light. The effects of light exposure vary from protein to protein and are dependent upon various formulation factors.[43,30] The aim of this section is to provide a brief overview on novel photodegradation products identified in therapeutic proteins upon light exposure (predominantly UV light).

Previously, Haywood et al.[53] have identified the photolytic cleavage of the Trp side chain (indole group) and formation of glycine hydroperoxide (GlyOOH) in the place of Trp on exposure of IgG1 to light with $\lambda = 254$ nm or $\lambda > 295$ nm. This photo-induced lysis proceeds via an intermediary radical cation ($TrpNH^{+\bullet}$) and leads to the formation of $C^{\bullet}$. This $C^{\bullet}$ likely adds oxygen followed by reaction with H donor yielding GlyOOH.

In another study, Bane et al.[45] have identified the formation of a triply oxidized His residue, a second doubly oxidized His residue, and Trp side chain cleavage in an IgG1 molecule following light exposure under ICH conditions. In this study they have proposed that singlet oxygen

initiates the oxidation of His leading to formation of endo-peroxide intermediates on the imidazole ring. The resulting endo-peroxides lead to the formation of hydroxylated imidazolones which were eventually converted into triply oxidized His product through hydrolysis or oxidation of hydroxyl imidazolone ring.[45] The endo-peroxides formed resultant of light exposure, can also be involved in formation of histidine (His-His) cross-links as reported by Liu et al.[43] The endo-peroxides formed are converted to the 2-oxo-histidine and His+32 intermediates, the latter is subjected to nucleophilic attack by the unmodified His and finally elimination of H_2O to form a His-His crosslinks.[43]

Disulfide bonds are sensitive to light-induced degradation, where recent studies by Mozziconacci et al. with model peptides (containing disulfide bonds),[50] oxytocin,[54] insulin,[55] and IgG1 mAb[56] have indicated the formation of novel photoproducts such as dithiohemiacetals, thioethers, vinyl thioethers, D-amino acids, and the conversion of cysteine to alanine and dehydroalanine.[48-51,54-57]

1.7 Potential implications of chemical degradation on immunogenicity of protein therapeutics

The potential cause for immunogenicity of protein therapeutics has proven to be difficult to predict so far, with many biologics inducing unwanted immune responses.[58] These immune responses are directed towards the therapeutic resulting in reduced efficacy, anaphylaxis and at times life threatening autoimmunity. Development of high affinity anti-therapeutic antibodies is the most probable effect of administering an immunogenic therapeutic.[58-60] Direct clinical evidence of the immunogenicity of chemical degradation products of therapeutic proteins could not found.[60] However, Chan et al.[61] have raised cytotoxic T lymphocytes (CTLs) that identified succinimide derivatives (intermediate during the deamidation or isomerization process) of

peptides but were less cross-reactive at high concentrations with unmodified parent peptide. Similarly, CTLs raised against the unmodified parent peptide did not identify the succinimide derivative, implying deamidation or isomerization can lead to autoimmune recognition.[61] Previously, Rasheed et al.[62] have demonstrated that human serum albumin (HSA) oxidized through ROS was a potent immunogen in rabbits inducing high-titer antibodies, while titer against the unmodified HAS was low. The IgG antibodies were specific to HAS oxidized through ROS, suggesting generation of neoepitopes by oxidation.[62] There are many factors that may be involved in the immunogenicity of a biotherapeutic, and these factors can be classified into two groups: 1) Patient and treatment-related factors and 2) Product-related factors. Genetics, disease state, dose, frequency and route of administration are grouped under patient and treatment related factors, whereas contaminants, impurities, chemical and physical degradants are grouped under product-related factors.[60] Previously, the immunogenicity of protein therapeutics has been largely associated with the formation of protein aggregates,[63-65] but recent studies propose that chemical degradation may also play an important role.[66-69] This can be explained in different ways: the resultant chemical modifications can induce protein aggregation (through covalent cross-links) and formation of neo-epitopes.[69] For example, Hermeling et al.[66] showed that recombinant human interferon alpha 2-b (IFNα2b) forms highly immunogenic aggregates upon oxidation via Cu^{+2}/ascorbate system. To explain the immunogenic nature of these protein aggregates, Torosantucci et al.[68] mapped the modifications in oxidized and immunogenic aggregates of IFNβ1a. On analysis, several oxidative modifications and covalent cross-links which contributed to the immunogenic nature of these aggregates were identified.[68]

1.8 Overview of this dissertation

Physical and chemical instability of proteins due to trace metals, hydroperoxides, and light-exposure are frequently encountered during production, purification, storage, drug administration etc. As described in the introduction, the repercussions of physical and chemical instability, specifically oxidation and aggregation can include decreased efficacy and increased immunogenicity. To better comprehend the consequences of chemical degradation of protein, the extent and nature of chemical degradation products should be characterized thoroughly. Understanding the underlying degradation mechanism would provide valuable insights to better stabilize and/or design protein pharmaceuticals.

1.8.1 Dissertation outline

Chapter 2 discusses development of an efficient and rapid method to monitor the oxidative degradation of protein pharmaceuticals: probing tyrosine oxidation with fluorogenic derivatization

Chapter 3 investigates the effect of various excipients on the extent of epimerization in UV light exposed mAb formulation.

Chapter 4 aims to understand the correlation between photo-degradation and aggregation propensity of an UVA light-exposed IgG1 mAb using hydrogen deuterium exchange mass spectrometry, biophysical techniques and structural modeling.

Chapter 5 exploring photo-degradation of rat growth hormone with extreme ultra-pressure liquid chromatography-mass spectrometry utilizing a meter-long microcapillary columns.

Chapter 6 summarizes our findings and conclusions of this dissertation and suggestions for future research directions.

1.9 References

1) Walsh G. Biopharmaceutical benchmarks 2014. Nat. Biotechnol. 2014; 32(10): 992-1000.
2) Leader B, Baca QJ, Golan DE. Protein therapeutics: a summary and pharmacological classification. Nat. Rev. Drug discovery. 2008; 7(1): 21.
3) Krejsa C, Rogge M, Sadee W. Protein therapeutics: new applications for pharmacogenetics. Nat. Rev. Drug discovery. 2006; 5(6): 507.
4) Pavlou AK, Reichert JM. Recombinant protein therapeutics—success rates, market trends and values to 2010. Nat. Biotechnol. 2004; 22(12): 1513-9.
5) Kimchi-Sarfaty C, Schiller T, Hamasaki-Katagiri N, Khan MA, Yanover C, Sauna ZE. Building better drugs: developing and regulating engineered therapeutic proteins. Trends Pharmacol. Sci. 2013; 34(10): 534-48.
6) Akash MS, Rehman K, Tariq M, Chen S. Development of therapeutic proteins: advances and challenges. Turkish J. Biol. 2015; 39(3): 343-58.
7) Carter PJ. Introduction to current and future protein therapeutics: a protein engineering perspective. Exp. Cell. Res. 2011; 317(9): 1261-9.
8) Lagassé HD, Alexaki A, Simhadri VL, Katagiri NH, Jankowski W, Sauna ZE, Kimchi-Sarfaty C. Recent advances in (therapeutic protein) drug development. F1000Research. 2017; 6.
9) Ecker DM, Jones SD, Levine HL. The therapeutic monoclonal antibody market. MAbs 2015; 7(1): 9-14.
10) Nelson AL, Dhimolea E, Reichert JM. Development trends for human monoclonal antibody therapeutics. Nat. Rev. Drug discovery. 2010; 9(10): 767.

11) Buss NA, Henderson SJ, McFarlane M, Shenton JM, de Haan L. Monoclonal antibody therapeutics: history and future. Curr. Opin. Pharmacol. 2012; 12(5): 615-22.
12) Liu JK. The history of monoclonal antibody development–Progress, remaining challenges and future innovations. Annals of Medicine and Surgery. 2014; 3(4): 113-6.
13) Udpa N, Million RP. Monoclonal antibody biosimilars. Nat. Rev. Drug Discov. 2016; 15(1): 13.
14) Wang W, Singh S, Zeng DL, King K, Nema S. Antibody structure, instability, and formulation. J. Pharm. Sci. 2007; 96(1): 1-26.
15) Schroeder HW, Cavacini L. Structure and function of immunoglobulins. J Allergy Clin Immuno. 2010; 125(2): S41-52.
16) Liu H, May K. Disulfide bond structures of IgG molecules: structural variations, chemical modifications and possible impacts to stability and biological function. MAbs. 2012; 4(1): 17-23.
17) Manning MC, Patel K, Borchardt RT. Stability of protein pharmaceuticals. Pharm Res. 1989; 6(11): 903-18.
18) Manning MC, Chou DK, Murphy BM, Payne RW, Katayama DS. Stability of protein pharmaceuticals: an update. Pharm Res. 2010; 27(4): 544-75.
19) Stadtman ER. Oxidation of free amino acids and amino acid residues in proteins by radiolysis and by metal-catalyzed reactions. Annu. Rev. Biochem. 1993; 62(1): 797-821.
20) Li S, Schöneich C, Borchardt RT. Chemical instability of protein pharmaceuticals: Mechanisms of oxidation and strategies for stabilization. Biotechnol. Bioeng. 1995; 48(5): 490-500.

21) Hovorka SW, Schöneich C. Oxidative degradation of pharmaceuticals: theory, mechanisms and inhibition. J. Pharm. Sci. 2001; 90(3): 253-69.

22) Torosantucci R, Mozziconacci O, Sharov V, Schöneich C, Jiskoot W. Chemical modifications in aggregates of recombinant human insulin induced by metal-catalyzed oxidation: covalent cross-linking via michael addition to tyrosine oxidation products. Pharm Res. 2012; 29(8): 2276-93.

23) Jiskoot W, Randolph TW, Volkin DB, Middaugh CR, Schöneich C, Winter G, Friess W, Crommelin DJ, Carpenter JF. Protein instability and immunogenicity: roadblocks to clinical application of injectable protein delivery systems for sustained release. J. Pharm. Sci. 2012; 101(3): 946-54.

24) Kerwin BA, Remmele RL. Protect from light: photodegradation and protein biologics. J. Pharm. Sci. 2007; 96(6): 1468-79.

25) Mallaney M, Wang SH, Sreedhara A. Effect of ambient light on monoclonal antibody product quality during small-scale mammalian cell culture process in clear glass bioreactors. Biotechnol Prog. 2014; 30(3): 562-70.

26) Sreedhara A, Yin J, Joyce M, Lau K, Wecksler AT, Deperalta G, Yi L, Wang YJ, Kabakoff B, Kishore RS. Effect of ambient light on IgG1 monoclonal antibodies during drug product processing and development. Eur. J. Pharm. Biopharm. 2016; 100: 38-46.

27) ICH, Q. B., Stability Testing: Photostability testing of new drug substances and products.1996.

28) Mason BD, Schöneich C, Kerwin BA. Effect of pH and light on aggregation and conformation of an IgG1 mAb. Mol. Pharm. 2012; 9(4): 774-90.

29) Wei Z, Feng J, Lin HY, Mullapudi S, Bishop E, Tous GI, Casas-Finet J, Hakki F, Strouse R, Schenerman MA. Identification of a single tryptophan residue as critical for binding activity in a humanized monoclonal antibody against respiratory syncytial virus. Anal. Chem. 2007; 79(7): 2797-805.

30) Qi P, Volkin DB, Zhao H, Nedved ML, Hughes R, Bass R, Yi SC, Panek ME, Wang D, DalMonte P, Bond MD. Characterization of the photodegradation of a human IgG1 monoclonal antibody formulated as a high-concentration liquid dosage form. J. Pharm. Sci. 2009; 98(9): 3117-30.

31) Steinmann D, Ji JA, Wang YJ, Schöneich C. Photodegradation of human growth hormone: a novel backbone cleavage between Glu-88 and Pro-89. Mol. Pharm. 2013; 10(7): 2693-706.

32) Fradkin AH, Mozziconacci O, Schöneich C, Carpenter JF, Randolph TW. UV photodegradation of murine growth hormone: chemical analysis and immunogenicity consequences. Eur. J. Pharm. Biopharm. 2014; 87(2): 395-402.

33) Pigault C, Gerard D. Influence of the location of tryptophanyl residues in proteins on their photosensitivity. Photochem. Photobiol. 1984; 40(3): 291-6.

34) Rao SC, Rao C, Balasubramanian D. The conformational status of a protein influences the aerobic photolysis of its tryptophan residues: melittin, β-lactoglobulin and the crystallins. Photochem. Photobiol. 1990; 51(3): 357-62.

35) Tallmadge DH, Borkman RF. The rates of photolysis of the four individual tryptophan residues in UV exposed calf γ-II crystallin. Photochem. Photobiol. 1990; 51(3): 363-8.

36) Bergson, G. (1958), Ark. Kemi 12, 233.

37) Barltrop JA, Hayes PM, Calvin M. The Chemistry of 1, 2-Dithiolane (Trimethylene Disulfide) as a Model for the Primary Quantum Conversion Act in Photosynthesis1a. J. Am. Chem. Soc. 1954; 76(17): 4348-67.

38) Pattison DI, Rahmanto AS, Davies MJ. Photo-oxidation of proteins. Photochem. Photobiol. 2012; 11(1): 38-53.

39) Davies MJ, Truscott RJ. Photo-oxidation of proteins and its role in cataractogenesis. J. Photochem. Photobiol. 2001; 63(1): 114-25.

40) Silva E, De Landea C, Edwards AM, Lissi E. Lysozyme photo-oxidation by singlet oxygen: properties of the partially inactivated enzyme. J. Photochem. Photobiol. 2000; 55(2): 196-200.

41) Shen HR, Spikes JD, Smith CJ, Kopeček J. Photodynamic cross-linking of proteins: V. Nature of the tyrosine–tyrosine bonds formed in the FMN-sensitized intermolecular cross-linking of N-acetyl-L-tyrosine. J. Photochem. Photobiol. 2000; 133(1): 115-22.

42) Verweu H, Steveninck JV. Model studies on photodynamic cross-linking. Photochem. Photobiology. 1982; 35(2): 265-7.

43) Liu M, Zhang Z, Cheetham J, Ren D, Zhou ZS. Discovery and characterization of a photo-oxidative histidine-histidine cross-link in IgG1 antibody utilizing 18O-labeling and mass spectrometry. Anal. Chem. 2014; 86(10): 4940-8.

44) Lei M, Carcelen T, Walters BT, Zamiri C, Quan C, Hu Y, Nishihara J, Yip H, Woon N, Zhang TY, Kao YH. Structure-based Correlation of Light-induced Histidine Reactivity in A Model Protein. Anal. Chem. 2017.

45) Bane J, Mozziconacci O, Yi L, Wang YJ, Sreedhara A, Schöneich C. Photo-oxidation of IgG1 and Model Peptides: Detection and Analysis of Triply Oxidized His and Trp Side Chain Cleavage Products. Pharm. Res. 2017; 34(1): 229-42.

46) Florence TM. Degradation of protein disulphide bonds in dilute alkali. Biochem. J. 1980; 189(3): 507-20.

47) Mozziconacci O, Kerwin BA, Schöneich C. Photolysis of an intrachain peptide disulfide bond: primary and secondary processes, formation of H2S, and hydrogen transfer reactions. J. Phys. Chem. B. 2010; 114(10): 3668-88.

48) Mozziconacci O, Kerwin BA, Schöneich C. Reversible hydrogen transfer reactions of cysteine thiyl radicals in peptides: the conversion of cysteine into dehydroalanine and alanine, and of alanine into dehydroalanine. J. Phys. Chem. B. 2011; 115(42): 12287-305.

49) Zhou S, Mozziconacci O, Kerwin BA, Schöneich C. The photolysis of disulfide bonds in IgG1 and IgG2 leads to selective intramolecular hydrogen transfer reactions of cysteine Thiyl radicals, probed by covalent H/D exchange and RPLC-MS/MS analysis. Pharm Res. 2013; 30(5): 1291-9.

50) Mozziconacci O, Sharov V, Williams TD, Kerwin BA, Schöneich C. Peptide cysteine thiyl radicals abstract hydrogen atoms from surrounding amino acids: the photolysis of a cysteine containing model peptide. J. Phys. Chem. B. 2008; 112(30): 9250-7.

51) Mozziconacci O, Schöneich C. Sequence-specific formation of D-amino acids in a monoclonal antibody during light exposure. Mol. Pharm. 2014; 11(11): 4291-7.

52) Martin SR, Bayley PM. Absorption and circular dichroism spectroscopy. Calcium-Binding Protein Protocols: Volume 2: Methods and Techniques. 2002:43-55.

53) Haywood J, Mozziconacci O, Allegre KM, Kerwin BA, Schöneich C. Light-induced conversion of Trp to Gly and Gly hydroperoxide in IgG1.Mol. Pharm.2013;10(3):1146-50.

54) Mozziconacci O, Schöneich C. Photodegradation of oxytocin and thermal stability of photoproducts. J. Pharm. Sci. 2012; 101(9): 3331-46.

55) Mozziconacci O, Williams TD, Kerwin BA, Schöneich C. Reversible Intramolecular Hydrogen Transfer between Protein Cysteine Thiyl Radicals and αC− H Bonds in Insulin: Control of Selectivity by Secondary Structure. J. Phys. Chem. B. 2008; 112(49): 15921-32.

56) Mozziconacci O, Kerwin BA, Schöneich C. Exposure of a monoclonal antibody, IgG1, to UV-light leads to protein dithiohemiacetal and thioether cross-links: a role for thiyl radicals?. Chem. Res. Toxicol51. 2010; 23(8): 1310-2.

57) Mozziconacci O, Kerwin BA, Schöneich C. Reversible hydrogen transfer between cysteine thiyl radical and glycine and alanine in model peptides: Covalent H/D exchange, radical− radical reactions, and L-to D-Ala conversion. J. Phys. Chem. B. 2010; 114(19): 6751-62.

58) Baker M, Reynolds HM, Lumicisi B, Bryson CJ. Immunogenicity of protein therapeutics: the key causes, consequences and challenges. Self/nonself. 2010; 1(4): 314-22.

59) Hermeling S, Crommelin DJ, Schellekens H, Jiskoot W. Structure-immunogenicity relationships of therapeutic proteins. Pharm. Res. 2004; 21(6): 897-903.

60) Singh SK. Impact of product-related factors on immunogenicity of biotherapeutics. J. Pharm. Sci. 2011; 100(2): 354-87.

61) Chen W, Ede NJ, Jackson DC, McCluskey J, Purcell AW. CTL recognition of an altered peptide associated with asparagine bond rearrangement. Implications for immunity and vaccine design. J Immunol. 1996; 157:1000–1005.

62) Rasheed Z, Ali R. Reactive oxygen species damaged human serum albumin in patients with Type I diabetes mellitus: Biochemical and immunological studies. Life. Sci. 2006; 79:2320–2328.

63) Wang W, Singh SK, Li N, Toler MR, King KR, Nema S. Immunogenicity of protein aggregates—concerns and realities. Int. J. Pharm. 2012; 431(1): 1-1.

64) Zhou J, Rossi J. Aptamers as targeted therapeutics: current potential and challenges. Nat. Rev. Drug Discov. 2017; 16: 181-202.

65) Moussa EM, Panchal JP, Moorthy BS, Blum JS, Joubert MK, Narhi LO, Topp EM. Immunogenicity of therapeutic protein aggregates. J. Pharm. Sci. 2016; 105(2): 417-30.

66) Hermeling S, Schellekens H, Maas C, Gebbink MF, Crommelin DJ, Jiskoot WI. Antibody response to aggregated human interferon alpha2b in wild-type and transgenic immune tolerant mice depends on type and level of aggregation. J. Pharm. Sci. 2006; 95(5): 1084-96.

67) Filipe V, Jiskoot W, Basmeleh AH, Halim A, Schellekens H, Brinks V. Immunogenicity of different stressed IgG monoclonal antibody formulations in immune tolerant transgenic mice. InMAbs 2012; (4)6: 740-752.

68) Torosantucci R, Sharov VS, van Beers M, Brinks V, Schöneich C, Jiskoot W. Identification of oxidation sites and covalent cross-links in metal catalyzed oxidized interferon beta-1a: potential implications for protein aggregation and immunogenicity. Mol. Pharm. 2013; 10(6): 2311-22.

69) Schöneich C. Novel chemical degradation pathways of proteins mediated by tryptophan oxidation: tryptophan side chain fragmentation. J. Pharm. Pharmacol. 2017.

Figures

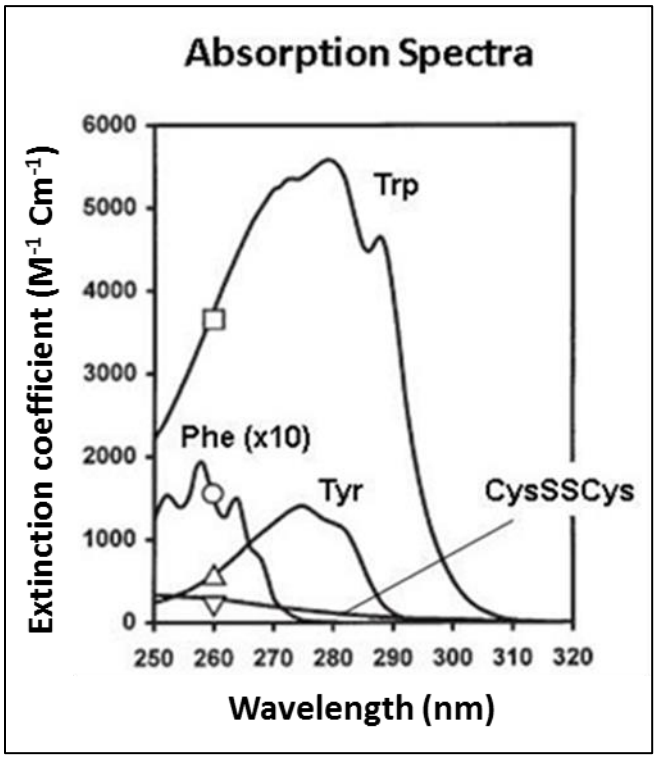

Figure 1. Absorption spectra of Trp, Phe, Tyr and CysSSCys (disulfide bond). The picture is reproduced from Martin SR et al. [52] by permission from the Springer e-book.

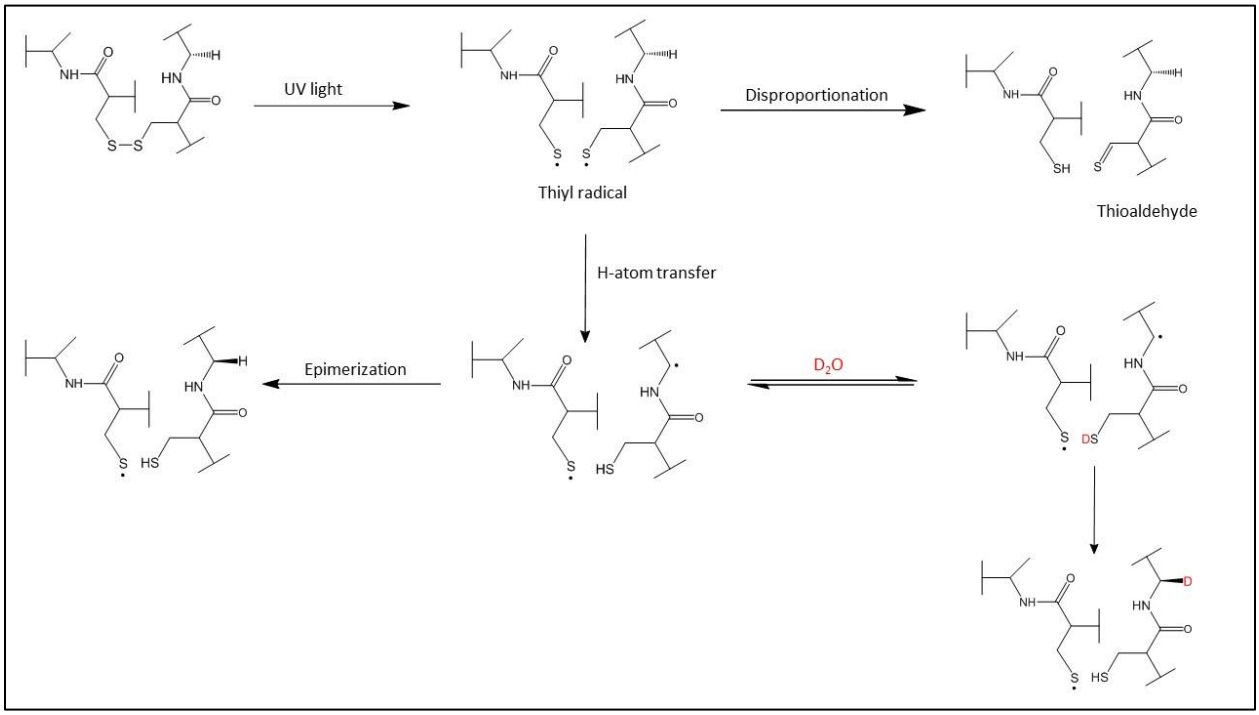

Figure 2. Light induced degradation of disulfide bond

Chapter.2 An efficient and rapid method to monitor the oxidative degradation of protein pharmaceuticals: probing tyrosine oxidation with fluorogenic derivatization

2.1 Introduction

Protein pharmaceuticals represent a fast growing class of therapeutics. Since the development of the first recombinant protein pharmaceuticals in 1982, more than 170 biotherapeutic products have been introduced to treat various diseases such as cancer, autoimmune diseases, allergy, infectious diseases, inflammation and various genetic disorders.[1-3] The global market for protein therapeutics is estimated to be worth $168 billion by 2017.[3] Much of the success of protein therapeutics is attributed to the influx of a large number of monoclonal antibodies into the pharmaceutical market.[4]

One of the most demanding tasks in the development of biotherapeutics is to maintain physical and chemical stability.[3] Protein unfolding, aggregation, surface adsorption and precipitation are major forms of physical instabilities encountered by protein therapeutics.[3-6] Chemical modifications involve covalent changes of chemical bonds, which ultimately lead to the formation of new chemical structures. Deamidation and oxidation are among the major chemical modification pathways of protein pharmaceuticals.[2, 3]

Methionine (Met), cysteine (Cys), tryptophan (Trp), tyrosine (Tyr), phenylalanine (Phe) and histidine (His) are significantly more sensitive to a series of oxidation pathways, due to the high reactivity of sulfur and aromatic rings towards various reactive oxygen species. [3, 8] Frequently, the chemical modifications of these amino acid residues result in structural and biologic consequences. For example, the formation of methionine sulfoxide (MetSO) in human IgG1 can impact its serum half-life [9], conformational stability [5], and the binding affinity to protein A and protein G columns used for purification.[10] Likewise, the oxidation of the other amino acids can also pose problems for the potency of protein pharmaceuticals. For example, the oxidation of a

single Trp residue is responsible for the loss of binding and biological activity upon (UV) light irradiation in MEDI-493, a monoclonal antibody (mAb) against respiratory syntical virus (RSV).[11]

Peptide bond flexibility, protein conformation and surface accessibility of amino acids affect the oxidation rates of amino acid residues.[8] Buffers, excipients, metal ions, light and temperature are also factors, which impact the oxidation pathways of proteins.[3,5,8] Autoxidation of polysorbates results in the formation of hydroperoxides which can oxidize proteins.[12] Polysorbates are the most common excipients used in protein formulations to prevent protein aggregation and protein surface adsorption.[12,13] Trace amounts of metals can be accidentally introduced into protein therapeutics during manufacturing and formulation through leaching from metal containers and excipients respectively.[14] These trace amounts of metal ions can induce metal-catalyzed oxidation.[15-17]

The oxidation of therapeutic proteins is monitored via a wide array of sensitive analytical techniques, including peptide mapping and mass spectrometry.[4,18-21] While offering high resolution and information on product identity, these techniques are time-consuming.

The aim of this study is to implement a fluorogenic derivatization method of oxidized Tyr and Phe amino acids as an orthogonal technique for the rapid screening of protein oxidation, and to evaluate whether a quantitative correlation exists between the oxidation of Tyr/Phe and Met for a given protein and specific oxidation conditions. The oxidation of Tyr and Phe generates aromatic vicinal diols such as 3, 4 dihydroxyphenylalanine (DOPA)[16] which can be derivatized with benzylamine derivatives.[22] Tryptophan oxidation yields several oxidation products, among them 5-hydroxy tryptophan (5-HTP), which can also be derivatized benzylamine derivatives.[23] DOPA and 5-HTP react with 4-amino methyl benzenesulfonic acid (ABS) to form a highly fluorescent

benzoxazole (**Scheme 1**; λ_{em} = 490nm, λ_{ex} = 360nm).[22,23] This method was initially developed to monitor oxidized proteins derived from tissue,[22,23] but is here applied to the screening of protein pharmaceuticals. To demonstrate that this fluorogenic method can be used as a high-throughput assay to screen for the stability of proteins, we evaluated this method with four proteins (bovine serum albumin (BSA), human growth hormone (hGH), a monoclonal antibody (IgG1) and insulin) exposed to oxidation via peroxyl radicals and metal-catalyzed reactions, respectively. Peroxyl radicals ($ROO^{\bullet}$) were generated through the thermal decomposition of 2,2'-azobis (2-methylpropionamidine) dihydrochloride (AAPH) [25] (**Scheme 2)**, a process that mimics the oxidation of proteins by peroxyl radicals generated from polysorbates.[24-26] Metal-catalyzed oxidation was initiated through the exposure of proteins to Cu (II)/L-ascorbic acid, or Fe (II)/H_2O_2 These conditions were selected to simulate the effect of trace amounts of metals inadvertently introduced into protein formulations during production and storage.[27,17] The oxidized proteins were reacted with ABS and subsequently placed on a UV-transilluminator (Fotodyne Inc., Hartland, WI, USA) to visualize the fluorescent products. For quantitative screening, the samples were prepared in a 96 well plate in order to allow simultaneous comparison of all proteins and their different responses to different oxidative stresses. Representatively for hGH we also quantified MetSO by mass spectrometry, and we related the mass spectrometry quantification of MetSO to the ABS derived fluorescence. For this, representative ABS fluorescence charts were built by integrating MetSO (quantified by mass spectrometry) and ABS fluorescence (measured by fluorescence spectroscopy) to serve as a tool for the rapid prediction of MetSO formation for a given protein.

2.2 Experimental methods

2.2.1 Materials

IgG1 (14 mg/ml) and hGH were provided by Genentech, Inc. (San Francisco, CA. Recombinant insulin containing 0.4% (w/w) zinc was purchased from Roche Applied Science (Indianapolis, IN). BSA, AAPH, monobasic and dibasic sodium hydrogen phosphate (Na_2HPO_4 and NaH_2PO_4), ethylenediaminetetraacetic acid (EDTA), L-ascorbic acid , copper dichloride ($CuCl_2$), sodium chloride (NaCl), iron (II) sulphate ($FeSO_4$), guanidine hydrochloride, potassium ferricyanide $K_3Fe(CN)_6$, iodoacetamide (IAA) , ammonium acetate ($NH_4C_2H_3O_2$), ammonium bicarbonate (NH_4HCO_3), dithiotheritol (DTT), bis (2-mercaptoehtyl) sulphone (BMS) and hydrogen peroxide (H_2O_2) were purchased form Sigma Aldrich (St. Louis, MO, USA). Trypsin/Lys-C, mass spectrometry grade, was purchased from Promega Corporation (Madison, WI, USA). SDS-PAGE running buffer (100mM Tris, 1.92M glycine and 0.1% (w/v) SDS at pH 8.25) and Precision plus Protein dual color standards were purchased from Bio-Rad (Hercules, CA, USA). Millipore Q water (milliQ water) was used for the preparation of all the solutions. Optimal water and acetonitrile (ACN), containing 0.1% (v/v) formic acid were purchased from Fisher Scientific (Waltham, MA). Amicon ultra-0.5 centrifugal filter devices equipped with a 10kDa cut off membrane were purchased from Millipore Inc., (Bedford, MA, USA). 4-Aminomethyl-benzylsulfonic acid (ABS) was synthesized according to published protocol [22].

2.2.2 AAPH oxidation

The model proteins (BSA, hGH, IgG1 and insulin) were dissolved at 1 mg/ml in 20 mM sodium phosphate buffer at pH 7.2. The reaction mixtures were prepared by mixing 200 µL of the model protein stock solution (1 mg/ml) with a series of concentrations of AAPH, and then incubated at 37 ^{o}C for 3 hours. The final concentrations of AAPH were 0 (control), 1, 2, 4, 8 and 16 mM.

Based on the rate of radical generation at 37 ^{o}C, 1.36 x 10^{-6} [AAPH] Ms^{-1} , [25] a 3 hour incubation with 16 mM AAPH generates a total of 2.35 x 10^{-4} M initial peroxyl radicals. With a concentration of hGH (1 mg/ml) at 4.5 x 10^{-5} M, the maximal ratio of [$ROO^{\bullet}$] / [hGH] = 5.2. To stop the reaction, the oxidized hGH samples were buffer exchanged with 100 mM phosphate buffer (pH 9.2) for 12 mins at 14,000 g (4 ^{o}C, 3 times) using Amicon ultra- 0.5 centrifugal filters equipped with a 10 kD cut-off membrane. In order to test whether we completely stopped the reaction we compared two samples (i) AAPH-exposed hGH, which was buffer exchanged, and (ii) AAPH-exposed hGH, which was buffer exchanged but incubated for 3 additional hours at 37 ^{o}C. After derivatization with ABS, both samples showed the same fluorescence intensity, indicating that all AAPH had been removed by buffer exchange.

2.2.3 Metal catalyzed oxidation

2.2.3.1 Cu (II) /L-ascorbate

Metal catalyzed oxidation of model proteins (1 mg/ml, in 20 mM sodium phosphate buffer, pH 7.2) by Cu (II)/L-ascorbic acid was performed by mixing model proteins with various concentrations of Cu (II) to reach final concentrations ranging from 5 µM to 20 µM. To allow binding of Cu (II) to the proteins, the samples were incubated with Cu (II) for ten minutes prior to the addition of L-ascorbic acid.[29] After ten mins, 500 µM of L-ascorbic acid was added to each sample. The final solution was incubated at 37 ^{o}C for 3 hours. The reactions were stopped by the addition of 50 µL of 50 mM EDTA.

2.2.3.2 Fe (II)/H_2O_2/EDTA

Separate stock solutions of EDTA (20 mM), Fe (II) (10 mM), and H_2O_2 (10 mM) were prepared in Ar-saturated ammonium acetate buffers (20 mM, pH 7.2). 500 µL of the EDTA solution was mixed with 400 µL of the Fe (II) solution in order to prepare a stock solution of EDTA/ Fe (II) at

1 mM. After mixing, the solution was again saturated with Ar. Subsequently 200 µL of the model protein stock solution (1 mg/ml, in 20 mM ammonium acetate buffer pH 7.2) was mixed with 10 µL of the Fe (II) /EDTA solution, and the oxidation reaction was started by the addition of 10 µL of the H_2O_2 stock solution. The samples were incubated at 37 ^oC for 3 hours. The reactions were stopped by the addition 250 µL DTPA (1 mM), and 10 µL of catalase (25 µM).

2.2.4 Fluorogenic derivatization

After exposure of the model proteins to AAPH and metal catalyzed oxidation, the oxidized proteins were buffer exchanged with 100 mM sodium phosphate buffer (pH 9.2) using Amicon ultra-0.5 centrifugal filter devices equipped with a 10 kDa cut-off membrane. The optimal conditions for the derivatization of DOPA in oxidized proteins with ABS were as follows: oxidized protein samples were mixed with $K_3Fe(CN)_6$ at a molar ratio of $K_3Fe(CN)_6$: protein = 30:1 in the presence of 10 mM ABS and followed by incubation of samples in the dark for 90 mins. The procedures for analysis of the derivatized samples are described in the next two sections.

2.2.5 Size exclusion chromatography (SEC)

SEC was performed on a Shimazdu HPLC system equipped with two Shimazdu LC-20AT pumps (Shimazdu, Columbia, MD) and coupled both to a photo-diode array detector (Prominence RF-20A, Shimazdu, Columbia, MD) and a fluorescence detector (RF-20A, Shimazdu, Columbia, MD). The samples (90 µL) were injected onto a TSK-GEL G3000swxl column (7.8 mm TD x 30 cm, 5 µm, Tosoh Biosciences, King of Prussia, PA, USA). The mobile phase consisted of 200 mM sodium phosphate buffer and 50 mM sodium chloride at pH 7.0, and was eluted through the column at a constant flow rate of 0.7 ml/min.

2.2.6 Steady-state fluorescence spectroscopy analysis

The steady-state fluorescence of protein samples derivatized with ABS was measured with a Shimazdu RF-5301PC-spectrofluorophotometer equipped with a 1-cm quartz cuvette. Fluorescence measurements at λ_{em}= 490 nm (λ_{exc} = 360 nm) were acquired both in a 500 µL 1-cm quartz cuvette (Starna cell, Atascadero, CA 93422) and on a 96 well plate model, respectively. The excitation and emission bandwidths were set at 5 nm.

2.2.7 Reduction and alkylation

Oxidized and control hGH samples were purified through Amicon ultra-0.5 centrifugal filter devices equipped with 10 kDa membranes. The purified hGH samples were reconstituted in 100 µL of ammonium bicarbonate buffer (50 mM, pH 7.5). The disulfide bonds were reduced by the addition of 50 µL BMS (5 mM stock solution in ACN), followed by incubation at 45 ^{o}C for 30 mins. The reduced cysteine residues were alkylated by the addition of 50 µL of IAA (25 mM in NH_4HCO_3 buffer 50 mM, pH 7.4), followed by incubation for 2 hours at 37 ^{o}C.

2.2.8 Trypsin/Lys-C digestion

150 µL of reduced and alkylated hGH (1 mg/ml) were mixed with 700 µL $HClO_4$ (0.5 M). The samples were centrifuged at 16,000 g at 4 ^{o}C for 20 mins and the resulting pellet washed twice with milliQ water. The pellet was reconstituted in 200 µL of NH_4HCO_3 buffer (50 mM, pH 8).The protein samples were digested with trypsin/ Lys-C (3 µg) in NH_4HCO_3 buffer (50 mM, pH 8) at 37 ^{o}C overnight. The proteolytic digests were purified using Amicon ultra-0.5 centrifugal devices equipped with 10 kDa membranes to separate undigested protein and trypsin/Lys-C from the tryptic peptides.

2.2.9 Sodium Dodecyl Sulfate Polyacrylamide Gel Electrophoresis

After reduction and alkylation of Cys residues, 20 µL solution containing either native or oxidized hGH (1 mg/ml), and its control were mixed with 1.1 X reducing sample buffer, which consisted of 68.89 mM Tris HCl at pH 7.0, 2.2% w/w SDS, 0.044% w/w bromophenol blue, 22.22% w/w glycerol, and 111.11 mM DTT. The samples were boiled at 100 ^{o}C for 2 mins after mixing. An aliquot of 20 µL of each sample was loaded onto a 4-20% polyacrylamide gel from Bio-Rad (Hercules, CA, USA). Molecular weight standards and Precision Plus Protein Dual Color Standards (Bio-Rad) were also loaded onto the same gel. The gel electrophoresis was run at a difference of potential of 200 V for 40 mins using 10-fold diluted running buffer. The fluorescence bands that contained protein derivatized with ABS, were visualized through a UV-transilluminator (λ = 302 nm).

2.2.10 In-Gel digestion

The fluorescent bands were excised for in-gel digestion, according to the protocol described by Shevchenko et al [30]. Briefly, the gel slices were first rinsed twice with 100 mM NH_4HCO_3 (pH 7.8) in H_2O/ACN (1:1 v/v) and then rinsed with 100% ACN at room temperature. The gel slices were dried using a Speedvac from Labconco Corp. (Kansas City, MO, USA). The dried gel slices were incubated for one hour at 4 ^{o}C in 200 µL of 50 mM acetic acid, containing 5 µg of sequencing-grade trypsin/Lys-C. An aliquot of 200 µL of 100 mM NH_4HCO_3 (pH 7.8) was then added to the samples prior to protein digestion. The samples were incubated at 37 ^{o}C for 8 hours. Upon completion of the digestion, the protein solutions were transferred into new 1.5-mL Eppendorf vials. The gel slices were rinsed three times with 100% ACN, and the rinsing solutions were combined with the solutions containing digested protein in the new Eppendorf

vials. The samples were concentrated using the Speedvac to reach a final volume of 20 µL for LC-MS/MS analysis.[30]

2.2.11 Mass spectrometry analysis

LC-ESI-MS experiments were performed on an Acquity UPLC system (Waters Corporation, Milford, MA) coupled to either a Xevo Q-TOF (Waters Corporation, U.K) or a linear ion trap quadrupole-Fourier transform (LTQ-FT) mass spectrometer (Thermo-Finnigan, Bremen, Germany).

2.2.11.1 Xevo Q-TOF mass spectrometry analysis

LC-MS analysis were performed on a Xevo Q-TOF mass spectrometer (Waters Corp.,U.K), equipped with a nanoAcquity (Waters Corp.,U.K) chromatograph and a BEH nanocolumn (75 µm x 150 mm C18, Waters Corp.). Aqueous (A) and organic (B) mobile phases consisted of optimal water and formic acid (FA) 99.9%: 0.1%, (v:v), and ACN and FA 99.9%: 0.1%, (v:v). Tryptic peptides were eluted within 70 mins by increasing mobile phase B linearly from 3 to 35% (v:v) within the first 50 mins, and by increasing the amount of B to 95% (v:v) within the following 20 mins. The flow rate was 0.3 µl/min. The Xevo Q-TOF was operated in the MS^E mode with all lenses optimized on the $[M + 2H]^{2+}$ ion for the $[Glu]^1$ -fibrinopeptide B. The cone voltage was 25 V, and Argon was admitted to the collision cell. The spectra were acquired using a mass range of 150-2,000 Da. The data were accumulated for 0.5 s per cycle. MS/MS measurements were performed by ramping the collision energy from 10V to 40V.

2.2.11.2 LTQ-FT mass spectrometry analysis

Experiments were carried out on a linear ion trap quadrupole-Fourier transform (LTQ-FT) ion cyclotron resonance mass spectrometer. The instrument was operated in the data dependent

acquisition (DDA) mode. All the lenses were optimized on the $[M+H]^+$ ion from leucine enkephalin. Tryptic digests were eluted on a non-porous Presto FF-C18 column (15 cm x 0.5 mm, 2 µm, Imtakt USA, Portland, USA) at a flow rate of 5 µl/min. The ESI source was operated with a spray voltage of 2.8 kV, a tube lens offset of 96 V and a capillary temperature of 200 ^{o}C. The mobile phases consisted of water, ACN and FA at a ratio of 99.9%:0%:0.1%, (v:v) for solvent A and 0%:99.9%:0.1%, (v:v) for solvent B. The raw files from the FT-ICR measurements were read by the Xcalibur 2.0 software package (Thermo Scientific, Waltham, MA) and analyzed with MassMatrix.[30]

2.2.12 Calibration curves

A calibration curve for mass spectrometry analysis was built by plotting the peak areas of the Glu-Fib peptide against a series of known concentrations of the Glu-Fib peptide. Glu-Fib was provided as lyophilized powder, to which 0.1% FA in optimal water was added to bring the concentration to 100 µM. A dilution series was prepared by addition of 0.1% FA in optimal water. Calibration curve built with concentrations ranging from 2-2000 nM **(**Fig. 1b). The calibration curves were built using peptide peak intensity measurements, which involved extraction of ion chromatograms from the LC-MS runs of the Glu-Fib peptide followed by calculation of peak areas. Calibration curves were built by plotting peak areas of the extracted ion chromatograms versus the theoretical concentrations. In the calibration curves, the slopes are representative of the sensitivities of the mass spectrometry method used for the analytes. The precision of the data was determined by measuring 3 replicates of one sample, which is represented by standard deviation. The two calibration curves were built to bracket the limit of quantification and the upper limit of linearity. Limit of quantification (LOQ, 5 nM) is the lowest concentration of the analyte that can be quantified. The upper limit of linearity (LOL, 2000 nM)

describes the highest concentration of analyte above which linearity cannot be established between concentration and peak area.[31]

2.2.13 The use of a 96 well-microplate to efficiently monitor oxidized proteins by ABS derivatization

To assess the presence of oxidized proteins in a large variety of protein samples we performed the fluorogenic derivatization with ABS in a 96 well microplate. BSA (1 mg/ml), IgG1 (1 mg/ml), insulin (1 mg/ml) and hGH (1 mg/ml) were oxidized with either AAPH, Fe (II)/H_2O_2/EDTA, or Cu(II)/L-ascorbate. After incubation, the samples were buffer exchanged with 100 mM sodium phosphate buffer (pH 9). Samples were centrifuged at 14,000 g for 12 mins in Amicon 0.5-ultra filters equipped with 10 kD cut-off membranes. After the centrifugation, samples were measured for protein concentration and adjusted accordingly before loading the samples into the well plate. 200 µL of each sample was transferred to a 96 well microplate. After loading the oxidized samples to the microplate, 50 µL of 60 mM ABS stock solution was added to the samples at final concentrations of 10 mM ABS, followed by the addition of 50 µL of 3 mM $K_3Fe(CN)_6$ stock solution to a final concentration of 500 µM. After 90 mins, the microplate was placed on a UV-Transilluminator (operated at λ = 302 nm) for visualization of the fluorescence, and subsequently placed in a spectrofluorometer to read the absolute intensities.

2.3 Results

The two objectives of this study were to establish a rapid screening method for Tyr and Phe oxidation and to evaluate whether there is a quantitative relationship between the oxidation of Tyr/Phe and Met for a given protein (representatively hGH) and a given oxidative stress system (representatively AAPH). Tyr/Phe oxidation to DOPA can easily be monitored by fluorescence

detection after ABS derivatization of DOPA, while the oxidation of Met to MetSO must be monitored by HPLC coupled to either UV or mass spectrometry detection.

The results section is divided into four sub-sections. First, we will present the results on hGH alone, along with the details regarding the derivatization of DOPA by ABS. In the second sub-section, we will characterize the formation of MetSO in oxidized hGH. The third sub-section will focus on the development of ABS fluorescence charts to relate the quantification of MetSO by LC-MS to the fluorescence detection of DOPA in oxidized hGH. Finally, the development of a high-throughput assay to simultaneously screen for the oxidative degradation of a series of model proteins will be described.

2.3.1 ABS derivatization to monitor the formation of DOPA in oxidized hGH

After ABS derivatization of hGH oxidized with AAPH, we observed the formation of the fluorescent benzoxazole (λ_{em} = 490 nm on excitation at λ_{exc} = 360 nm) (Fig. 2, blue, a). The control (non-oxidized hGH), which underwent the same protocol for ABS derivatization showed little fluorescence (Fig. 2, black, b).

The ABS-dependent fluorescence intensity increases with the increase in concentration of AAPH (1 mM to 16 mM) used to oxidize hGH, indicating an AAPH-dependent increase of Tyr/Phe oxidation (Fig. 3). However, this increase is not linear over the range of AAPH concentration suggesting different sensitivity of different Phe/Tyr residues to AAPH derived oxidation. Similar observations were made by SEC analysis and fluorescence detection (Fig. 4, Fig. S3). hGH degradation induced by AAPH was monitored using SEC coupled to diode array detector (Fig. S4), indicating increase in aggregation with oxidizing power of the AAPH system.

2.3.2 SDS-PAGE analysis of ABS-derivatized oxidized hGH

After the incubation of hGH with different initial concentrations of AAPH (ranging from 1 mM to 16 mM), the protein was derivatized with ABS, followed by reduction and alkylation of derivatized hGH. The samples were then fractioned by SDS-PAGE.

The fluorescence intensity increased from lane 2 to lane 7 (Fig. 5) for both monomers and dimers (covalent aggregates) of hGH, which indicates the presence of oxidized Tyr and / or Phe that are derivatized with ABS, in both monomer and dimer. In addition, as we progress from lane 2-7, a smear of fluorescence starts to appear in the higher molecular weight region indicating the formation of higher molecular weight aggregates with oxidized Tyr and / or Phe. These observations confirm that the formation of DOPA increases with the increase in the initial concentration of AAPH.

2.3.3 Identification of DOPA and ABS derivatized peptides

The most intense fluorescent bands (corresponding to monomers) from the SDS–PAGE were excised and subjected to in-gel digestion, and the tryptic peptides were extracted and analyzed by LC-MS/MS. After oxidation of hGH, MS/MS analysis of the proteolytic peptides indicates hydroxylation of Tyr-35 in the tryptic peptide QEFEEAYIPK, where the fragment ions y3, y4, b3, and b4 demonstrate an increase of +16 Da of Tyr-35 (Fig. 6). After ABS-tagging of oxidized hGH, the LC-MS analysis of the tryptic digest revealed that the mass of the peptide QEFEEAYIPK increased by +197 Da, as expected for derivatization of DOPA with ammonia and ABS. The MS/MS spectrum confirms the conversion of Tyr 35 into benzoxazole (Fig. 7**)** and the structure is shown in the insert of Fig.7. Indeed, the parent ion with m/z of 1450.39 corresponds to an increase of +197 Da in comparison to the original tryptic peptide

QEFEEAYIPK. The series of y1-y4, and b1-b4 fragment ions indicate that the mass increase of 197 Da is located at Tyr-35. We also detected derivatization of DOPA with two ABS molecules (Fig. 8**)**, consistent with the reaction mechanism of ABS derivatization**.**[22,23] This twofold derivatized parent ion with m/z 1620.39 corresponds to an increase of +366 Da relative to the original tryptic peptide QEFEEAYIPK. This tryptic peptide originally contains also Phe, which is an additional potential target for oxidation.[14] The series of y5-y8 and b1-b3 fragment ions shows no sign of derivatization at the original Phe-32 residue. The increase of +366 Da is located between the fragment ions y3 and y4, demonstrating that the addition of two molecules of ABS occurred at the original Tyr-35 residue. We observe no significant oxidation of Tyr-103 under our reaction conditions. However, this is not surprising as low yields of Tyr-103 oxidation were previously observed for much stronger oxidizing conditions, where [ROO$^{\bullet}$] / [hGH] = 30.[28] In contrast, under our experimental conditions, [ROO$^{\bullet}$] / [hGH] = 5.2.

2.3.4 Identification of MetSO by LC-MS

hGH is a single chain protein consisting of 191 amino acids residues which contains three Met residues Met-14, Met-125, and Met-170 (Table 1). Only Met-14 and Met-125 were oxidized to MetSO with significant yields after incubation of hGH with various concentrations of AAPH.[28]

After oxidation of hGH, the MS/MS spectrum of the tryptic peptide LFDNAMLR showed that Met-14 was oxidized to MetSO. The fragment ions y3 and b6 confirm an increase of +16Da at Met-14 (Fig. 9). Our analysis also revealed that Met-125 in the tryptic peptide DLEEGIQTLMGR was oxidized to MetSO**.** The latter was demonstrated by its MS/MS spectrum, which indicated through the formation of the y3 and b10 fragment ions that oxidation, occurred at Met-125 (Fig. 10).

MetSO in oxidized hGH was quantified as follows: The sum of the ion intensities of the oxidized tryptic peptides LFDNA(MetSO)LR and DLEEGIQTL(MetSO)GR was compared to the Glu-Fib calibration curve (Fig. 11). To compensate any potential variation of the amount of MetSO to the variability of the recovery of the peptides after digestion, the MetSO containing peptides were normalized to the intensity of the oxidation resistant peptide SNLELLR. Quantification of MetSO was achieved assuming that MetSO containing peptides ionized similarly than the Glu-Fib peptide during ESI.

2.3.5 Correlation of DOPA fluorogenic derivatization with MetSO formation in oxidized hGH

The steady-state fluorescence intensities of ABS-derivatized hGH were plotted against the amount of MetSO detected by LC-MS (Fig. 12). The plot shows two distinct regions: for fluorescence intensities up to ca. 330 au, a ca. 6.6-fold increase in fluorescence (between ca. 50 and 330 a.u.) is accompanied by a ca. 5-fold increase in MetSO. However, for fluorescence intensities between 330 and 600 a.u., a < 2-fold increase in fluorescence intensity is accompanied by an almost 3-fold increase in MetSO. The existence of these specific regions can be rationalized by different sensitivities of various Tyr and Met residues towards oxidation. Nevertheless, these charts containing plots of fluorescence vs. MetSO permitted to predict the amount of MetSO without performing an LC-MS analysis. The robustness of this method was tested by the incubation of hGH with various AAPH concentrations which were not used to build the fluorescence vs. MetSO plots. For example, hGH was oxidized in presence of 7 mM AAPH for 3 hours at 37 ^{o}C. The oxidized hGH was reacted with ABS and the measured fluorescence intensity of 370 au was used to estimate the amount of MetSO to 1.6 nanomoles (± 0.054). This value for MetSO was reasonably close to the yield of MetSO 1.705 nanomoles (± 0.019)

independently determined by mass spectrometry. We note, that a fluorescence chart built for one specific protein cannot be used to predict the oxidation of another protein, due to differences in sequence and, most likely, in the sensitivities of Met and Tyr to oxidation in different proteins. Hence, separate fluorescence charts have to be constructed for individual proteins.

2.3.6 Fluorescence visualization of ABS derivatized protein samples by UV-transilluminator

The model proteins (hGH, IgG1, insulin and BSA) were exposed to various oxidation conditions, followed by derivatization with ABS and fluorescence visualization on the UV-Transilluminator. Experiments were performed in a 96 well plate (one entire column on the microplate was loaded with the same protein). Model proteins exposed to AAPH, Cu (II)/L-ascorbate and Fe (II)/H_2O_2 were loaded to columns 1-4, 6-9 and 10-12, respectively in the microplate (Fig. 13). The first two wells in column 5 (5a and 5b) were loaded with derivatization reagents alone (ABS and $K_3Fe(CN)_6$) to monitor the background. Rows a and e were always loaded with non-oxidized (control) proteins exposed to derivatizing conditions with ABS. Table 2 presents the individual conditions for each well. Upon visualization (Fig.13), protein samples that were exposed to stronger oxidation conditions always showed stronger fluorescence intensities as compared to protein samples exposed to lower levels or no oxidation. There was minimal fluorescence in the non-oxidized controls. The ABS derivatized fluorescence intensities of the representative samples are presented in the supplementary material (Fig. S5).

2.4 Discussion

The length and intricacy of the development process for protein pharmaceuticals require the development of fast and affordable stability tests. The latter have already been developed for

screening products, ranging from early stage[36] to late stage formulation development.[37] The benefits of high-throughput screening rely on a rapid analysis, which permits to collect a substantial amount of data to preclude the release of unstable products. In the pharmaceutical industry any process, which can fulfill these requirements can help in introducing protein pharmaceuticals faster into the market. Another advantage of high-throughput screening is the possibility to analyze a broad variety of samples (e.g. different proteins) at the same time.[36,37]

We have developed a quick and sensitive chemical assay to monitor the level of oxidation of proteins. Our assay is based on the derivatization of DOPA with ABS, which specifically allows for the detection of oxidation products of Phe and Tyr.[14,22,23] We adapted our assay to a 96 well microplate framework, where four different non-oxidized (control) and oxidized model proteins (IgG1, insulin, hGH and BSA) were ABS-derivatized in a single microplate. The latter was placed on a UV-Transilluminator to reveal the specific fluorescence of the benzoxazole product, which resulted from the reaction between DOPA and ABS. This plate could also be read in a high throughput fashion on a fluorescence plate reader. The fluorescence values could be correlated to a previously generated interpolation curve like has been made for hGH.

Model proteins were exposed to increasing amounts of peroxyl radicals ($ROO^{\bullet}$), which were generated by thermolysis of AAPH in air saturated aqueous solution at a rate of 1.36×10^{-6} [AAPH] Ms^{-1}.[38] Our assay correlates the increase of fluorescence intensities, resulting from the derivatization of DOPA by ABS, with the exposure of proteins to increasing amount of $ROO^{\bullet}$ (Fig 3). Based on a calibration curve generated by Sharov et al.,[22] the amount of DOPA generated on hGH by exposure to increasing amounts of peroxyl radicals from AAPH was estimated to be between 1.02 pico moles (1.1 µmoles per mole of protein) and 6.1 pico moles (6.66 µmoles per mole of protein). Under our experimental conditions, the latter corresponds to a

fluorescence intensity between 70 and 600 a.u. on our plate reader. Therefore, under our experimental conditions the ratio of Met oxidation over Tyr/Phe oxidation in hGH, was ca. 767:1. We also did observe DOPA by LC-MS analysis but its level was below the limit of quantification by MS.

MetSO represents one of the major degradation products in protein therapeutics, which can potentially impact protein pharmaceuticals.[8,9] In addition, MetSO is frequently monitored as a representative oxidation product of protein pharmaceuticals. Typically, MetSO is detected by peptide mapping in combination with LC-MS analysis, which does not permit rapid screening of multiple formulations. Our fluorogenic assay shows that after exposure of hGH to AAPH, the amount of DOPA in oxidized hGH correlates quantitatively with the formation of MetSO which was measured by LC-MS. Based on our observations the key to this correlation is likely the parallel reaction of ROO$^{\bullet}$ with both Tyr and Met, as outlined in **Scheme 3**. Upon thermolysis of AAPH in air, the formation of carbon-centered radicals yields ROO$^{\bullet}$ (**Scheme 2**) which oxidize tyrosine to tyrosyl radicals (TyrO$^{\bullet}$, **Scheme 3, reaction 1**). TyrO$^{\bullet}$ can further react with peroxyl radicals to form DOPA (**Scheme 3, reaction 2**), which can be derivatized with ABS to form the fluorescent benzoxazole derivative (**Scheme 1**). In parallel, ROO$^{\bullet}$ reacts via two-electron oxidation with Met yielding MetSO and an alkoxyl radical [39] (RO$^{\bullet}$, **Scheme 3, reaction 3**). RO$^{\bullet}$ can oxidize Tyr to yield DOPA via formation of TyrO$^{\bullet}$ (**Scheme 3, reactions 4 and 5**). Because DOPA and MetSO are formed simultaneously and originate from the same oxidants (i.e. RO$^{\bullet}$, ROO$^{\bullet}$), the identification and characterization of one of these oxidation products allows for predicting the formation of the others. We note that analogous linear correlations between DOPA and MetSO formation can also be expected for other oxidants, except that the absolute values

may vary depending on the preference of the specific oxidants for Tyr and Met, respectively. The only exception will be peroxides in the absence of metals, where peroxides would react nearly exclusively with Met to generate MetSO (i.e., in the absence of metals, no Fenton-type reaction is expected). However, as most proteins will show trace of metal contaminants such conditions are frequently not met in pharmaceutical formulations.

2.5 Conclusions

Our rapid fluorescence based screening allows for the fast comparison of the stability of multiple formulations, for example in 96 well plates. Subsequent in depth LC-MS analysis can then be limited to the most promising formulations, resulting in significant saving of time and resources.

2.6 References

1) Benjamin L, Quentin, J.B, David E. Golan. Protein therapeutics: a summary and pharmacological classification. Nat. Rev. Drug. Discov. 2008; 7: 21-39.

2) Li S, Schöneich C, Borchardt, R, T. Chemical instability of protein pharmaceuticals. Mechanisms of oxidation and strategies for stabilization. Biotechnol Bioeng. 1995; 48: 490-500.

3) Manning, C M, Chou D K, Murphy M B, Payne, W R, Katayama, S, D. Stability of Protein Pharmaceuticals: An Update. Pharm Res. Rev. 2010; 27(4): 544-575.

4) Hawe A, Wiggenhorn M, Van De Weert M, Garbe H J, Mahler H C, Wim Jiskoot. Forced Degradation of Therapeutic Proteins. J Pharm Sci Rev. 2011; 101 (3): 895-913.

5) Wang Wei. Instability, stabilization, and formulation of liquid protein pharmaceuticals. *Int* J Pharm. Rev. 1999; 185: 129-188.

6) Schöneich C., Hageman J M, Borchardt, T B. Stability of Peptides and Proteins. 1997.

7) Zhong X, Neumann P, Corbo M, Loh E. Recent advances in biotherapeutics Drug discovery and Development. Intech

8) Torosantucci R, Schöneich C, Wim Jiskoot. Oxidation of therapeutic proteins and peptides: structural and biological consequences. Pharm Res. Rev. 2014; 31: 541-553.

9) Wang W, Vlasak J, Li Y, Pristatsky P, Fang Y, Pittman T, Roman J, Wang Y, Prueksaritanont T, Ionescu, R. Impact of methionine oxidation in human IgG1 Fc on serum half-life of monoclonal antibodies. Mol.Immunology. 2010; 860-866

10) Gaza-Bulesco G, Faldu S, Hurkmans K, Chumsae C, Liu H. Effect of methionine oxidation of a recombinant monoclonal antibody on the binding affinity to protein A and Protein G. *J Chromatogr B*. 2008; 870: 55-62.

11) Wei Z, Feng J, Lin HY, Mullapudi S, Bishop E, et al. (2007) Identification of a single tryptophan residue as critical for binding activity in a humanized monoclonal antibody against respiratory syntical virus. Anal Chem. 2007; 79: 2797-2805.

12) Kerwin B. Polysorbates 20 and 80 used in the formulation of protein biotherapeutics: structure and degradation pathways. J Pharm Sci. 2008: 97: 2924-35.

13) Donbrow M, Azaz E, Pillersdorf A. Autoxidation of polysorbates. J Pharm Sci. 1978; 67: 1676-81.

14) Zhou S, Mozziconacci O, Kerwin A B, Schöneich C. Fluorogenic tagging methodology applied to characterize oxidized tyrosine and phenylalanine in an immunoglobulin monoclonal antibody. Pharm Res. 2013; 30: 1311-1327.

15) E. R. Stadtman. Olivier, C, N. Metal-catalyzed oxidation of proteins. J Biol Chem. 1991; 266 (4): 2005-2008.

16) E. R. Stadtman. Oxidation of free amino acid residues in proteins by radiolysis and metal- catalyzed reactions. Annu. Rev. Biochem. 1993; 62: 797-821.

17) Mozziconacci O, Junyan A. Ji, Wang, J, Schöneich C. Metal-Catalyzed Oxidation of Protein Methionine Residues in Human Parathyroid Hormone (1-34): Formation of Homocysteine and a Novel Methionine-Dependent Hydrolysis Reaction. Mol. Pharm. 2012; 10: 739-755.

18) Chen G, Pramanik N B. Application of LC/MS to proteomics studies: current status and future prospects. Drug Discovery Today. 2009; 14: 465-471.

19) Chen G, Warrack M B, Goodenough K A, Wei H, Wang-inverson B D, Tymiak A A. Characterization of protein therapeutics by mass spectrometry: recent developments and future developments. Drug Discovery Today. 2011; 16: 58-64.

20) Schöneich C, Sharov, V, S. Mass spectrometry of protein modifications by reactive oxygen and nitrogen species. Free Radic Biol Med. 2006; 41: 1507-1520.

21) Igor A. Kaltashov , Cedric E. Bobst, Rinat R. Abzalimov, Guanbo Wang, Burcu Baykal, Shunhai Wang. Advances and challenges in analytical characterization of biotechnology products: Mass spectrometry-based approaches to study properties and behavior of protein therapeutics. Biotechnol Adv. 2012; 30, 210-222

22) Sharov V S, Dremina E S, Galeva N A, Gerstenecker G S, Li X, Dobrowsky R T, Stobaugh J F, Schöneich C. Fluorogenic tagging of peptide and protein 3-Nitrotyrosine with 4-(Amino methyl)-benzenesulfonicacid for quantitative analysis of protein tyrosine nitration. Chromatographia. 2010; 71: 37-53.

23) Sharov V S, Dremina, Pennington J, Killmer J, Asmus C, Thorson, M, Hong S J, Li X, Stobaugh J F, Schöneich C. Selective fluorogenic derivatization of 3-nitrotyrosine and 3,4-dihydroxyphenylalanine in peptides: a method designed for quantitative proteomic analysis. Methods Enzymol. 2008; 441: 19-32.

24) Ravuri S. K. Kishore, Sylvia Kiese, Stefan Fischer, Astrid Pappenberger, Ulla Grauschopf, Hanns-Christian Mahler. The degradation of polysorbates 20 and 80 and its potential impact on the stability of biotherapeutics. Pharm Res. 2011; 28(5): 1194-1210.

25) Betigeri S, Thakur A, Raghavan K. Use of 2-2'- Azobis (2- Amidinopropane) Dihydrochloride as a reagent tool for evaluation of oxidative stability of Drugs. Pharm Res. 2005; 22: 310-317.

26) Werber J, Wang J Y, Milligan M, Li M, Ji A J. Analysis of 2-2'- Azobis (2-Amidinopropane) Dihydrochloride degradation and hydrolysis in aqueous solution. J Pharm Sci. 2011; 100(8): 3307-3315.

27) Ji J, Zhang B, Cheng. W, Wang. J.Y. Methionine, tryptophan, and Histidine Oxidation in a Model protein, PTH: Mechanisms and stabilization. J Pharm Sci. 2009; 98: 4485-4500.

28) Steinmann D, J. A. Ji, Y. J. Wang, Schöneich C. Oxidation of human growth hormone by oxygen-centered radicals: formation of Leu-101 hydroperoxides and Tyr-103 oxidation products. Mol. Pharm. 2012; 9: 803-814.

29) Zhao F, Ghezzo-Schöneich E, Aced G I, Hong J, Milby T, Schöneich C. Metal-catalyzed oxidation of histidine in human growth hormone. Mechanism, isotope effects, and inhibition by a mild denaturing alcohol. J Biol Chem. 1997; 272: 9019-9029.

30) Shevchenko A, Tomas H, Havli J, Olsen J V, Mann M. In-gel digestion for mass spectrometric characterization of proteins and proteomes. Nat Protoc. 2007; 1: 2856-2860.

31) Xu H, Freitas. MassMatrix: a database search program for rapid characterization of proteins and peptides from tandem spectroscopy data. Proteomics. 2009; 9: 1548-1555.

32) Mani R D, Abbatiello E S, Carr A S. Statistical characterization of multiple-reaction monitoring mass spectrometry (MRM-MS) assays for quantitative proteomics. BioMed Central. 2012; 13.

33) Seema B, Ajit T, Raghavan K. Use of 2,2'- Azobis(2-Amidinopropane) Dihydrochloride as a Reagent Tool for Evaluation of Oxidative Stability of Drugs. Pharm.Res. 2005; 22.

34) Clare L. Haekins, Michael J. Davies. Generation and propagation of radical reactions on proteins. Biochim Biophys Acta. 2001; 1504: 196-219.

35) Berges J, Trouillas P, Houee-Levin C. Oxidation of protein tyrosine or methionine residues: From the amino acid to peptide. J Phys Conf Ser. 2011; 261.

36) White R. E. High-throughput screening in drug metabolism and Pharmacokinetic support of drug discovery. Annu. Rev. Pharmacol. Toxicol. 2000; 40: 133-157.

37) Capelle M, Gurny R, Arvinte T. High throughput screening of protein formulation stability: Practical considerations. Eur. J .Pharm. Biopharm. 2007; 65: 131-148.

38) Niki E. Free radical initiators as source of water-or lipid-soluble peroxyl radicals. Methods Enzymol. 1990; 186: 100-108.

39) Schöneich C. Methionine oxidation by reactive oxygen species: reaction mechanisms and relevance to Alzheimer's disease. Biochim Biophys Acta. 2005; 1703(2): 111-119.

Schemes

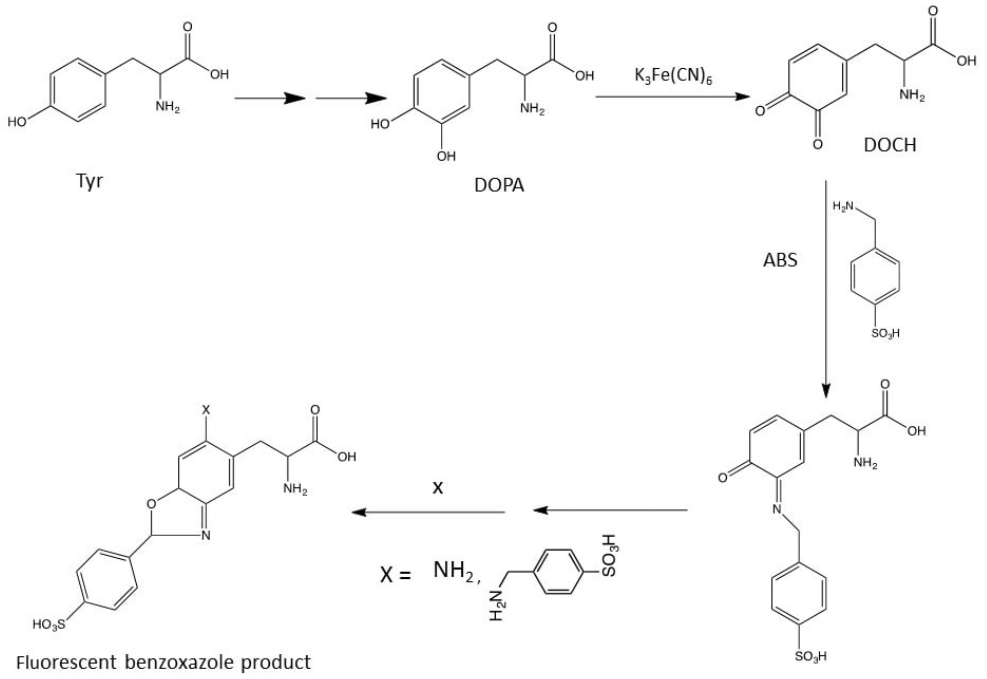

Scheme 1: Schematic representation of the fluorogenic derivatization of DOPA with ABS.

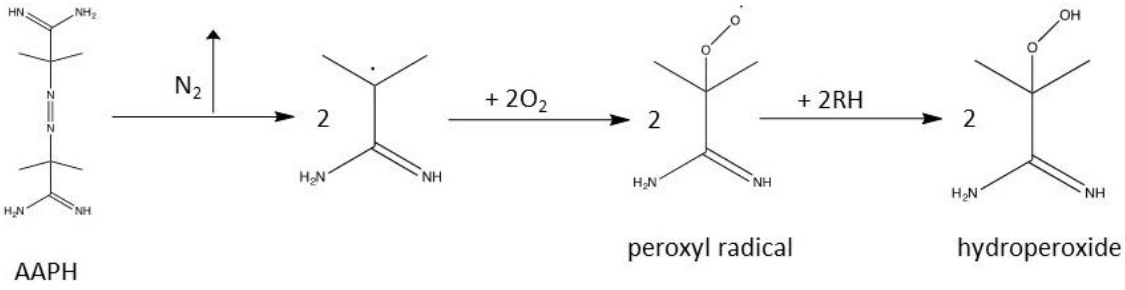

Scheme 2: Mechanism of thermolysis of AAPH, production and reaction of peroxyl radicals under aerobic conditions.

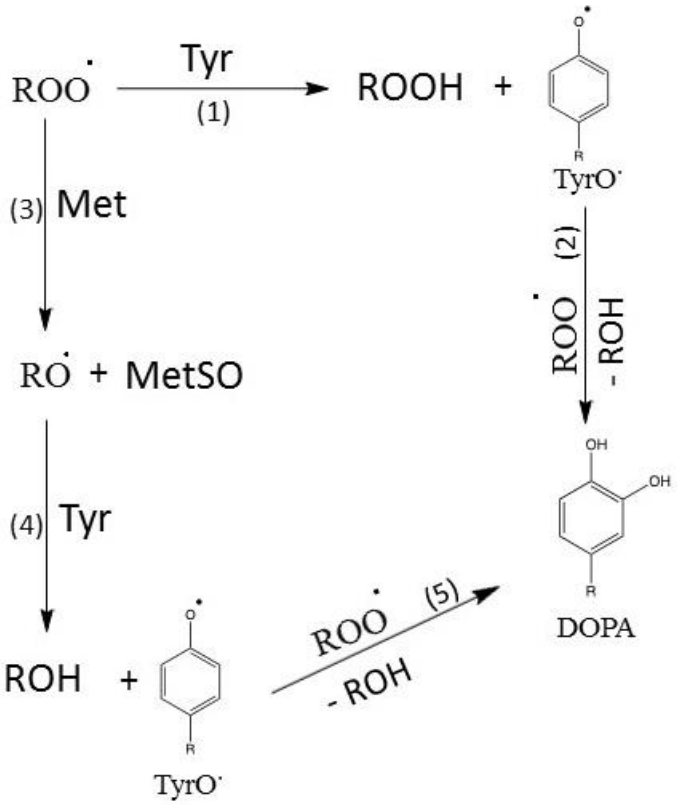

Scheme 3: Oxidation of Tyr and Met initiated by peroxyl radical.

Tables

Methionine	Tryptic peptide	m/z
Met-14	**LFDNAMLR**	**979.50**
Met-125	**DLEEGIQTLMGR**	**1361.67**
Met-170	**DMDKVETFLR**	**1253.61**

Table 1: List of methionine containing tryptic peptides obtained after digestion of hGH with trypsin/Lys-C.

hGH control	IgG1 control	Insulin control	BSA control	tagging reagents	hGH control	IgG1 control	Insulin control	BSA control	hGH control	IgG1 control	Insulin control
hGH + 1mM AAPH	IgG1 + 1mM AAPH	Insulin + 1mM AAPH	BSA + 1mM AAPH	tagging reagents	hGH 5µM Cu(II) + 500µM L-Asc	IgG1 5µM Cu(II) + 500µM L-Asc	Insulin 5µM Cu(II) + 500µM L-Asc	BSA 5µM Cu(II) + 500µM L-Asc	hGH 10µM Fe(II) + 500µM H_2O_2	IgG1 10µM Fe(II) + 500µM H_2O_2	Insulin 10µM Fe(II) + 500µM H_2O_2
hGH + 4mM AAPH	IgG1 + 4mM AAPH	Insulin + 4mM AAPH	BSA+ 4mM AAPH	-	hGH 10µMCu(II) + 500µM L-Asc	IgG1 10µMCu(II) + 500µM L-Asc	Insulin 10µM Cu(II) + 500µM L-Asc	BSA 10µM Cu(II) + 500µM L-Asc	hGH 20µM Fe(II) + 500µM H_2O_2	IgG1 20µM Fe(II) + 500µM H_2O_2	Insulin 20µM Fe(II) + 500µM H_2O_2
hGH + 8mM AAPH	IgG1 + 8mM AAPH	Insulin + 8mM AAPH	BSA+ 8mM AAPH	-	hGH 20µMCu(II) + 500µM L-Asc	IgG1 20µMCu(II) + 500µM L-Asc	Insulin 20µM Cu(II) + 500µM L-Asc	BSA 20µM Cu(II) + 500µM L-Asc	_	_	_
hGH control	IgG1 + control	Insulin + control	BSA control	-	hGH control	IgG1 control	Insulin control	BSA control	hGH control	IgG1 control	Insulin control
hGH + 1mM AAPH	IgG1 + 1mM AAPH	Insulin + 1mM AAPH	BSA + 1mM AAPH	-	hGH 5µM Cu(II) + 500µM L-Asc	IgG1 5µM Cu(II) + 500µM L-Asc	Insulin 5µM Cu(II) + 500µM L-Asc	BSA 5µM Cu(II) + 500µM L-Asc	hGH 10µM Fe(II) + 500µM H_2O_2	IgG1 10µM Fe(II) + 500µM H_2O_2	Insulin 10µM Fe(II) + 500µM H_2O_2
hGH + 4mM AAPH	IgG1 + 4mM AAPH	Insulin + 4mM AAPH	BSA + 4mM AAPH	-	hGH 10µM Cu(II) + 500µM L-Asc	IgG1 10µM Cu(II) + 500µM L-Asc	Insulin 10µM Cu(II) + 500µM L-Asc	BSA 10µM Cu(II) + 500µM L-Asc	hGH 20µM Fe(II) + 500µM H_2O_2	IgG1 20µM Fe(II) + 500µM H_2O_2	Insulin 20µM Fe(II) + 500µM H_2O_2
hGH + 8mM AAPH	IgG1 + 8mM AAPH	Insulin + 8mM AAPH	BSA + 8mM AAPH	-	hGH 20µM Cu(II) + 500µM L-Asc	IgG1 20µM Cu(II) + 500µM L-Asc	Insulin 20µM Cu(II) + 500µM L-Asc	BSA 20µM Cu(II) + 500µM L-Asc	_	_	_
1	2	3	4	5	6	7	8	9	10	11	

Table 2: 96-well plate loaded with IgG1, hGH, insulin and BSA oxidized under the indicated conditions and derivatized with ABS. The symbol "-" indicates empty wells.

Figures

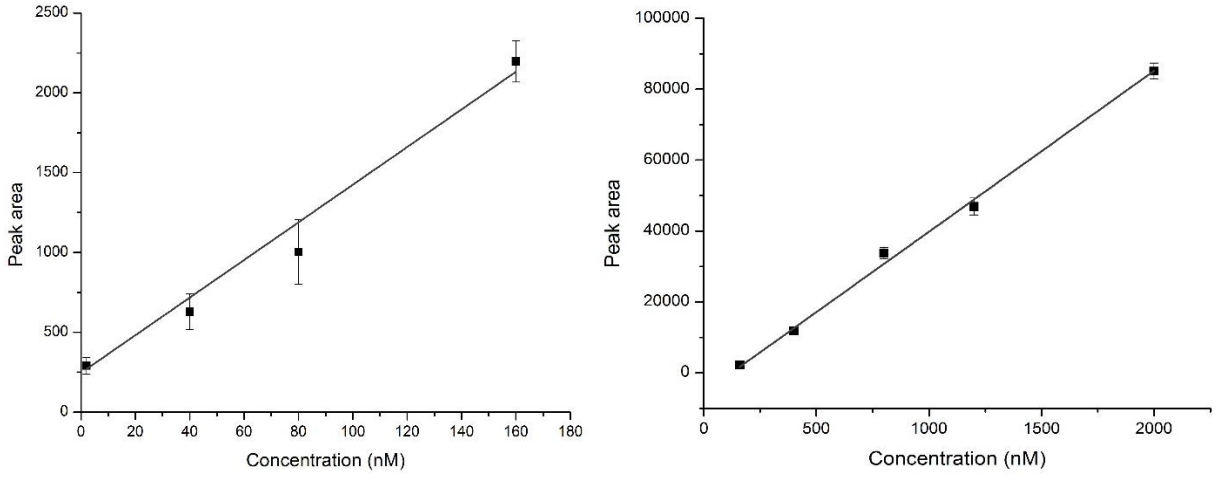

(a) **(b)**

Figure 1. Calibration curves obtained on Xevo-QTOF, using Glu-Fib standard peptide. (**a**) Glu-Fib concentration: 2 – 160 nM. (**b**) Glu-Fib concentration: 160-2000 nM.

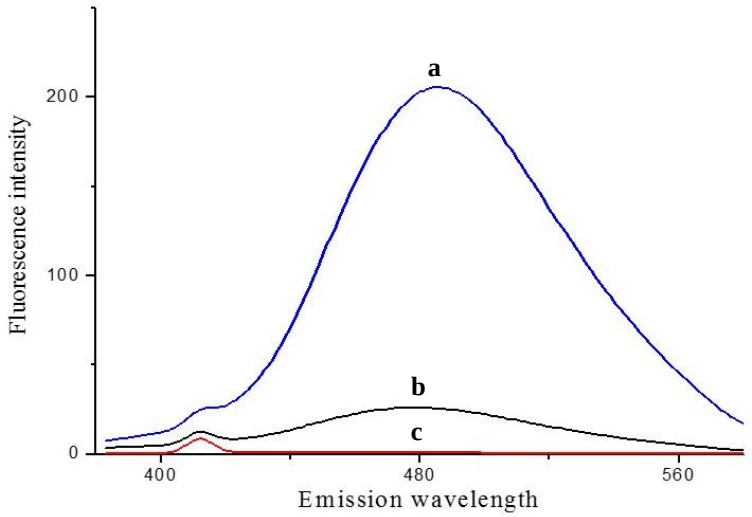

Figure 2. Steady state fluorescence monitored after ABS derivatization of **a**) hGH oxidized with 2mM AAPH at 37ºC for 3 hours (blue), **b**) non-oxidized hGH (black), **c**) the background fluorescence of the hGH oxidized with 2mM AAPH for 3 hours at 37ºC, prior to ABS derivatization (red).

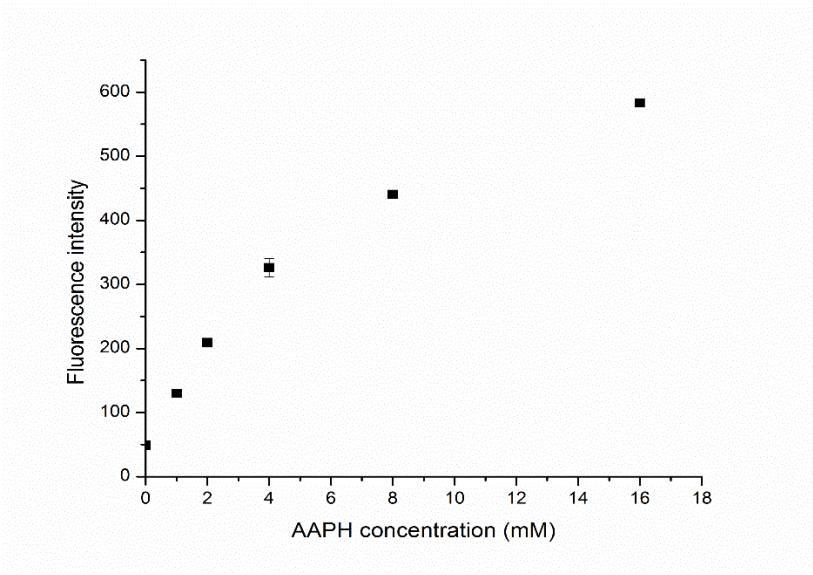

Figure 3. Fluorescence (λ_{em} max) after ABS derivatization of hGH (1mg/ml), oxidized in the presence of different initial concentrations of AAPH ranging from 0 (non-oxidized) to 16 mM, at 37ºC for 3 hours and monitored by steady-state fluorescence as shown in Fig. 2.

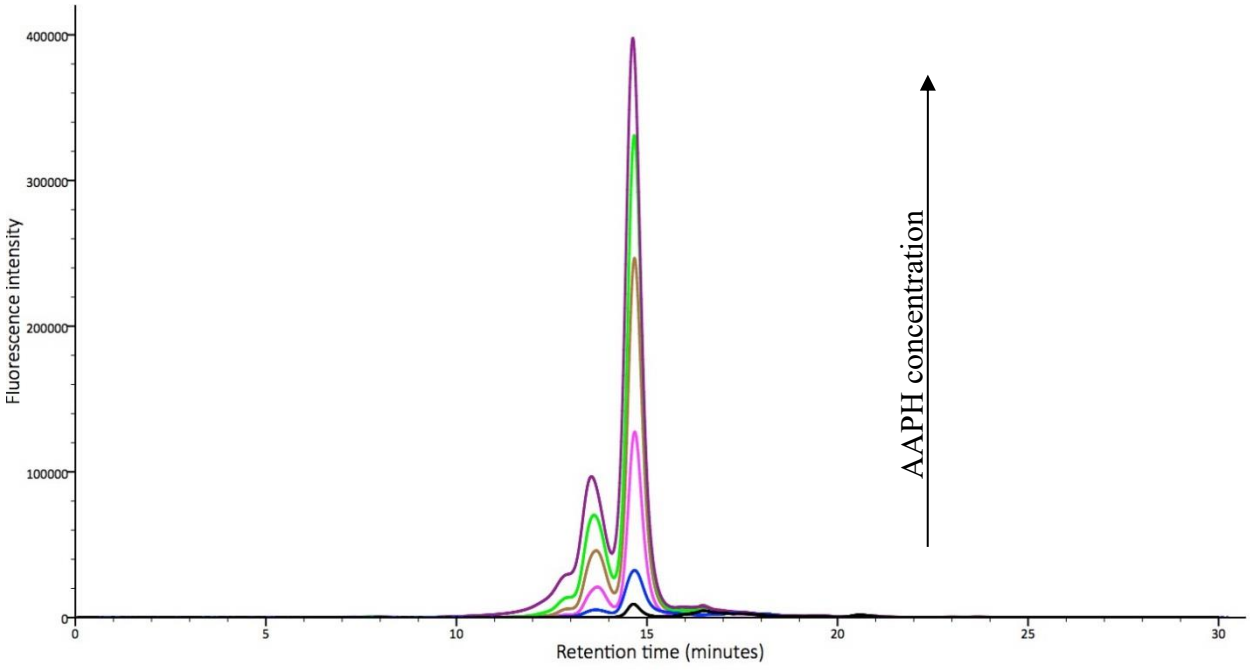

Figure 4. Size exclusion chromatography (SEC) of ABS tagged oxidized hGH (1mg/ml). Fluorescence detection (Ex **360nm**-Em **490nm**) of **a**) non-oxidized but ABS-derivatized (black), oxidized hGH obtained after incubation of hGH with **b**) 1 mM AAPH (dark blue), **c**) 2 mM AAPH (pink), **d**) 4 mM AAPH (brown), **e**) 8 mM (green) and with **f**) 16 mM AAPH (purple) for 3 hours at 37ºC.

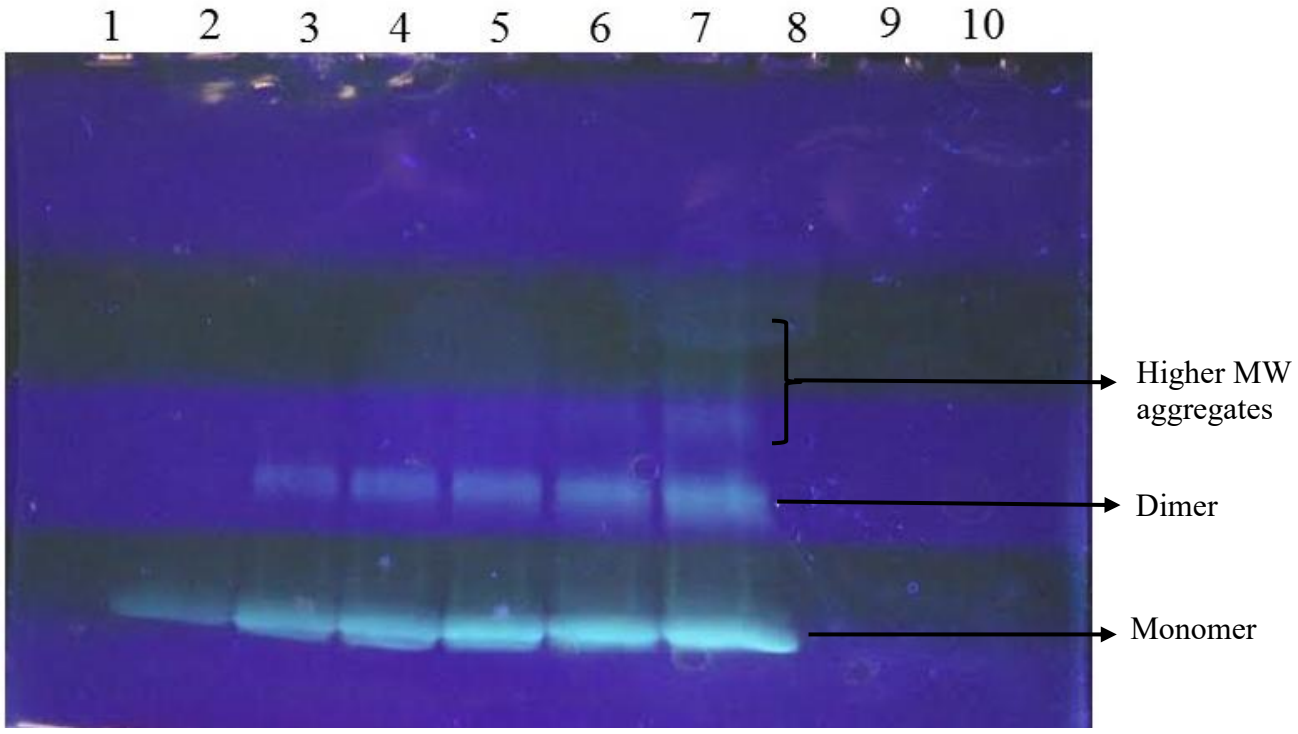

Figure 5. SDS-PAGE analysis (reducing conditions) and fluorescence visualization of oxidized hGH (1mg/ml) after ABS derivatization. Fluorescence was recorded by UV Transilluminator (Lane-1: molecular weight standards, Lane-2 hGH non-oxidized (control), Lane-3: hGH oxidized with 1mM AAPH, Lane-4: hGH oxidized with 2mM AAPH, Lane-5: hGH oxidized with 4mM AAPH, Lane-6: hGH oxidized with 8mM AAPH, Lane-7: hGH oxidized with 16mM AAPH, Lane-8: derivatization reagents, Lane-9 and 10: empty.

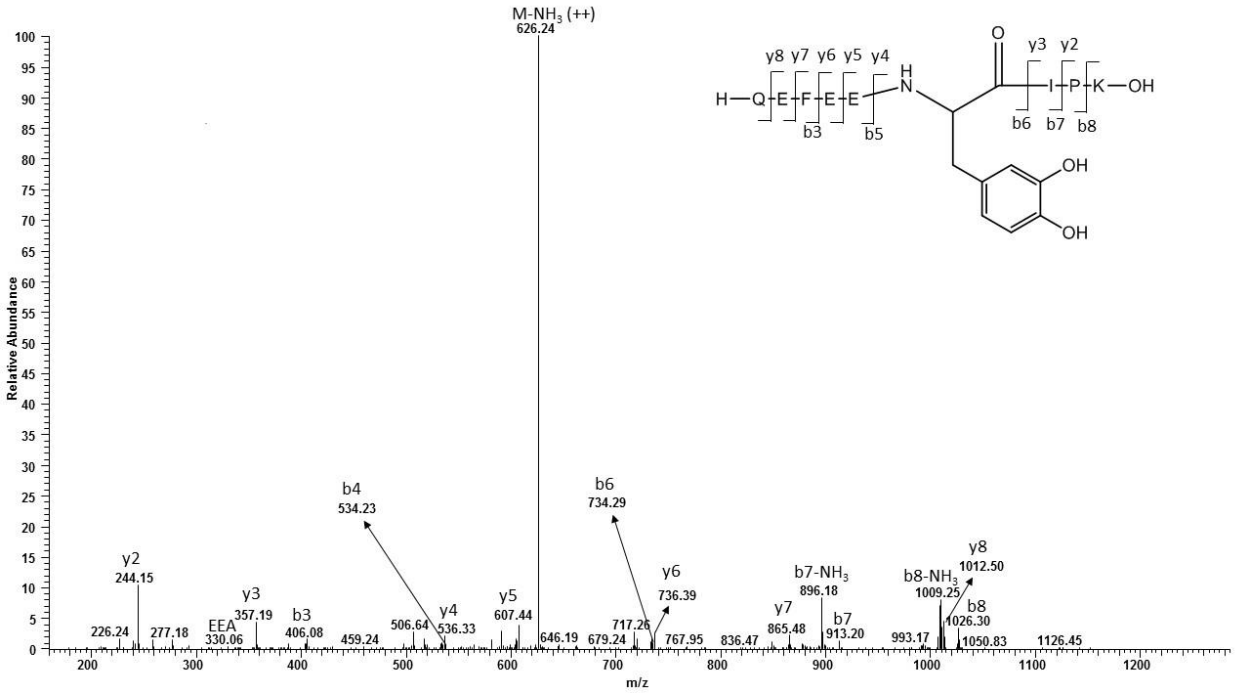

Figure 6. Collision-induced dissociation (CID) obtained on an FT-LTQ mass spectrometer of the oxidized tryptic peptide QEFEEY (+16 Da) IPK.

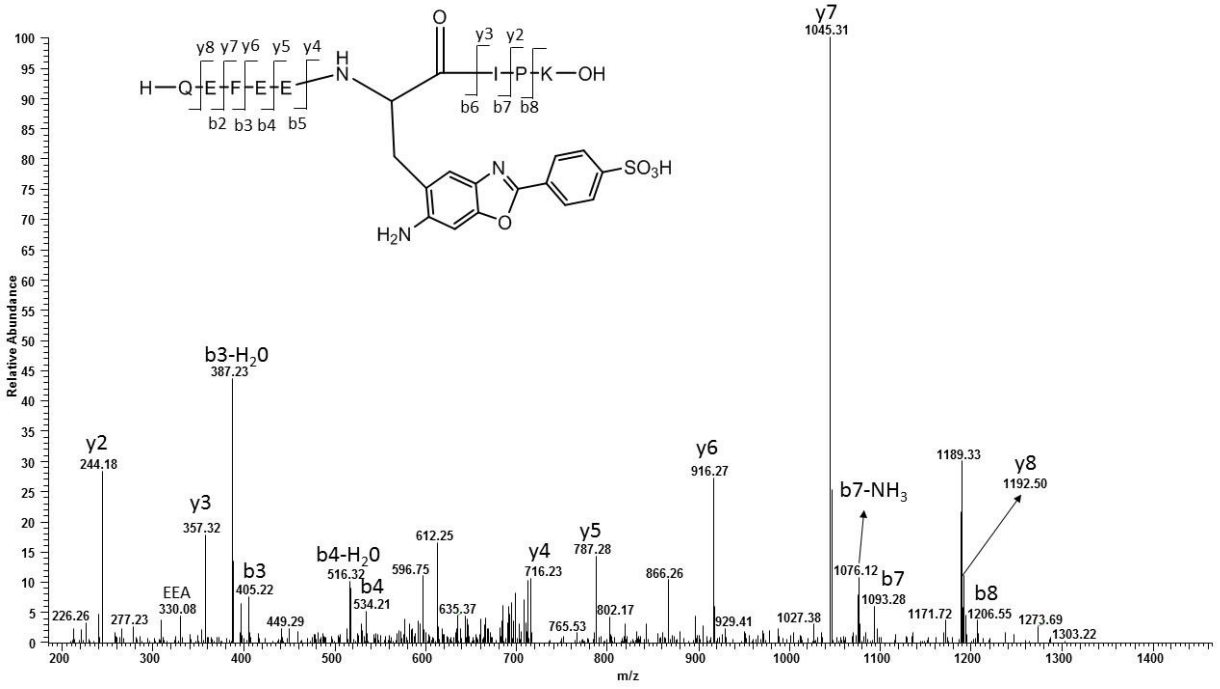

Figure 7. Collision-induced dissociation (CID) obtained on an FT-LTQ mass spectrometer of the tryptic peptide QEFEEY(+197 Da)IPK, generated through oxidation and ABS derivatization of hGH.

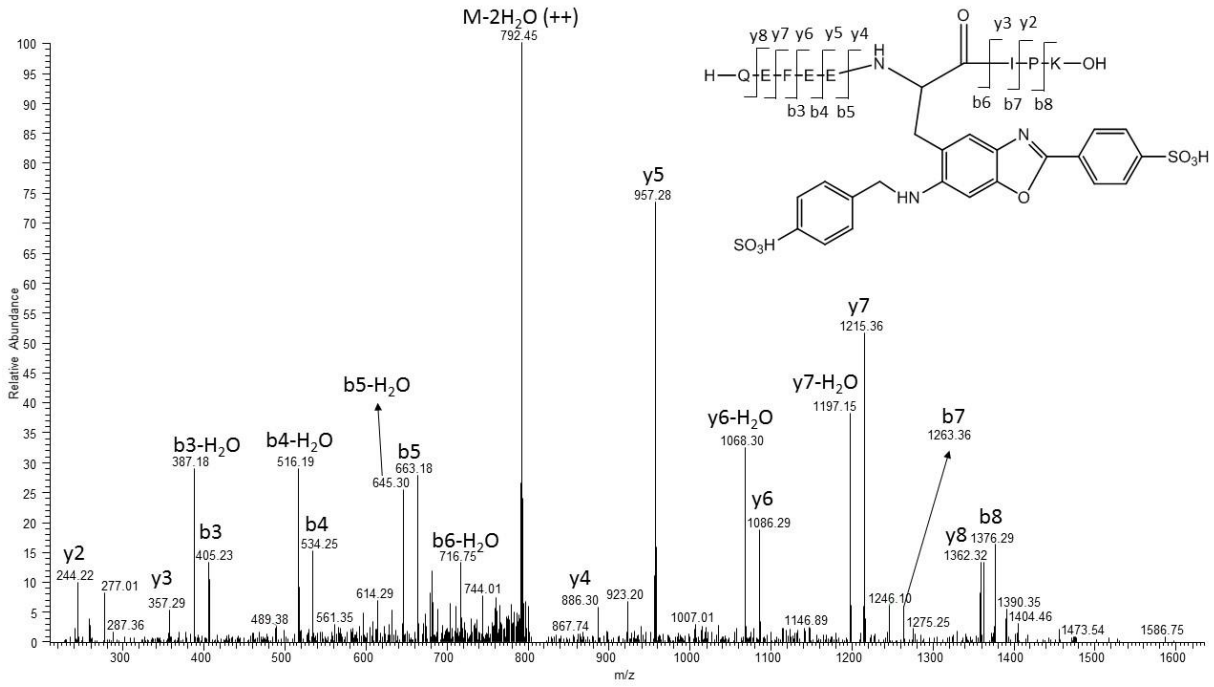

Figure 8. Collision-induced dissociation (CID) obtained on an FT-LTQ mass spectrometer of the tryptic peptide QEFEEY(+366 Da)IPK, generated through oxidation and ABS derivatization of hGH.

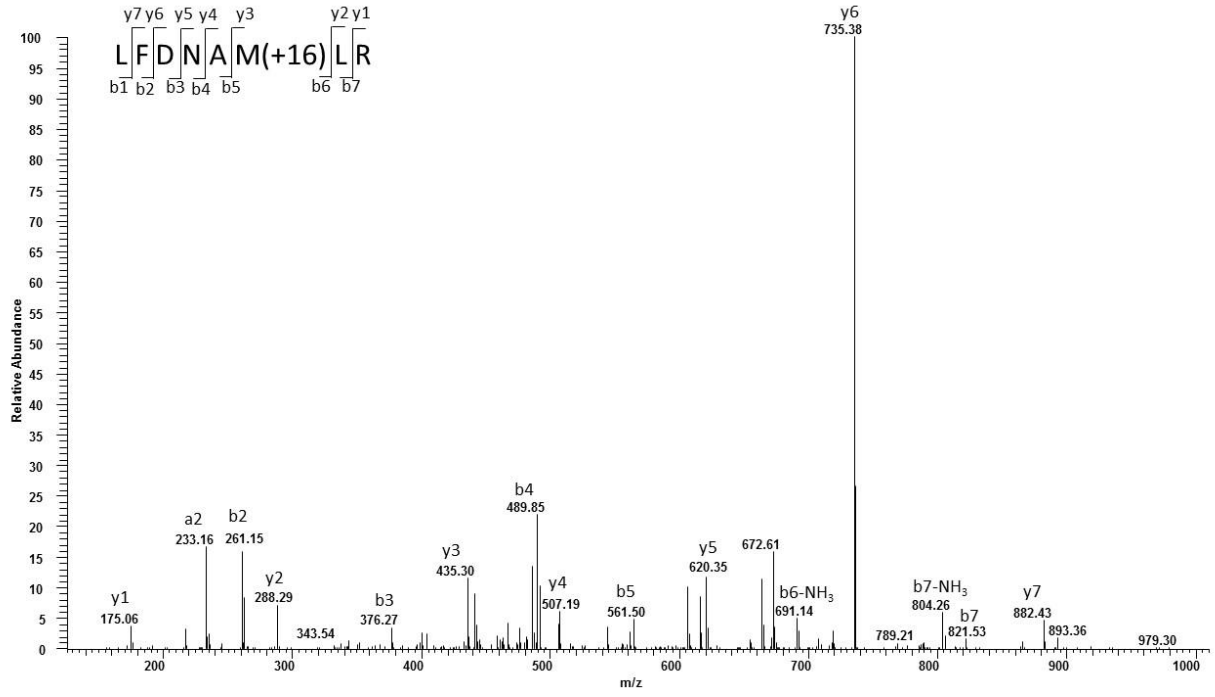

Figure 9. Collision-induced dissociation (CID) obtained on an FT-LTQ mass spectrometer of the oxidized tryptic peptide LFDNAM (+16 Da) LR. The peptide is the result of tryptic digestion of oxidized hGH.

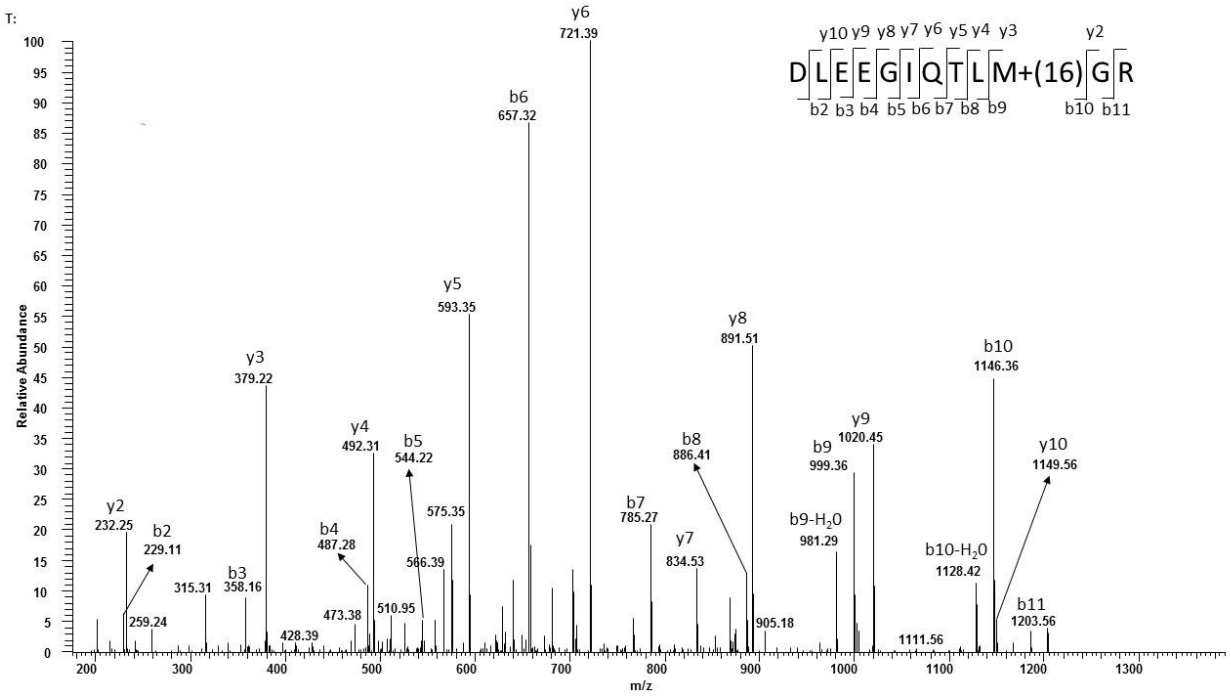

Figure 10. Collision-induced dissociation (CID) obtained on an FT-LTQ mass spectrometer of the oxidized tryptic peptide DLEEGIQTLM (+16 Da) GR. The peptide is the result of tryptic digestion of oxidized hGH.

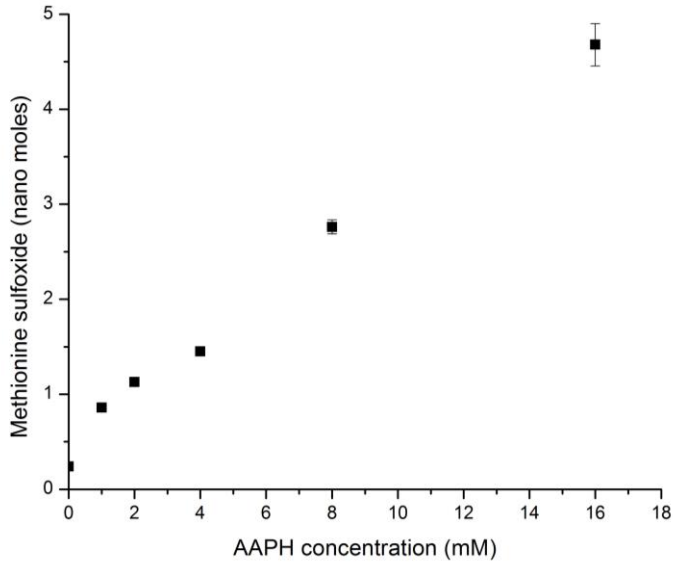

Figure 11. LC-MS analysis: Formation and quantification of MetSO during oxidation of hGH by serial concentration of AAPH ranging from 0 (non-oxidized) to 16mM on incubation for 3 hours at 37ºC. The data points represent the mean of four different experiments ± standard deviation.

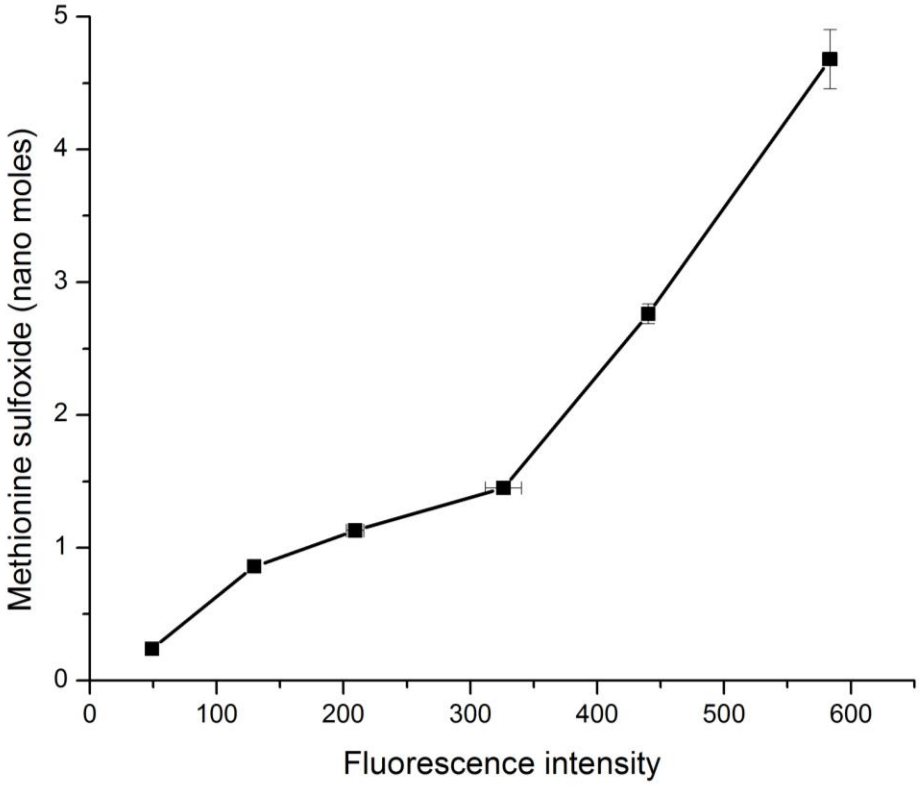

Figure 12. ABS fluorescence chart acquired after plotting fluorescence of ABS tagged DOPA against the amount of MetSO detected by LC-MS in hGH oxidized with increasing concentration of AAPH incubated at 37°C for 3 hours. Each data point represents the mean of four different experiments ± standard deviation.

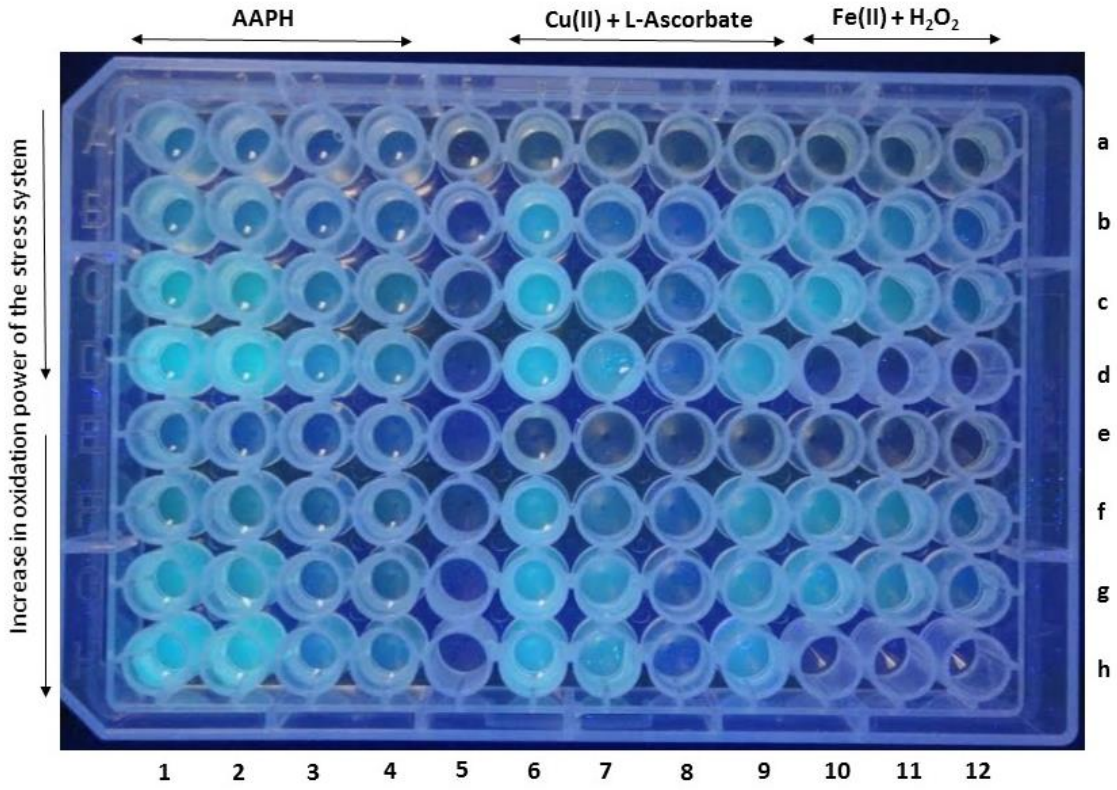

Figure 13. Fluorescence visualization on a UV-Transilluminator ($\lambda = 302nm$). IgG1, hGH, Insulin and BSA protein samples were oxidized with respective oxidative stressing systems and derivatized with ABS.**1a** hGH control, **1b-1d** hGH oxidized with 1, 4, 8 mM AAPH respectively, **2a** IgG1 control, **2b-2d** IgG1 oxidized with 1, 4, 8 mM AAPH respectively, **3a** Insulin control, **3b-3d** Insulin oxidized with 1, 4, 8 mM AAPH respectively, **4a** BSA control, **4b-4d** BSA oxidized with 1, 4, 8 mM AAPH respectively. **5a** tagging reagents, **5b** 100mM dibasic sodium phosphate buffer. **6a** hGH control, **6b-6d** hGH oxidized with 5, 10, 15 µM Cu (II) respectively and 500µM L-Ascorbic acid, **7a** IgG1 control, **7b-7d** IgG1 oxidized with 5, 10, 15 µM Cu (II) respectively and 500µM L-Ascorbic acid, **8a** Insulin control, **8b-8d** Insulin oxidized with 5, 10, 15 µM Cu (II) respectively and 500µM L-Ascorbic acid, **9a** BSA control, **9b-9d** BSA oxidized with 5, 10, 15 µM Cu (II) respectively and 500µM L-Ascorbic acid. **10a** hGH control, **10b-10c** hGH oxidized with 10, 20 µM Fe (II) + H_2O_2, **11a** IgG1 control, **11b-11c** IgG1 oxidized with 10, 20 µM Fe (II) + H_2O_2, **12a** Insulin control, **12b-12c** Insulin oxidized with 10, 20 µM Fe (II) + H_2O_2.

Supplementary figures

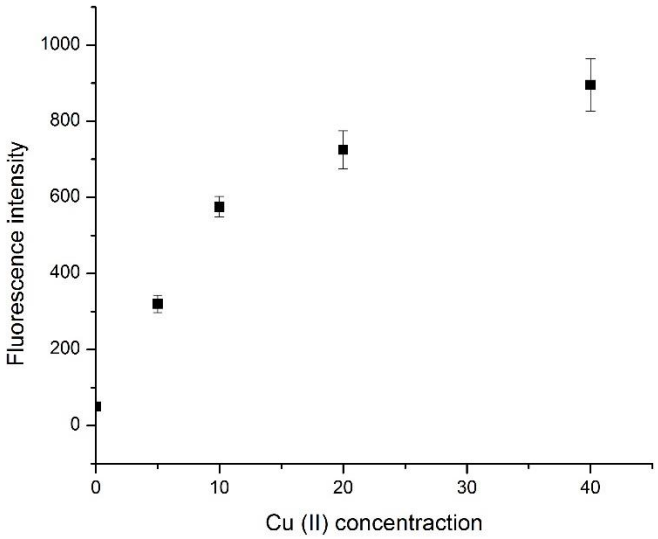

Fig. S1 Fluorescence after ABS derivatization of hGH (1mg/ml), oxidized in the presence of different initial concentrations of Cu (II) ranging from 0 (non-oxidized) to 40µM, at 37°C for 3 hours and monitored by steady-state fluorescence as shown in Fig. 2. Each data point represents the mean of four different experiments ± standard deviation.

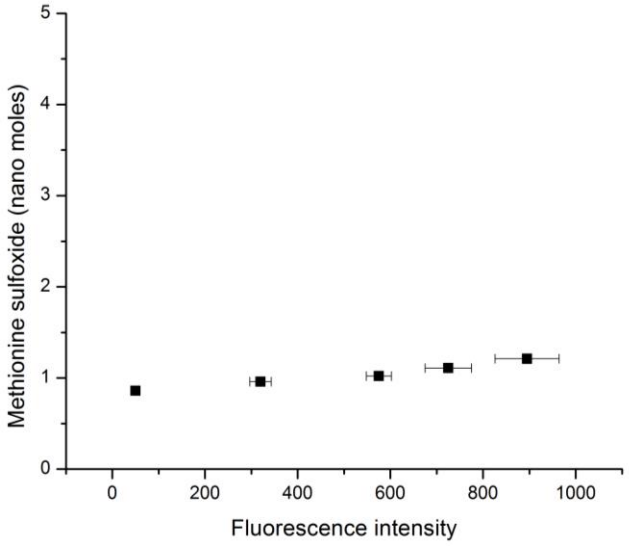

Fig. S2 LC-MS analysis: Formation and quantification of MetSO during oxidation of hGH by serial concentration of Cu (II) ranging from 0 (non-oxidized) to 40µM on incubation for 3 hours at 37°C. Each data point represents the mean of four different experiments ± standard deviation.

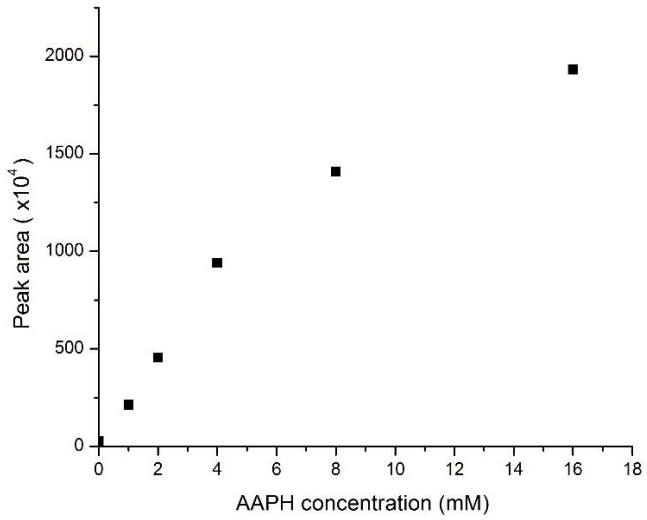

Fig. S3 Quantification of fluorescent peak area of hGH (1mg/ml), oxidized in the presence of different initial concentrations of AAPH ranging from 0 (non-oxidized) to 16 mM, at 37ºC for 3 hours and monitored by SEC analysis and fluorescence detection as shown in Fig. 4.

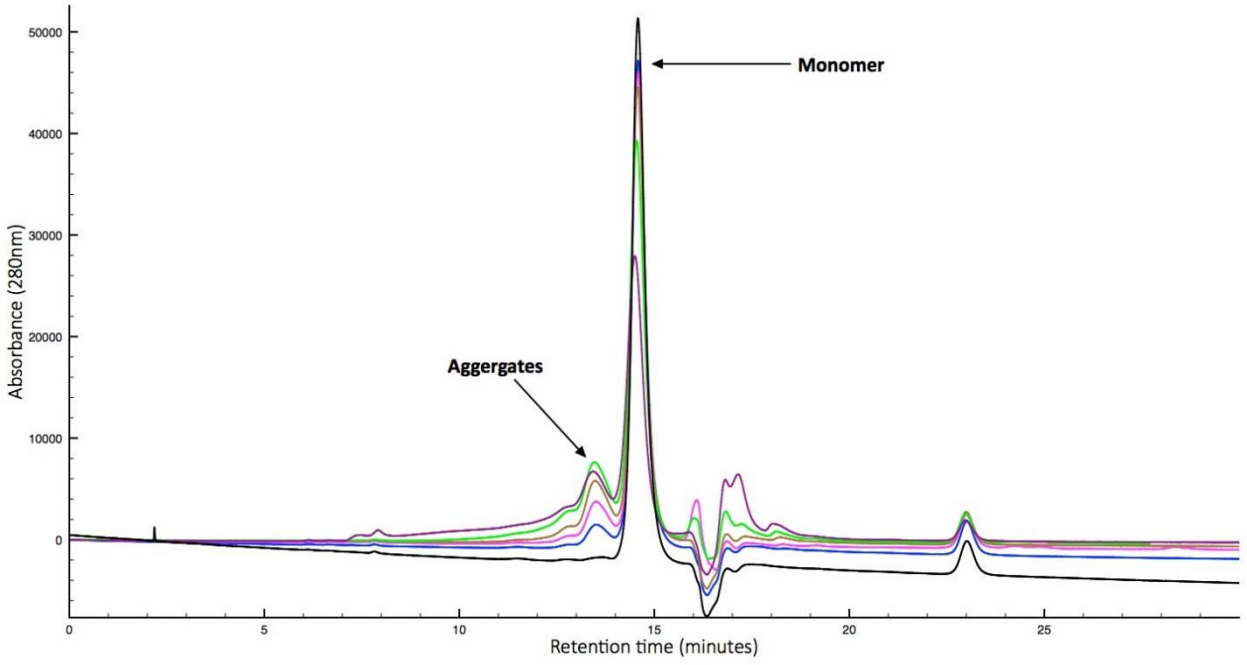

Fig. S4 SEC-UV chromatograms (λ = 280nm) to monitor hGH degradation on incubation with AAPH. **a**) non-oxidized but ABS-derivatized (black), oxidized hGH obtained after incubation of hGH with **b**) 1 mM AAPH (dark blue), **c**) 2 mM AAPH (pink), **d**) 4 mM AAPH (brown), **e**) 8 mM (green) and with **f**) 16 mM AAPH (purple) for 3 hours at 37ºC.

AAPH					Cu (II) + L-Ascorbate				Fe (II) + H_2O_2			
41.5	30.7	27.2	22.7	7.1	41.3	28.4	18.7	29.4	47.3	33.1	21.4	**a**
135.9	125.4	57.7	51.9	9.3	228.5	109.7	34.1	127.1	149.1	135.9	47.2	**b**
325.4	435.7	117.6	107.3	-	414.8	243.1	48.4	151.7	169.3	151.4	61.4	**c**
450.9	545.5	221.9	197.5	-	598.3	315.3	62.4	179.2	-	-	-	**d**
47.4	23.9	21.5	24.1	-	37.8	29.5	16.8	32.6	41.4	39.4	25.9	**e**
127.6	131.7	69.1	54.3	-	219.4	111.3	37.9	133.4	154.9	132.6	49.6	**f**
327.1	445.1	109.8	101.8	-	431.9	229.9	42.6	161.4	165.6	158.9	63.9	**g**
465.7	575.3	206.3	185.3	-	617.3	329.8	60.6	185.3	-	-	-	**h**
1	**2**	**3**	**4**	**5**	**6**	**7**	**8**	**9**	**10**	**11**	**12**	

Fig. S5 Fluorescence intensity readings of respective protein samples, measured using spectrofluorophotometer (measurements of well plate in Fig. 13) . IgG1, hGH, Insulin and BSA protein samples were oxidized with respective oxidative stressing systems and derivatized with ABS.**1a** hGH control, **1b-1d** hGH oxidized with 1, 4, 8 mM AAPH respectively, **2a** IgG1 control, **2b-2d** IgG1 oxidized with 1, 4, 8 mM AAPH respectively, **3a** Insulin control, **3b-3d** Insulin oxidized with 1, 4, 8 mM AAPH respectively, **4a** BSA control, **4b-4d** BSA oxidized with 1, 4, 8 mM AAPH respectively. **5a** tagging reagents, **5b** 100mM dibasic sodium phosphate buffer. **6a** hGH control, **6b-6d** hGH oxidized with 5, 10, 15 µM Cu (II) respectively and 500µM L-Ascorbic acid, **7a** IgG1 control, **7b-7d** IgG1 oxidized with 5, 10, 15 µM Cu (II) respectively and 500µM L-Ascorbic acid, **8a** Insulin control, **8b-8d** Insulin oxidized with 5, 10, 15 µM Cu (II) respectively and 500µM L-Ascorbic acid, **9a** BSA control, **9b-9d** BSA oxidized with 5, 10, 15 µM Cu (II) respectively and 500µM L-Ascorbic acid. **10a** hGH control, **10b-10c** hGH oxidized with 10, 20 µM Fe (II) + H_2O_2, **11a** IgG1 control, **11b-11c** IgG1 oxidized with 10, 20 µM Fe (II) + H_2O_2, **12a** Insulin control, **12b-12c** Insulin oxidized with 10, 20 µM Fe (II) + H_2O_2.

Chapter 3. Identification of D-amino acids in light-exposed mAb formulations

3.1 Introduction

In the last three decades, monoclonal antibodies (mAbs) have made a considerable metamorphosis from being scientific tools to one of the leading group of biotherapeutics.[1] Currently, there are approximately 30 mAbs that have been approved for clinical practice in the United States and Europe for various disease conditions, with global sales reaching approximately $86.7 billion in 2015.[2, 3]

All mAbs have an identical fundamental immunoglobulin (Ig) structure composed of two heavy (≅ 50 kDa) and two light (≅ 25 kDa) polypeptide chains, connected through disulfide bonds. Each heavy chain is comprised of one variable (V_H) and three constant (C_H1, C_H2 and C_H3) domains, whereas each light chain is composed of one variable (V_L) domain and one constant (C_L) domain. The Ig's are further classified into five isotypes, referred to as IgA, IgD, IgE, IgG, and IgM based on the structure of their constant domains. Presently, the therapeutically most widely used isotype is IgG.[3, 4] IgGs can be further classified into four subclasses based on the pattern of interchain disulfide bonds: IgG1, 2, 3 and 4. Among these four subclasses, IgG1, 2 and 4 are used as therapeutics, while IgG3 is rarely used because of its low serum half-life.[4]

MAbs are susceptible to various kinds of physical and chemical degradation. Aggregation, precipitation and surface adsorption are some of the major forms of physical instabilities, whereas deamidation, oxidation and fragmentation represent some of the major forms of chemical instabilities.[5] Both physical and chemical stability of mAbs can be influenced by various external factors such as pH, temperature, excipient impurities, light-exposure, etc.[5, 6] Protein therapeutics are subjected to light-exposure during various stages of their developmental process, such as production, purification, packaging, storage and administration to the patient.[7]

The peptide backbone, aromatic amino acids (Tyr, Trp and Phe), His and disulfide bonds are the primary targets of photodegradation in proteins.[7, 8] In recent years, the pharmaceutical industry has become more cognizant of the marked sensitivity of biotherapeutics to light exposure. As of now, light-exposure of biotherapeutics has been reported to cause aggregation, oxidation, fragmentation, covalent cross-linking, discoloration and color formation.[8-10] Therefore, intrinsic photostability testing of drug molecules has become an essential part of stress testing to demonstrate that light exposure does not result in unacceptable changes.[11]

IgG1 represents the most predominant subclass of IgG in human serum and has also been the preferred choice for the development of mAb therapeutics. One of the fundamental structural hallmarks of the IgG1 subclass is the arrangement of disulfide bonds. IgG1 contains a total of 16 disulfide bonds comprised of four interchain disulfide bonds in the hinge region and twelve intrachain disulfide bonds associated with twelve separate domains. These disulfide bonds play an important role in maintaining the tertiary and quaternary structure of the protein.[12] However, these disulfide bonds are prone to photodegradation via direct photolysis and or electron transfer from photo-irradiated Trp, generating cysteine thiyl radicals (CysS$^{\bullet}$). Thiyl radicals are known to react via reversible hydrogen transfer reactions with C-H bonds of adjacent amino acids.[13] These intramolecular hydrogen transfer reactions yield carbon-centered radicals, which eventually may result in the formation of protein hydroperoxides (in presence of oxygen),[14] aggregates (covalent cross-links)[8] or protein fragmentation.[15] These reversible hydrogen transfer reactions can be probed using covalent deuterium incorporation onto particular amino acids when protein photo-irradiation is performed in D_2O.[16-18] Previous studies have identified covalent deuterium incorporation due to reversible hydrogen transfer reaction between CysS$^{\bullet}$ and C-H (as shown in Scheme 1) in UV light-exposed peptides and proteins.[16-19] These hydrogen transfer reactions can

also result in the epimerization (L to D) of amino acids. Mozziconacci et al. have demonstrated the thiyl radical dependent conversion of L-Ala into D-Ala in disulfide linked model peptides [18] and the selective epimerization of L-Tyr into D-Tyr and L-Val into D-Val in a UV light-exposed mAb. [19]

Protein structure can influence the formation of carbon centered radicals in multiple ways. Primarily, the accessibility of C-H bond of an amino acid to the protein $CysS^{\bullet}$ generated during photolysis can be affected by protein structure and dynamics.[20] Secondarily, homolytic bond dissociation energies (BDE) of C-H bonds at the C-alpha carbon are influenced by the type of protein secondary structure, in which the amino acid is located, where $BDH_{\text{random coil}} < BDH_{\beta\text{-sheet}} < BDH_{\alpha\text{-helix}}$. [21] Moreover, excipients have been shown to change surface properties of proteins, leading to changes in secondary and tertiary structure.[22,23] Some of the widely used excipients can be categorized into the following groups, protein stabilizers (polyols, sugars, salts), surfactants (polysorbate 20 and polysorbate 80) and amino acids .[23] In this study, we aim to understand the effect of various formulation excipients such as arginine (L-Arg), methionine (L-Met), leucine (L-Leu), sucrose and glucose on the site specificity and extent of epimerization in UV light-exposed mAbs using covalent deuterium incorporation and amino acid analysis, respectively. We chose these formulations because the physical analysis of the secondary structure of an IgG1 has already been documented in such formulations. Previously, Thakkar et al.[24] have assessed the conformational stability of IgG1 mAb in presence of L-Arg and sucrose excipients; through this study L-Arg was found to be a destabilizer, whereas sucrose was found to be a stabilizer of mAb. In the same study, Thakkar et al.[24] have postulated that the potential reason for the destabilizing effect of L-Arg was the suppression of the intermolecular β-

structure-rich intermediate structure formation, which potentially stabilizes partially altered structures; in contrast, sucrose stabilizes the β-structure-rich intermediary structure. [24]

The formation of D-amino acids could impose local conformational changes in proteins, potentially leading to the formation of partially unfolded structures, which can serve as precursors for the formation of higher molecular weight structures. Therefore, we performed a quantitative analysis of D-amino acid formation in monomer and aggregates of a mAb exposed to light. For experimental purposes, we chose light of λ = 254 nm and λ > 295 nm (λ_{max} = 305 nm) as an investigative tool. These conditions are different from those recommended by the ICH1QB guidelines, but allowed for controlled and rapid experimental procedures using light of a limited wavelength region (instead of the broad wavelength region recommended by the ICH, i.e. 320-800 nm, which is less suitable for mechanistic studies). Light-induced mAb aggregates were separated from monomers using size exclusion chromatography (SEC), and the extent of epimerization was monitored using amino acid analysis.

3.2 Experimental methods

3.2.1 Materials

The mAb (50 mg/ml) was provided by Genentech, Inc. (San Francisco, CA). Monobasic sodium hydrogen phosphate (NaH_2PO_4), dibasic sodium hydrogen phosphate (Na_2HPO_4), monobasic potassium hydrogen phosphate (KH_2PO_4), dibasic potassium hydrogen phosphate (K_2HPO_4), guanidine hydrochloride, iodoacetamide (IAA), sodium acetate, ammonium bicarbonate, dithiothreitol (DTT), bis (2-mercaptoethyl) sulphone (BMS), brij surfactant, N-acetyl-L-cysteine (NAC), o-phthaldialdehyde (OPA), L-Arg, L-Met, L-Leu, glucose and trypsin (from porcine pancreas) were purchased form Sigma Aldrich (St. Louis, MO, USA). Deuterium oxide (99.9%

D) was purchased from Cambridge Isotope Laboratories Inc. Millipore Q water (milliQ water) was used for the preparation of all the solutions. Sucrose, methanol, trifluoroacetic acid (TFA), optimal water and acetonitrile (ACN), containing 0.1% (v/v) formic acid were purchased from Fisher Scientific (Waltham, MA). Amicon ultra-0.5 centrifugal filter devices equipped with a 10 kDa cut-off membrane were purchased from Millipore Inc (Bedford, MA, USA).

3.2.2 UV irradiation

3.2.2.1 Sample preparation

A stock solution of the mAb was dialyzed against 50 mM sodium phosphate buffer (pH 5.5) at 5 ^{o}C using 10 kDa molecular weight cut-off membranes (Slide-A-Lyzer, Thermo scientific, Rockford, IL) for 24 hours. Subsequently, the stock solution was concentrated to 150 mg/mL using Amicon ultra-0.5 centrifugal filters devices equipped with a 10 kDa cut-off membranes (Millipore, Billerica, MA). The concentrations of mAb stock solutions were measured by UV-spectroscopy at 280 nm, where Abs 0.1% (=1 g/L) = 1.523 cm^{-1}.[25]

3.2.2.2 Preparation of excipient solutions

Solutions which were prepared in D_2O will be referred as deuterated solutions, and the solutions prepared in H_2O will be referred as non-deuterated solutions. Deuterated or non-deuterated excipient solutions were prepared by dissolving L-Arg (10 mg/ml), L-Met (10 mg/ml), L-Leu (10 mg/ml), glucose (10 mg/ml), or sucrose (10 mg/ml. pD values are reported after correcting pH electrode measurements for the deuterium isotope effects (pD = pH + 0.4).[26] The pH and pD was adjusted with HCl and DCl stock solutions, respectively to reach a pH/pD of 5.5.

3.2.2.3 Preparation of mAb samples for UV irradiation

Aliquots of 100 µL of concentrated mAb (150 mg/mL) were diluted with 500 µL of either H_2O or D_2O containing individual excipients (each excipient at a concentration of 10 mg/mL, pH/pD of 5.5, and final protein concentration of 25 mg/mL). Each sample was split into two, of which 300 µL were UV irradiated and the other 300 µL were used as a control sample. The samples were purged with argon (Ar) for 90 mins prior to UV irradiation. The samples were UV irradiated for 60 min at $\lambda = 254$ in quartz tubes, or $\lambda_{max} = 305$ nm in pyrex tubes. For proof of concept, we exposed the mAb solutions to $\lambda = 254$ nm light as these experimental conditions would allow us to rapidly optimize the detection of D-amino acids. The UV light with $\lambda_{max} = 305$ nm corresponds to a spectral distribution of approximately 90% of photons in 280 nm – 320 nm wavelength range. Importantly, protein Trp residues show absorption bands which can extend to about 320 nm,[7,27] such that these conditions would allow us to examine specifically the D-amino acid formation induced by Trp photo-ionization. All photo-irradiation experiments were performed in a UV-irradiator (Rayonet, The Southern New England Ultraviolet Company, Branford, CN) equipped with four UV-lamps (RMR-305 or RMR-254).

3.2.3 Reduction, alkylation and digestion

All the samples prepared in either D_2O or H_2O were exchanged into ammonium bicarbonate buffer (NH_4HCO_3, 50 mM, pH 8) using Amicon ultra-0.5 centrifugal filter devices equipped with a 10 kDa cut-off membrane (Millipore, Billerica, MA). After the buffer exchange, for each sample a volume of approximately 75 µL was recovered and diluted with 425 µL of NH_4HCO_3 buffer and exchanged a second time using an Amicon ultra-0.5 centrifugal filter, as described above. After the second exchange, the samples were reconstituted in a final volume of 300 µL of

NH_4HCO_3 buffer. An aliquot of 30 µL of buffer exchanged mAb samples (25 mg/ml) were placed in 270 µL of guanidine hydrochloride (6 M, pH 8 in 50 mM NH_4HCO_3 buffer) and incubated at 60 ^oC in the presence of 5 mM bis-(2-mercaptoethyl) sulfone (BMS) for 30 mins for the reduction of disulfide bonds. The reduced cysteines were alkylated at 45 ^oC with 20 mM iodoacetamide (IAA). After one hour of incubation the samples were mixed with 300 µL (1:1 v/v) of 1M perchloric acid and centrifuged at 14,000 g for 20 mins at 4 ^oC. The supernatant was discarded and the resulting pellet was washed with 50 mM NH_4HCO_3 buffer for three times by slowly adding the buffer without disturbing the pellet. After three washes, the pellet was reconstituted in 500 µL of 50 mM NH_4HCO_3 buffer (pH 8.0) and sonicated for few seconds and 25 µg of trypsin (from procaine pancreas) was added. The samples were incubated at 37 ^oC for 2 hours. After 2 hours, another 25 µg of trypsin (from porcine pancreas) were added and the incubation was continued overnight at 37 ^oC. The digestion was stopped by the addition of 10 µL of formic acid and the samples were purified through Amicon ultra-0.5 centrifugal filter devices equipped with a 10 kDa cut-off membrane to discard undigested protein and trypsin.

3.2.4 Size exclusion chromatography (SEC)

Buffer exchanged mAb samples (both control and irradiated) at 25 mg/mL were diluted to 1 mg/mL using 200 mM sodium perchlorate buffer and 50 mM sodium chloride (pH 6.0). SEC was performed on a Shimazdu HPLC system equipped with two Shimazdu LC-20AT pumps (Shimazdu, Columbia, MD), coupled to a Prominence RF-20A photo-diode array detector (Shimazdu, Columbia, MD). The samples (90 µL) were injected onto a TSK-GEL SuperSW3000 column (4.6 mm ID x 30 cm, Tosoh Biosciences, King of Prussia, PA, USA). The mobile phase consisted of 200 mM sodium perchlorate buffer and 50 mM sodium chloride at pH 6.0, and was eluted through the column at a constant flow rate of 0.25 mL/min. Aliquots of 90 µg of mAb

were injected for each analytical characterization. Monomer and aggregate fractions were collected, using the fraction collector (FRC-10A, Shimazdu, Columbia, MD) connected to the system, by making several injections. The collected fractions were pooled and concentrated using Amicon Ultra-15 centrifugal devices with 10 kDa cut-off membrane (Millipore, Billerica, MA).

3.2.5 UPLC-MS analysis: Identification of the peptides showing covalent deuterium incorporation

LC-MS analysis was performed on a Xevo Q-TOF mass spectrometer (Waters Corp., Milford, MA), equipped with a nanoAcquity (Waters Corp, Milford, MA) set of pumps delivering a mixture of mobile phase A consisting of optimal water and formic acid 99.9%: 0.1%, (v:v), and mobile phase B, consisting of ACN and formic acid 99.9%: 0.1%, (v:v) at a flow rate of 0.3 µl/min. A volume of 0.5 µL of the mAb digest was injected onto reverse-phase CSH nanocolumn (75 µm x 150 mm C18, Waters Corp.). Peptides were eluted with linear gradient ranging from 3-35% of mobile phase B within 60 mins.

3.2.6 HPLC UV-Vis analysis: Purification of the peptides showing covalent deuterium incorporation

A volume of 100 µL of the digests were injected onto a reverse-phase C18 column (Vydac 218TP, 250 x 4.6 mm, 5 µm) that was connected to a set of pumps (LC-20AT, Shimazdu, Columbia, MD), delivering a mixture of mobile phase A (100% H_2O, 0.1% TFA) and B (100% ACN, 0.1% TFA) at a flow rate of 0.5 mL/min. The C18 column was placed in a column heater and maintained at 25 ^oC. The mixture of mobile phases A and B was delivered according to the

following gradient program: between 0 and 2 mins the mixture of solvents contained 97% of mobile phase A and 3% of mobile phase B. After 2 mins, the mobile phase B was linearly increased to 28% within 128 mins. The chromatograms were monitored with a diode array detector (SPD-M20A, Shimazdu, Columbia, MD). Proteolytic peptides were collected using a fraction collector (FRC-10A, Shimazdu, Columbia, MD), followed by concentrating the fractions to a volume of 100 μL using a CentriVap concentrator (Labconco, Kansas City, MO).

3.2.7 Amino acid analysis

Amino acid analysis consisted of two steps, complete hydrolysis of the substrate (protein or peptide) using optimized conditions, which would avoid/ minimize amino acid epimerization during hydrolysis, followed by chromatographic analysis and quantification of L- and D-amino acids.

3.2.7.1 Acid hydrolysis of mAb

The protein concentration of all the fractions (monomer and aggregates) was adjusted to 5 mg/mL. A custom made glass microplate was used to perform the acid hydrolysis reaction of the collected fractions. The glass microplate and 6 N HCl (Pierce, Thermo Scientific, Rockford, IL) were placed in a glove bag, which was saturated with nitrogen. A volume of 200 μL of 6 N HCl (nitrogen saturated) was added to each well. The glass microplate was sealed prior to be removed from the glove bag. The sealed glass microplate was transferred to an oven (Precision, Winchester, VA) and incubated at 130 ^{o}C for 45 mins. The hydrolyzed samples were vacuum dried and reconstituted in 200 μL aqueous sodium acetate solution (25 mM, pH 6.5) in the glass microplate.

3.2.7.2 HPLC analysis of L- and D-amino acids

Volumes of 50 μL of hydrolyzed protein solutions prepared in 25 mM aqueous sodium acetate (pH 6.5) were transferred to a polystyrene 96 well microplate and placed in an auto-sampler (Shimadzu, Columbia, MD). Three different stock solutions were prepared in order to derivatize the amino acids with OPA and NAC. Solution S1 consisted of 9,967 μL of K_2HPO_4 (190 mM, pH 9.5) buffer, and 33 μL of Brij-35 solution (35% w:v). Solution S2 consisted of 5.5 mg of OPA, and 12 mg of NAC in 265 μL of methanol and 4,735 μL of K_2HPO_4 (190mM, pH 9.5) buffer. Solution S3 consisted of sodium phosphate buffer, NaH_2PO_4 (200 mM, pH 4.5). Solutions S1, S2 and S3 were always placed in the auto-sampler at 5 ^oC. The solutions were mixed together using the auto-sampler to ensure the reproducibility of the derivatization reaction. The solutions were mixed as follows: 50 μL of each S1, S2 and hydrolyzed protein solution were mixed together. During the next one minute, the solution was mixed by soaking and dispensing 100 μL of the solution using the syringe in the auto-sampler. After mixing, the solution was left for one more minute at 5 ^oC in the dark. Then, 150 μL of S3 were added to the solution. Again, the final solution was mixed for one minute by soaking and dispensing of 100 μL of the solution using the syringe in the auto-sampler. Then, 50 μL of the final solution was injected onto a reverse-phase capillary C18 column (Supelcosil LC-18-T, 150 x 4.6 mm, 5 μm), which was attached to a set of pumps (Shimadzu, Columbia, MD), delivering a mixture of solvents A (25 mM sodium acetate, pH 6.5 and 5 μM sodium azide) and B (100% methanol) at a flow rate of 0.5 mL/min. The C18 column was always maintained at 35 ^oC. The mixture of solvents A and B was delivered according to the following gradient program: between 0-15 mins the mixture of solvents consisted of 100% solvent A. After 15 mins, solvent B was increased to 35% within 125

mins. Subsequently, the column was washed for 5 mins with 50% solvent B, and re-equilibrated for 40 mins with 100% solvent A prior to the next injection. The chromatograms were recorded with a fluorescence detector (RF-20A, Shimadzu, Columbia, MD).

3.2.8 Incubation with D-amino acid oxidase

The flavoprotein D-amino acid oxidase (DAAO) is a widely used tool for *in vitro* enzymatic assays for the detection of D-amino acids.[29,30] DAAO oxidizes D-amino acids with a strict enantioselectivity to produce the corresponding α-keto acids and ammonia.[31] This property of DAAO was used to confirm the presence of D-amino acids in our protein hydrolysates.

An enzyme stock solution was prepared by addition of 0.2 mg of DAAO from porcine kidney (EC number: 1.4.3.3, Sigma, St. Louis, MO) and 0.5 mg of catalase from bovine liver (EC number: 1.11.1.6, Sigma, St. Louis, MO) to 1 mL of Tris buffer (200mM, pH 8.3). The final reaction mixture was prepared by addition of 75 µL of enzyme stock solution to 25 µL of protein hydrolysate, and incubated at 37 ^{o}C for 1 hour. After the incubation, the protein hydrolysate were purified using Amicon Ultra-15 centrifugal devices with 10 kDa cut-off membrane (Millipore, Billerica, MA) to remove DAAO and catalase from the reaction mixture.

3.3 Results

3.3.1 Enrichment of monomer and aggregates using SEC

The formation of D-amino acids could impose local conformational changes in proteins, potentially leading to the formation of partially unfolded structures, which can serve as precursors for the formation of higher molecular weight structures. Therefore, we performed a

quantitative analysis of D-amino acid formation in monomers and aggregates of a mAb exposed to UV light.

MAb samples in various formulations (pH 5.5) were exposed to UV light for 60 mins. Analytical SEC was used to estimate the content of aggregates, monomers and fragments in both control and UV irradiated mAb formulations (Fig. 1, 2, Fig. S1 and S2). The chromatograms showed several important differences in UV irradiated samples when compared to their respective control samples. The loss of monomer peak (at retention time, t_R = 12 min) in UV light-exposed samples was accompanied by an increase in earlier eluting peaks (aggregates), eluting with t_R ca. 9 and 10 mins (Fig.1a). The monomer peak also widened upon light exposure. In addition, we observed formation of a peak eluting with t_R = 14.5 mins (likely fragments). While the control samples predominantly contained monomer, and low levels of aggregates (3.7%, ± 0.47), the mAb samples exposed to UV light (λ = 254 nm) in presence of either L-Arg, L-Met, glucose, L-Leu, or sucrose contained 43.6 % (± 4.15), 31.3 % (± 4.99), 35.5 % (± 5.18), 31.6% (± 4.89), and 41.3% (± 6.9) of aggregates, respectively (Fig. S3a). For all conditions examined, when compared to mAb samples exposed to UV light at λ = 254 nm, mAb samples exposed to UV light at λ_{max} = 305 nm contained relatively less amount of aggregates and fragment species (Fig. S3).

SEC connected to a fraction collector was used to isolate both monomer and aggregate fractions. Approximately 3 injections for each original mAb sample were made for the isolation of monomer and aggregate species, followed by pooling and concentration of the samples to obtain sufficient protein quantities for future experiments. All the fractions were stored at 4 ^{o}C until further analysis.

3.3.2 Amino acid analysis of monomers and aggregates

Monomer and aggregates of interest were subjected to acid hydrolysis, followed by derivatization with NAC and OPA. The derivatized L- and D-amino acids were separated by reverse-phase liquid chromatography coupled to a fluorescence detector (Fig. S4).

3.3.2.1 Amino acid analysis of monomer and aggregates resultant of UV irradiation at λ_{max} = 305 nm

Amino acid analysis of control (not UV-irradiated) mAb hydrolysate lead to the identification of the following amino acids: (i) L-Asp, (ii) L-Glu, (iii) L-Ser, (iv) L-Thr, (v) L-Arg, (vi) L-Ala, (vii) L-Lys, (viii) L-Tyr, (ix) L-Met, (x) L-Val, (xi) L-Phe, (xii) L-Ile, and (xiii) L-Leu. Under typical acid hydrolysis conditions Asn and Gln are completely hydrolyzed to Asp and Glu, respectively. Trp was completely degraded and Cys cannot be directly determined from the acid-hydrolyzed samples. Ser and Thr are partially hydrolyzed and usually loss of about 10 and 5 %, respectively. Ser and Thr residues can undergo β-elimination during hydrolysis.[28]

For example, comparison of amino acid analyses of aggregates (Fig. 3, brown trace) resultant of UV light exposure (λ_{max} = 305 nm) of mAb in L-Arg formulation and control mAb monomer (Fig. 3, green trace) in L-Arg formulation revealed presence of D-Glu (Fig. 3a), D-Ala (Fig. 3b) and D-Val (Fig. 3c) in aggregates resultant of UV light exposure. The absence of D-amino acids in control mAb monomer suggest that D-Glu, D-Ala, and D-Val are generated during UV irradiation (λ_{max} = 305 nm) of mAb in L-Arg formulation. Amino acid analyses of monomers and aggregates, resultant of light-exposure of mAb at λ_{max} = 305 nm in different formulation (L-Arg, L-Met, L-Leu, glucose and sucrose) also revealed formation of D-Val, D-Glu and low levels D-Asp in all the samples.

Absence of D-Glu, D-Ala and D-Val in all control mAb samples also suggests that our experimental conditions (hydrolysis for 45 minutes) were sufficiently mild to limit D-amino acid formation during hydrolysis. On contrary, D-Asp was identified in both control and light-exposed mAb samples, suggesting that D-Asp is either present in starting material or generated during hydrolysis or sample preparation.

3.3.2.2 Amino acid analysis of monomer and aggregates resultant of UV irradiation at λ = 254 nm

Amino acid analyses of monomers and aggregates, resultant of light-exposure of mAb at λ = 254 nm in different formulation (L-Arg, L-Met, L-Leu, glucose and sucrose) reveals formation of D-Val, D-Glu and low levels D-Asp in all the samples (Fig. S5). The absence of D-amino acids in control mAb monomer suggest that D-Glu and D-Val are generated during UV irradiation (λ = 254 nm) of mAb in various formulations.

3.3.3 Quantification of D-amino acids in monomers and aggregates

After amino acid analysis, the extent of epimerization in monomers and aggregates was determined by dividing the peak areas of the respective peaks of D-amino acids by the sum of peak areas for both the respective D- and L-amino acids, as shown in the formula below:

$$\%\, D-amino\ acid = \frac{Peak\ area\ of\ D-amino\ acid\ peak}{Peak\ area\ of\ D-amino\ acid\ peak + Peak\ area\ of\ L-amino\ acid\ peak} \quad \text{X } 100$$

Quantitative analysis for monomers (Fig. 4a) and aggregates (Fig. 4b), resultant of light-exposure of mAb at λ_{max} = 305 nm in different formulation reveals formation of D-Val, D-Glu

and low levels D-Asp (around 0.3%) in all the samples, whereas D-Ala was only identified in aggregates formed resultant of UV irradiation (λ_{max} = 305 nm) of mAb in L-Arg formulation. For example, amino acid analysis of aggregates resultant of light-exposure in the L-Arg-containing formulation revealed 13.03 % (± 0.52) of D-Val, 6.69 % (± 0.8) of D-Glu, and 0.21% (± 0.03) of D-Ala.

Quantitative analysis for monomers (Fig. 5a) and aggregates (Fig. 5b), resultant of light-exposure of mAb at λ = 254 nm in different formulation reveals formation of D-Val and D-Glu, while low levels D-Asp (around 0.3%) were present in all the samples. For example, amino acid analysis of aggregates resultant of light-exposure in L-Arg formulation revealed 4.47 % (± 0.42) of D-Val, and 2.79 % (± 0.18) of D-Glu.

3.3.4 Identification of D-amino acid containing peptide sequences in UV irradiated mAb

Our strategy to identify D-amino acid-containing sequences in light-exposed mAb is based on covalent deuterium incorporation during photo-irradiation of the protein in D_2O.[19] Peptides incorporating deuterium can be detected by HPLC-MS/MS analysis, their retention time recorded, and then peptides eluting with these retention parameters can be fractionated after photo-irradiation in H_2O. Peptides of interest were fractionated, collected, and subjected to acid hydrolysis, followed by derivatization with NAC and OPA for amino acid analysis.

3.3.4.1 Covalent incorporation of deuterium during UV irradiation of mAb in D_2O

The HPLC-MS analysis of the proteolytic peptides obtained after light-exposure (λ_{max} = 305 nm) of mAb formulations in D_2O and H_2O unveiled five ions with m/z 756.37, 635.30, 356.8, 1030.5, and 1193.58, which covalently incorporated deuterium after light-exposure in D_2O (Fig. 6, 7 and

8). MS/MS analysis permitted identification of the sequences of the respective peptide ions with covalent incorporation of deuterium (Table 1). The ions with m/z 1030.5, 1193.51 and 356.8 corresponds to heavy chain sequence H51-H59, H51-H60 and H287-H296, respectively. After light-exposure of mAb at λ_{max} = 305 nm, only the peptide segments H51-59 and H287-H296 that showed covalent incorporation of deuterium were fractionated for amino acid analysis.

3.3.4.2 Fractionation and amino acid analysis of proteolytic peptides H51-H59 and H287-H296

The proteolytic peptides obtained after UV irradiation at λ_{max} = 305 nm of mAb in the L-Arg-containing formulation were fractionated by HPLC and monitored by UV-detection. The collected fractions were reanalyzed by LC-MS analysis to ensure the purity of each fraction (Fig. 9). The HPLC-MS analysis of fraction 23 revealed peptide segment H287-H296 co-eluting with another peptide ion with a mass of m/z 521.3. The peptide ion with m/z 521.3 could not be identified by MS/MS analysis, due to poor fragmentation. The amino acid analysis of fraction 23 (H287-H296 and peptide segment with m/z 521.3) revealed presence of D-Val along with other L-amino acids.

The HPLC-MS analysis of fraction 18 revealed H51-H59 and H319-H324 (proteolytic peptide with no covalent incorporation of deuterium) co-eluting with each other. The amino acid analysis of peptide segments in fraction 18 (H51-H59 and H319-H324) revealed the presence of D-Ala along with other L-amino acids.

3.3.5 Incubation with DAAO

Amino acid analysis enabled identification of D-Val, D-Ala and D-Glu in monomers and aggregates of light-exposed mAb. To confirm the presence of D-amino acids in light-exposed

mAb samples, we utilized the ability of DAAO to selectively oxidize D-amino acids to the corresponding α-keto acids.[29-31] A comparison of the amino acid analyses of the mAb hydrolysates prior and subsequent to DAAO treatment revealed the complete disappearance of D-Val (Fig. S6), D-Ala (Fig. S7), and D-Glu, consistent with the assignment of these peaks to the respective D-amino acids.

In addition, comparison of the amino acid analyses of the fraction 23 hydrolysate prior and subsequent to DAAO treatment revealed the complete disappearance of D-Ala, consistent with the assignment of the peak to D-Ala. Incubation of fraction 18 with DAAO also lead to the disappearance of the signal for D-Val; however, a residual signal co-eluting with D-Val remained due to a contamination of DAAO with an unknown compound, as revealed by control experiments with DAAO alone (Fig. S8). This contamination did not affect the analysis of total mAb hydrolysate after treatment with DAAO, due to the significantly larger quantity of D-Val present after hydrolysis of the entire protein.

3.4 Discussion

Due to the chirality of the α-carbon (Cα), all amino acids with the exception of Gly can undergo epimerization (conversion of L-amino acid to D-amino acid). Although only L-amino acids are used for the synthesis of proteins, D-amino acids have been identified in various proteins from human tissue, resultant of post-translational modifications (PTM). For example, D-Asp was detected in various proteins from human tissue such as eye lens, skin and bone in elderly people, and a high proportion of D-Asp and D-Ser were found in amyloid plaques of Alzheimer's disease. [32-34] Tao et al. have reported on the epimerization of crystallin proteins extracted from the sheep eye lens,[35] showing a considerable degree of isomerization and epimerization in

disordered N-terminal and C-terminal domains.[35,36] Even though these modifications are not as abundant as the commonly studied PTMs, such as resulting from oxidation and phosphorylation, they can affect the higher order structure of a protein, in turn affecting the biological activity of a protein. [31] All the examples presented earlier are associated with the identification of D-amino acids in biological samples, but recently there has been some evidence showing the formation of D-amino acids in therapeutic proteins. Amano et al. have identified specifically the racemization of Cys220 in the hinge region of IgG1 upon incubation of the protein at 50 ºC and pH 9.[37] Likewise, Zhang et al. have identified the racemization of disulfide Cys residues (HC Cys220; LC Cys214) in the hinge region of an IgG1 incubated under basic pH conditions.[38] In both of these studies reversible β-elimination of Cys residues has been presented as the underlying reaction mechanism for the base-catalyzed racemization of the hinge region disulfide bond. [37,38] In another study, Mozziconacci et al. have identified the formation of D-amino acids in specific sequences of a UV light-exposed IgG1. [19]

Photo-irradiation of proteins can lead to the formation of thiyl radicals by various mechanisms.[39-41] UV light at λ_{max} = 305 nm is essentially absorbed by aromatic amino acids (Trp, Tyr, Phe).[7,27] Here, the absorption of light by Trp produces an excited state, which can eventually ionize to form a hydrated electron and a radical cation.[7] The hydrated electron can reduce a disulfide bond to form a disulfide radical anion, which further dissociates into cysteine thiyl radicals (CysS$^{\bullet}$) and Cys. Instead, UV light at λ = 254 nm can be directly absorbed by the disulfide bond, leading to the homolytic cleavage of the disulfide bonds and generating a pair of CysS$^{\bullet}$ radicals.[13,16-19,40] The resultant CysS$^{\bullet}$ radicals formed upon light-exposure can participate in intramolecular hydrogen atom abstraction from adjacent C-H bonds, leading to the formation of carbon-centered radicals. [13-16] If such intramolecular hydrogen atom transfer proceed between CysS$^{\bullet}$ and a C-H

bond of the chiral carbon, the resulting carbon atom exhibits two prochiral faces. The reverse hydrogen atom transfer can lead to formation of either L- or D- amino acid. [17]

3.4.1 Effect of various excipients on the extent of epimerization in UV irradiated mAb formulations

The formation of D-amino acids could impose local conformational changes in proteins, potentially leading to the formation of partially unfolded structures, which can serve as precursors for the formation of higher molecular weight structures. Therefore, we performed a quantitative analysis of D-amino acid formation in monomer and aggregates of a mAb exposed to light. In this study, a variety of excipients were added to a mAb formulation, such as protein stabilizers (sucrose, glucose) and amino acids (L-Arg, L-Met and L-Leu).

The quantitative analysis for monomers (Fig. 4a) and aggregates (Fig. 4b), resultant of light-exposure of mAb at λ_{max} = 305 nm in different formulation revealed existence of D-Val, D-Glu and low levels D-Asp in all the samples, whereas D-Ala was only identified in aggregates formed resultant of UV irradiation (λ_{max} = 305 nm) of mAb in L-Arg formulation. The quantitative analysis of monomers (Fig. 5a) and aggregates (Fig. 5b), resultant of light-exposure of mAb at λ = 254 nm in different formulation revealed the formation of D-Val and D-Glu, while low levels D-Asp were present in all the samples.

Interestingly, a quantitative analysis revealed higher yields of D-amino acids for both monomers and aggregates resultant of UV irradiation (λmax = 305 nm and λ = 254 nm) of mAb in the L-Arg containing formulation when compared to mAb in other formulations (in L-Met, L-Leu, sucrose and glucose). This can be rationalized by an increase in mAb flexibility in the C_H1 and C_H2 domains in the presence of L-Arg, [24,42] which can increase the probability of D-amino acid

formation. In contrast, sugars (sucrose and glucose) are known to increase the compactness and rigidity of a protein in aqueous solution. For example, the stabilizing effect of sucrose on protein structure was explained by Timasheff et al. by "preferential exclusion" mechanism.[43] Based on this mechanism, sucrose is preferentially excluded from the protein surface increasing the chemical potential of the solution. According to Le Chatlier's principle, to counteract the changes imposed by preferential exclusion a new equilibrium is established to reduce thermodynamically unfavorable states, during which proteins adopt to a smaller surface area with a more compact and rigid structures.[42-44] This rigid nature (less flexibility) of mAb in the presence of sugars can minimize the extent of intra-molecular hydrogen transfer reactions thus reducing the magnitude of epimerization.

3.4.2 Effect of various excipients on the site-specificity of the epimerization in UV irradiated mAb formulations

Intramolecular hydrogen transfer reactions can be monitored using covalent incorporation of deuterium when photolysis of disulfide bond happens in presence of D_2O. In this study, we have identified selective addition of deuterium into five peptides for mAb in L-Arg and L-Met formulations, and four peptides for mAb in sucrose, glucose and L-Leu formulations (Table. 1 and Table 2). These results illustrate that protein CysS$^{\bullet}$ radicals generated resultant of photolysis of disulfide bonds in mAb abstract hydrogen atoms from specific sequences. The differences in deuterium incorporation in mAb in presence of various formulations suggest an influence of mAb conformation on protein CysS$^{\bullet}$ radical formation and reactivity. Protein conformation can influence the formation of carbon-centered radicals by controlling the accessibility of C-H bond to the protein CysS$^{\bullet}$ radicals formed during light-exposure. However, covalent deuterium incorporation alone does not allow us to identify if a specific amino acid is potentially

epimerized, as intramolecular H atom transfer between CysS$^{\bullet}$ and C-H bond of a non-chiral atom will still exhibit covalent deuterium incorporation, but will not be involved in epimerization. As a proof of concept, the amino acid analyses of peptide segments H51-H59 and H287-H296 (peptide segments that showed covalent incorporation of deuterium) revealed presence of D-Ala and D-Val, respectively.

The peptide segment H51-H59 is present in the complementarity-determining region (CDR), thus presence of epimerized amino acids is likely to have an effect on the binding affinity of a mAb to the target and, therefore have an effect on its potency.

3.5 Conclusion

Our results show that UV light-exposure (λ_{max} = 305 nm and λ = 254 nm) can induce epimerization of particular amino acid residues in mAb. As the epimerization of certain amino acids could lead to loss of biological activity of IgG, high extra care should be taken to limit the exposure of proteins to light.

3.6 References

1) Udpa N, Million P R. Monoclonal antibodies biosimilars. Nat Rev Drug Discov. 2016; (15): 13-14.

2) Hansel T T, Kropshofer H, Singer T, Mitchell A J, George T J A. The safety and side effects of monoclonal antibodies. Nat Rev Drug Discov. 2010; (9): 327-338.

3) Justin K H L. The history of monoclonal antibody development–Progress, remaining challenges and future innovations. Ann Med Surg. 2014; (3.4): 113-116.

4) Reichert JM, Valge-Archer VE. Development trends for monoclonal antibody cancer therapeutics. Nat. Rev. Drug Discov. 2007; 6(5): 349-56.

5) Manning M C, Chou D K, Murphy B M, Payne R W, Katayama D S. Stability of protein pharmaceuticals: an update. Pharm Res. 2010; 27 (4): 544-575.

6) Bommana R, Mozziconacci O, Wang YJ, Schöneich C. An Efficient and Rapid Method to Monitor the Oxidative Degradation of Protein Pharmaceuticals: Probing Tyrosine Oxidation with Fluorogenic Derivatization. Pharm Res. 2017; 18: 1-6.

7) Kerwin B A, & Remmele R L. Protect from light: photodegradation and protein biologics. J Pharm Sci. 2007; 96(6): 1468-1479.

8) Mozziconacci O, Kerwin B A, Schöneich C. Exposure of a monoclonal antibody, IgG1, to UV-light leads to protein dithiohemiacetal and thioether cross-links: a role for thiyl radicals?. Chem Res Toxicol. 2010; 23(8): 1310-1312.

9) Qi P, Volkin D B, Zhao H, Nedved M L, Hughes R, Bass, Yi C S, Panek E M, Wang D, Dalmonte P, Bond, M. D. Characterization of the photodegradation of a human IgG1 monoclonal antibody formulated as a high-concentration liquid dosage form. J Pharm Sci. 2009; 98(9): 3117-3130.

10) Mason B D, Schöneich C, Kerwin B A. Effect of pH and light on aggregation and conformation of an IgG1 mAb. Mol Pharm. 2012; 9(4): 774-790.

11) ICH harmonized tripartite guideline: guideline for the photostability testing of new drug substances and products. J Postgrad Med. 2001; 47: 264.

12) Liu H, May K. Disulfide bond structures of IgG molecules: structural variations, chemical modifications and possible impacts to stability and biological function. MAbs 2012; 4(1): 17-23.

13) Mozziconacci O, Kerwin B A, Schöneich C. Photolysis of an intrachain peptide disulfide bond: primary and secondary processes, formation of H2S, and hydrogen transfer reactions. J Phys Chem B. 2010; 114(10): 3668-3688.

14) Steinmann D, Ji JA, Wang YJ, Schöneich C. Oxidation of human growth hormone by oxygen-centered radicals: formation of Leu-101 hydroperoxide and Tyr-103 oxidation products. Mol. Pharm. 2012; 9(4): 803-14.

15) Steinmann D, Ji JA, Wang YJ, Schöneich C. Photodegradation of human growth hormone: a novel backbone cleavage between Glu-88 and Pro-89. Mol. Pharm. 2013; 10(7): 2693-706.

16) Zhou S, Mozziconacci O, Kerwin BA, Schöneich C. The photolysis of disulfide bonds in IgG1 and IgG2 leads to selective intramolecular hydrogen transfer reactions of cysteine Thiyl radicals, probed by covalent H/D exchange and RPLC-MS/MS analysis. Pharm Res. 2013; 30(5): 1291-9.

17) Mozziconacci O, Williams TD, Schöneich C. Intramolecular hydrogen transfer reactions of thiyl radicals from glutathione: formation of carbon-centered radical at Glu, Cys, and Gly. Chem. Res. Toxicol. 2012; 25(9): 1842-61.

18) Mozziconacci O, Kerwin BA, Schöneich C. Reversible hydrogen transfer between cysteine thiyl radical and glycine and alanine in model peptides: Covalent H/D exchange, radical− radical reactions, and L-to D-Ala conversion. J. Phys. Chem. B. 2010; 114(19): 6751-62.

19) Mozziconacci O, Schöneich C. Sequence-specific formation of D-amino acids in a monoclonal antibody during light exposure. Mol Pharm. 2014; 11(11): 4291-7.

20) Rauk A, Armstrong DA. Influence of beta-sheet structure on the susceptibility of proteins to backbone oxidative damage: preference for C(alpha)-centered radical formation at glycine residues of antiparallel beta-sheets. J Am Chem Soc. 2000; 122: 4185–92.

21) Rauk A, Yu D, Armstrong DA. Oxidative damage to and by cysteine in proteins: an ab initio study of the radical structures, C−H, S−H, and C−C bond dissociation energies, and transition structures for H abstraction by thiyl radicals. J Am Chem Soc.1998; 120: 8848–55.

22) Chi EY, Krishnan S, Randolph TW, Carpenter JF. Physical stability of proteins in aqueous solution: mechanism and driving forces in nonnative protein aggregation. Pharm Res. 2003; 20(9): 1325-36.

23) Kamerzell TJ, Esfandiary R, Joshi SB, Middaugh CR, Volkin DB. Protein–excipient interactions: Mechanisms and biophysical characterization applied to protein formulation development. Adv. Drug Deliv. Rev. 2011; 63(13): 1118-59.

24) Thakkar SV, Joshi SB, Jones ME, Sathish HA, Bishop SM, Volkin DB, Middaugh CR. Excipients differentially influence the conformational stability and pretransition dynamics of two IgG1 monoclonal antibodies. J. Pharm. Sci. 2012; 101(9): 3062-77.

25) Pace CN, Vajdos F, Fee L, Grimsley G, Gray T. How to measure and predict the molar absorption coefficient of a protein. Protein Sci. 1995; 4(11): 2411-23.

26) Covington AK, Paabo M, Robinson RA, Bates RG. Use of the glass electrode in deuterium oxide and the relation between the standardized pD (paD) scale and the operational pH in heavy water. Anal. Chem. 1968; 40(4):700-6.

27) Martin SR, Bayley PM. Absorption and circular dichroism spectroscopy. Calcium-Binding Protein Protocols: Volume 2: Methods and Techniques. 2002:43-55.

28) Fountoulakis M, Lahm HW. Hydrolysis and amino acid composition analysis of proteins. J. Chromatogr. A. 1998; 826(2): 109-34.

29) Molla G, Piubelli L, Volontè F, Pilone MS. Enzymatic detection of D-amino acids. Unnatural Amino Acids: Methods and Protocols: 273-89.

30) Sacchi S, Rosini E, Caldinelli L, Pollegioni L. Biosensors for D-amino acid detection. Unnatural Amino Acids: Methods and Protocols: 313-24.

31) Tedeschi G, Pollegioni L, Negri A. Assays of d-amino acid oxidases. Unnatural Amino Acids: Methods and Protocols. 2012: 381-95.

32) Fujii N. D-amino acid in elderly tissues. Biological and Pharmaceutical Bulletin. 2005; 28(9): 1585-9.

33) Tomiyama T, Asano S, Furiya Y, Shirasawa T, Endo N, Mori H. Racemization of Asp23 residue affects the aggregation properties of Alzheimer amyloid beta protein analogues. J. Biol. Chem. 1994; 269(14): 10205-8.

34) Huang L, Lu X, Gough PC, De Felippis MR. Identification of racemization sites using deuterium labeling and tandem mass spectrometry. Anal. Chem. 2010; 82(15): 6363-9.

35) BN Tao Y, Julian RR. Identification of amino acid epimerization and isomerization in crystallin proteins by tandem LC-MS. Anal. Chem. 2014; 86(19): 9733-41.

36) Lyon YA, Sabbah GM, Julian RR. Identification of Sequence Similarities among Isomerization Hotspots in Crystallin Proteins. J. Proteome Res; 16(4): 1797-805.

37) Amano M, Hasegawa J, Kobayashi N, Kishi N, Nakazawa T, Uchiyama S, Fukui K. Specific racemization of heavy-chain cysteine-220 in the hinge region of immunoglobulin gamma 1 as a possible cause of degradation during storage. Anal. Chem. 2011; 83(10): 3857-64.

38) Zhang Q, Flynn GC. Cysteine racemization on IgG heavy and light chains. J. Biol. Chem. 2013; 288(48): 34325-35.

39) Schöneich C. Mechanisms of protein damage induced by cysteine thiyl radical formation. Chem Res Toxicol. 2008; 21(6): 1175-9.

40) Mozziconacci O, Sharov V, Williams TD, Kerwin BA, Schöneich C. Peptide cysteine thiyl radicals abstract hydrogen atoms from surrounding amino acids: the photolysis of a cystine containing model peptide. J. Phys. Chem. B. 2008; 112(30): 9250-7.

41) Schöneich C. Thiyl radicals and induction of protein degradation. Free radical research. 2016; 50(2): 143-9.

42) Manikwar P, Majumdar R, Hickey JM, Thakkar SV, Samra HS, Sathish HA, Bishop SM, Middaugh CR, Weis DD, Volkin DB. Correlating excipient effects on conformational and storage stability of an IgG1 monoclonal antibody with local dynamics as measured by hydrogen/deuterium-exchange mass spectrometry. J. Pharm. Sci. 2013; 102(7): 2136-51.

43) Arakawa T, Timasheff SN. Stabilization of protein structure by sugars. J. Biochem. 1982 ;21(25): 6536-44.

44) Lee JC, Timasheff SN. 1981. The stabilization of proteins by sucrose. J. Biol. Chem 256(14):7193–7201.

Schemes

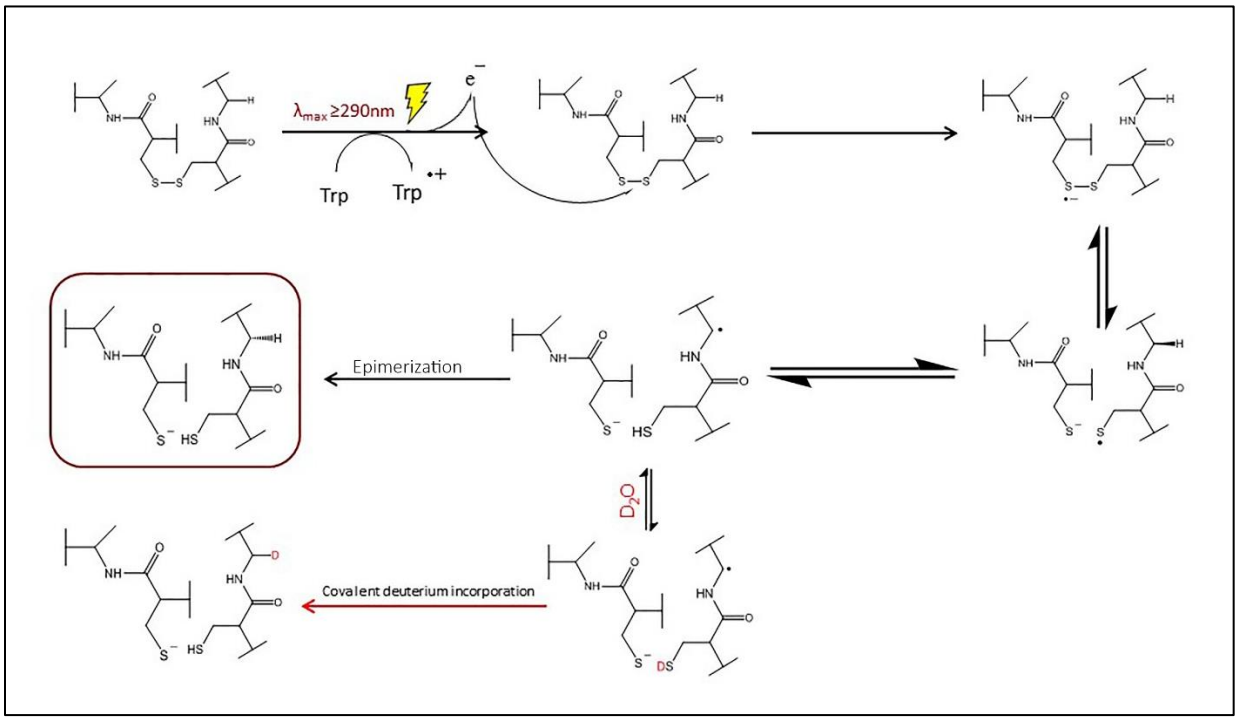

Scheme 1: The intramolecular H atom transfer occurring between the thiyl radical of the cysteine residue and C-H bond.

Tables

Position	L-Arg	L-Met	L-Leu	Sucrose	Glucose
H51-H59	✓	✓	✓	✓	✓
H51-H60	✓	✓	✓	✓	✓
H287-H296	✓	✓	×	×	×
H353-H357	✓	✓	✓	✓	✓
H392-H397	✓	✓	✓	✓	✓

Table 1. List of proteolytic peptides with covalent deuterium incorporation after UV light-exposure (λ_{max} = 305 nm) of mAb in five (L-Arg, L-Met, L-Leu, sucrose and glucose) different formulations.

Figures

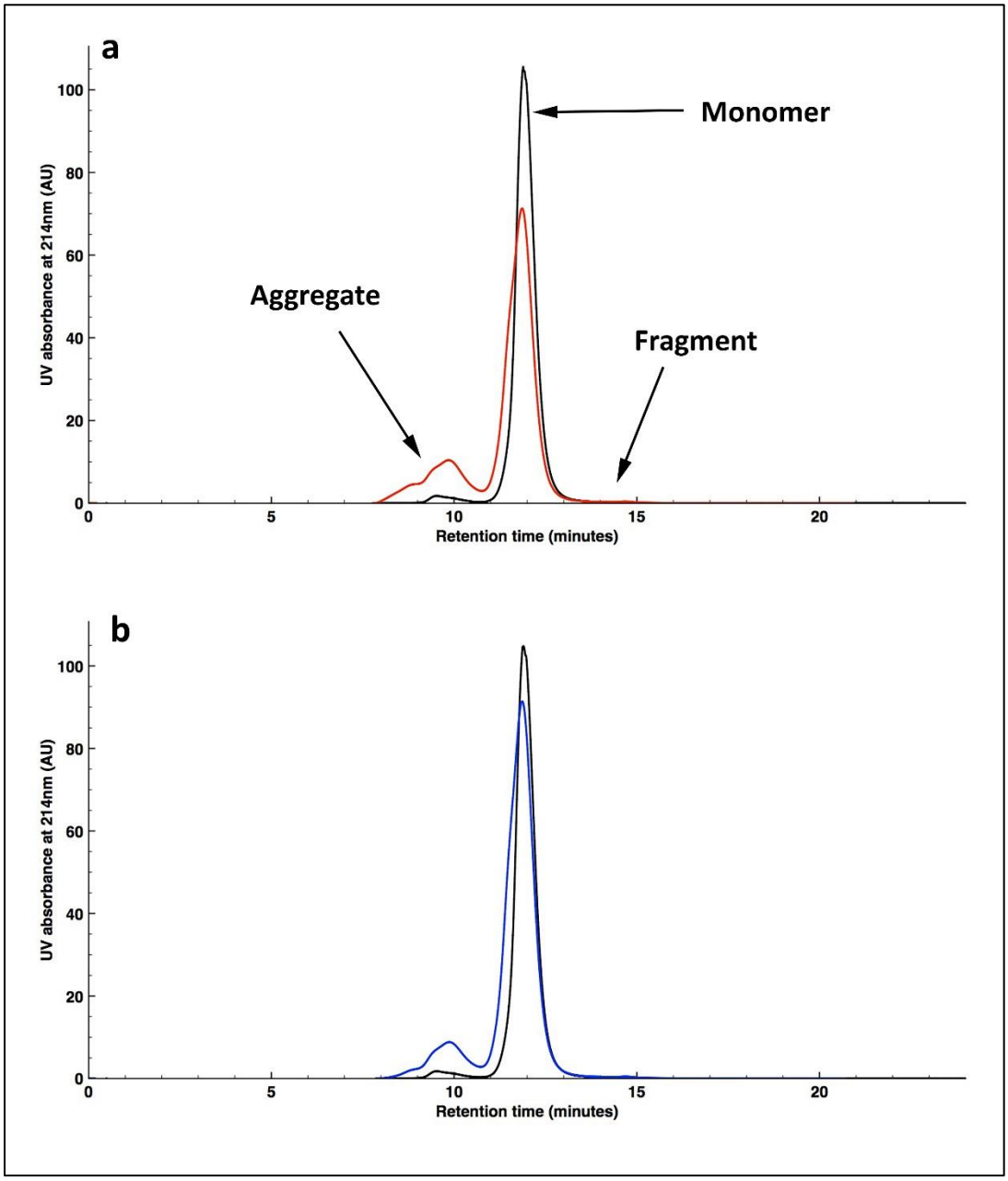

Figure 1. SEC analysis of mAb samples exposed to UV (λ_{max} = 305 nm) irradiation for 60 min. (a) Overlay of SEC chromatograms of mAb in L-Arg formulation, without light exposure (control, black trace) and exposure to UV light for 60 min (red trace). (b) Overlay of SEC chromatograms of mAb in L-Met formulation, without light exposure (control, black trace) and exposure to UV light for 60 min (blue trace).

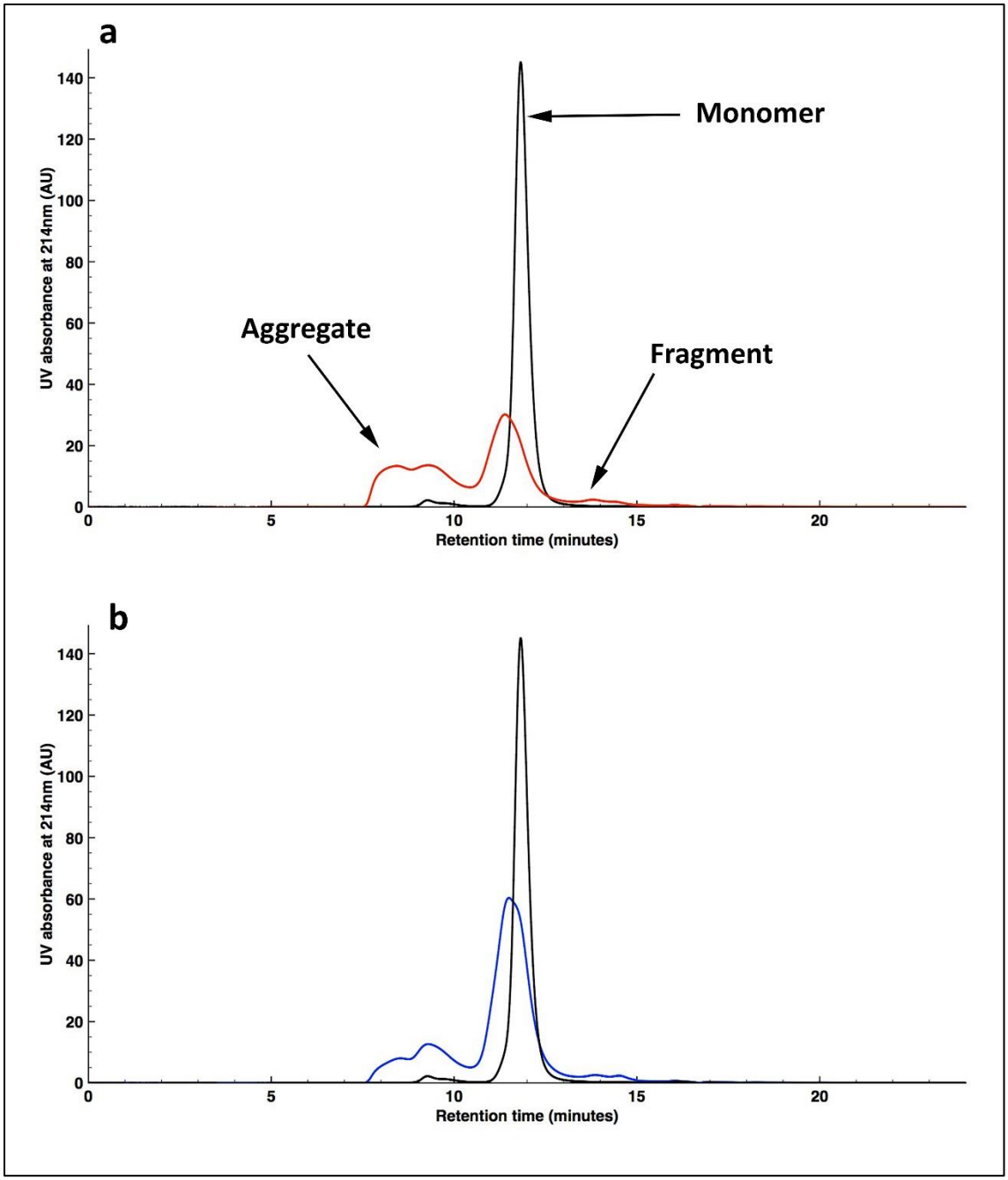

Figure 2. SEC analysis of mAb samples exposed to UV (λ = 254 nm) irradiation for 60 min. (a) Overlay of SEC chromatograms of mAb in L-Arg formulation, without light exposure (control, black trace) and exposure to UV light for 60 min (red trace). (b) Overlay of SEC chromatograms of mAb in L-Met formulation, without UV irradiation (control, black trace) and with UV irradiation for 60 min (blue trace).

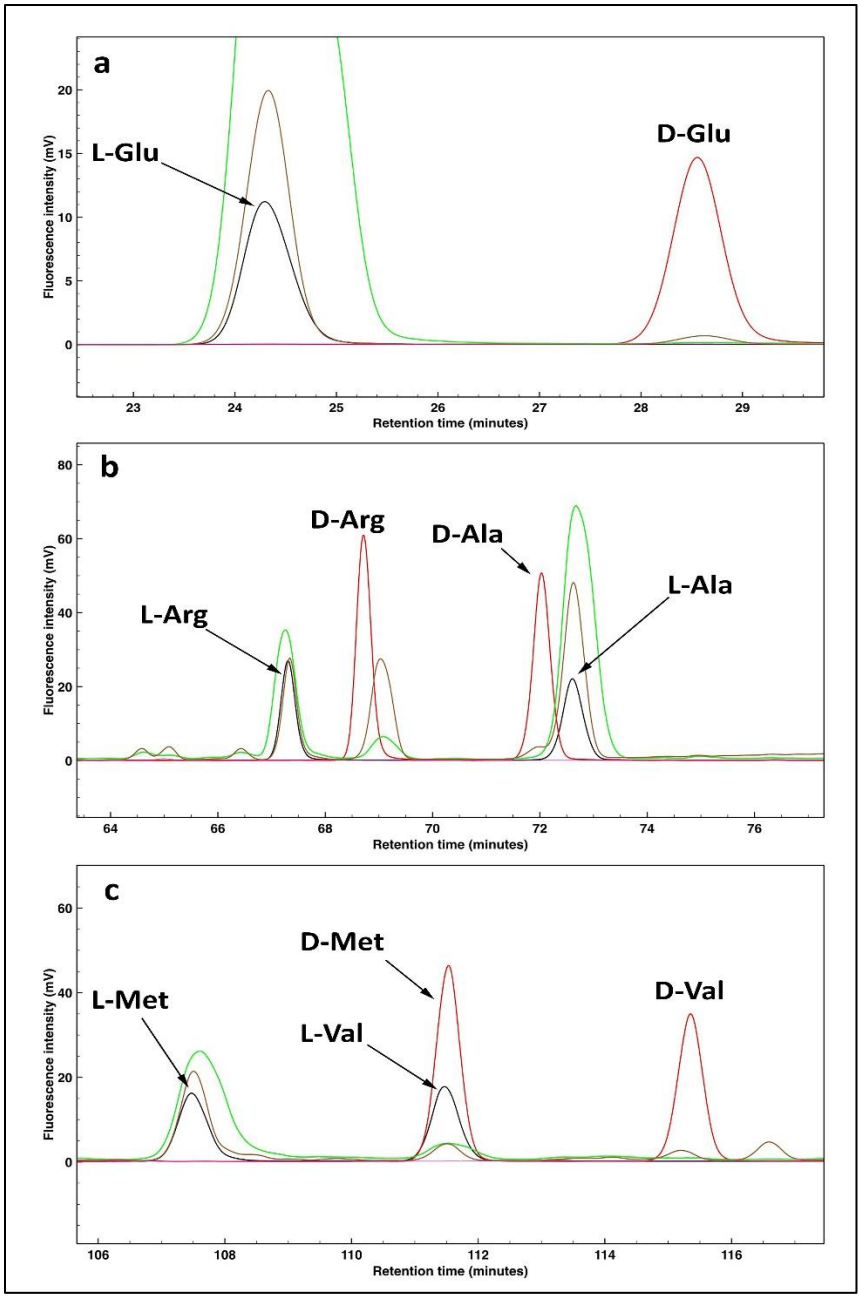

Figure 3. Amino acid analysis of aggregates resultant of UV irradiation (λ_{max} = 305 nm) of mAb in L-Arg formulation (brown trace) and control mAb in L-Arg formulation (green trace). Amino acid standards L-Glu (black trace, a), D-Glu (red trace, a) L-Arg (black trace, b), D-Arg (red trace, b), L-Ala (black trace, b), D-Ala (red trace, b), L-Met (black trace, c), D-Met (red trace, c), L-Val (black trace, c) and D-Val (red trace, c). The HPLC chromatograms are recorded using a fluorescence detector (λ_{ex} = 340 nm and λ_{em} = 455 nm).

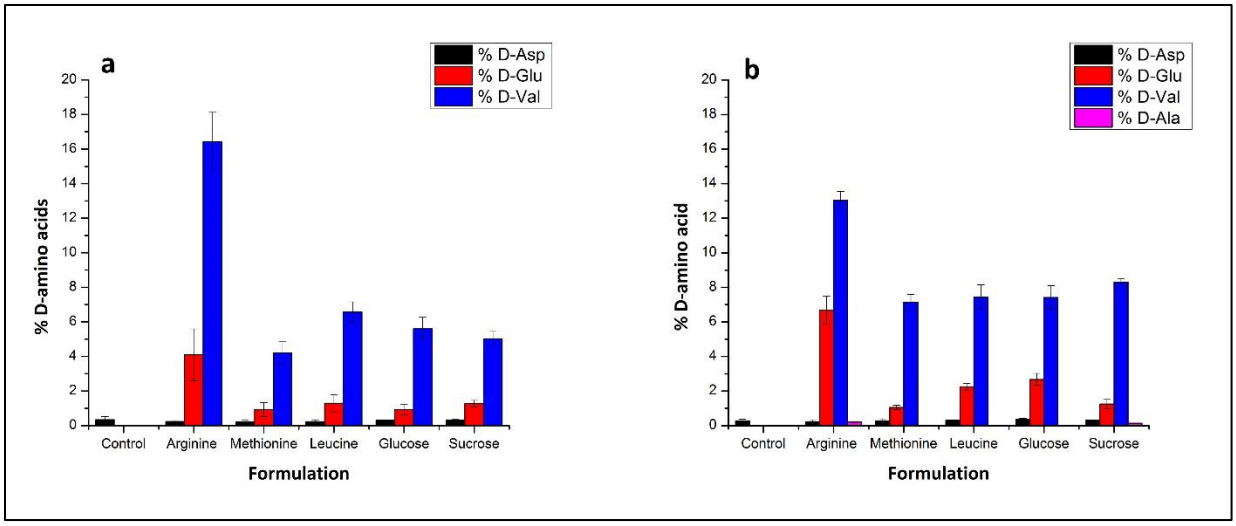

Figure 4. Quantitative analysis of D-amino acids identified in (a) monomer, and (b) aggregate fractions generated after UV (λ_{max} = 305 nm) irradiation of mAb in L-Arg, L-Met, L-Leu, glucose and sucrose formulations. Error bars represent standard deviation from three independent samples.

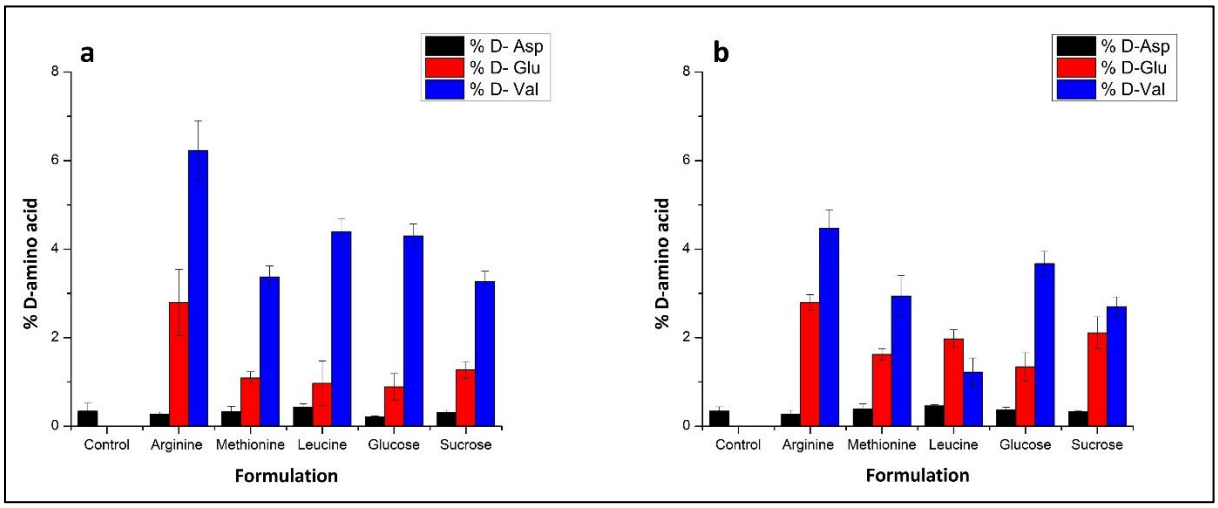

Figure 5. Quantitative analysis of D-amino acids identified in (a) monomer, and (b) aggregate fractions generated after UV (λ = 254 nm) irradiation of mAb in L-Arg, L-Met, L-Leu, glucose and sucrose formulations. Error bars represent standard deviation from three independent samples.

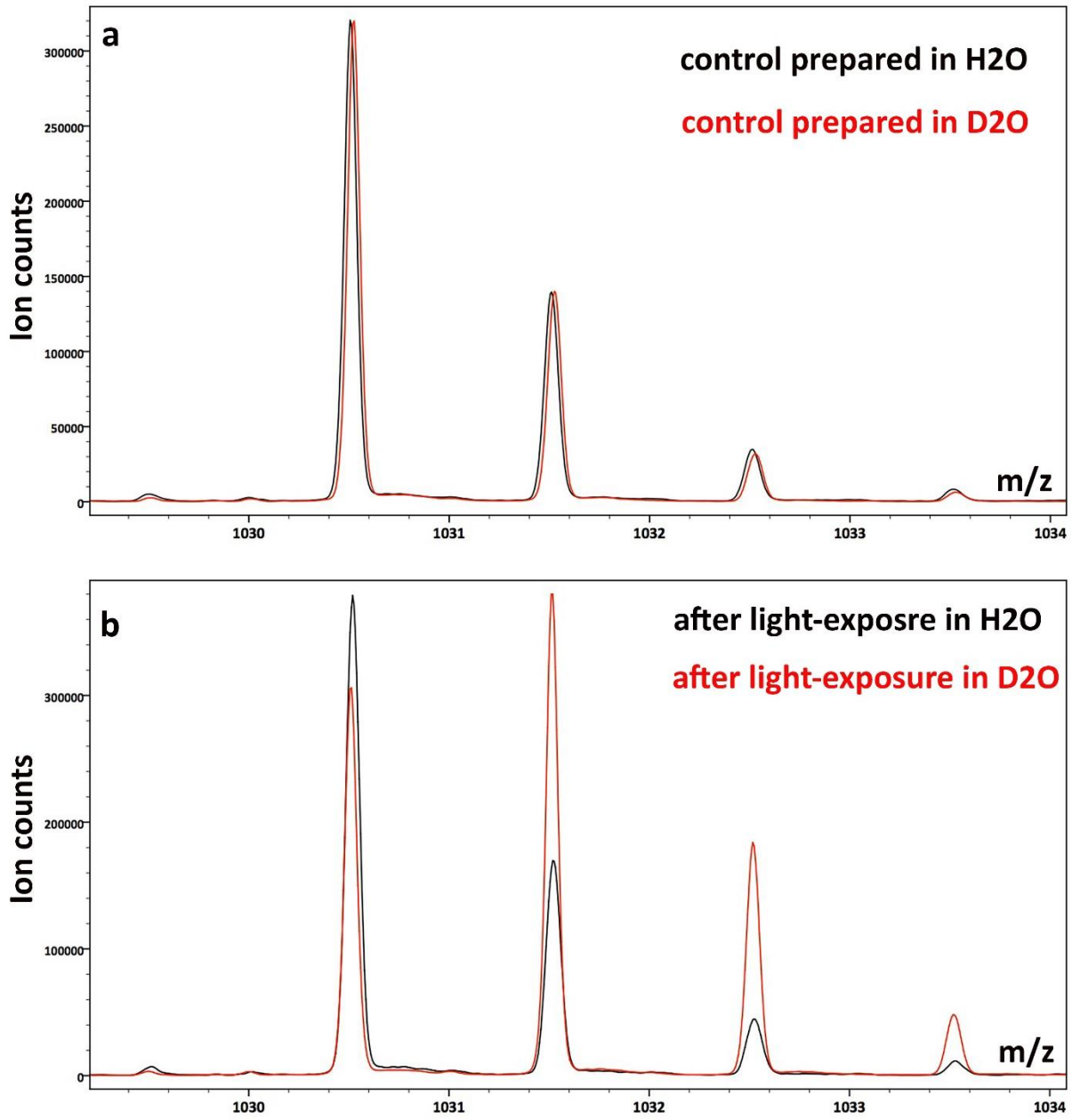

Figure 6. Comparison of the isotopic distributions of the ion with m/z 1030.44 (H51-H59) generated after the digestion of control mAb in H_2O (a, black) and D_2O (a, red), and UV irradiated (λ_{max} = 305 nm) mAb in non-deuterated (H_2O, b, black) and deuterated (D_2O, b, red) L-Arg-containing formulation.

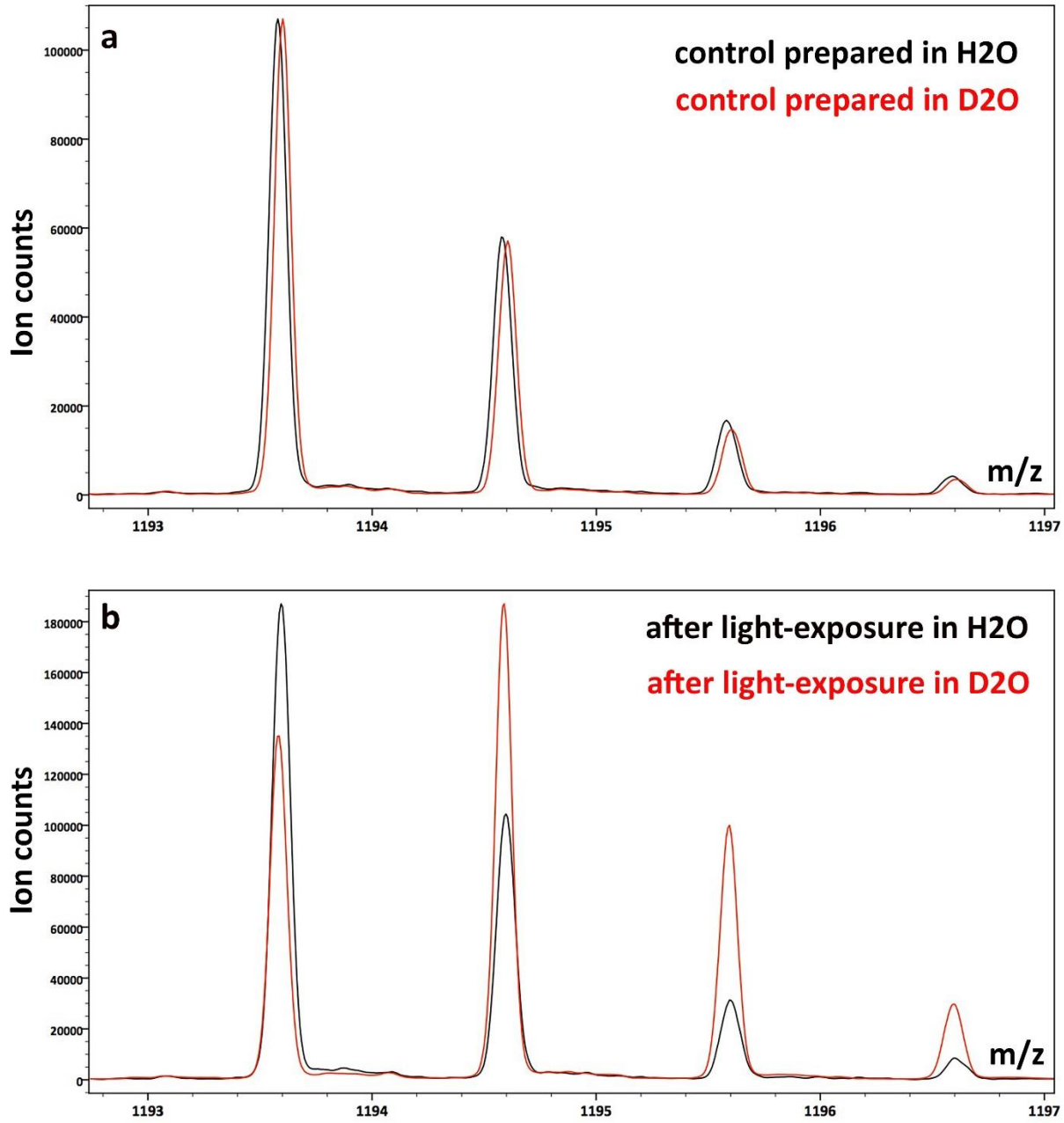

Figure 7. Comparison of the isotopic distributions of the ion with m/z 1193.51 (H51-H60) generated after the digestion of control mAb in H_2O (a, black) and D_2O (a, red), and UV irradiated (λ_{max} = 305 nm) mAb in in non-deuterated (H_2O, b, black) and deuterated (D_2O, b, red) L-Arg-containing formulation.

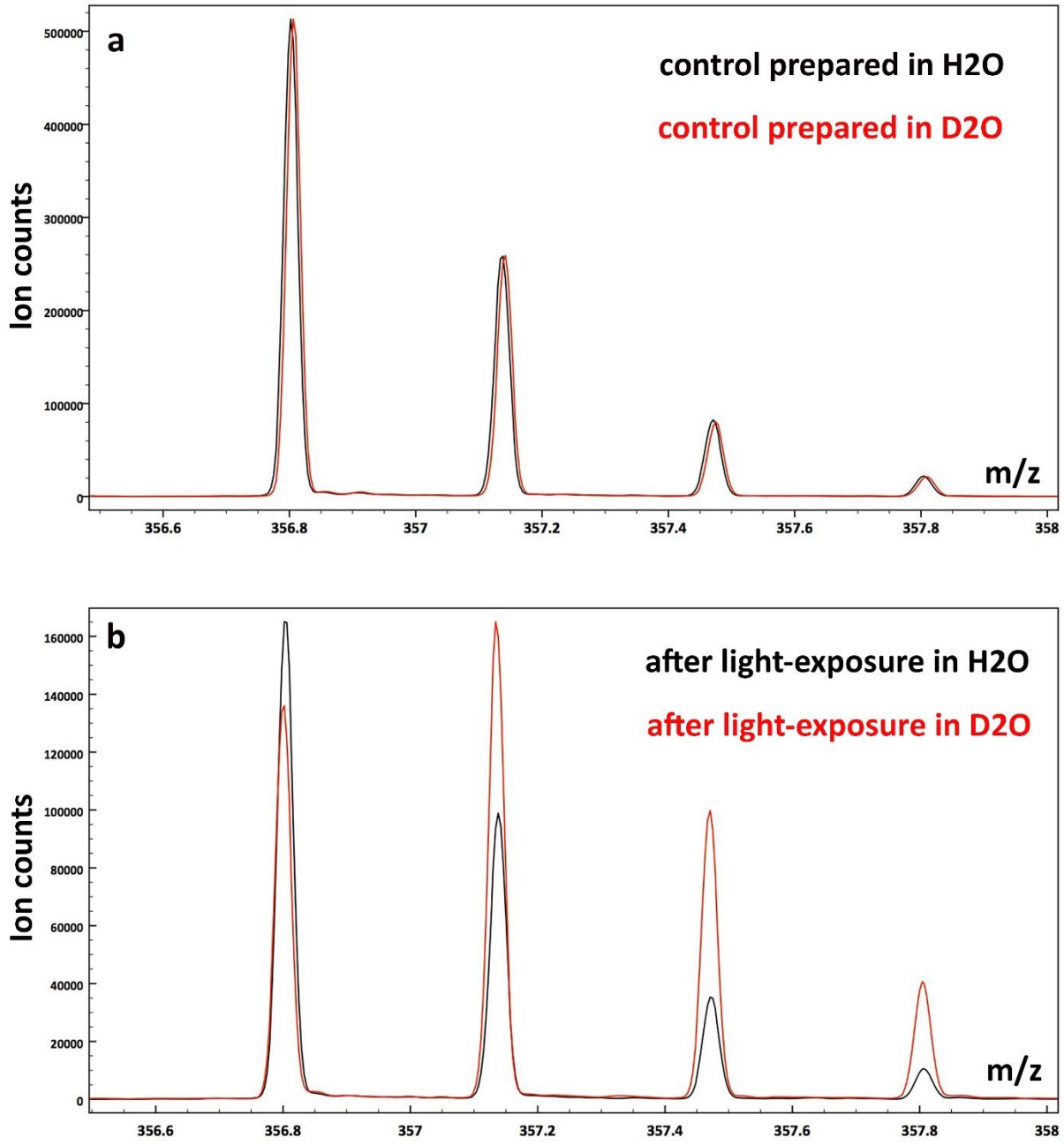

Figure 8. Comparison of the isotopic distributions of the ion with m/z 356.8 (H287-H296) generated after the digestion of control mAb in H_2O (a, black) and D_2O (a, red), and UV irradiated (λ_{max} = 305 nm) mAb in in non-deuterated (H_2O, b, black) and deuterated (D_2O, b, red) L-Arg-containing formulation.

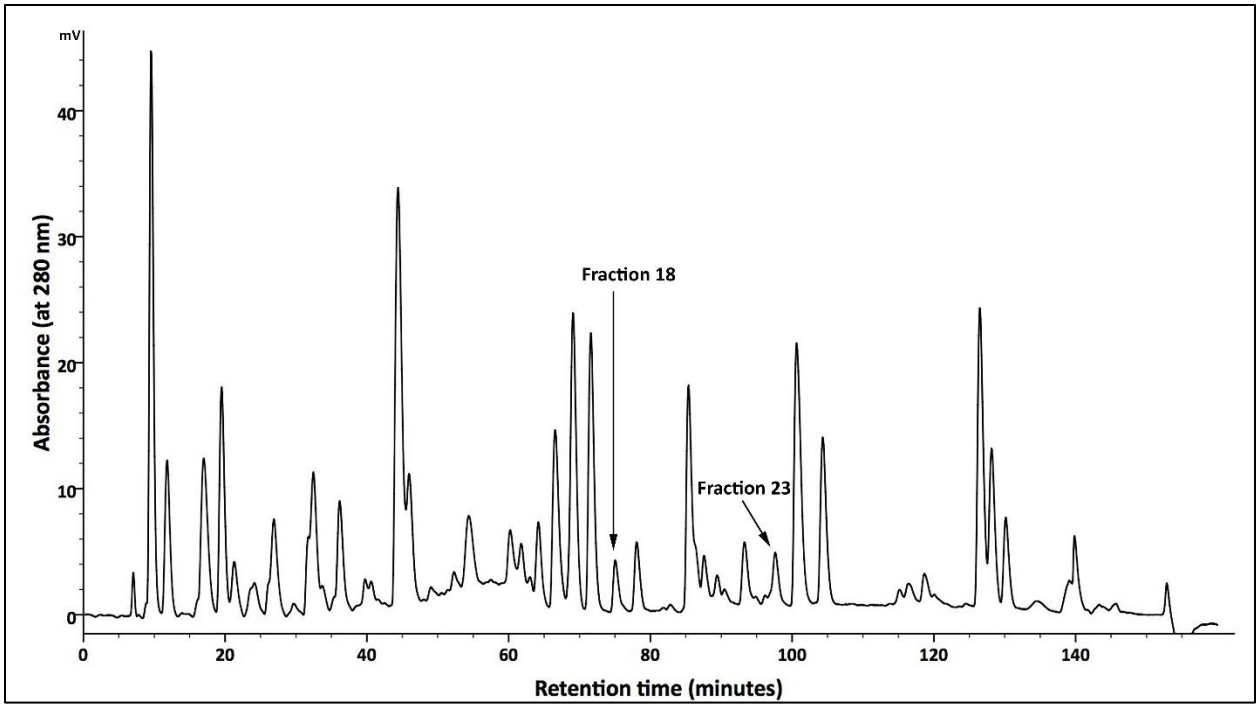

Figure 9. HPLC chromatogram, recorded at $\lambda = 280$ nm, of a proteolytic digest of a mAb, which had been UV-irradiated ($\lambda_{max} = 305$ nm) in an L-Arg-containing formulation. Chromatographic peaks were collected into individual fractions. Proteolytic peptides with covalent incorporation of deuterium were present eluting in fraction 18 and 23. The purity of these fractions was assessed by LC-MS analysis.

Supplementary material

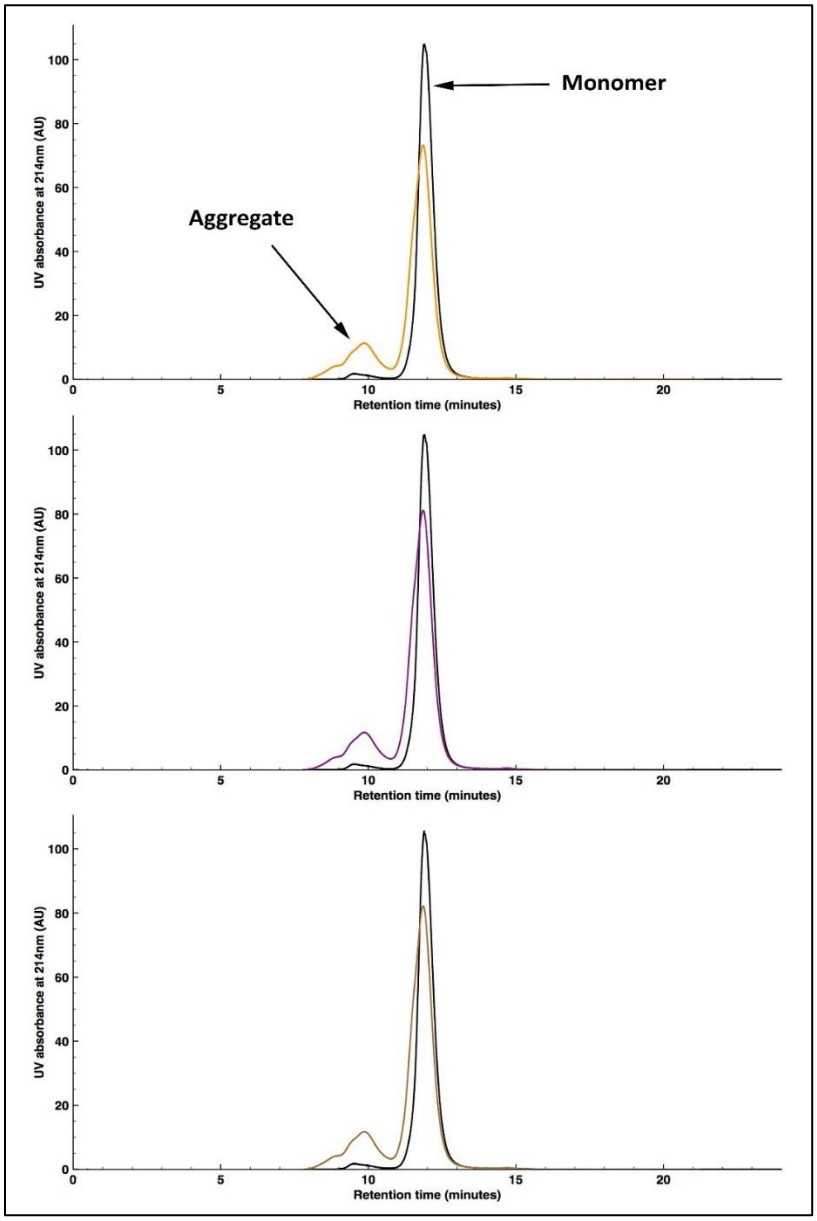

Fig S1: SEC analysis of mAb samples exposed to UV (λ_{max} = 305 nm) light for 60 min. (a) Overlay of SEC chromatograms of mAb in (a) leucine formulation, without light exposure (control, black trace) and exposure to UV light for 60 min (orange trace), (b) glucose formulation, without light exposure (control, black trace) and exposure to UV light for 60 min (purple trace), (c) sucrose formulation, without light exposure (control, black trace) and exposure to UV light for 60 min (brown trace).

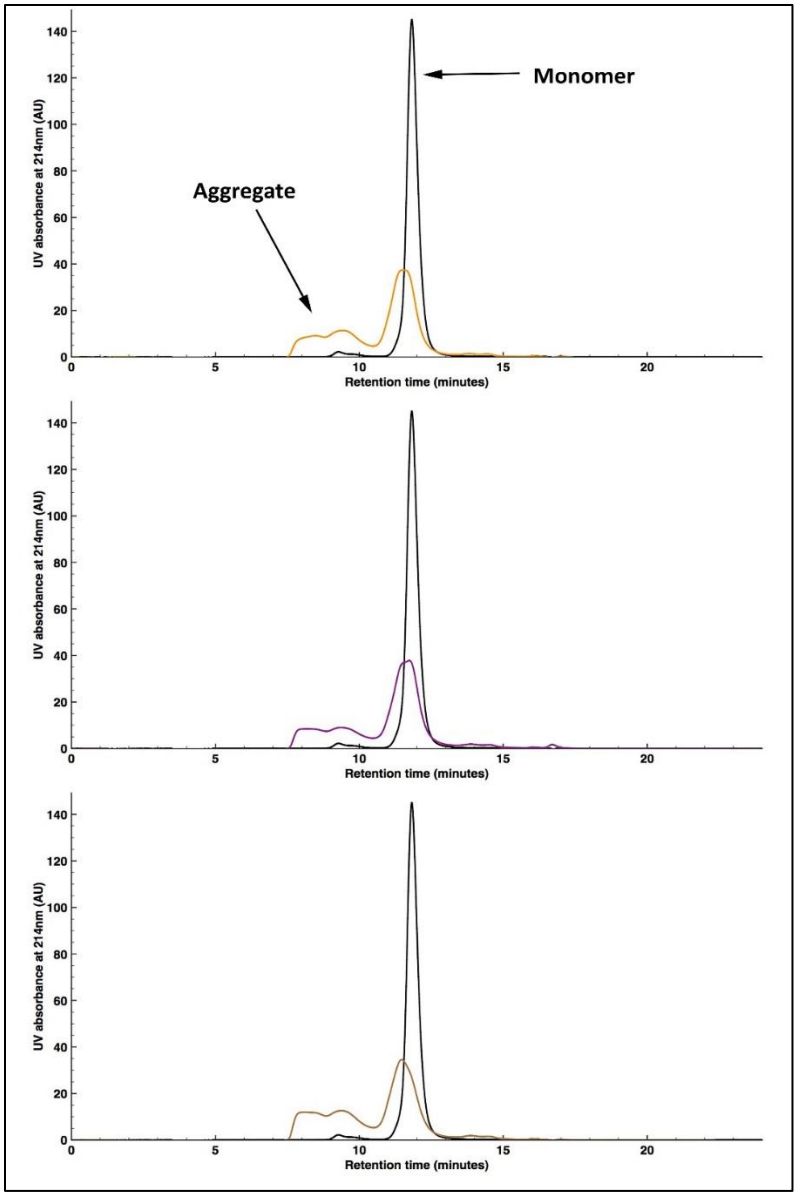

Fig S2: SEC analysis of mAb samples exposed to UV (λ = 254 nm) light for 60 min. Overlay of SEC chromatograms of mAb in (a) leucine formulation without light exposure (control, black trace) and exposure to UV light for 60 min (orange trace), (b) glucose formulation, without light exposure (control, black trace) and exposure to UV light for 60 min (purple trace), (c) sucrose formulation, without light exposure (control, black trace) and exposure to UV light for 60 min (brown trace).

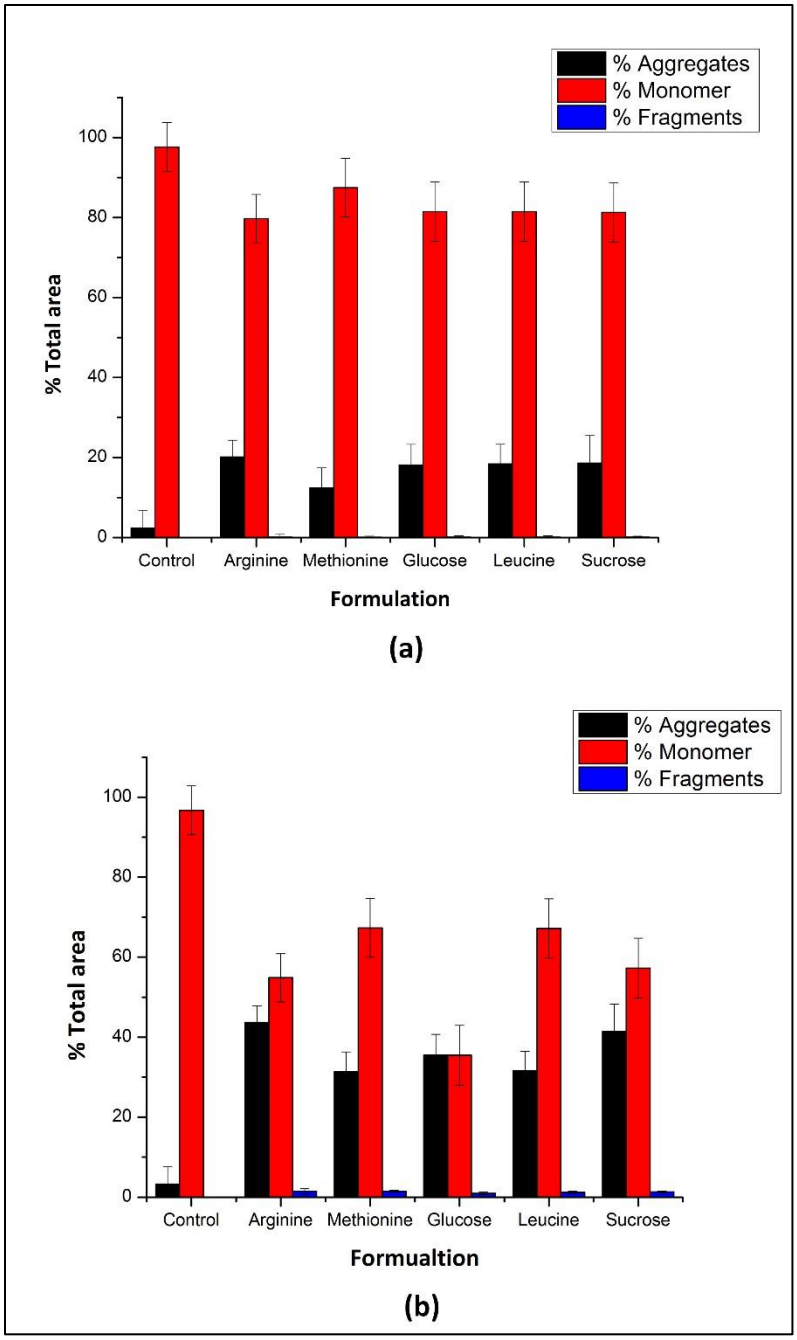

Fig S3: SEC analysis of mAb samples in different formulations before (control) and after UV light exposure for 60 min. The bar graphs represent the amount of aggregates, monomer and fragments of mAb as measured on (a) UV light exposure at λ_{max} = 305 nm and (b) UV light exposure at λ = 254 nm.

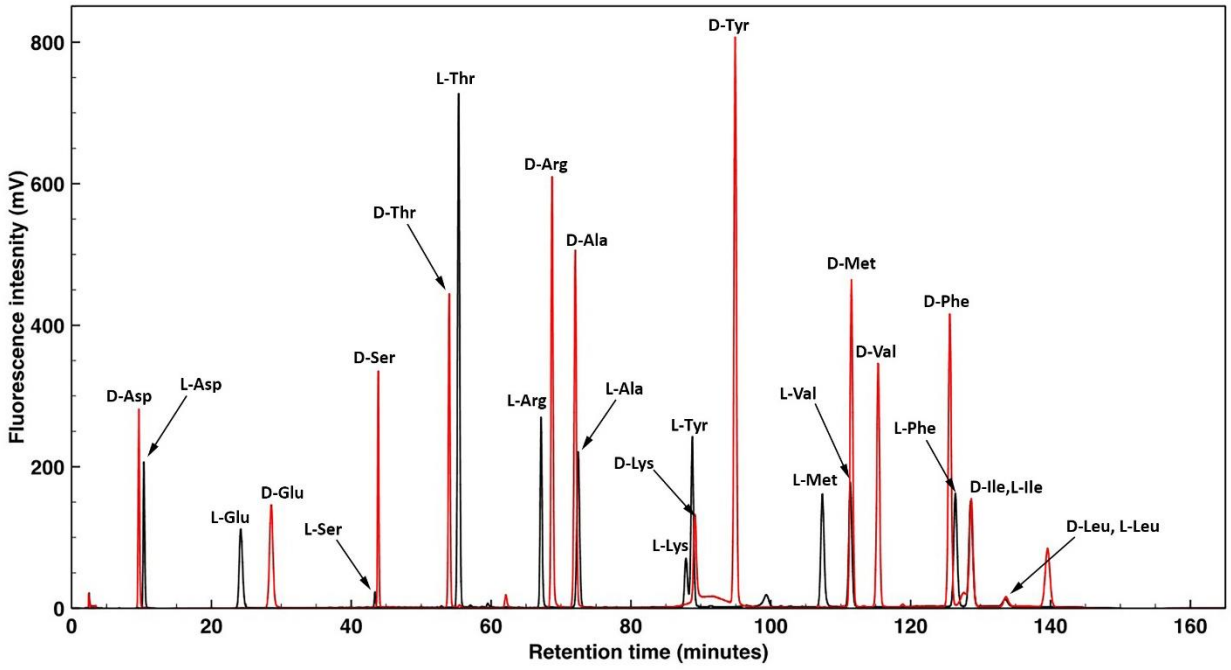

Fig S4. Amino acid analysis of L and D amino acid standards. The HPLC chromatograms are recorded using a fluorescence detector (λ_{ex} = 340 nm and λ_{em} = 455 nm).

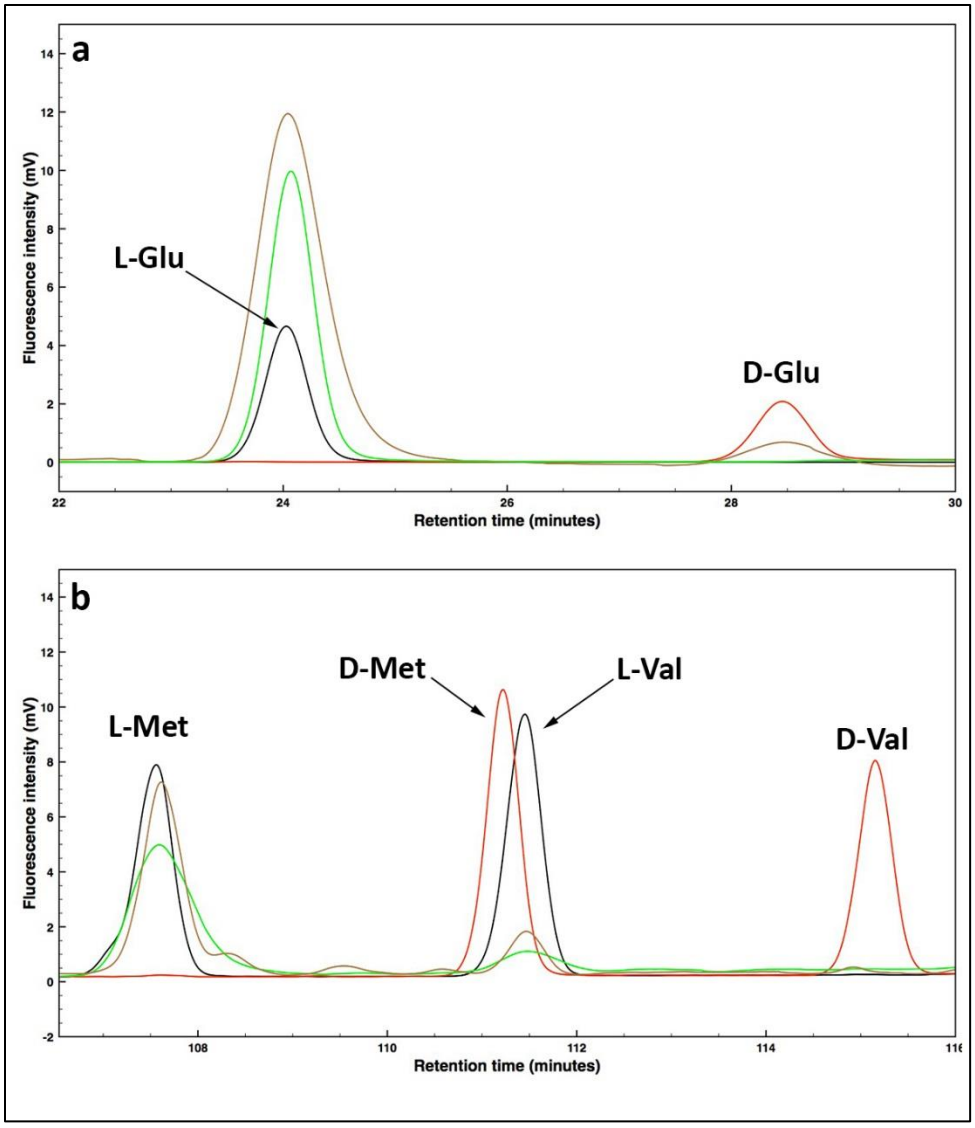

Fig S5. Amino acid analysis of aggregates resultant of UV irradiation (λ_{max} = 254 nm) of mAb in L-Arg formulation (brown trace) and control mAb in L-Arg formulation (green trace). Amino acid standards L-Glu (black trace, a), D-Glu (red trace, a), L-Met (black trace, b), D-Met (red trace, b), L-Val (black trace, b) and D-Val (red trace, b). The HPLC chromatograms are recorded using a fluorescence detector (λ_{ex} = 340 nm and λ_{em} = 455 nm).

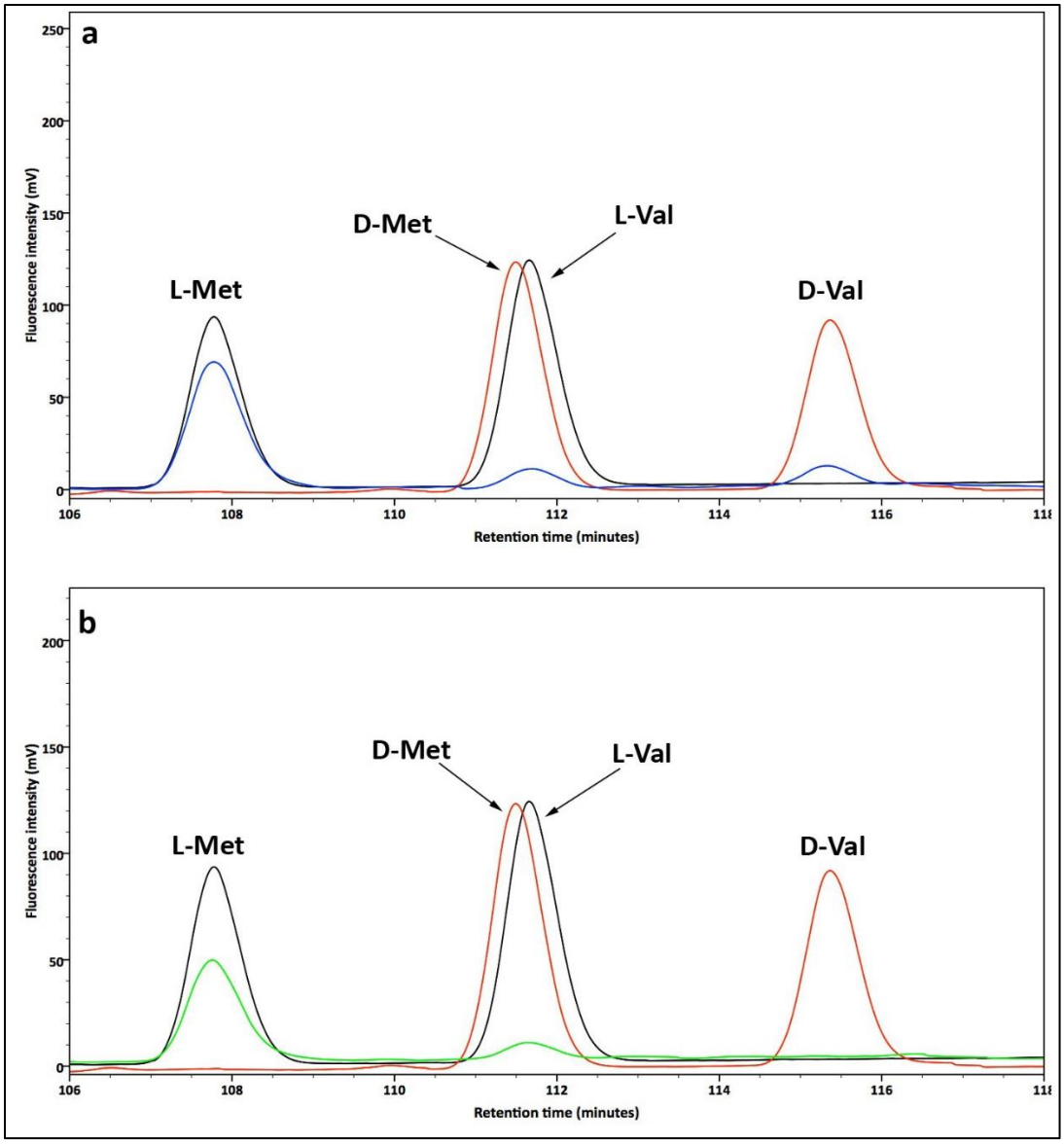

Fig S6. Amino acid analysis of aggregates resultant of UV irradiation (λmax = 305 nm) of mAb in L-Arg formulation (blue trace) and after treating with DAAO (b, green trace). a) Amino acid standards L-Met (black trace), D-Met (red trace), L-Val (black trace), and D-Val (red trace, a). The HPLC chromatograms are recorded using a fluorescence detector (λ_{ex} = 340 nm and λ_{em} = 455 nm).

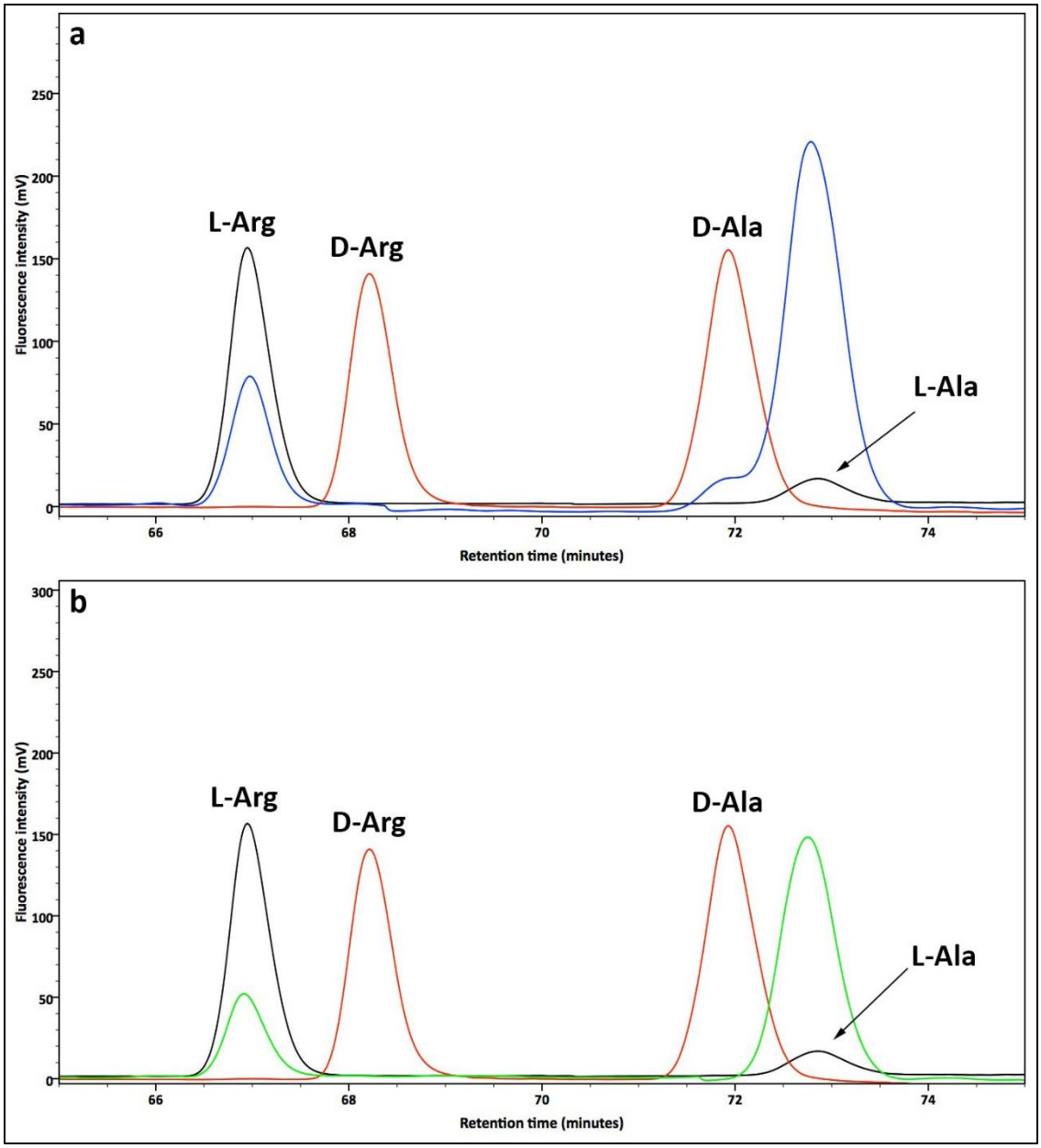

Fig S7. Amino acid analysis of aggregates resultant of UV irradiation (λmax = 305 nm) of mAb in L-Arg formulation (blue trace) and after treating with DAAO (b, green trace). a) Amino acid standards L-Arg (black trace), D-Arg (red trace), L-Ala (black trace), and D-Ala (red trace, a). The HPLC chromatograms are recorded using a fluorescence detector (λ_{ex} = 340 nm and λ_{em} = 455 nm).

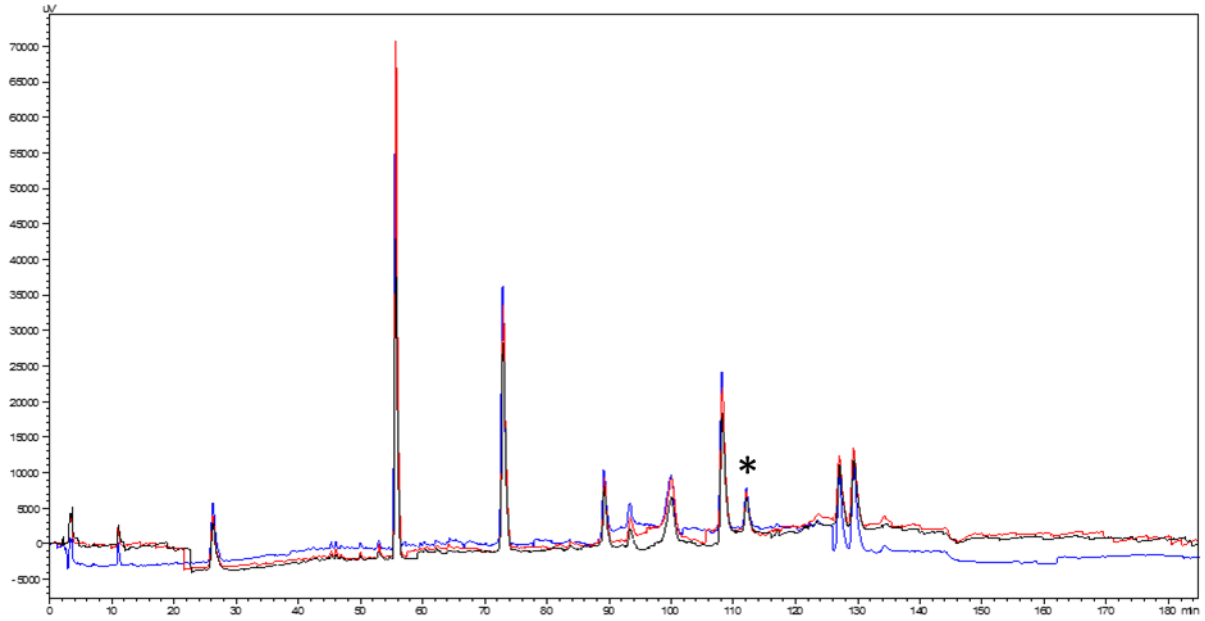

Fig S8. Amino acid analysis of blank (buffer solution, triplicates) after treating with DAAO. The HPLC chromatograms are recorded using a fluorescence detector (λ_{ex} = 340 nm and λ_{em} = 455 nm).

"*" impurity peak co-eluting with D-Val peak during amino acid analysis of protein or peptide hydrolysates.

Chapter 4. Understanding the increased aggregation propensity of a light exposed IgG1 mAb using hydrogen exchange mass spectrometry, biophysical characterization, and structural analysis

4.1 Introduction

Biopharmaceutical drugs are a fast growing class of therapeutics, which include peptides, recombinant therapeutic proteins such as, insulin, monoclonal antibodies and antibody-drug conjugates (ADC).[1] In the past 30 years, the number of biopharmaceutical drugs on the market increased from 13 to 210, amassing US$163 billion in product sales.[2] This increase in demand for biologic drugs revolutionized the development pipelines in many pharmaceutical companies. In the last decade, there was an increase in the number of biotech products (large molecule drugs) in clinical trials by 155%, from 355 in 2001 to 907 in 2012.[2] The extraordinary success of biotech products is attributed to advantages such as high target specificity, high potency and low side effects.[1-4] Currently monoclonal antibodies (mAbs) are the largest selling protein therapeutics in the market, with a global value of US$86.7 billion in 2015.[3]

Therapeutic mAbs are complex glycoproteins that belong to the immunoglobulin (Ig) family. Based on the structure of their constant regions, Ig's are categorized into five groups, IgA, IgD, IgE, IgG, and IgM.[4-5] Currently, most prevalent group of Ig's in the market is IgG. IgGs are composed of two identical light and heavy chains connected through inter-chain disulfide bonds. Each heavy chain is composed of one variable domain (V_H) and three constant domains (C_H1, C_H2 and C_H3). Each light chain is composed of one variable domain (V_L) and one constant domain (C_L). The variable regions of heavy chain and light chain combine to form the antigen-binding site (Fab), whereas the constant regions combine to form the fragment crystallizable (Fc) domain.[4-6] IgGs can be further classified into four subclasses based on the pattern of inter-chain disulfide bonds: IgG1, 2, 3 and 4. Among these four subclasses, IgG1, 2 and 4 are used as therapeutics, while IgG3 is rarely used because of its low serum half-life. [4-7]

Similar to other protein therapeutics, IgG mAbs are prone to various types of chemical and physical instability. Deamidation, oxidation and fragmentation are some of the major forms of chemical instability; correspondingly, aggregation, denaturation and precipitation are some of the major forms of physical instability.[8] These instabilities can lead to loss of activity and, in some cases, can cause unwanted immunogenic responses.[8-11] The chemical and physical stability of therapeutic proteins can be impacted by various external processing-related or handling-related factors such as extreme pH, temperature, freeze thaw, excipient impurities, mechanical stress, light exposure, and so on.[8]

Therapeutic proteins are exposed to light during various stages of their developmental process. Chromatographic processes during purification routinely use UV light (280 nm and 214 nm) for detection. Light exposure can also occur during storage, fill and finish processes, visual inspection and packaging.[12] Some types of protein therapeutics are diluted into IV bags before administering to the patient, where they can be exposed to ambient light.[12, 13] Previous studies have identified traces of UVA and UVB light in emissions of fluorescent lamps. [13, 14]

The aromatic amino acids (Trp, Tyr and Phe), peptide backbone and cysteine (disulfide bonds) are the principal targets of photodegradation in proteins.[12] Photodegradation in proteins begins with absorption of light, resulting in excitation of electron to higher energy state (singlet state) followed by distinct processes including, relaxation by fluorescence to ground state or undergo inter system crossing forming triplet state, reaction with oxygen to generate singlet oxygen ($^1O_2$) species or excited state photochemical processes such as photoionization. Photoionization leads to the release of electron from the residues, resulting in formation of solvated electron (e^-_{aq}) and a radical cation followed by deprotonation yielding an uncharged radical. The reactive oxidation species ($^1O_2$) produced on light exposure can initiate photo oxidation in proteins. [12,15] For

example, UV light exposure of an IgG1 mAb induced oxidation of Trp in a complementarity-determining region (CDR) resulting in significant decrease in its biological activity.[16] Recently various novel modifications were also identified in IgG1 mAbs due to photodegradation, for example, a doubly oxidized His 289 in the Fc region of IgG1,[17] a triply oxidized His,[18] inter molecular His-His crosslinks (220, HC),[19] conversion of Trp to Gly and Gly hydroperoxide,[20] and Trp side chain cleavage products.[18] Another important consequence of light exposure is photoionization, which results in electron transfer to the disulfide bonds, resulting in the formation of thiolate and thiyl radical. A pair of thiyl radicals can also be formed via direct photolysis (at λ = 254 nm) of disulfide bridges. Thiyl radicals can participate in reversible hydrogen transfer reactions with adjacent amino acids leading to the formation of dithiohemiacetal, thioether, vinyl thioether crosslinks and epimerized amino acids.[21,22] All these chemical photodegradation products can act as precursors for physical instability in proteins e.g. aggregation, fragmentation etc. [8]

There are a limited number of studies that have examined the effect of light on physical and conformational attributes in mAbs. Previously Qi et al.[23] have shown formation of yellow color in highly concentrated (100 mg/mL) IgG1 mAbs on exposure to light. In the same study, they also observed a decrease in biological activity and increase in aggregation and fragmentation with increase in duration of light exposure.[23] Mason et al.[24] studied the effect of pH and UVB light (λ_{max} = 302 nm) exposure on protein conformation using various biophysical techniques. By DSC analysis, they identified prominent changes in thermal transition temperatures, indicating a decrease in conformational stability because of light exposure. While the tertiary structure of the mAb remained intact, but analysis of the secondary structure revealed changes in β-sheet structure.[24]

Among the various degradation pathways that occur in mAbs on exposure to light, aggregation has been one of the major concerns, as protein aggregates are potentially immunogenic.[25-27] In consequence, it is important to understand the aggregation pathways of mAbs upon exposure to light.

In this study, we aim to understand the underlying mechanism behind the increased aggregation propensity of an IgG1 mAb due to UVA light exposure. A mAb sample was exposed to UVA light for up to 72 hours followed by isolation of monomer and dimer fractions from the samples formed due to light exposure using SEC coupled to a fraction collector. Hydrogen/deuterium exchange mass spectrometry (H/D-MS) was used to explore changes in local flexibility of isolated monomers, and dimers from the light exposed mAb samples compared to non-light exposed control mAb. Biophysical characterization including far- and near-UV CD and DSC were used to explore changes in secondary and tertiary stricture and thermal stability of the isolated monomers and dimers compared to the control mAb. In conjugation with experimental results, computational analyses were also applied to understand potential molecular mechanisms of higher order structural changes due to light exposure in mAbA and likely pathways of aggregation. The changes observed in higher order structure, thermal stability, and accelerated stability are correlated with changes in local flexibility due to photo-induced chemical changes in the mAb. Moreover, the possible underlying mechanism of increased aggregation propensity due to light exposure is discussed in the context of an established aggregation hotspot in the literature.

4.2 Experimental methods

4.2.1 Materials

MAbA was expressed and purified at Eli Lilly and company, Branchburg, NJ. Deuterium oxide (99+ atom %), tris (2-carboxyethyl) phosphine hydrochloride (TCEP), trifluoroacetic acid (TFA) and iodoacetamide (IAA) were purchased from Sigma Aldrich (St. Louis, MO). Monobasic sodium phosphate monohydrate, dibasic sodium phosphate anhydrous, sodium chloride, LC-MS grade water and acetonitrile (ACN), 10X NUPAGE® reducing agent, Novex sharp pre-stained broad range molecular weight marker and SYPRO Ruby Protein Gel stain were purchased from Fischer scientific (Hampton, NH). Sequencing grade modified trypsin, PNGase F and Glu-c were purchased from Promega (Madison, WI). Guanidine hydrochloride (Gdn-HCl), dithiothreitol (DTT), and Tris hydrochloride (Tris HCl) were purchased from Thermo Scientific (Waltham, MA). Type I glass vials and stoppers were purchased from Schott Glass (Lebanon, PA) and West Pharmaceuticals (West Whiteland, PA), respectively.

4.2.2 UVA light exposure of mAbA

Light exposure experiments were performed using an ICH ES2000 Reach-IN (Environmental Specialties, Inc., Raleigh, NC) photo chamber equipped with near-ultraviolet (UVA) lamps and cool white fluorescent bulbs to allow exposure to UV and visible spectral regions respectively. The near UV lamp has an emission spectrum ranging approximately from 315-400 nm with λ_{max} = 350 nm. UVA light exposure was run at factory 'default' flux conditions of 22 W/m^2. The guidelines for 100% ICH conditions are 200 W h/m^2 of UVA light. [28, 29]

Consistently, 500 µL of mAbA was added to 2 mL type I glass vials capped with autoclaved rubber stoppers and placed vertically in the photo chamber. The samples were irradiated for 9 hours (100% ICH dose = 1X), 24 hours (2.5X ICH) and 72 hours (8X ICH). The chamber temperature was controlled at 25 ^{o}C throughout the light exposure experiments.

4.2.3 Size exclusion chromatography (SEC) analysis and fraction collection

Samples were analyzed using a Dionex (Sunnyvale, CA) high performance liquid chromatography system with UV absorbance detection at 280 nm and 214 nm respectively. A TSKgel G3000SWxl (Tosoh bioscience, King of Prussia, PA) 7.8 mm x 30 cm column with 5 µm particle size was used for SEC analysis. The SEC mobile phase contained 47 mM sodium phosphate and 300 mM sodium chloride, at pH 7. Isocratic flow conditions at 0.5 mL/min with column maintained at 25 ^{o}C was used to separate various sized species present in the mAbA samples. 75 µg of mAbA were loaded on the SEC column per injection. Fractions corresponding to monomer and dimer fractions were collected using the fraction collector connected to the system by making approximately 10 injections. The collected fractions were pooled and concentrated using Amicon Ultra-15 centrifugal devices with 10,000 MWCO membranes.

4.2.4 SEC and multi-angle light scattering (MALS) Analysis

SEC-MALS analysis of mAbA samples was performed using an Agilent (Santa Clara, CA) 1100 HPLC connected to a Dawn HELEOS II MALS detector in series with Optilab rEX refractive index detector (Wyatt Technology Corporation, Santa Barbara CA). 20 µL of mAbA at 2.5 mg/mL protein concentration was loaded on a TSK gel 3000SWXL column (TOSOH biosciences, King of Prussia, PA) connected to the SEC instrument. Data analysis was performed using Astra software Version 6.1 (Wyatt Technology Corporation, Santa Barbara, CA).

4.2.5 Sodium dodecyl sulfate polyacrylamide gel electrophoresis analysis

Nonreducing and reducing (10X NUPAGE® reducing agent) SDS-PAGE analysis were performed on precast Novex 4%-12% Tris-Glycine gels from Invitrogen (Carlsbad, CA). The Novex sharp pre-stained broad range molecular weight marker that covers the range of 3.5–260 kDa was used. 1.25 µg of mAbA was loaded on to each lane and the separation was achieved by using 45 mA and 200 V of electricity for 45 min. The gels were stained with SYPRO Ruby Protein Gel stain for 30 min, followed by destaining for 60 min. Bio-Rad ChemiDoc XRS+ was used to for gel documentation.

4.2.6 Differential scanning calorimetry (DSC)

Monomer and dimer fractions in SEC buffer were diluted to 1 mg/mL protein using 47 mM sodium phosphate and 300 mM sodium chloride, at pH 6.1 and analyzed with a MicroCal VP-Capillary DSC instrument (Malvern instruments Inc, Westborough, Massachusetts). Scans were collected from 20 to 90 ^{o}C at 60 ^{o}C/h. The raw DSC data were buffer and baseline subtracted, concentration normalized, and then fit to a multi-state model with 3 transitions using the MicroCal LLC DSC plug-in for Origin 7.0 software to calculate the thermal transition temperatures. The onset temperature of thermal unfolding (T_{onset}) represent the temperature where the heat capacity value reached 0.2 Kcal/mol ^{o}C. The reported T_m and T_{onset} values are an average of three independent runs.

4.2.7 Circular dichroism (CD) analysis

Far- and near-UV CD data are acquired using a Chirascan Plus CD spectropolarimeter fitted with an autosampler (Applied Photophysics, Leatherhead, UK). Monomer and dimer fractions in SEC

buffer were diluted to 2 mg/mL protein using the same SEC buffer (pH 6.1). The autosampler arm was used to load samples from a plate in to the cuvette and then for washing and rinsing the cuvette following analysis. Far-UV CD data was acquired in a 0.01 cm pathlength flow-through cuvette (Applied Photophysics, Leatherhead, UK) from 190-260 nm wavelength at 1 nm bandwidth, step size of 1 nm, and scan time of 1 sec per point. Near-UV CD data was acquired in a 0.5 cm pathlength open top flow through cuvette (Applied Photophysics, Leatherhead, UK) from 250-350 nm wavelength at 1 nm bandwidth, step size of 1 nm, and scan time of 2 second per point. The reported data are average of three repeat scans for any sample. All CD data were acquired at ambient room temperature. Water and bovine serum albumin standards were analyzed by far- and near-UV CD before and after all sample analyses to confirm no drift of instrument performance from historical data or during the sample runs (data not shown).

4.2.8 Accelerated stability study

500 µL of protein samples were filled into 2 mL type I glass vials and exposed to UVA light for 9, 24 and 72 hours, respectively. The light exposed samples, along with controls (no light exposure), were then subjected to an accelerated stability study in which samples were stored in triplicates at 5 ^{o}C, 25 ^{o}C and 35 ^{o}C and analyzed using SEC after storage for 30 days and 90 days along with initial time point samples.

4.2.9 Intact mass analysis

Monomer and dimer fractions were diluted into LC-MS grade water to a concentration of 0.5 mg/mL protein. 100 µL of a 0.5 mg/mL sample was mixed with 2.5 µL of 1 M Tris-HCl buffer (pH 8.0) and 2 µL of 2 U/mL PNGase F (Promega, Madison, WI). The mixture was incubated overnight at 37 °C. The samples were mixed with 1 µL of 50 mg/mL DTT (in 125mM Tris-HCl

buffer) and incubated at 37 °C for 45 min to reduce the disulfide bonds. 0.5 µg of the reduced protein was injected onto an Acquity UPLC BEH300 C4 1.7 µm, 1.0 X 50 mm column connected to Waters Xevo G2 QTOF (Milford, MA) mass spectrometer operating in ESI positive mode. Mobile phases A and B consisted of 0.05% (V/V) trifluoroacetic acid (TFA) in LC-MS grade water and 0.04% TFA in LC-MS grade ACN, respectively. A linear gradient of 20-90% mobile phase B in 12 min was used at a flow rate of 70 µL/min to elute mAbA from the RPLC column (Acquity UPLC BEH300 C4 1.7 µm, 1.0 X 50 mm). Molecular masses were acquired by deconvoluting the multiply charged ion peaks using the MaxENT procedure in the MassLynx software (Waters, Milford, MA).

4.2.10 Peptide mapping

100 µg of mAbA were mixed with 20 µL of 7 M Gdn-HCl, 125 mM Tris-HCl buffer (pH 8.0). The disulfide bonds of the mAbA samples were then reduced by addition of 1 µL of 50 mg/mL DTT (in 125 mM Tris-HCl buffer) and incubated at 37 °C for 45 min, followed by alkylation with 3 µL of 50 mg/mL IAA (in 125mM Tris-HCl buffer) solution in the dark at room temperature for 30 min. 170 µL of 100 mM Tris buffer (pH 8.0) was then added to achieve a total volume of 300 µL. The reduced and alkylated samples were digested by the addition of 50 µL of 0.1 µg/µL sequencing grade trypsin (enzyme: protein 1: 20, w: w) and incubation at 37 ºC for 2 hours, followed by the addition of 25 µL of 0.1 µg/µL Glu-C (enzyme: protein 1: 40, w: w) and further incubation for 2 hours at 37 ºC. The digestion was quenched by the addition of 1 µL of 50% TFA in water. All the digested samples were analyzed by LC/MS/MS^{E} using a Waters nano Acquity UPLC system coupled to a Waters Synapt G2-S mass spectrometer (Milford, MA). Tryptic peptides were separated using an Acquity UPLC BEH C18 1.7 micrometer, 1.0 X 150 mm reverse phase column and the ions were analyzed by mass spectrometry between values of

m/z 100 and m/z 2000. Data acquisition was achieved in the MS^E continuum mode by ramping up the collision energy from 22 V to 55 V. Mobile phase A was 0.05% (V/V) trifluoroacetic acid (TFA) in LC-MS grade water and mobile phase B was 0.04% TFA in ACN. Peptides were eluted with a linear gradient of 1% B to 35% B in 135 min followed by washing the column with 90% ACN for 15 min, after which the column was equilibrated with 1% ACN for 8 min with a flow rate of 50 µL/min. Trypsin and Glu-C digestion resulted in 95% coverage for both monomer and dimer fractions. Peptide mapping data were analyzed using MassLynx software.

4.2.11 Hydrogen/Deuterium exchange mass spectrometry (H/D-MS)

The monomer and dimer fractions isolated from control and UVA light exposed mAbA were analyzed by H/D-MS using a Waters HDX manager system, connected to a Synapt G2-S mass spectrometer. All the starting protein stocks were adjusted to 10 mg/mL protein using 47 mM sodium phosphate and 300 mM sodium chloride at pH 6.1. Sample preparation for H/D-exchange experiments were carried out using a two-arm H/DX PAL robot (LEAP Technologies, Carrboro, NC). 4 µL mAbA sample was mixed with 76 µL of labeling buffer (47 mM sodium phosphate, 300 mM sodium chloride in 99+ atom% D_2O, pH 6.1) in a 1:20 (v/v) ratio to initiate H/D exchange. The pH values mentioned here are reported as is recorded using a glass pH probe without further conversion to pD. The exchange reaction was quenched at four time points (50, 100, 1000, 10000 sec) by 1:1 dilution (40 µL) with ice-cold quench buffer (0.4 M TCEP, 4 M Gdn-HCl, 200 mM sodium phosphate) at 1 ^oC resulting in a final pH ~ 2.5. The quenched solution is maintained at 1 ^oC. 20 µL of the quenched solution were immediately injected into the sample loop of the refrigerated HDX-Manager compartment, housing the reversed-phase column, trap and the pepsin column at 0.5^oC during the course of the experiments. The samples were passed through an immobilized pepsin column (AB applied science, 2.1 x 30 mm), desalted

on a Waters VanGuard precolumn trap (Acquity UPLC BEH C18 1.7 µm) for 5 min at 0.3 mL/min and then the peptides were separated on a reversed phase column (Acquity UPLC BEH C18 1.7 µm, 1.0 x 50 mm) at a flow rate of 50 µL/min. Mobile phase A was 0.1 % formic acid in LC-MS grade water and mobile phase B was 0.1% formic acid in LC-MS grade ACN. Peptides were eluted with a linear gradient of 3% to 15% mobile phase B in 1 min, followed by linear increase from 15% to 40% in next 5 min and directed in to a Waters Synapt G2-S mass spectrometer running in the positive ESI mode. The data were acquired in the MS^E mode with a scan over m/z 255 to m/z 2000, with lock spray correction using leucine encephalin. Two additional gradients from 40-90% mobile phase B and 3-90% mobile phase B were built at the end of the gradient cycle for each sample injection to allow clean-up of the reversed phase column and trap. In addition, after sample digestion through the pepsin column, two cocktail mixes of a) 5% acetonitrile, 5% isopropanol, and 20% acetic acid in water and b) 2M guanidine hydrochloride in 100mM phosphate at pH 2.5 were injected in 100 µL volumes consecutively to pass through the pepsin column to minimize carry-over.[31] No major carry-over issues were observed following this cleaning protocol for the RPLC column, trap and the pepsin column.

4.2.12 H/D-MS data analysis

A peptide list was generated by identifying the resulting peptide segments after online pepsin digestion of non-deuterated mAbA sample using the BiopharmaLynx software (Waters), with mass tolerance set at 10 ppm for singly charged precursor ions and 30 ppm for MS^E fragment ions. A total of 118 and 112 peptide segments were identified covering approximately 90% and 85% of primary sequence of mAbA in monomer and dimer fractions, respectively. HD Examiner (Sierra analytics, Modesto, CA) was used to calculate the mass increase due to deuterium uptake for the different peptic peptide segments and conditions. Statistically significant differences

between mAbA control and light exposed samples (monomer and dimer fractions) were identified using a 99% confidence interval for the current data set which was calculated using the method of Houde et al.[32] H/D exchange data were mapped onto the homology model of mAbA. Back-exchange measured using fully deuterated control peptide segments ranged from 18-25 %.

4.2.13 Homology model of mAbA, sequence, and structural analysis

Homology modeling was performed based on protein sequence of mAbA in the Molecular Operating Environment (MOE) (Chemical Computing Group, Montreal, Canada), using 1HZH as a template for full IgG1. Amber10: EHT force field was used for the following structural analysis in MOE. Solvent accessible surface area (SASA) and surface exposure (%) for each residue was calculated based on the static model structure using the protein properties analysis module (MOE). Spatial aggregation propensity (SAP) was computed according to the method reported by Chennamsetty et al. (2010) in the Accelrys Discovery Studio 4.0 software (San Diego, CA). The modeled structure of mAbA was also prepared and computed for electrostatic potential using Accelrys Discovery Studio 4.0 software. In addition, the online tool AGGRESCAN was used to analyze primary sequence for the prediction and evaluation of "hot spots" of aggregation in polypeptides. [33] All structure model figures were generated by MOE.

4.3 Results

We start by defining three terms that will be used throughout the remainder of the document. First, the term “control” refers to a mAbA sample that was directly diluted from the stock solution. Second, “dark control” refers to samples that were identically treated as light exposed samples, but placed in a card board box in the photo chamber to prevent light exposure. Third, “stressed” samples refer to mAbA samples that were exposed to UVA light.

4.3.1 UVA light induce increased aggregation with higher exposure time

MAbA samples in 25 mM sodium phosphate buffer (pH 6.1) were exposed to UVA light for various time points: 9 hours (100% ICH dose = 1X), 24 hours (2.5X ICH) and 72 hours (8X ICH). The apparent molar mass of the various sized species generated due to light exposure were independently confirmed using SEC-MALS analysis (Supplementary Material, Fig. S1). The percent of dimers and higher molecular weight species (HMWS) increased with increasing duration of UVA light exposure (Fig 1a). SEC connected to a fraction collector was used to isolate both monomer and dimer fractions. The amount of dimers formed in control and light exposed mAbA samples ranged from 4 – 12%, as measured by SEC. Dark controls contained similar amount of aggregates as the control samples. Approximately 10 injections of each original mAbA sample were made for isolation of monomer and dimer species followed by pooling and concentrating the samples to obtain enough protein quantities for future experiments. The purity of the collected fractions was determined using analytical SEC. Monomer fractions (Fig. 1b) were 98% pure and eluted at approximately 16 min, whereas the dimer fractions (Fig. 1c) were 94 – 96% pure with traces of monomer species and eluted at 14 min. Purified fractions were always stored at 2-8 ^{o}C until further analysis.

Comparison of non-reducing and reducing SDS-PAGE (Supplementary Material, Fig.S2) indicates formation of non-reducible covalent species in light exposed samples. Formation of higher molecular weight species (HMWS) increased (appearance of new bands above the heavy chain band) with increase in the duration of light exposure, which is in agreement with the SEC data. Along with HMWS there was a parallel increase in the formation of fragments, which are detected as lower molecular weight bands observed below the band of intact protein in non-reducing SDS-PAGE.

4.3.2 UVA light induced oxidation of selective Met residues in mAbA

Both monomer and dimer fractions were analyzed using LC-MS to determine the effect of light on chemical degradation of mAbA. Through intact mass analysis (Supplementary Material, Fig. S3), peaks with a mass increase of ~32 Da were identified exclusively on HCs of mAbA samples exposed to light. The intensity of these additional peaks increased with the increase in duration of light exposure. Less intense peaks with a mass increase of ~16 Da were also observed. Peptide mapping was used to identify the distribution of modifications. On analysis, selective peptides with methionine (Met) showed an additional peak with mass increase of 16 Da. It was confirmed by MS/MS that the mass increase was due to the oxidation of Met residues to methionine sulfoxide (MetSO). The extent of oxidation was determined by dividing the extracted ion chromatogram (EIC) peak areas of the MetSO containing peptides by the total peak areas of MetSO containing peptides and non-oxidized Met containing peptides.

There are six Met residues in the heavy chain of mAbA, out of which Met 257 and Met 433 were extensively oxidized in both monomer (Fig. 2a) and dimer (Fig. 2b) fractions. The extent of Met oxidation increased with the duration of light exposure for both monomer and dimer fractions. Table. 1 summarizes oxidation levels of Met residues in UVA light exposed mAbA (monomer) as well as the calculated solvent accessible surface area (SASA) of the respective Met residues. There were some peptides which showed probable low levels of Tyr and His oxidation, but lack of good MS/MS fragmentation to further confirm the modification, limited us in identifying these modifications.

4.3.3 UVA light reduced thermal stability of mAbA monomer and dimer fractions

Thermal unfolding by DSC was used to compare the conformational stability of mAbA monomer and dimers isolated from control and UVA light exposed mAbA samples. Figure 3a shows a representative DSC thermograms of mAbA (1 mg/mL, pH 6.1 in SEC buffer), which display three distinct thermal transition temperatures denoted as T_m1, T_m2, and T_m3. Values for the onset temperatures (T_{onset}) (Table. 2) were also determined. A gradual decrease in T_{onset} and T_m1 were observed for monomers and dimers (Table. 2, Supplementary Material, Fig.S4) collected from mAbA exposed to increasing doses of UVA light. 72 hours UVA light exposure caused ~ 11 ^oC decrease in T_{onset}, ~ 1.4 ^oC decrease in T_m1, ~ 0.5 ^oC decrease in T_m2 in both monomer and dimer fractions compared to the control. ~ 0.5 ^oC and ~ 0.2 ^oC decrease in T_m3 are also observed for monomer and dimer fractions compared to the control mAb.

4.3.4 UVA light exposure induced changes in tertiary structure of mAbA dimers

The near-UV CD data for the monomer and dimer fractions (Fig. 3a, 3b) of mAbA show changes due to light exposure compared to the control. The magnitude of the changes are higher than usual instrument variability, and hence indicate changes in tertiary structure of mAbA due to UVA exposure. The differences are very distinctive in dimer fractions (Fig. 3b) collected from UVA light exposed samples. No differences in near UV-CD spectra was observed between monomer and dimer fractions in the control sample (data not shown).

The far-UV CD data for the monomer and dimer fractions of mAbA (Supplementary material, Fig.S5) show no major changes due to increasing UVA light exposure compared to the control indicating no major change in secondary structure of the monomer/dimer fractions. All the spectra displayed intense negative band between 215-220 nm demonstrating β-sheet rich nature of mAbA. No difference in far UV-CD spectra was observed between control monomer and dimer samples (data not shown).

4.3.5 UVA light exposure decreases accelerated storage stability of mAbA

The impact of pre-exposure to UVA light was assessed on accelerated storage stability of mAbA samples. The protein samples were stored in stoppered type I glass vials at three temperatures (5 ^{o}C, 25 ^{o}C and 35 ^{o}C) for up to 90 days after the light exposure, and analyzed by SEC to quantify the percent of monomer, aggregates and fragments species that were generated. SEC chromatograms of mAbA were analyzed immediately (day 0) after light exposure (9 hours, 24 hours and 72 hours). While non-photo irradiated samples contained predominantly monomer (Fig. 4b), with low levels of aggregates (4.2%, Fig. 4a) and fragments (0.16%, Fig. 4c), whereas mAbA samples exposed to UVA light for 9, 24 and 72 hours contained 6.52% (± 0.32), 8.81% (± 0.47) and 12.82% (± 0.42) of aggregates (Fig. 4a) respectively and 0.27% (± 0.027), 0.39% (± 0.031) and 0.59% (± 0.029) fragments (Fig. 4c), respectively at day 0.

Upon accelerated storage, the light exposed mAbA samples had a major decrease in monomer content and elevation in aggregate and fragment content. For example, the control sample showed only slow increase of aggregate content from 4.2% (± 0.33) at day 0 to 4.57% (± 0.27), 4.7% (± 0.30) and 4.9% (± 0.39) respectively, upon incubation at 5 ^{o}C (black solid line), 25 ^{o}C (black dashed line) and 35 ^{o}C (black dotted line) for 90 days, respectively, but the 72 hours

photo-irradiated sample showed a rapid increase in aggregate content from 12.82% (± 0.71) at day 0 to 19.89% (± 0.93), 23.86% (± 0.56) and 25.69% (± 0.82) on incubation for 90 days at 5 ^{o}C (blue solid line), 25 ^{o}C (blue dashed line) and 35 ^{o}C (blue dotted line), respectively (Fig. 4a). Similarly, other stressed (9 hours and 24 hours UVA light exposed) samples also exhibited rapid decrease of monomer and increase of aggregate content, compared to control samples (Fig. 4).

4.3.5 H/D-MS analysis of mAbA monomers and dimers

H/D-MS analysis was used to evaluate the changes in local dynamics of mAbA due to UVA light exposure. MAbA monomer and dimers fractions generated due to 72 hours UVA light exposure along with the control mAbA monomer sample were labeled with deuterium using deuterated solutions containing 47 mM sodium phosphate and 300 mM sodium chloride (pH 6.1) in 99+ atom % D_2O at 25 ^{o}C. The exchange was quenched at different time points (50 sec, 100 sec, 1,000 sec and 10,000 sec), followed by proteolysis using a pepsin column and analysis by LC-MS. A total of 118 and 112 peptide segments were identified covering approximately 90% and 85% of the primary sequence in the monomer and dimer fractions, respectively, collected from mAbA which was exposed to light for 72 hours.

Deuterium uptake plots were generated for each peptide by plotting the mass increase for each peptide vs exposure time (seconds) in D_2O. Fig. 5 shows deuterium uptake plots of six representative peptide segments from mAbA control monomer, and monomer and dimers from 72 hours light exposed mAbA. Comparison of the H/D exchange profiles of 118 peptic peptide segments showed no significant changes in deuterium uptake for majority of the peptide segments compared between control and 72 hours UVA light exposed monomer or dimer species. However, three specific segments (Fig.5) HC 147 - 156 in the C_H1 domain, HC 242–256

and HC 301–323 in the C_H2 domain showed increased in deuterium uptake in both UVA exposed monomer and dimer samples compared to the control monomer. For example, in monomer fractionated from 72 hours UVA light exposed mAbA the HC 247–256 segment (peptide number 53) in the C_H2 domain exchanged more quickly with largest difference, relative to the control evident at 50 sec. In the C_H2 domain there were also a series of overlapping peptide segments (Supplementary Material, Fig.S6) covering HC 242-256, which are located at the N-terminus of the C_H2 domain displayed increased deuterium uptake in UVA light exposed monomer and dimer when compared to control monomer.

H/D-MS analysis of dimer fractions revealed several segments with increased deuterium uptake, (Fig.5 and Supplementary material, Fig.S7) HC 116-125, and HC 155-170 in C_H1 domain, HC 242-256, and HC 301-315 in C_H2 domain and HC 376–385 in C_H3 domain indicating regions with decreased strength of H-bonding or increased solvent exposure due to UVA light induced chemical changes. Analysis also revealed several segments, HC 51–59 in V_H domain, HC 204–213 in C_H1 domain and LC 95–99 in V_L domain with decrease in deuterium uptake as compared to control monomer.

Differential exchange plots were used to visualize and estimate the impact of light induced chemical changes on H/D exchange across all the mAbA peptides. The relative mass difference (Δm) is the difference in average mass of a peptide segments between two states, (eg. state 1: light exposed and state 2: control).

Ordinal numbers (peptide numbers) were assigned to each peptide segment based on the ascending order of sequence midpoint of each peptide segment from the N-terminus to the C-terminus. The relative mass difference (Δm) for each peptide segment was plotted on the vertical

axis vs the peptide number on the horizontal axis of the difference plots (Fig. 6). MAbA segments with positive Δm indicate regions of increased deuterium uptake, implying increase in local flexibility due to UVA light exposure, whereas negative Δm indicate regions of decreased deuterium uptake implying decrease in local flexibility. A 99% confidence interval of ± 0.59 Da (Supplementary material, Fig.S8) was calculated based on the standard deviations from the entire dataset and is represented by a black horizontal dashed line in Figure. 6. A measured Δm greater or smaller than 0.59 Da for at least one labeling time point indicate a significant difference in local flexibility in the corresponding peptide segment. Most regions of mAbA monomers or dimers did not have any significant changes in flexibility due to UVA light exposure, whereas few segments had statistically significantly changes.

Following analysis, the segments showing significant changes in deuterium uptake are color coded on to the homology model of mAbA (Fig. 7a, 7b). Regions with significant increase and decrease in deuterium uptake are color coded with red and blue, respectively.

4.3.7 Structure-based and sequence-based computational analysis of mAbA

Three-dimensional structure based analysis of mAbA including SAP (spatial aggregation propensity), SCM (spatial charge map) and other molecular descriptors were calculated (Supplementary material, Fig.S9). The results indicated that mAbA bear hydrophilic surface overall, with a net charge of 9.3 when calculated at pH 6.1. Furthermore, there is no strong negatively charged patch or charge imbalance identified on the surface of the mAbA by SCM analysis or electrostatic potential analysis. The three regions with decreased deuterium uptake identified from dimer sample, one (HC 204-213) is the outer β-sheet stretch located on C_H1 domain, adjacent to the region showing increased deuterium uptake (HC 151-170), an inner β-

sheet on C_H1 (Fig. 8b). The other two regions with decreased uptake are located on the Fv domain; composed of a partial CDR-H2 loop and CDR-L3 loop (Fig. 8a). A closer look of these regions reveals that charge and polar residues (D, E, K, Y, N) are dominant on the surface, with the exception of a surface exposed Trp residue. On the other hand, plotting the regions with increased deuterium uptake (either monomer or dimer) indicates that they are predominantly located at the constant regions of mAbA (C_H1, C_H2 and C_H3) and mostly buried or partially buried. HC 116-125 is the linker connecting the Fv to the C_H1 domain, it is known to be a flexible region involving elbow movement of the F_{ab} domain. HC 151-170 is a long stretch consisting of two anti-parallel β-sheets, located at the center of C_H1 domain. The other three regions (major increase of uptake) cluster around the inner core of the C_H2 domain (2 β-sheets), plus a nearby loop on the top of the C_H3 that interfacing with the C_H2 domain. The β-sheet (HC 242-256) with the most significant increase in deuterium uptake is directly adjacent to the carbohydrates packed between the two C_H2 domains of the Fc dimer. The last residue of this region (HC 242-256) is followed directly by Met 257, located at the C_H2-C_H3 elbow. Met 257 and Met 433, the top two residues showing highest rate of oxidation upon photo-stress of mAbA are three-dimensionally close with each other.

In addition to the spatial aggregation propensity analysis, AGGRESCAN was used to probe the aggregation prone sequences in the constant domains of mAbA based on the primary sequence. The hot spots identified by AGGRESCAN included HC 144-155, HC 176-193, HC 243-248, HC 303-316, and HC 367-378, which are then plotted on the mAbA homology model (Fig. 7c). In comparison with the plot based on the HDX results of dimer (Fig. 7b), several AGGRESCAN hot spots overlap and coincide with the regions of increased uptake.

4.4 Discussion

Protein aggregation represents a process during which two or more protein molecules (monomers) associate to form stable complexes. Aggregates may be tethered by strong non-covalent/covalent forces, which may require a marked level of conformational alteration (unfolding or misfolding) in order to expose highly aggregation-prone sequence of amino acids (aggregation "hot spots"), which may form strong inter-protein contacts between the monomers.[34] The aggregation propensity of a given protein can be influenced by its environmental factors such as, the solution pH, ionic strength, concentration of co-solutes, mechanical stresses, exposure to light, etc.[8]

The main aim of this study was to investigate the molecular mechanism of increased aggregation propensity of an IgG1 mAb following exposure to UVA light. Light exposure of protein therapeutics has been known to induce oxidation, fragmentation, covalent cross-links, discoloration, yellow color formation and aggregation.[16-24] In this study, a monoclonal antibody of IgG1 subclass, mAbA was exposed to UVA light for three different time points: 9 hours (100% ICH), 24 hours (2.5X ICH) and 72 hours (8X ICH). SEC was used to separate and collect monomer and dimer fractions of the UVA exposed mAbA sample, and the fractions were analyzed by a variety of techniques to monitor their conformational, physical and chemical stability as well as aggregation propensity on storage. A dependence of duration of light exposure on the rate of aggregation of mAbA on accelerated storage was observed from SEC (Fig. 1a) and SDS-PAGE (Fig. S2) data. The extent of aggregation increased with an increase in the duration of light exposure. Non-reducible covalent species with molecular weight ranging approximately between 140 kD – 260 kD were identified upon UVA light exposure (Fig. S2).

The amount of non-reducible species also increased with increase in duration of light exposure, the trend being 9 hours < 24 hours < 72 hours. The high degree of covalent character in UVA light exposed mAbA can be rationalized by the formation of photo induced non-reducible covalent crosslinks. Previously Liu et al. [19] have discovered formation of photo-oxidative cross-links across two identical conserved His residues on two separate heavy chains. In other studies, Mozziconacci et al. [21, 22] have identified formation of thioether, vinyl thioether and dithiohemiacetal crosslinks. The cleavage and formation of these C-S (carbon-sulfur) crosslinks may occur through photo induced homolytic cleavage of the disulfide bonds. These type of covalent crosslinks could account for the multiple non-reducible higher molecular weight species detected by reduced SDS-PAGE analysis.

The majority of IgG1 and IgG2 class mAbs have two conserved Met residues, Met 257 and Met 433 located in the C_H2 and C_H3 domains, respectively. In this study, UVA light exposure of mAbA resulted in extensive oxidation of Met 257 and Met 433 in both monomer (Fig. 2a) and dimer (Fig. 2b) fractions. Similar observations were made by Liu et al.[35] where they observed preferential oxidation of Met 257 and Met 433 in another light exposed IgG1 mAb. The oxidation of these Met residues [to Met sulfoxide (+16) or Met sulfone (+32)] has been shown to decrease circulation half-life, protein A binding, FcRn binding and thermal stability.[36-38] Oxidation of mAbA upon light exposure may involve formation of reactive oxygen species (ROS) such as: singlet oxygen, superoxide and hydrogen peroxide, which are shown to oxidize the proteins.[12, 39] For example, Alavattam et al.[39] have shown that the surface exposed Trp residues are capable of transferring light energy to oxygen, converting it to various ROS and finally into hydrogen peroxide which led to chemical instability of a mAb.

In this study, we observed extensive oxidation of Met 257 and Met 433 residues, with SASA values of 27.96 and 0, respectively (Table.1). Residues that are more solvent exposed were anticipated to be more available for chemical degradation. On contrary, Met 433 with zero SASA was highly oxidized. This could be because of its close proximity to Met 257 (highly oxidized), which may induce oxidation of Met 433 due to small conformational changes due to oxidation.[40,41]

To understand the effect of light exposure on mAbA and to study the underlying mechanism of aggregation, we investigated the conformation of mAbA before and after UVA light exposure. DSC is normally used to test the thermal stability of proteins.[42,43] In our study, thermograms of intact mAbA revealed three transitions. The transition with largest experimental enthalpy represents unfolding of the Fab segment, while the second and third transition temperatures represent unfolding of C_H2 and C_H3 domains, respectively.[42,43] From the data (Table. 2), it is evident that the UVA light exposure affects the thermal stability of mAbA. There was decrease in T_{onset} and T_{m1} by ~11 ^oC and ~1.4 ^oC, respectively in 72 hours UVA light exposed monomer when compared to control monomer and decrease in T_{onset} and T_{m1} by ~11 ^oC and ~1.4 ^oC, respectively in dimer fractionated from 72 hours UVA light exposed sample when compared to control dimer. Monomer and dimer fractions separated from mAbA samples exposed to increasing durations of UVA light, showed decrease in T_{onset} and T_{m1} values, while the T_m2 and T_m3 unfolding transitions showed relatively smaller decreases (~ 0.5 ^oC). Larger decreases in T_{onset} and T_{m1} values indicate changes in conformational stability in the F_{ab} domain resultant of light exposure.

Analyzing the dimer species fractionated from UVA light exposed samples, near-UV CD (Fig. 3a, 3b) detected significant changes in tertiary structure on UVA light exposure. This indicates

that, the environment of the disulfide bonds, and aromatic residues in the antibody are impacted by the chemical changes on UVA light exposure. Methionine oxidation along with changes in dynamics could cause disruption of tertiary structure of light exposed dimer samples when compared to control dimer. However, only minor changes in the magnitude of MRE was observed and no new peaks or deletion of peaks were observed indicating the changes in tertiary structure of mAbA was not extensive due to light exposure. No changes were observed by far UV-CD between the UVA light exposed monomer, dimer and the control indicating insignificant changes to the secondary structure.

To understand the impact of UVA light exposure on accelerated storage stability, a study was performed, where mAbA samples were exposed to various durations of light exposure (9 hours, 24 hours and 72 hours) followed by incubation at different temperatures (5 ^{o}C, 25 ^{o}C and 35 ^{o}C) for up to 90 days and later analyzed using SEC. The results (Fig. 4) indicate that 72 hours of light exposure resulted in significant increase in aggregation from approximately 12.82% at time zero to 25.69%, as compared to increase from 4.2% to 4.7% for control sample on storage at 35 ^{o}C for 90 days. This data proved that chemical changes imparted to the mAb due to light exposure significantly increase the aggregation propensity of mAbA on accelerated storage conditions.

4.4.1 Identification of potential aggregate interfaces in dimers formed resultant of UVA light exposure

H/D-MS analysis of dimers fractionated from 72 hours UVA light exposed mAbA revealed (Fig. 5) peptide segments with increase in protection against deuterium uptake. Three segments HC 204–213, HC 51–59, and LC 95–99 showed significant protection towards hydrogen exchange in

the dimer fraction. Segment HC 204-213 is located in the C_H1 domain, whereas HC 51–59, and LC 95–99 are located in the F_{ab} arm. Interestingly, HC 204-213 segment shares some of the same residues as in HC 206-242 has been previously identified by Iacob et al.[30] as an aggregation interface in a native (not result of any stress) IgG1 mAb dimer, also showing protection towards exchange in dimer form compared to monomer.

Identification of segments with decrease in uptake in F_{ab} and C_H1 regions demonstrate probable formation of F_{ab}-F_{ab} or F_{ab}-C_H1 or C_H1-C_H1 interfaces in the dimers. However, long distance interactions between specific segments cannot be ruled out based on the results of H/D exchange results alone. Previously several groups have examined protein-protein interfaces of antibody aggregates. For example, Arora et al.[44] have identified the interface of reversible self-association in the F_{ab} region in IgG1 mAb at high concentration. Hydroxyl radical foot printing was used to locate the interface of the antibody dimer by Deperatla el al.[45]. Zhang et al.[46] identified Fab-Fab interactions in the CDR region in irreversible aggregates generated resultant of heat exposure.

4.4.2 Integrating experimental data with structural and computational analysis

Comparison of the H/D-MS data of monomer and dimer plotted on the mAb structure (Fig. 7a, 7b) revealed one interesting feature, which is that the additional peptide regions with increased uptake (on dimer species) reside on area of inter-domain interfaces. HC 116-125 is the linker between V_H and C_H1 domain; and HC 376-385 is a turn between the two β-sheets of C_H3 domain, contributing to the C_H2-C_H3 interface. It suggests that the active regions (increase uptake) spread from one domain to another domain through either linker or direct contacts. In combination of the findings from the near-UV CD experiment (Fig. 3a, 3b), which indicated additional tertiary structure changes in dimer, one can imagine that the local structural

perturbation in monomer (intra-domain) likely propagate to other domains in dimer species (inter-domain). This could be the result of dimer formation or one leading reason of dimer association.

The common implication of decreased uptake is that the regions are protected by protein-protein interactions. The three regions with decreased uptake in dimer species are surface exposed peptide segments, all on the Fab domain (Fig. 7b), suggesting F_{ab}-mediated dimer formation. Among them, HC 51-59 and LC 95-99 are part of CDR-H2 and CDR-L3 loop, unique to mAbA. Three-dimensionally, they form a connected stretch on the F_{ab} CDR surface, which was named as site 1 (Fig. 8c). The global surface feature of mAbA is hydrophilic based on SAP, SCM and electrostatic potential analysis. Zooming into the site 1 area on the F_{ab} CDR surface, there is a small but strong hydrophobic spot (Tyr 94 of LC) standing out in the region of LC 95-99 (Fig. 8c). The rest of the surface in this protected area consists mostly charged and polar resides (K, D, E, Y). The SAP hotspot (Tyr 94 of LC) may drive dimeric association. Yet we cannot rule out intermolecular interaction of mAbA through charge or polar interactions. The third peptide region with decreased uptake (HC 204-213) is further down in C_H1 domain that precedes the upper hinge of mAbA and was named site 2 (Fig. 8d). Taking into account the locations of these protected regions and the geometry of IgG structure, more than one potential orientations likely co-exist for the dimeric association for mAbA after UVA exposure. Dimeric interfacing through site 1 is likely a head to head contact by the F_{ab} arms of two mAbA, which resembles the elongated form described by Plath et al.[47]. On the other hand, dimer association through the site 2 is likely the side to side interaction through C_H1 domain, an example shown as the compact form by Plath et al.[47] Presumably site 2 dimer association is common to all IgGs, whereas site 1 dimer association is mAbA specific.

In this study, the hotspots identified by AGGRESCAN based on sequence analysis coincide with several regions with increased deuterium uptake, which are also the hydrophobic cores of the constant domains. The two methionines with highest oxidation upon UVA light exposure (Met 257 and Met 433) are located at the elbow regions between C_H2 and C_H3 domains. Met 257 is directly connected to the strand (HC 242 - 256, highest uptake). Met 433 is close to the strand (HC 376 - 385, increased uptake) in C_H3. It is plausible that the oxidation of Met 257 and Met 433 upon light exposure induces local perturbations and populates firstly to regions of proximity within the C_H2 domain and C_H3 domain, displaying increased uptake. If local structural changes lead to domain unfolding, the AGGRESCAN predicted hotpots could be the sites that are prone to start a cascade of events that lead to high molecular weight aggregate formation.

4.4.3 Changes in thermal stability do not correlate with local flexibility

DSC data showed small changes in T_m2 and T_m3 in the 72 hours light exposed sample, indicating that the chemical changes and the significant increases in flexibility observed in the C_H2 and C_H3 domains have minor impact on thermal stability of these domains in mAbA. However, DSC indicated somewhat larger changes in T_{onset} and T_m1 in the 72 hours light exposed monomer sample compared to the control monomer in spite of no major chemical changes seen in the Fab, except a significant increase in local flexibility of the 147-156 segment in the C_H1 domain. Several other segments in the Fab experienced changes in flexibility in the dimer, however no major changes in thermal stability was observed between the dimer and monomer fractions. This shows a total lack of correlation between large changes in thermal stability and local flexibility in the Fab region.

4.4.4 Changes in local flexibility of 'aggregation hotspots' induce higher aggregation

UVA light exposure caused significant increases in local flexibility in two particular domains: in the C_H1 domain (HC 147 – 156), and in the C_H2 domain (HC 242-256 and HC 301-323) of monomer fractionated from 72 hours UVA light exposed mAbA (Fig. 5). In contrast, significant increases in local flexibility in dimer fractionated from 72 hours UVA light exposed mAbA were identified in three particular domains: in the C_H1 domain (HC 116 – 125, and HC 151- 170), in the C_H2 domain (HC 242-256, and HC 301-323), and in the C_H3 domain (HC 376–385). The largest increase in local flexibility was observed in the two specific segments of the C_H2 domain that are predicted to be aggregation prone by the sequence based predictor (AGGRESCAN). These hydrophobic segments in the C_H2 domain of mAbA likely initiate the aggregation pathway. Previously several studies have shown that increased flexibility in the same segments in the C_H2 domain as is observed in this study is correlated with loss of stability in IgG1 mAbs. [48-50] A conformational comparison between mAb dimer and monomer by Iacob et al.[30] revealed rapid deuteration of the same segment in the C_H2 domain in the dimer demonstrating an increase in local flexibility in this region on dimer formation. Other researchers have shown that oxidation of Met 257 in IgG1 mAbs resulted in increased deuterium uptake in an 11-amino acid segment (FLFPPKPKDTL) that also cover the 242-256 segment in the C_H2 domain in mAbA located immediately before Met 257.[32,41] It has been postulated that oxidation of Met 257 and Met 433 increase the distance between two sulfur atoms, thus disrupting the hydrophobic interactions therefore resulting in increase in local dynamics.[41]

Photo-stability is routinely screened for new candidate mAbs in preclinical development. Generally, an appropriate control strategy is designed for candidates that show greater degradation liability on photo-exposure. Exploring the correlations between photo-induced damage such as oxidation in case of mAbA, conformational and accelerated storage stability, changes in local flexibility, and computationally predicted aggregation hotspots can identify aggregation prone sequences in a mAb. Such information may be used during protein engineering to reduce the potential for long term aggregation propensity thereby increasing the safety of these types of biotherapeutics. Future studies may be designed with mAbs looking at the impact on aggregation propensity due to different types of light-induced chemical degradation. One way to limit oxidation in such studies will be to do the photo-exposure experiments in sealed vials containing only nitrogen in the headspace. Moreover, the similarity of the data presented in this report with data from other mAbs can also produce platform learning for IgG1 mAbs.

4.5 Conclusions

Comprehensive understanding of aggregation propensity of protein pharmaceuticals is a vital task in development of protein therapeutics in the biopharmaceutical industry. In this study, we demonstrated use of H/D-MS to explore changes in local flexibility due to UVA light exposure on an IgG1 mAb accompanied with computational analysis for identification of aggregation prone regions, and biophysical analysis using circular dichroism and differential scanning calorimetry to explore changes in higher order structure and thermal stability. Our results indicate that UVA light exposure induced methionine oxidation, caused larger changes in the F_{ab} domain with smaller changes in C_H2 and C_H3 domains, and increased deuterium exchange in

three segments in the C_H2 and C_H3 domains in the monomer and dimer. We also identified formation of possible F_{ab}-F_{ab} and F_{ab}-C_H1 interaction interface in dimers, formed resultant of UVA light exposure. Computational analysis identified potential aggregation prone regions in C_H2 and C_H3 domains of the mAbA. Increased deuterium exchange was specifically observed in two of these aggregation hotspots (HC 242 – 256, and HC 376 - 385) in the 72 hours light exposed mAbA monomer and dimer fractions. Hence increased local flexibility in the C_H2 domain due to UVA light exposure correlates with increased aggregation propensity of this IgG1 mAb.

4.6 References

1. Walsh G. Biopharmaceutical benchmarks. Nat Biotechnol. 2014; 32(10): 992-1000.

2. Mitragotri S, Burke A P, Langer R. Overcoming the challenges in administering biopharmaceutical: formulation and delivery strategies. Nat Rev Drug Discov. 2014; (13): 655-672.

3. Udpa N, Million P R. Monoclonal antibodies biosimilars. Nat Rev Drug Discov. 2016; (15): 13-14.

4. Hansel T T, Kropshofer H, Singer T, Mitchell A J, George T J A. The safety and side effects of monoclonal antibodies. Nat Rev Drug Discov. 2010; (9): 327-338.

5. Justin K H L. The history of monoclonal antibody development–Progress, remaining challenges and future innovations. Ann Med Surg. 2014; (3.4): 113-116

6. Nelson A L, Dhimolea, E. and Reichert, J.M. Development trends for human monoclonal antibody therapeutics. Nat Rev Drug Discov. 2010; (9): 767–774.

7. Buss N A, Henderson S J, McFarlane M, Shenton J M, de Haan L. Monoclonal antibody therapeutics: history and future. Curr Opin Pharmacol. 2012; (12.5): 615-622.

8. Manning M C, Chou D K, Murphy B M, Payne R W, Katayama D S. Stability of protein pharmaceuticals: an update. Pharm Res. 2010; 27 (4): 544-575.

9. Zheng J Y, Janis L J. Influence of pH, buffer species, and storage temperature on physicochemical stability of a humanized monoclonal antibody LA298. Int J Pharm. 2006; 308 (1): 46-51.

10. Bertolotti-Ciarlet A, Wang W, Lownes R, Pristatsky P, Fang Y, McKelvey, Li Y, Li Y, Drummond J, Prueksaritanont T, Vlasak J. Impact of methionine oxidation on the binding of human IgG1 to FcRn and Fcγ receptors. Mol Immunol. 2009; 46(8): 1878-1882.

11. Wang W, Singh S K, Li N, Toler M. R, King K R, Nema S. Immunogenicity of protein aggregates concerns and realities. Int J Pharm. 2012; 431(1): 1-11.

12. Kerwin B A, & Remmele R L. Protect from light: photodegradation and protein biologics. J Pharm Sci. 2007; 96(6): 1468-1479.

13. Sreedhara A, Glover Z K, Piros N, Xiao N, Patel A, Kabakoff B. Stability of IgG1 monoclonal antibodies in intravenous infusion bags under clinical in-use conditions. J Pharm Sci. 2012; 101(1): 21-30.

14. Sayre R M, Dowdy J C, Poh-Fitzpatrick M. Dermatological risk of indoor ultraviolet exposure from contemporary lighting sources. Photochemi Photobiol. 2004 80(1): 47-51.

15. Davies M J. Singlet oxygen-mediated damage to proteins and its consequences. Biochem Biophys Res Commun. 2003; 305(3): 761-770.

16. Wei Z, Feng J, Lin H Y, Mullapudi S, Bishop E, Tous G I, Cases-Finet J, Hakki F, Strouse R, Schenerman M A. Identification of a single tryptophan residue as critical for binding activity in a humanized monoclonal antibody against respiratory syncytial virus. Anal Chem. 2007; 79(7): 2797-2805.

17. Amano M, Kobayashi N, Yabuta M, Uchiyama S, & Fukui K. Detection of histidine oxidation in a monoclonal immunoglobulin gamma (IgG) 1 antibody. Anal Chem. 2014; 86(15): 7536-7543.

18. Bane J, Mozziconacci O, Yi L, Wang Y J, Sreedhara A, Schöneich C. Photo-oxidation of IgG1 and Model Peptides: Detection and Analysis of Triply Oxidized His and Trp Side Chain Cleavage Products. Pharm Res. 2017; 34(1): 229-242.

19. Liu M, Zhang Z, Cheetham J, Ren D, Zhou Z S. Discovery and characterization of a photo-oxidative histidine-histidine cross-link in IgG1 antibody utilizing 18O-labeling and mass spectrometry. Anal Chem. 2014; 86(10): 4940-4948.

20. Haywood J, Mozziconacci O, Allegre K M, Kerwin B A, Schöneich C. Light-induced conversion of Trp to Gly and Gly hydroperoxide in IgG1. Mol Pharm. 2013; 10(3): 1146-1150.

21. Mozziconacci O, Kerwin B A, Schöneich C. Photolysis of an intrachain peptide disulfide bond: primary and secondary processes, formation of H2S, and hydrogen transfer reactions. J Phys Chem B. 2010; 114(10): 3668-3688.

22. Mozziconacci O, Kerwin B A, Schöneich C. Exposure of a monoclonal antibody, IgG1, to UV-light leads to protein dithiohemiacetal and thioether cross-links: a role for thiyl radicals?. Chem Res Toxicol. 2010; 23(8): 1310-1312.

23. Qi P, Volkin D B, Zhao H, Nedved M L, Hughes R, Bass, Yi C S, Panek E M, Wang D, Dalmonte P, Bond, M. D. Characterization of the photodegradation of a human IgG1 monoclonal antibody formulated as a high-concentration liquid dosage form. J Pharm Sci. 2010; 98(9): 3117-3130.

24. Mason B D, Schöneich C, Kerwin B A. Effect of pH and light on aggregation and conformation of an IgG1 mAb. Mol Pharm. 2012; 9(4): 774-790.

25. Purohit V S, Middaugh C R, Balasubramanian S V. Influence of aggregation on immunogenicity of recombinant human Factor VIII in hemophilia A mice. J Pharm Sci. 2006; 95(2): 358-371.

26. Rosenberg A S. Effects of protein aggregates: an immunologic perspective. AAPS J. 2006; 8(3): E501-E507.

27. Fradkin AH, Mozziconacci O, Schöneich C, Carpenter JF, Randolph TW. UV photodegradation of murine growth hormone: chemical analysis and immunogenicity consequences. Eur. J. Pharm Biopharm. 2014; 87(2): 395-402.

28. ICH harmonized tripartite guideline: guideline for the photostability testing of new drug substances and products. J Postgrad Med 47: 264.

29. Hawe A, Wiggenhorn M, van de Weert M, Garbe JH, Mahler HC, Jiskoot W. Forced degradation of therapeutic proteins. J Pharm Sci. 2012; 101(3): 895-913.

30. Iacob R E, Bou-Assaf G M, Makowski L, Engen J R, Berkowitz S A, Houde D. Investigating monoclonal antibody aggregation using a combination of H/DX-MS and other biophysical measurements. J Pharm Sci. 2013; 102(12): 4315-4329.

31. Majumdar R, Manikwar P, Hickey JM, Arora J, Middaugh CR, Volkin DB, Weis DD. Minimizing carry-over in an online pepsin digestion system used for the H/D exchange mass spectrometric analysis of an IgG1 monoclonal antibody. J Am Soc Mass Spectrom. 2012; 23(12): 2140-2148.

32. Houde D, Berkowitz S A, Engen J R. The utility of hydrogen/deuterium exchange mass spectrometry in biopharmaceutical comparability studies. J Pharm Sci. 2011; 100: 2071−2086.

33. bioinf.uab.es/aggrescan/

34. Roberts CJ. Therapeutic protein aggregation: mechanisms, design, and control. Trends in Biotechnol. 2014; 32(7): 372-80.

35. Liu H, Gaza-Bulseco G, Zhou L. Mass spectrometry analysis of photo-induced methionine oxidation of a recombinant human monoclonal antibody. J Am Soc Mass Spectrom. 2009; 20(3):525-8.

36. Liu D, Ren D, Huang H, Dankberg J, Rosenfeld R, Cocco MJ, Li L, Brems DN, Remmele Jr RL. Structure and stability changes of human IgG1 Fc as a consequence of methionine oxidation. Biochemistry. 2008; 47(18):5088-100.

37. Bertolotti-Ciarlet A, Wang W, Lownes R, Pristatsky P, Fang Y, McKelvey T, Li Y, Li Y, Drummond J, Prueksaritanont T, Vlasak J. Impact of methionine oxidation on the binding of human IgG1 to FcRn and Fcγ receptors. Mol Immunol. 2009; 46(8):1878-82.

38. Wang W, Vlasak J, Li Y, Pristatsky P, Fang Y, Pittman T, Roman J, Wang Y, Prueksaritanont T, Ionescu R. Impact of methionine oxidation in human IgG1 Fc on serum half-life of monoclonal antibodies. Mol Immunol. 2011; 48(6): 860-6.

39. Sreedhara A, Lau K, Li C, Hosken B, Macchi F, Zhan D, Shen A, Steinmann D, Schöneich C, Lentz Y. Role of surface exposed tryptophan as substrate generators for the antibody catalyzed water oxidation pathway. Mol. Pharm. 2012; 10(1): 278-288.

40. Xu K, N Uversky V, Xue B. Local flexibility facilitates oxidization of buried methionine residues. Protein Pept Letters. 2012; 19(6): 688-97.

41. Zhang A, Hu P, MacGregor P, Xue Y, Fan H, Suchecki P, Olszewski L, Liu A. Understanding the conformational impact of chemical modifications on monoclonal antibodies with diverse sequence variation using hydrogen/deuterium exchange mass spectrometry and structural modeling. Anal Chem. 2014; 86(7): 3468-3475.

42. Garber E, Demarest SJ. A broad range of Fab stabilities within a host of therapeutic IgGs. Biochem. Biophys Res Commun. 2007; 355(3): 751-7.

43. Ionescu RM, Vlasak J, Price C, Kirchmeier M. Contribution of variable domains to the stability of humanized IgG1 monoclonal antibodies. J Pharm Sci. 2008; 97(4): 1414-1426.

44. Arora J, Hickey JM, Majumdar R, Esfandiary R, Bishop SM, Samra HS, Middaugh CR, Weis DD, Volkin DB. Hydrogen exchange mass spectrometry reveals protein interfaces and distant dynamic coupling effects during the reversible self-association of an IgG1 monoclonal antibody. MAbs. 2015; 7(3): 525-539.

45. Deperalta G, Alvarez M, Bechtel C, Dong K, McDonald R, Ling V. Structural analysis of a therapeutic monoclonal antibody dimer by hydroxyl radical footprinting. MAbs. 2013; 5(1): 86-101.

46. Zhang A, Singh SK, Shirts MR, Kumar S, Fernandez EJ. Distinct aggregation mechanisms of monoclonal antibody under thermal and freeze-thaw stresses revealed by hydrogen exchange. Pharm Res. 2012; 29(1): 236-50.

47. Plath F, Ringler P, Graff-Meyer A, Stahlberg H, Lauer ME, Rufer AC, Graewert MA, Svergun D, Gellermann G, Finkler C, Stracke JO. Characterization of mAb dimers reveals predominant dimer forms common in therapeutic mAbs. 2016; MAbs 8 (5): 928-940.

48. Majumdar R, Manikwar P, Hickey JM, Samra HS, Sathish HA, Bishop SM, Middaugh CR, Volkin DB, Weis DD. Effects of salts from the Hofmeister series on the conformational stability, aggregation propensity, and local flexibility of an IgG1 monoclonal antibody. Biochemistry. 2013; 52(19): 3376-89.

49. Houde D, Arndt J, Domeier W, Berkowitz S, Engen JR. Characterization of IgG1 conformation and conformational dynamics by hydrogen/deuterium exchange mass spectrometry. Anal Chem. 2009; 81(7): 2644-51.

50. Zheng K, Bantog C, Bayer R. The impact of glycosylation on monoclonal antibody conformation and stability. MAbs. 2011; 3(6): 568-576.

Tables

Methionine	Location	% oxidized	SASA Score
Met 34	HC	2.8	0.002
Met 83	HC	0	2.054
Met 109	HC	17.37	0
Met 257	HC	56.25	27.96
Met 363	HC	4.46	47.21
Met 433	HC	57.74	0

Table 1. Sites of methionine oxidation in UVA light exposed mAbA samples.

Sites of methionine oxidation identified by LC-MS/MS analysis in mAbA samples exposed to UVA light for 72 hours. The solvent accessible surface area (SASA) was calculated based on the static model structure using the protein properties analysis module (MOE).

	T_{onset} (°C)			T_m1 (°C)			T_m2 (°C)			T_m3 (°C)		
Sample type	Mean	SD	ΔT_{onset}	Mean	SD	ΔT_m1	Mean	SD	ΔT_m2	Mean	SD	ΔT_m3
Monomer												
Control	54.5	0.3	-	68.6	0.5	-	73.7	0.1	-	82.2	< 0.1	-
UVA 9 hrs	51.1	0.7	-3.4	67.9	< 0.1	-0.7	73.6	0.3	-0.1	82.1	< 0.1	-0.1
UVA 24 hrs	47.2	0.6	-7.3	67.7	< 0.1	-0.9	73.5	0.2	-0.2	82.0	0.2	-0.2
UVA 72 hrs	43.5	0.4	-11	67.2	0.12	-1.4	73.2	< 0.1	-0.5	81.7	0.2	-0.5
Dimer												
Control	55.9	0.4	-	68.1	< 0.1	-	73.6	< 0.1	-	82.1	< 0.1	-
UVA 9 hrs	52.1	0.4	-3.8	67.5	< 0.1	-0.6	73.3	0.2	-0.3	82.0	0.6	-0.1
UVA 24 hrs	49.2	0.9	-6.7	67.2	< 0.1	-0.9	73.2	< 0.1	-0.4	81.9	< 0.1	-0.2
UVA 72 hrs	45.4	0.4	-10.5	66.7	< 0.1	-1.4	73.1	<0.1	-0.5	81.9	< 0.1	-0.5

Table 2. Thermal onset temperature (Tonset) and Thermal melting temperatures (Tm1, Tm2, and Tm3) for monomer and dimer fractions collected from UVA light exposed mAbA samples as measured by DSC

mAbA solution at 1 mg/mL contained 47 mM sodium phosphate and 300 mM sodium chloride at pH 6.1. The difference in melting temperature (ΔT_m) was obtained from $T_{m,\ light\ exposed} - T_{m,\ control}$.
Mean and standard deviation (SD) are based on three separate measurements.

Figures

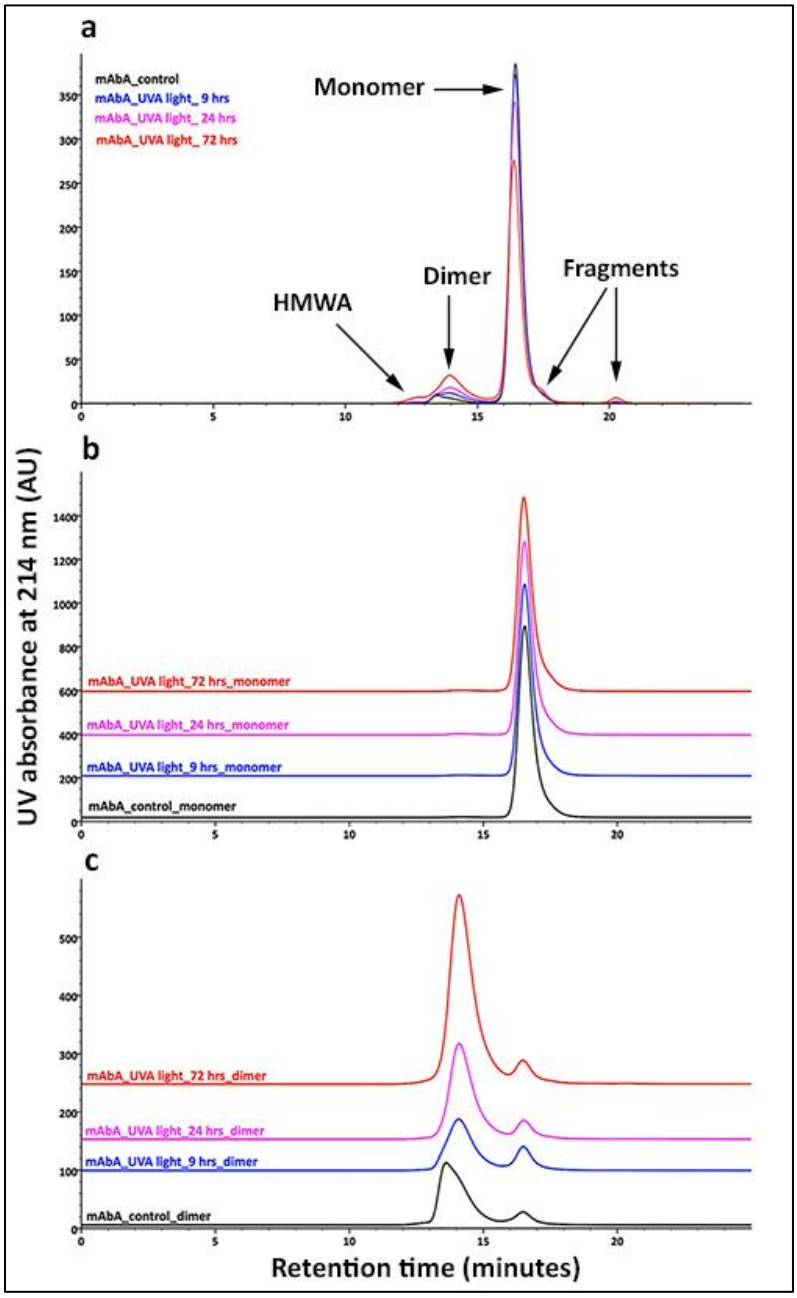

Figure 1. SEC analysis of mAbA samples exposed to UVA light. (a) Overlay of SEC chromatograms of mAbA exposed to increasing durations of UVA light. Samples were prepared in 25 mM sodium phosphate buffer (pH 6.1), without light exposure (control) (black trace) and exposure to UVA light for 9 hours (blue trace) or 24 hours (magenta trace) or 72 hours (red

trace). Overlay of SEC chromatograms showing purity of monomer (b) and dimer (c) fractions obtained after several injections and concentration of mAbA samples using SEC fraction collector. Each injection contained 125 µg of mAbA and monitored at 214 nm.

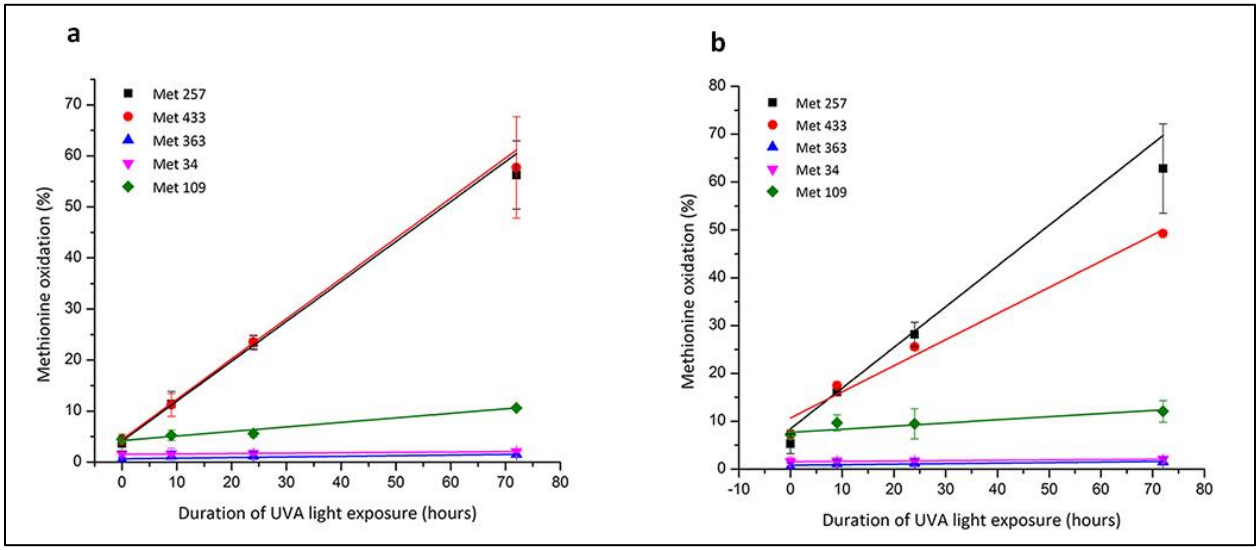

Figure 2. LC-MS analysis: Characterization of monomer and dimer fractions obtained from UVA light exposed mAbA samples. Correlation between methionine oxidation levels and duration of UVA light exposure, in (a) monomer and (b) dimer fractions. Error bars represent standard deviation from three independent samples.

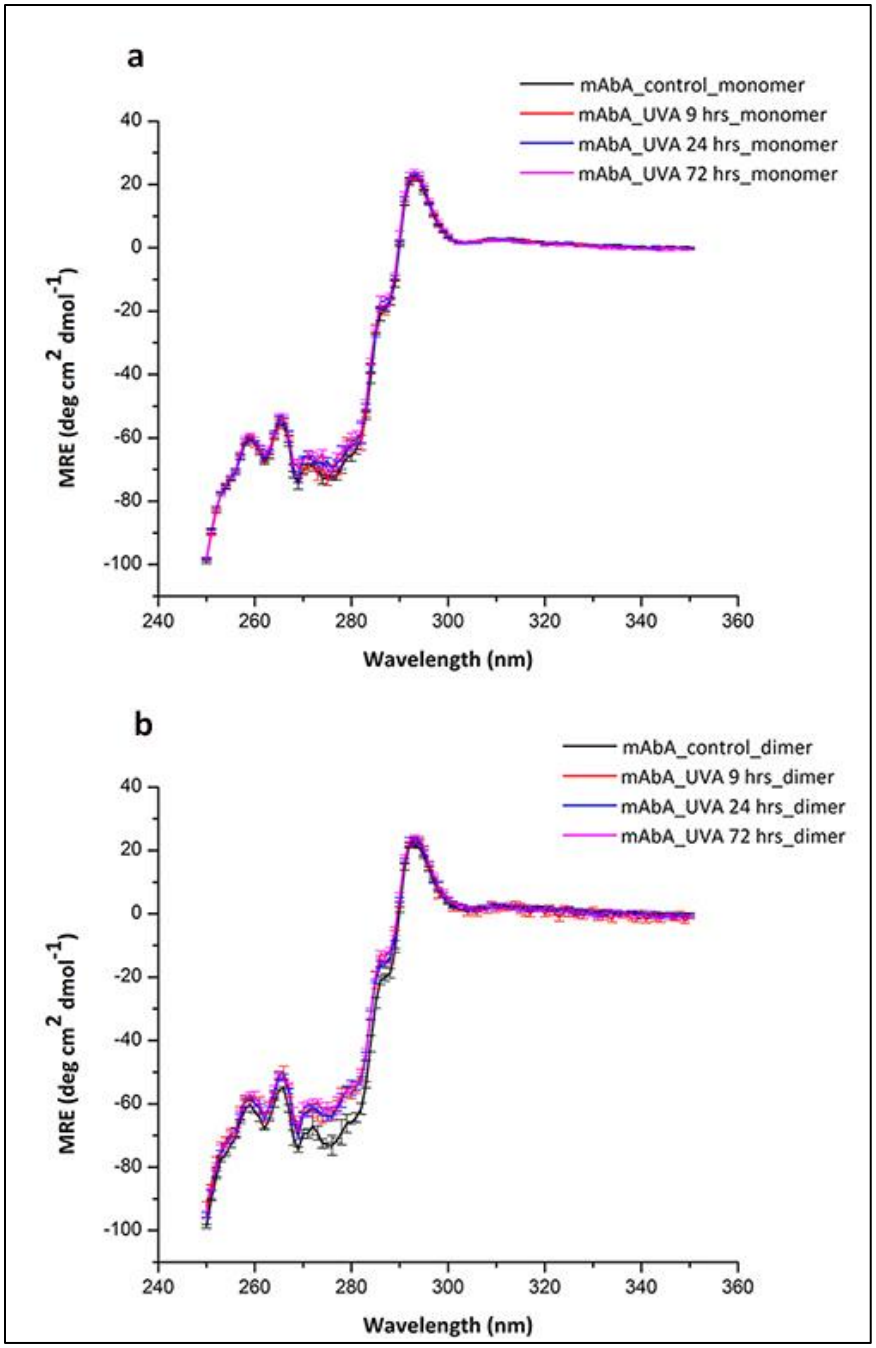

Figure 3. Near-UV spectra (n=3) of monomer (a) and dimers (b) isolated from mAbA samples exposed to increasing durations of UVA light exposure (0, 9, 24, 72 hours).

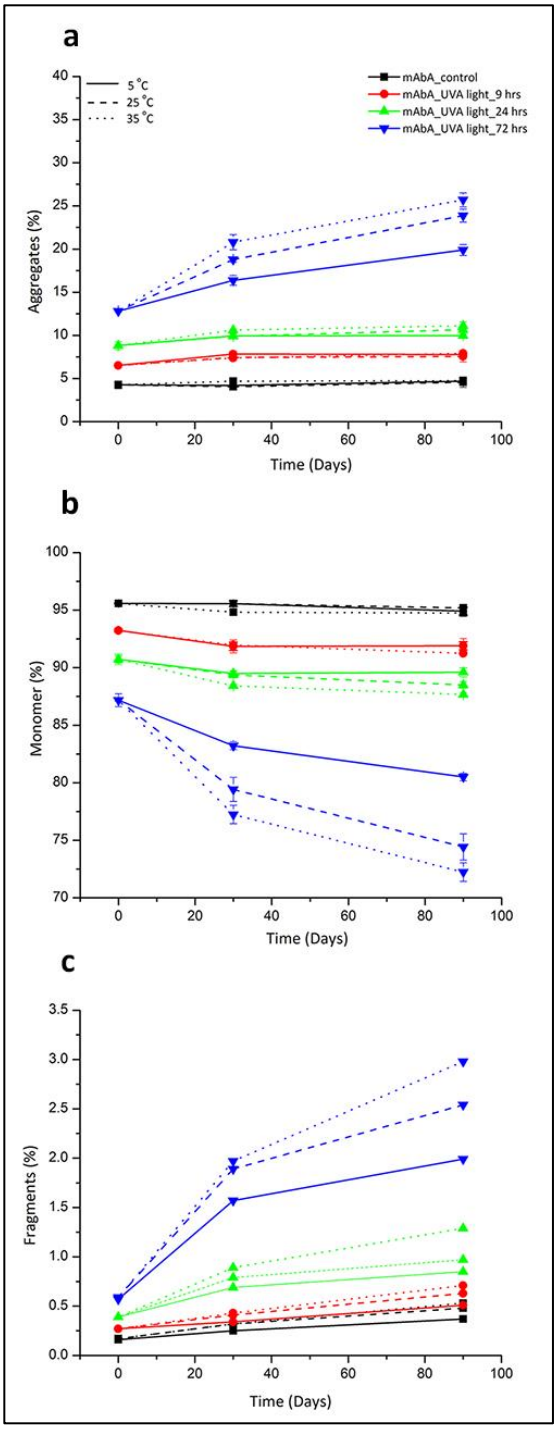

Figure 4. Effect of pre-exposure to UVA light on stability of mAbA during storage under accelerated conditions (5 ^{o}C, 25 ^{o}C and 35 ^{o}C) monitored by SEC. Changes in stability is represented as (a) % monomer, increase of (b) % aggregates and (c) % fragments. Error bars represent standard deviation from three independent samples.

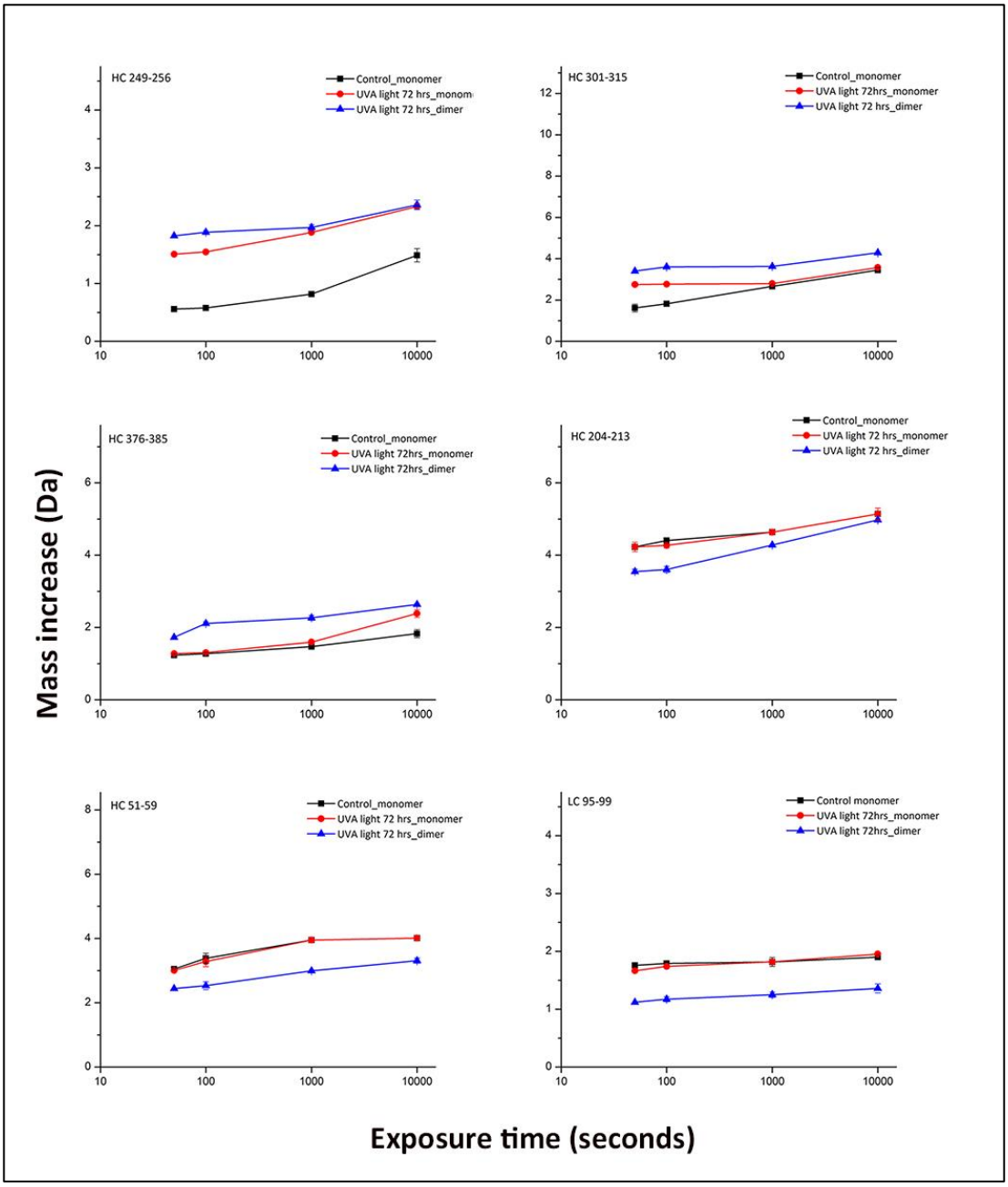

Figure 5. Deuterium uptake curves of six peptide segments from different regions of monomer and dimer fractions isolated from control mAbA and mAbA sample exposed to UVA light for 72 hours. Peptide segment identity is shown on each plot. The vertical axis on each graph represent the maximum possible exchange for each segment. The error bars represent standard deviation for three independent experiments.

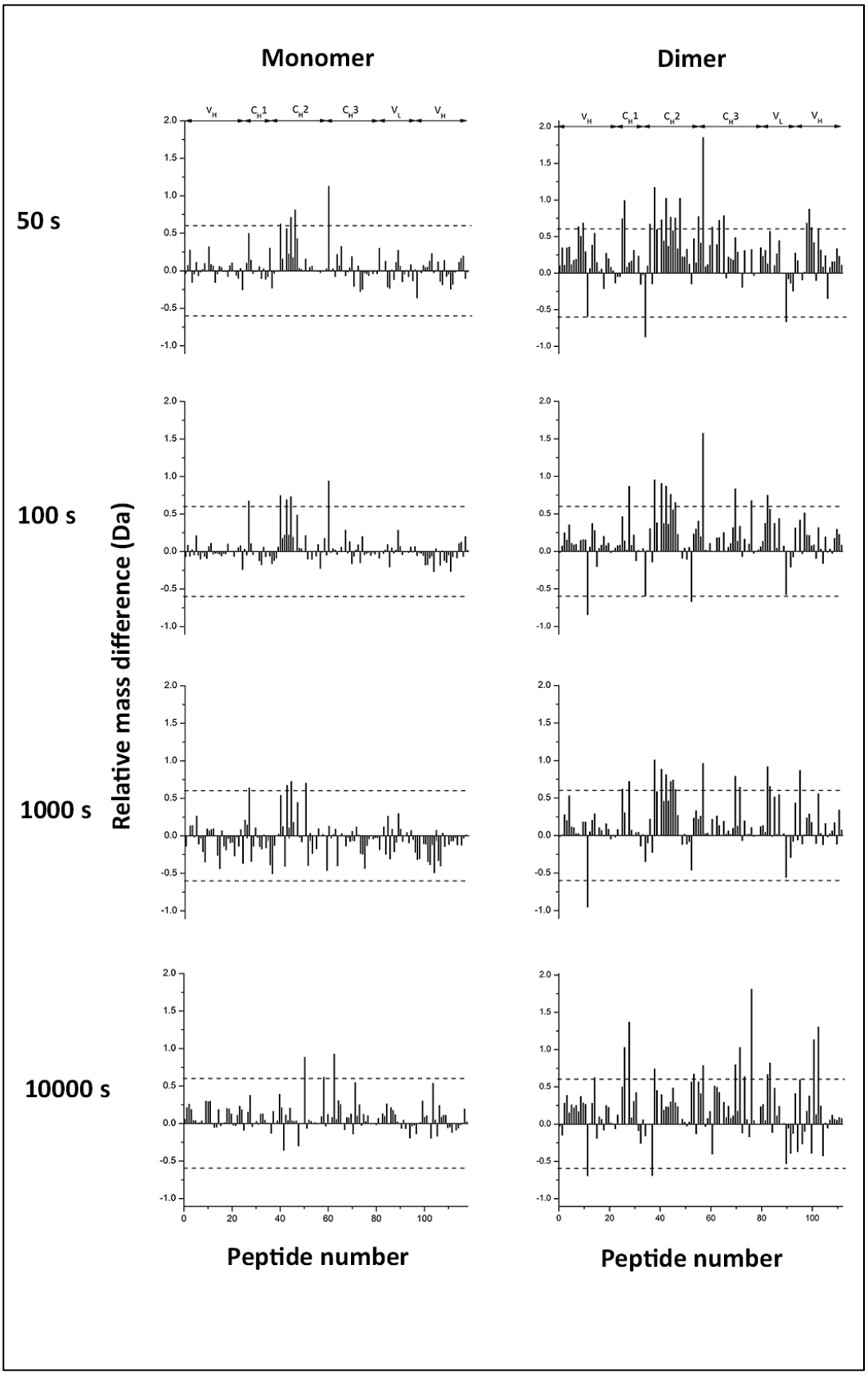
Monomer
Dimer
50 s
100 s
1000 s
10000 s
Relative mass difference (Da)
Peptide number
Peptide number

Figure 6. Relative mass difference (Δm) for all peptide segments of UVA light exposed (for 72 hours) mAbA, compared with control (no light exposure) monomer as measured by H/D-MS. Each vertical bar represents the mass difference of the average deuterium uptake of each peptide segment, at four different exchange time points (50, 100, 1000, and 10000 s). The x-axis represents the peptide number, arranged in ascending order starting with N-terminus of heavy chain and ending with C-terminus of the light chain. The horizontal dotted line represents the 99% confidence limit (± 0.59 Da) for a significant mass difference. The domain locations of the representative peptide segments are shown on the top.

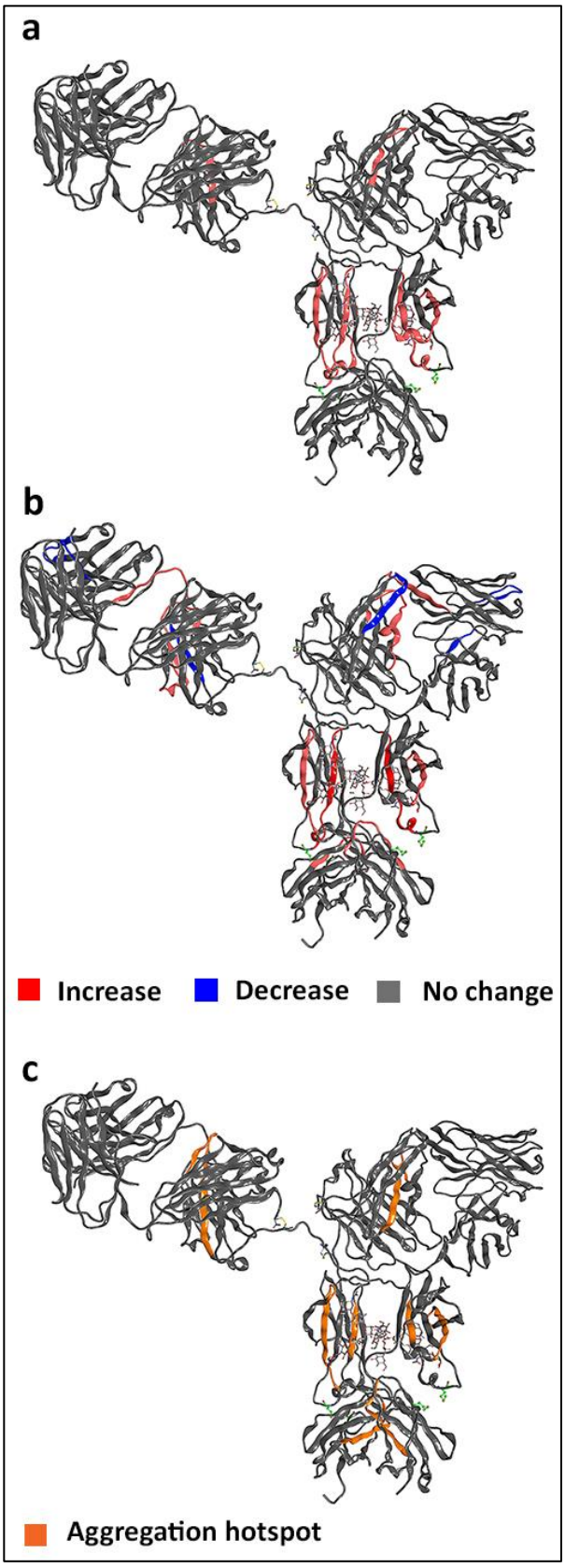
a
b
Increase
Decrease
No change
c
Aggregation hotspot

Figure 7. Effect of UVA light exposure on deuterium uptake of various segments of mAbA as measured by H/D-MS and plotted onto the homology model of mAbA. The color code is acquired from comparison of average deuterium uptake of monomer and dimer species fractionated from mAbA exposed to UVA light for 72 hours, compared with mAbA control monomer. The peptides segments that showed significant differences are indicated on the homology model. (a) Monomer, (b) Dimer and (c) Aggregation prone regions identified by AGGRESCAN are labeled with orange color.

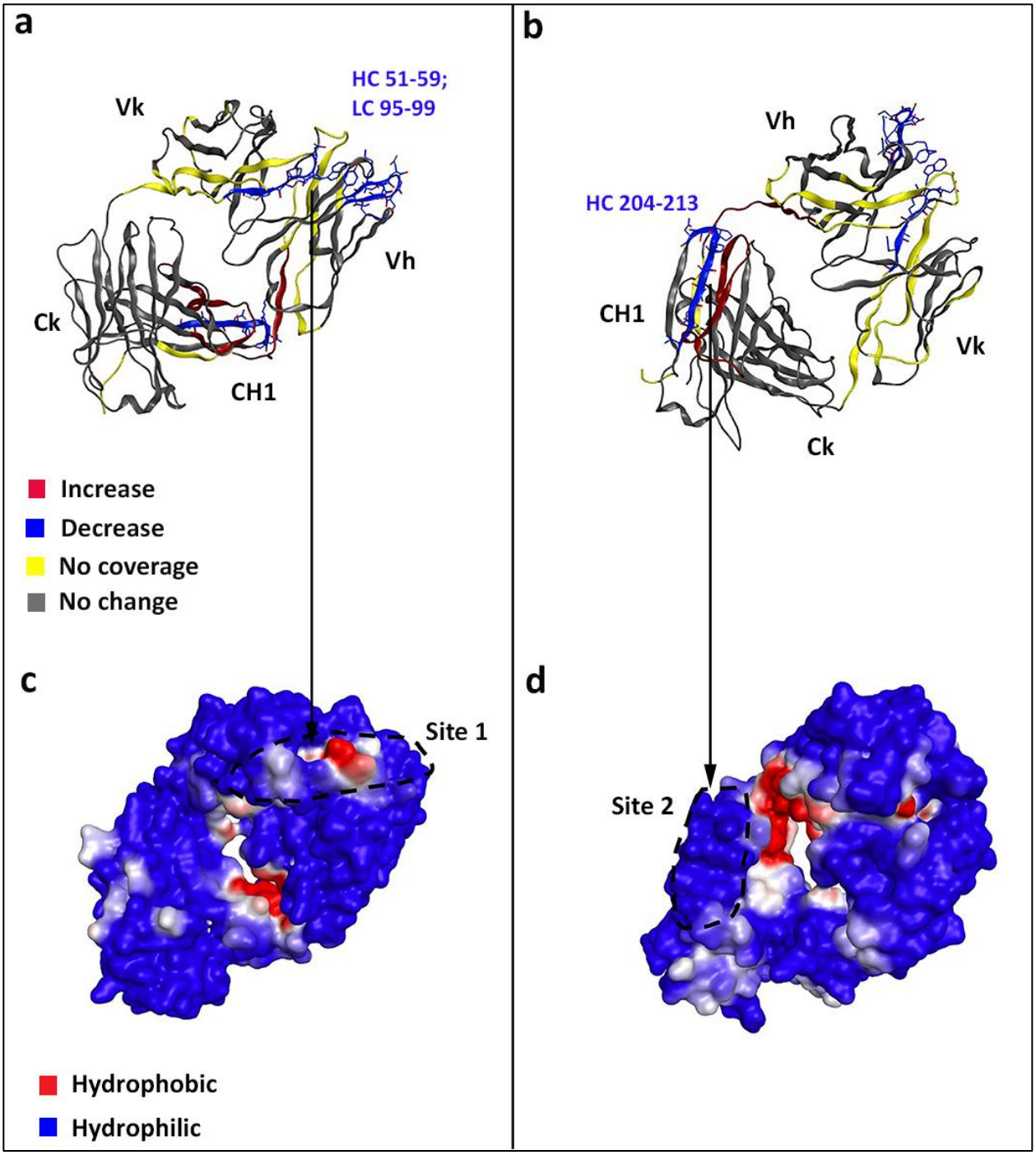

Figure 8. Effect of UVA light exposure on deuterium uptake of various segments of mAbA as measured by H/D-MS and plotted onto a homology model of the mAbA F_{ab} CDR surface (a, b). The spatial aggregation propensity (SAP) values at R = 5 Å are mapped onto the molecular surface of the mAbA F_{ab} CDR surface (c, d).

Supplementary material

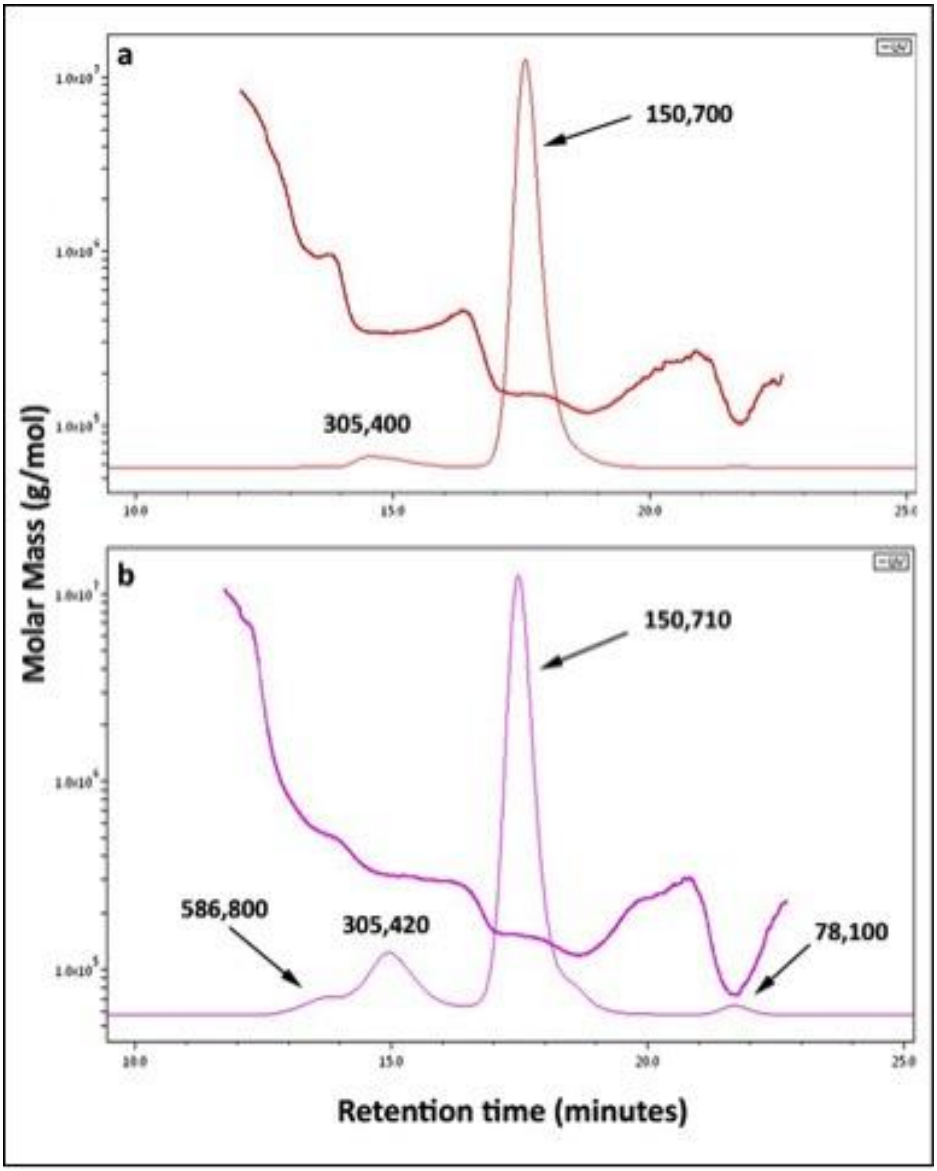

Fig. S1 SEC-MALS analysis of mAbA (1 mg/mL) (a) control and (b) exposed to UVA light for 72 hours. The left vertical axis is labeled as molar mass (g/mol). The solid vertical lines represent UV absorbance at 280 nm and horizontal line represents light scattering intensity. The average apparent molar mass of various species in the chromatogram was reported by the ASTRA software.

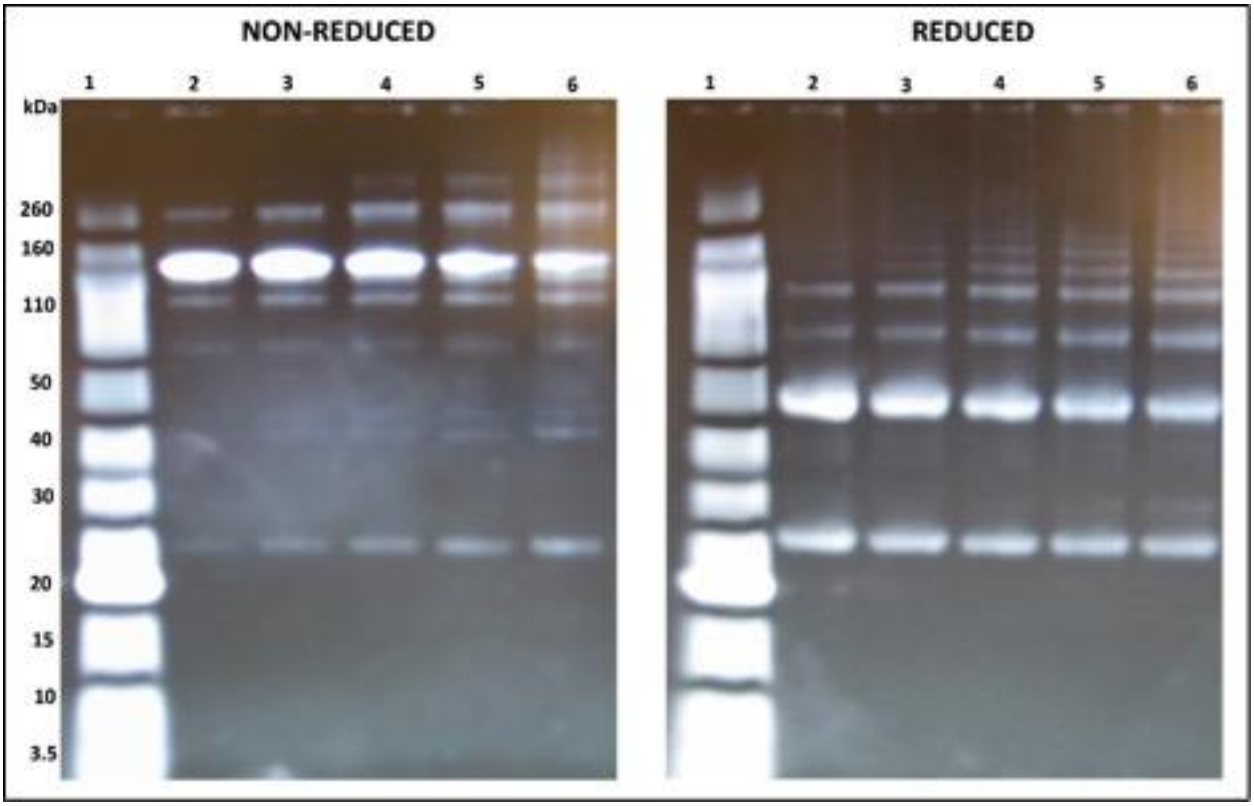

Fig. S2 Non-reduced and Reduced SDS-PAGE of mAbA samples exposed to increase in durations of UVA light: lane 1 molecular weight (kDa) standards, lane 2 control sample, lane 3 exposed 9 hours sample, lane 4 exposed 24 hours sample, lane 5 exposed 72 hours sample and lane 6 exposed 144 hours sample.

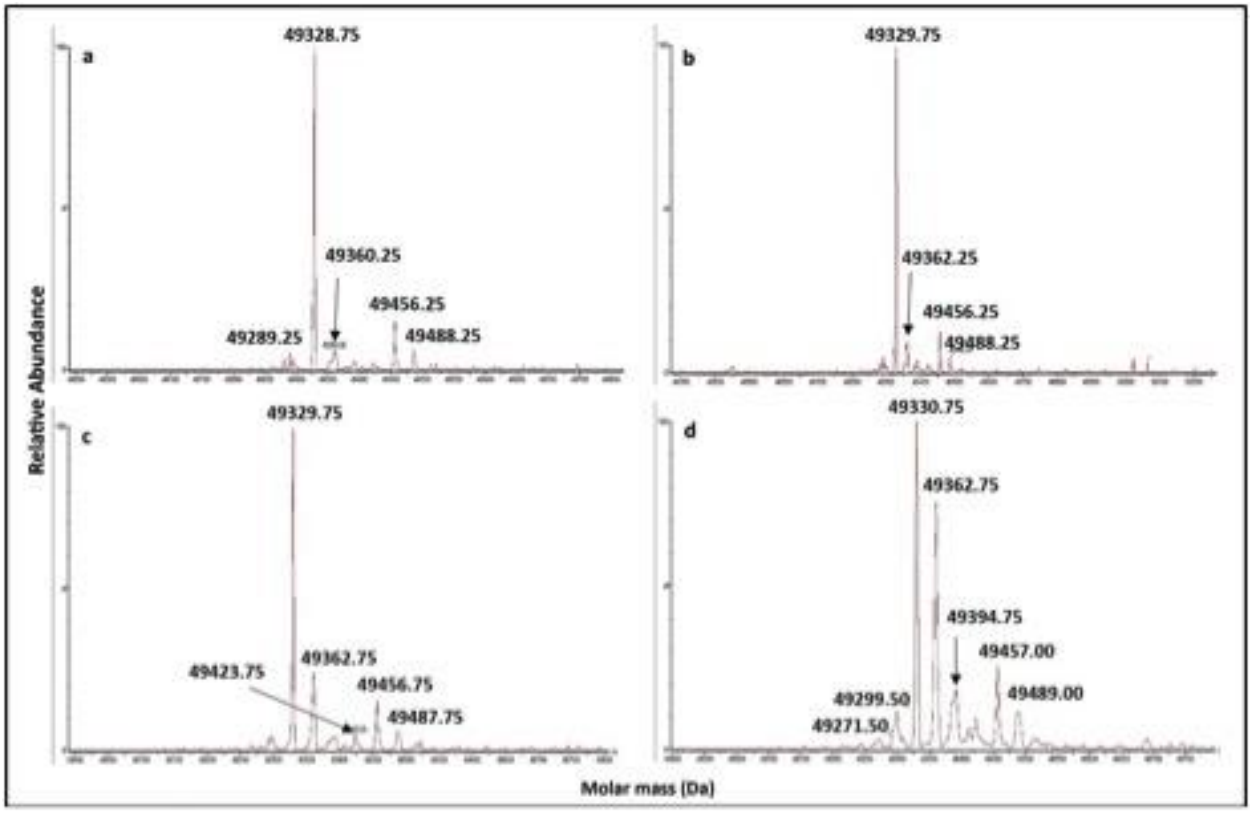

Fig. S3 Deconvoluted mass spectra of the heavy chain resultant of reduction of mAbA (a) control, exposed to UVA light for (b) 9 hours, (c) 24 hours, and (d) 72 hours.

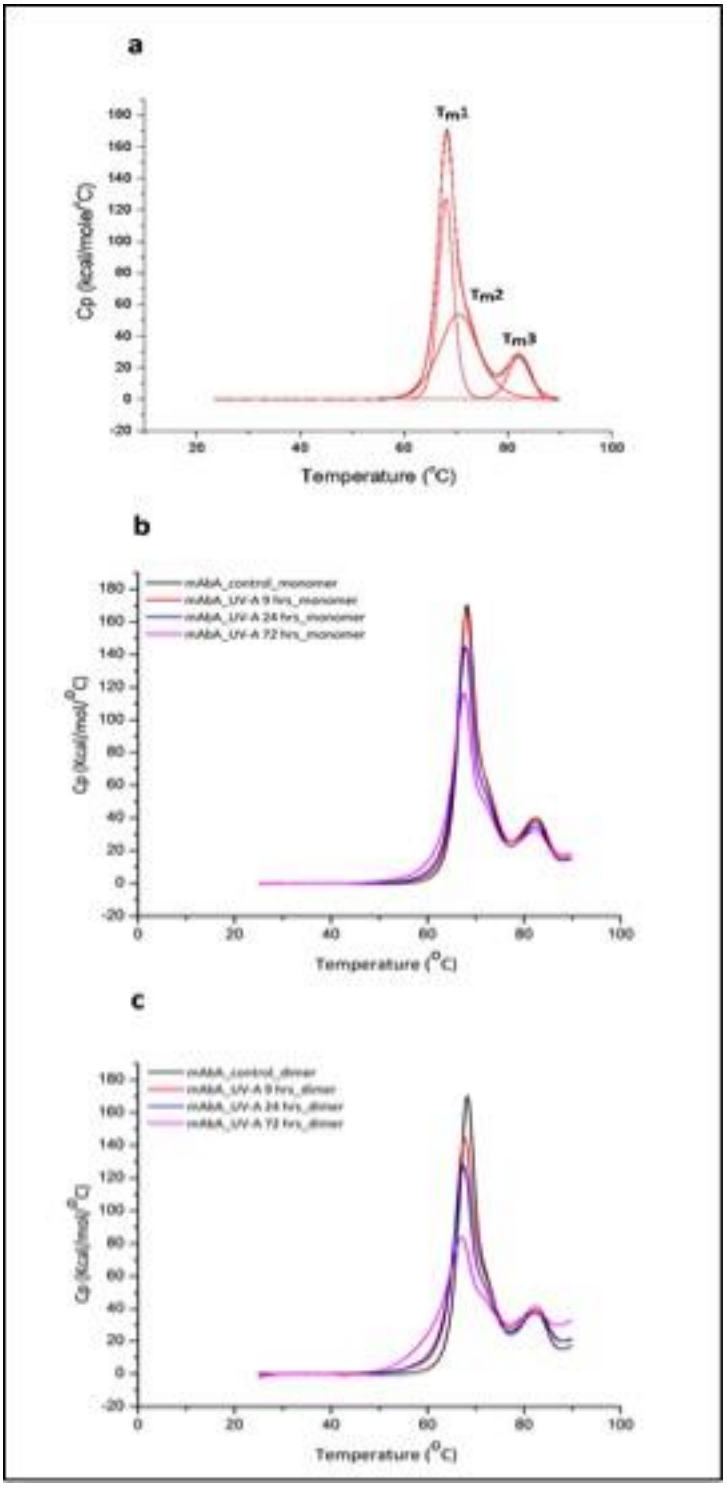

Fig. S4 DSC thermograms of mAbA exposed to UVA light. (a) Illustration of curve-fitted DSC thermograms for mAbA with T_m1, T_m2 and T_m3. Conformational stability of monomer (b) and dimer (c) fractions collected from mAbA samples exposed to UVA light.

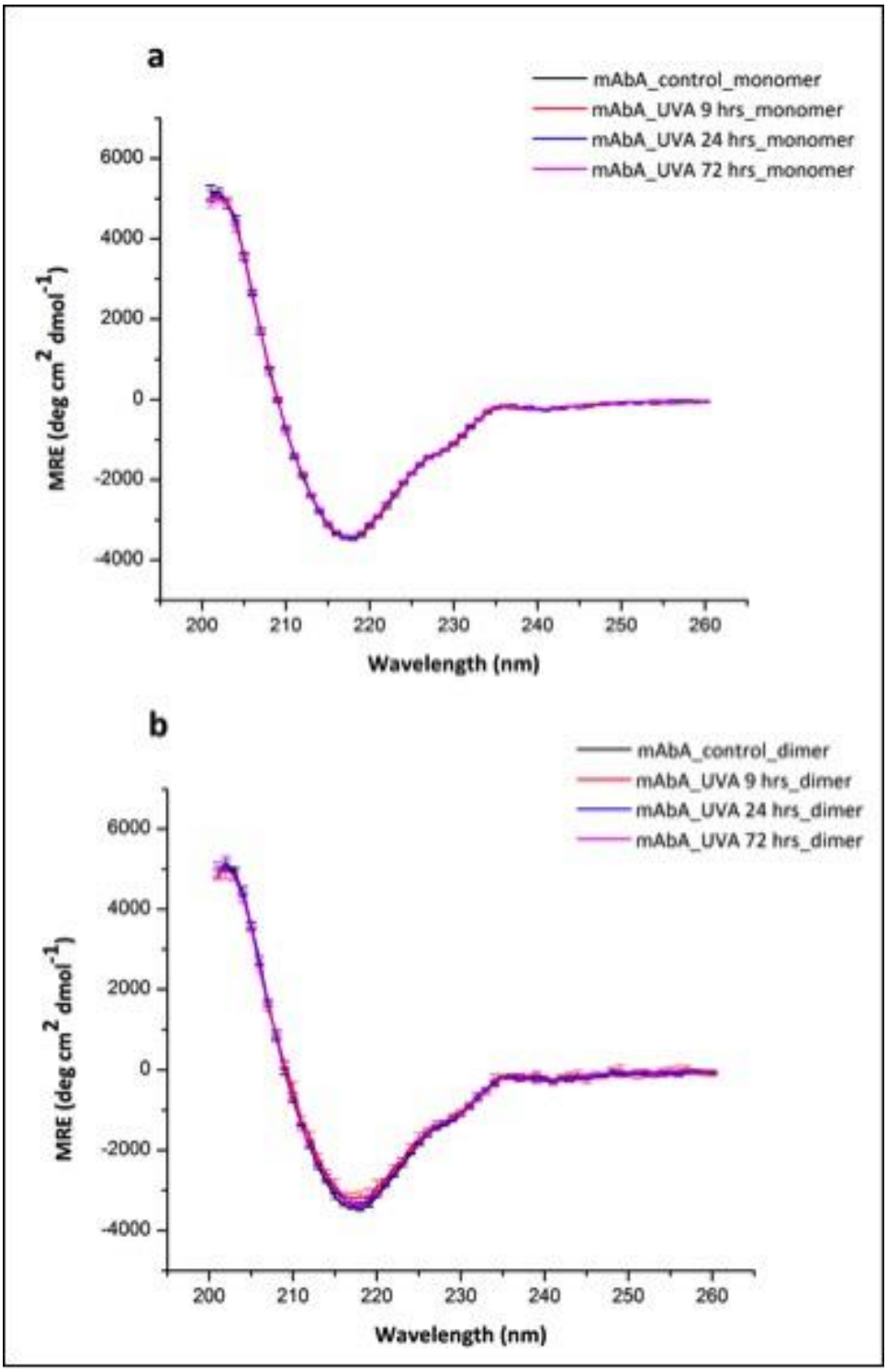

Fig. S5 Far-UV spectra (n=3) of (a) monomer and (b) dimers isolated from mAbA samples exposed to increasing durations of UVA light exposure (0, 9, 24, 72 hours).

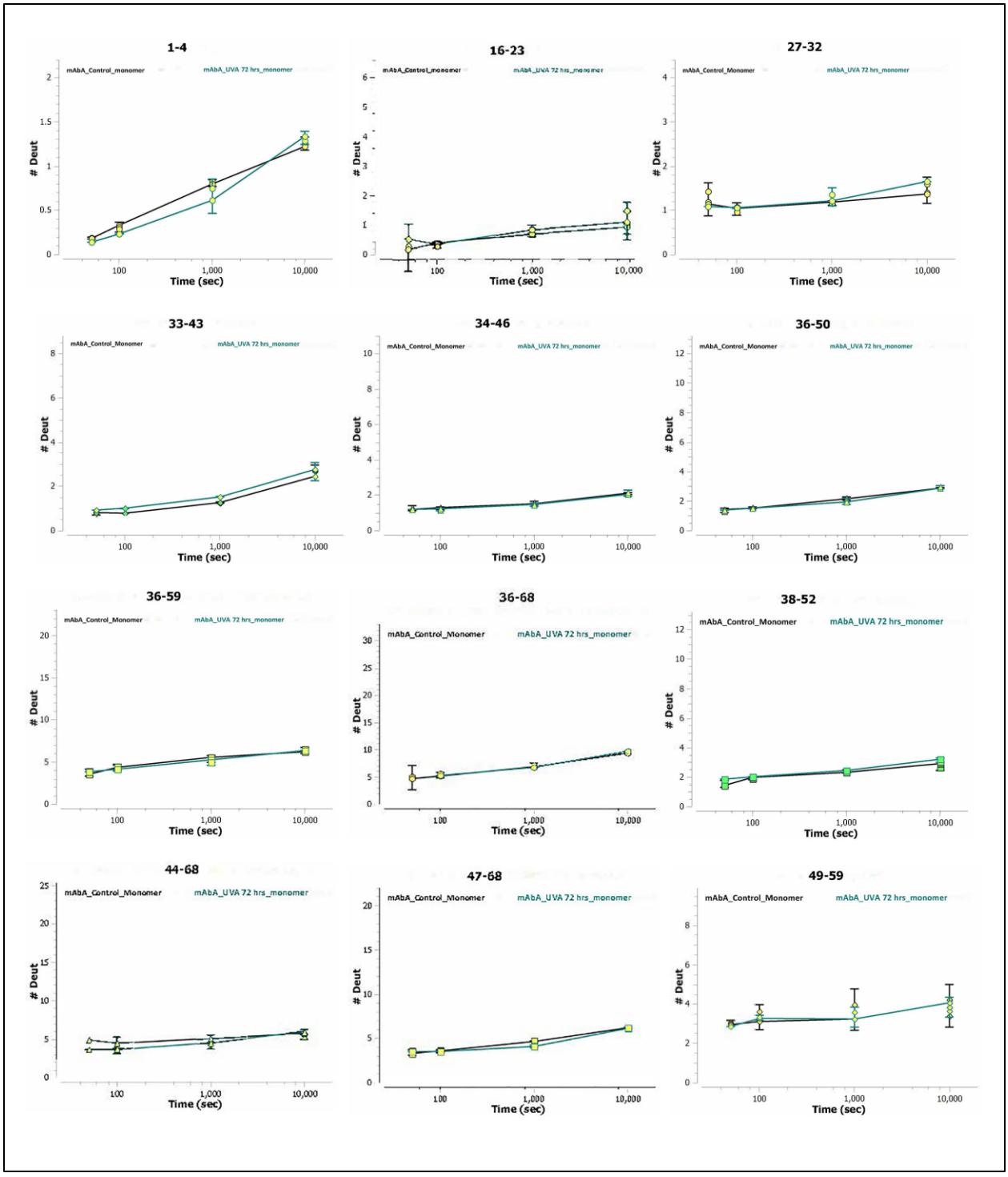

Fig. S6 Deuterium uptake curves for the segments from monomer fractionated from mAbA exposed to UVA light for 72 hours vs control monomer. Peptide segments containing oxidized Met residues were not readily found by HD-Examiner and hence are not reported. **(Heavy chain)**

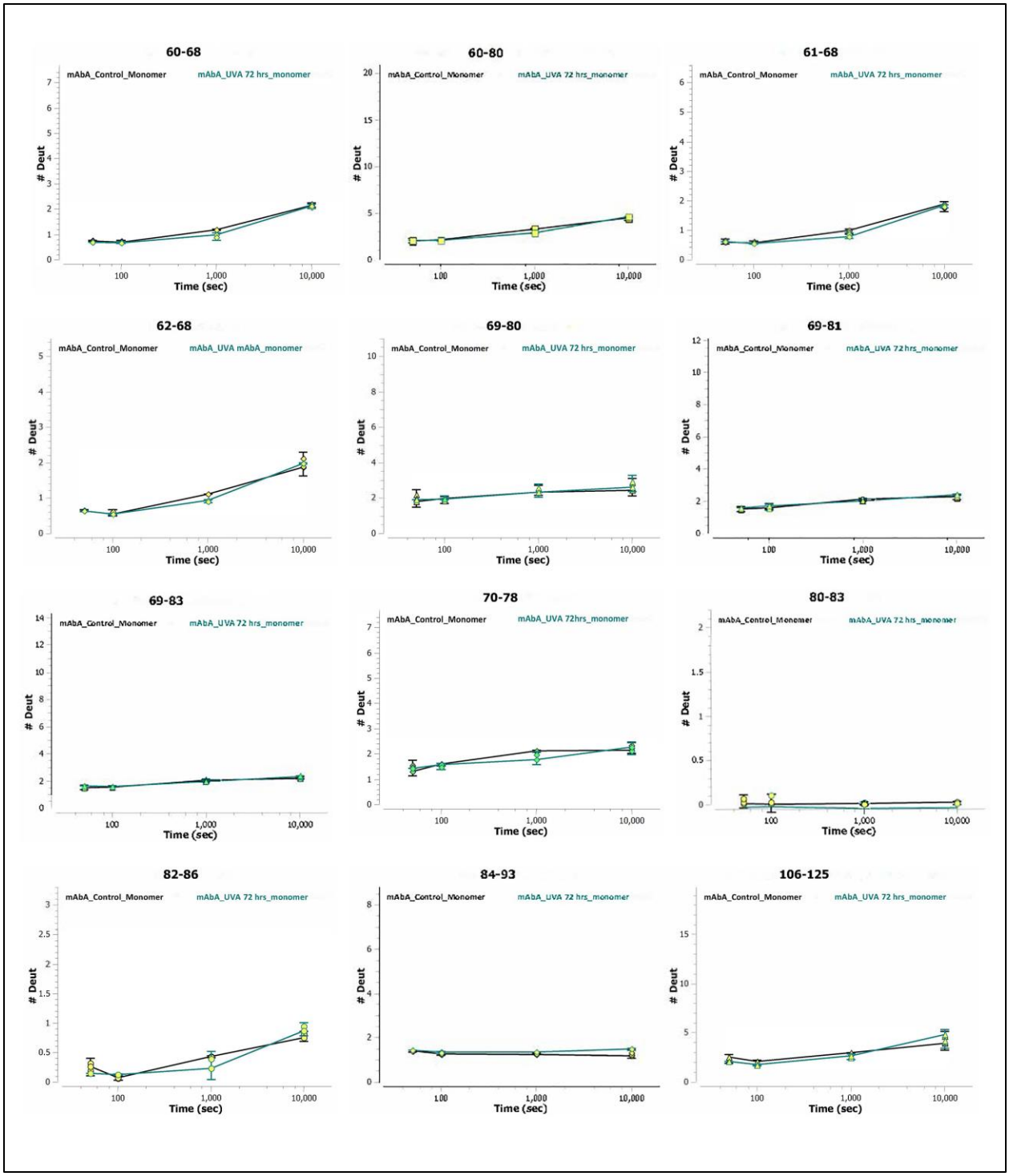

Fig. S6 Deuterium uptake curves for the segments from monomer fractionated from mAbA exposed to UVA light for 72 hours vs control monomer. Peptide segments containing oxidized Met residues were not readily found by HD-Examiner and hence are not reported. **(Heavy chain)**

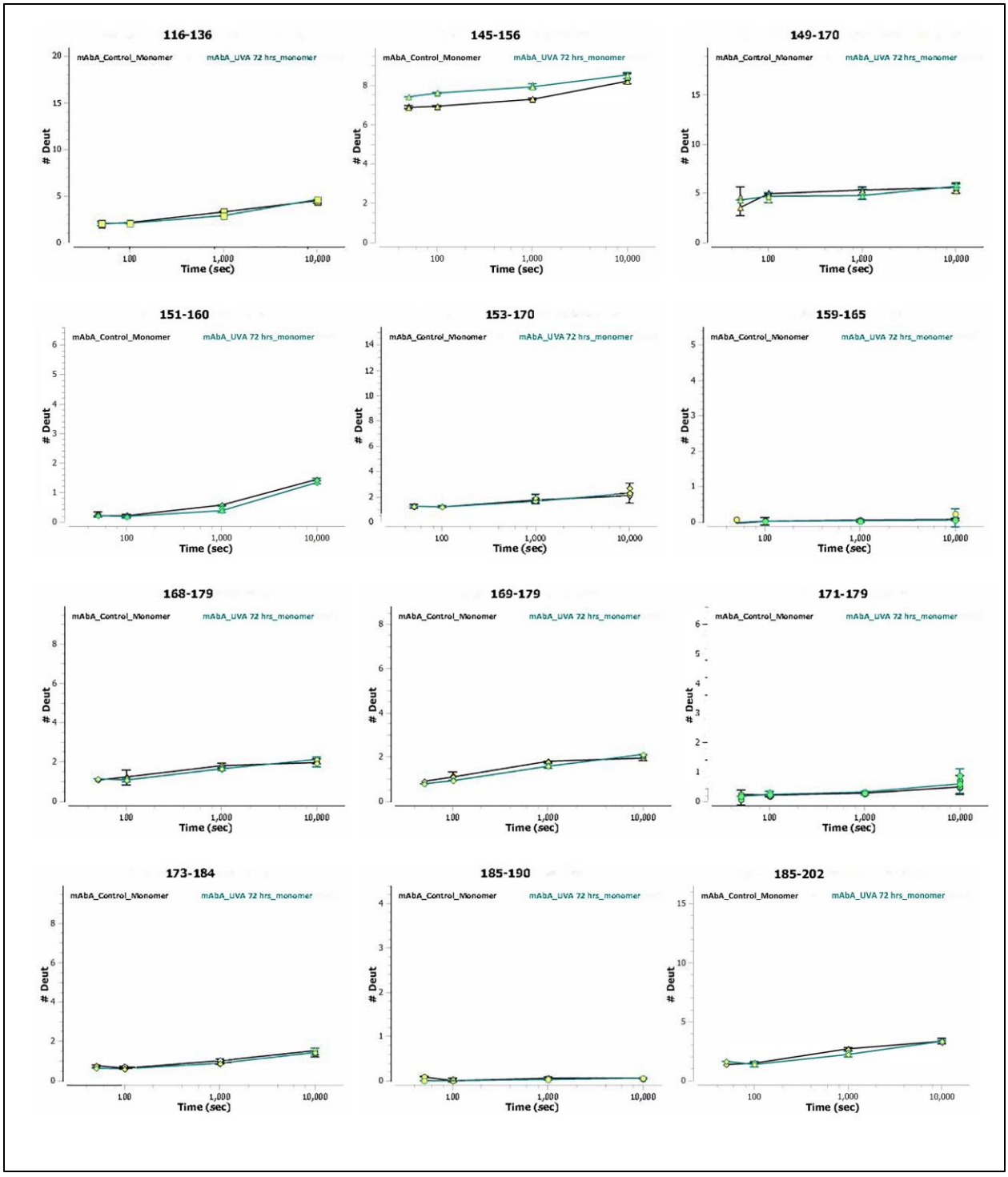

Fig. S6 Deuterium uptake curves for the segments from monomer fractionated from mAbA exposed to UVA light for 72 hours vs control monomer. Peptide segments containing oxidized Met residues were not readily found by HD-Examiner and hence are not reported. **(Heavy chain)**

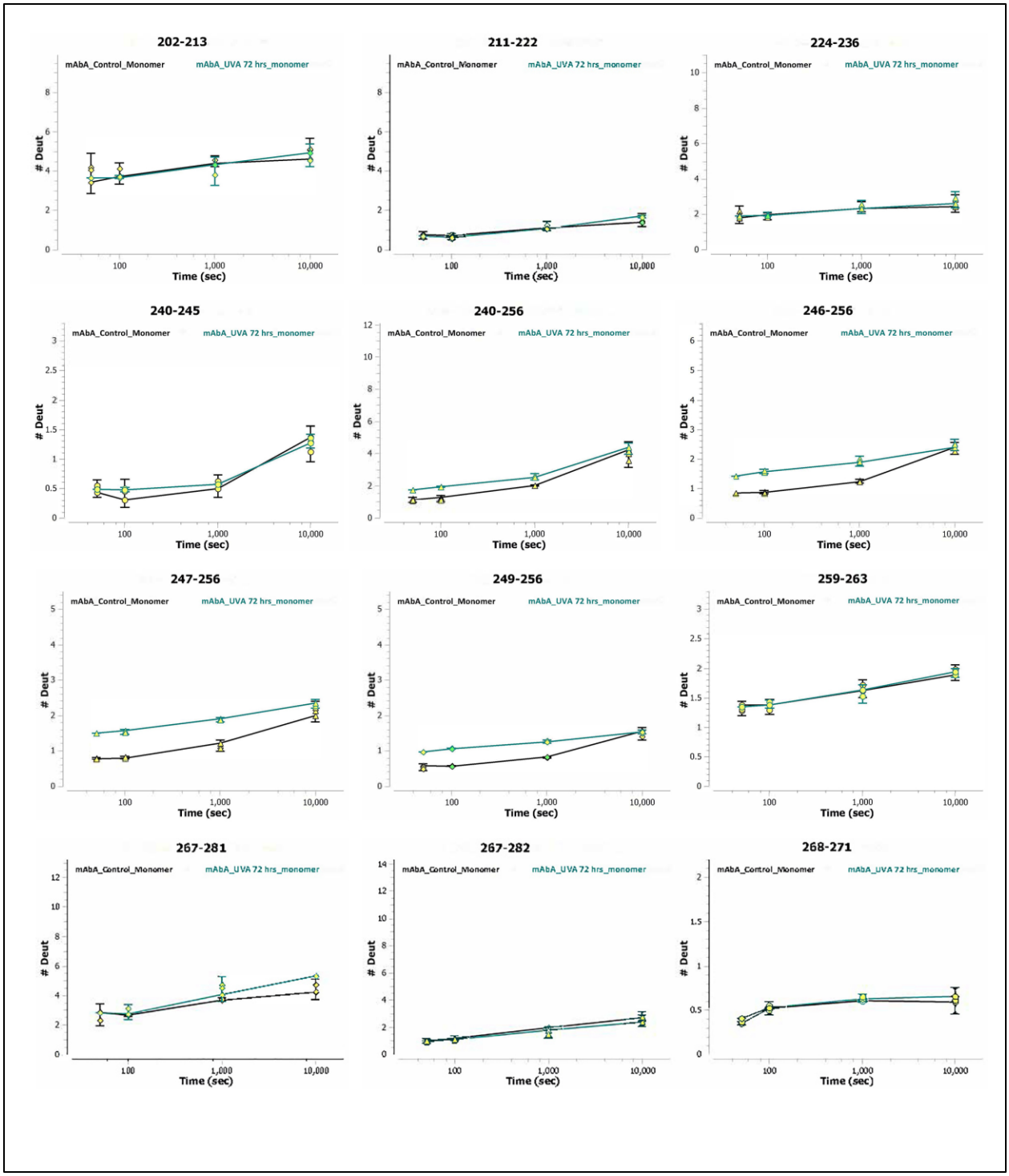

Fig. S6 Deuterium uptake curves for the segments from monomer fractionated from mAbA exposed to UVA light for 72 hours vs control monomer. Peptide segments containing oxidized Met residues were not readily found by HD-Examiner and hence are not reported. **(Heavy chain)**

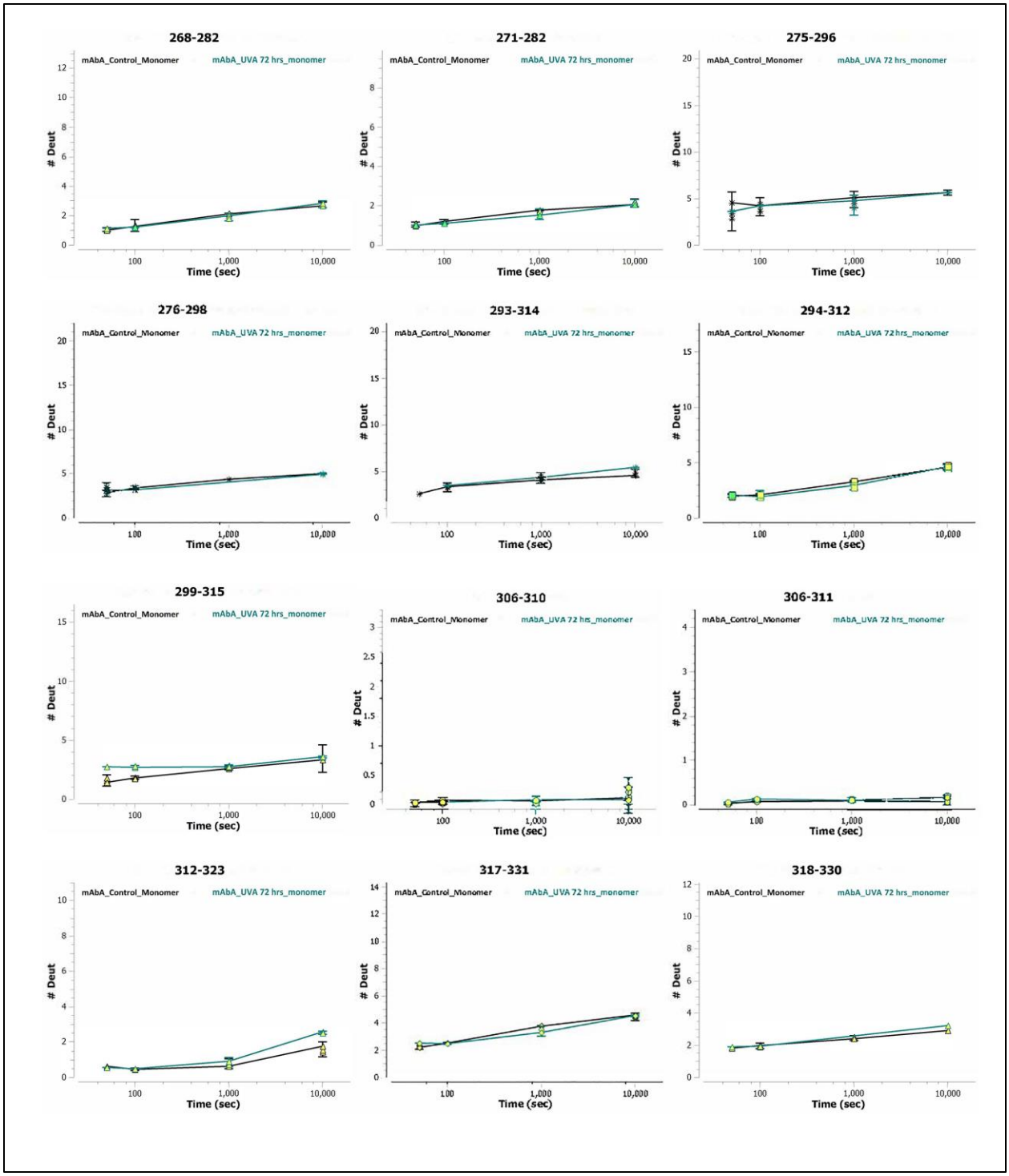

Fig. S6 Deuterium uptake curves for the segments from monomer fractionated from mAbA exposed to UVA light for 72 hours vs control monomer. Peptide segments containing oxidized Met residues were not readily found by HD-Examiner and hence are not reported. **(Heavy chain)**

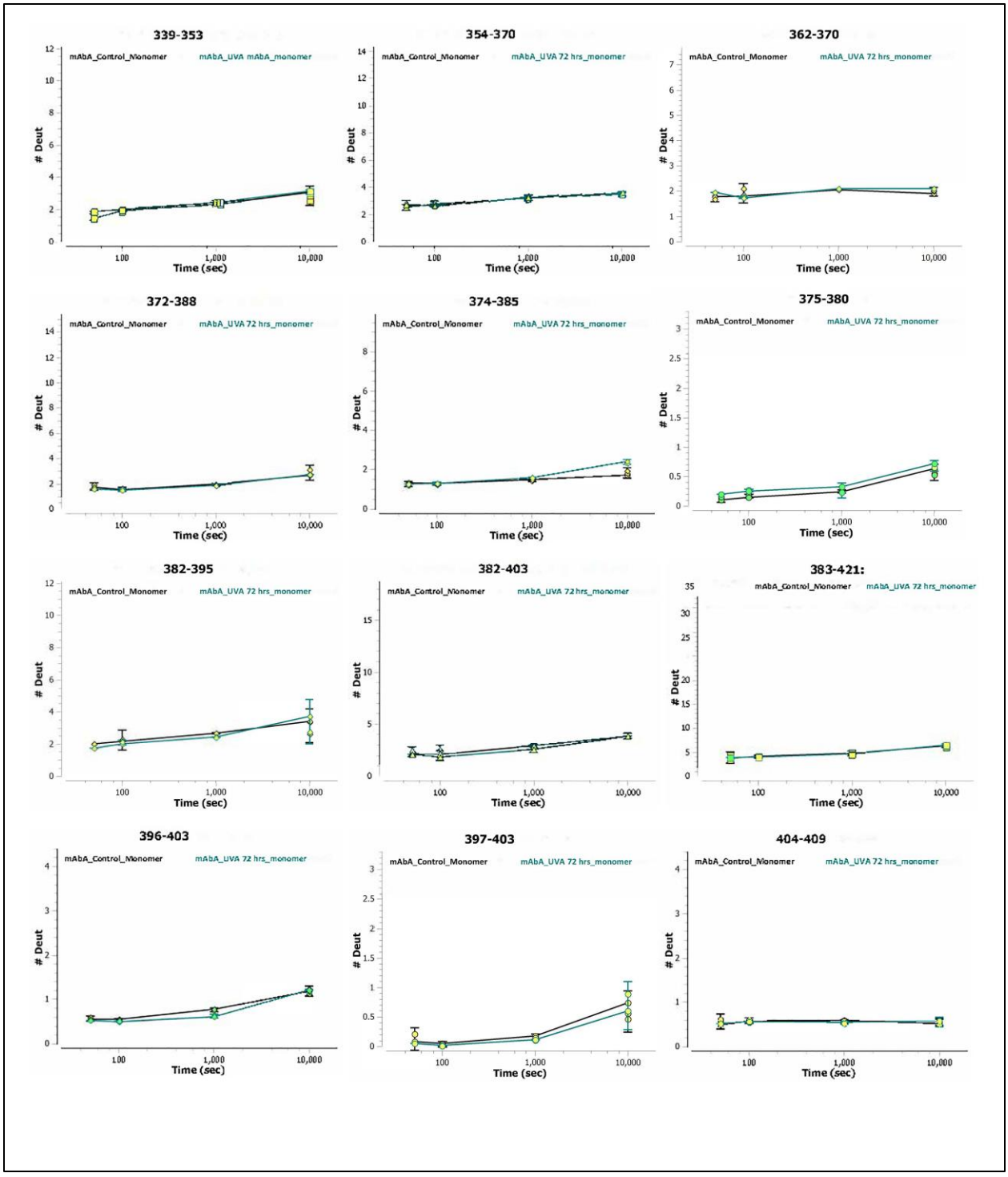

Fig. S6 Deuterium uptake curves for the segments from monomer fractionated from mAbA exposed to UVA light for 72 hours vs control monomer. Peptide segments containing oxidized Met residues were not readily found by HD-Examiner and hence are not reported. **(Heavy chain)**

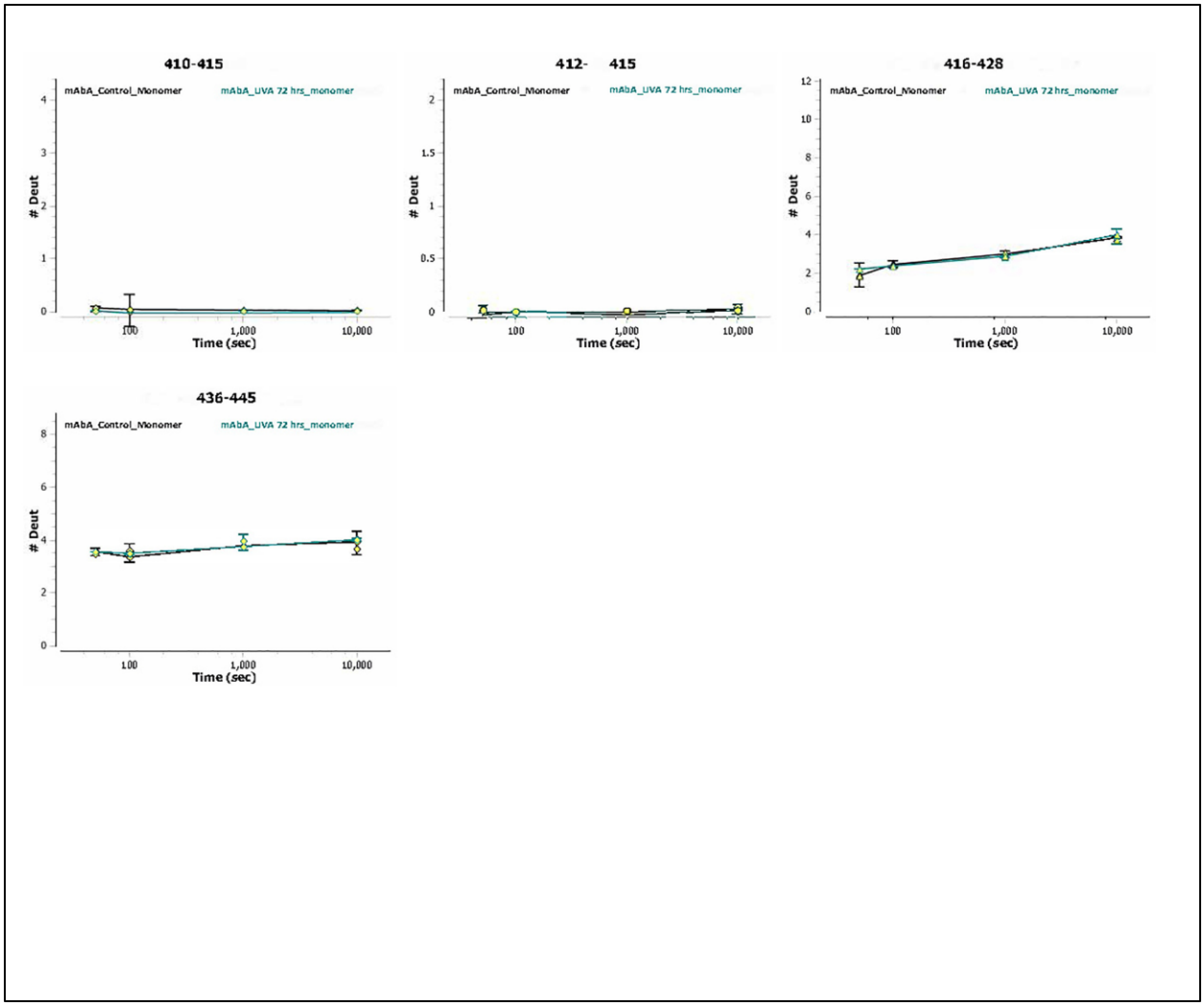

Fig. S6 Deuterium uptake curves for the segments from monomer fractionated from mAbA exposed to UVA light for 72 hours vs control monomer. Peptide segments containing oxidized Met residues were not readily found by HD-Examiner and hence are not reported. **(Heavy chain)**

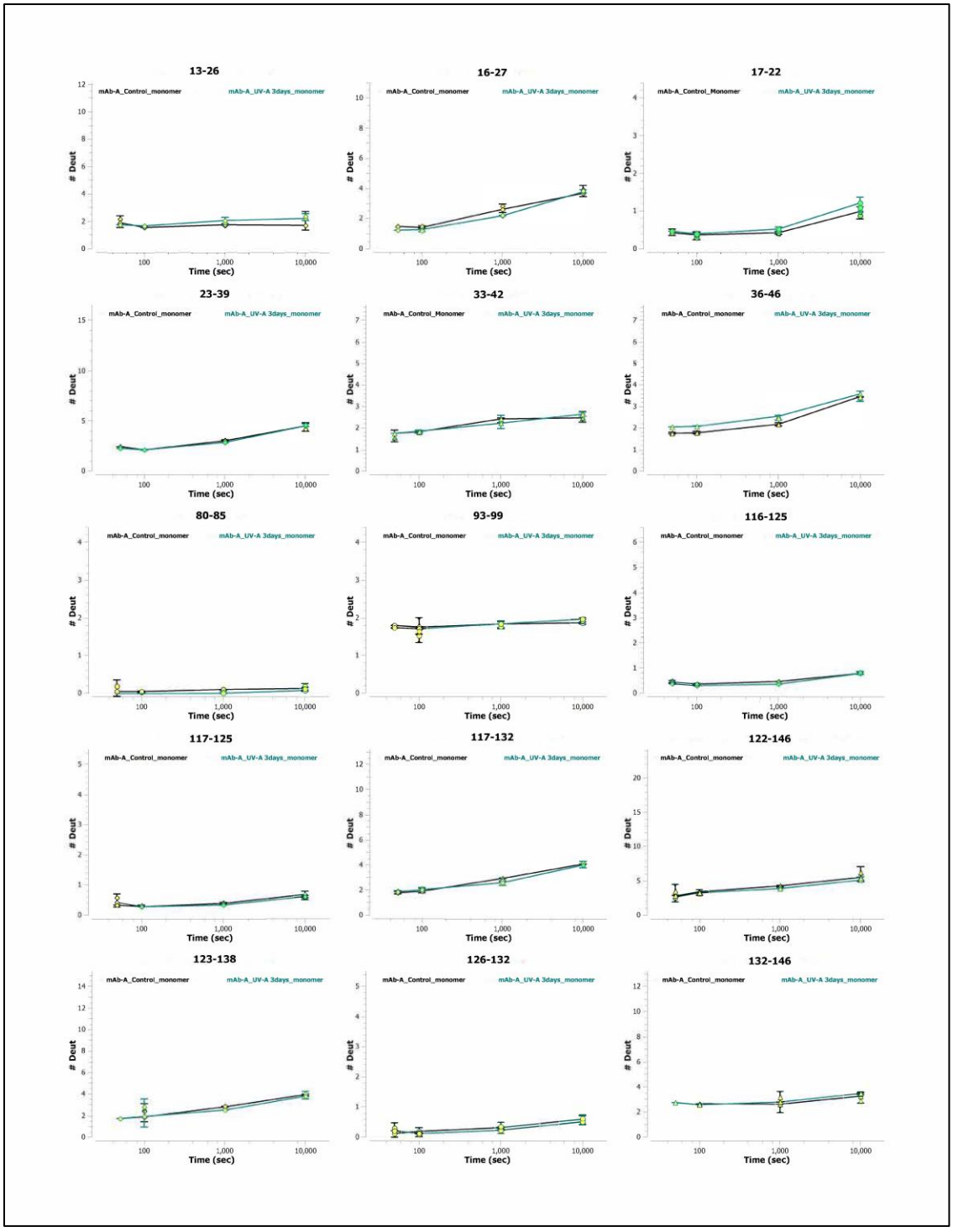

Fig. S6 Deuterium uptake curves for the segments from monomer fractionated from mAbA exposed to UVA light for 72 hours vs control monomer. Peptide segments containing oxidized Met residues were not readily found by HD-Examiner and hence are not reported. **(Light chain)**

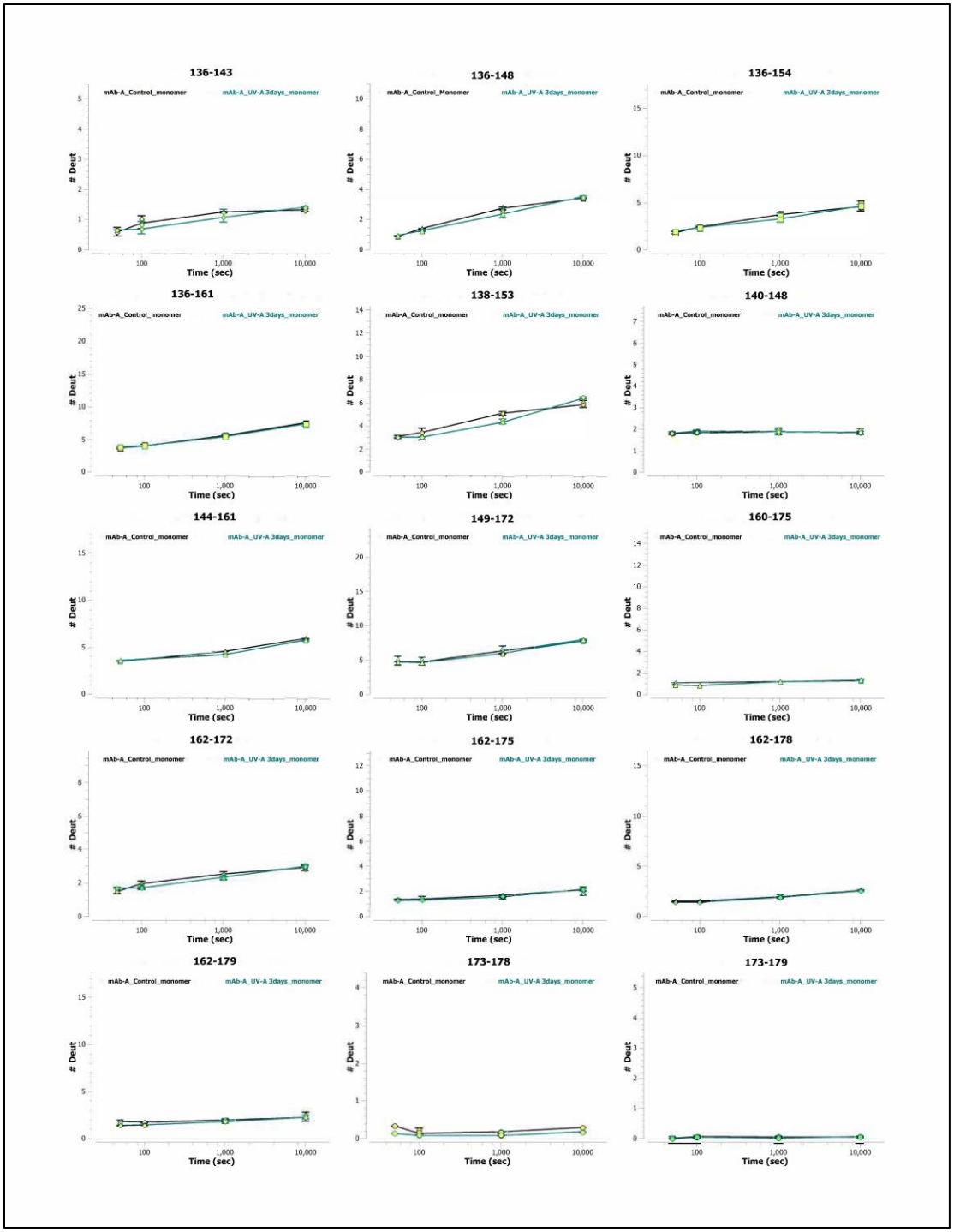

Fig. S6 Deuterium uptake curves for the segments from monomer fractionated from mAbA exposed to UVA light for 72 hours vs control monomer. Peptide segments containing oxidized Met residues were not readily found by HD-Examiner and hence are not reported. **(Light chain)**

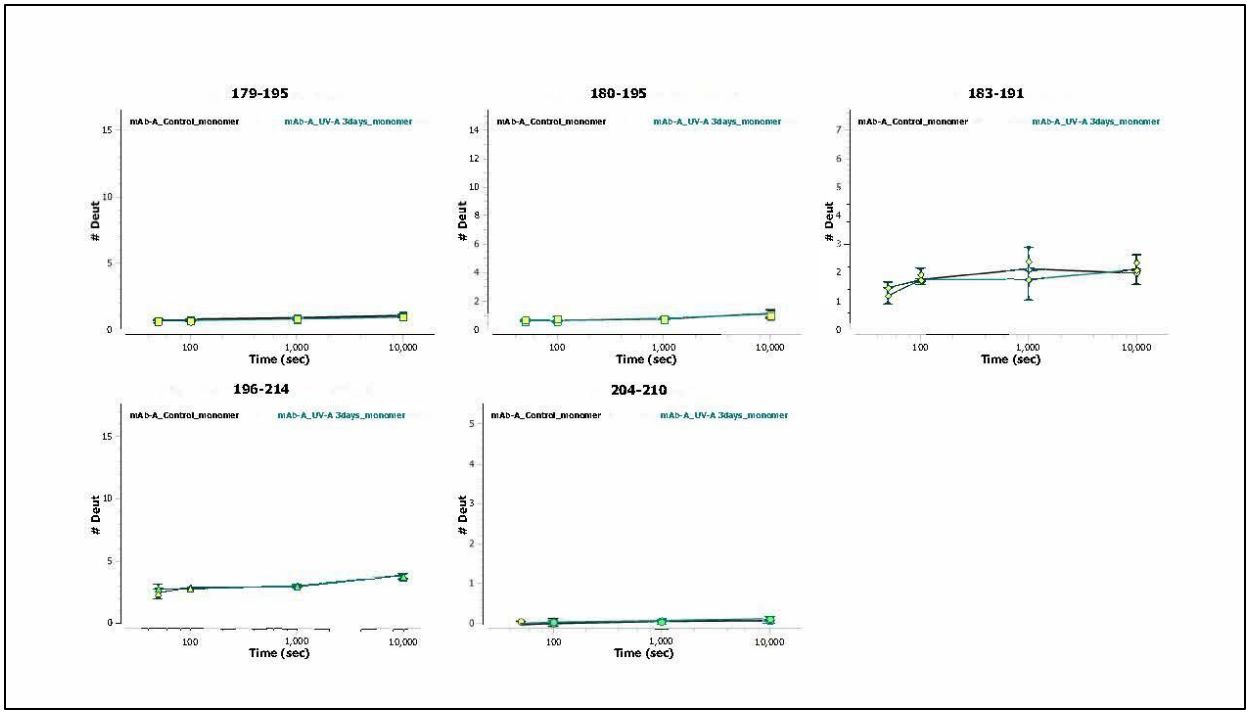

Fig. S6 Deuterium uptake curves for the segments from monomer fractionated from mAbA exposed to UVA light for 72 hours vs control monomer. Peptide segments containing oxidized Met residues were not readily found by HD-Examiner and hence are not reported. **(Light chain)**

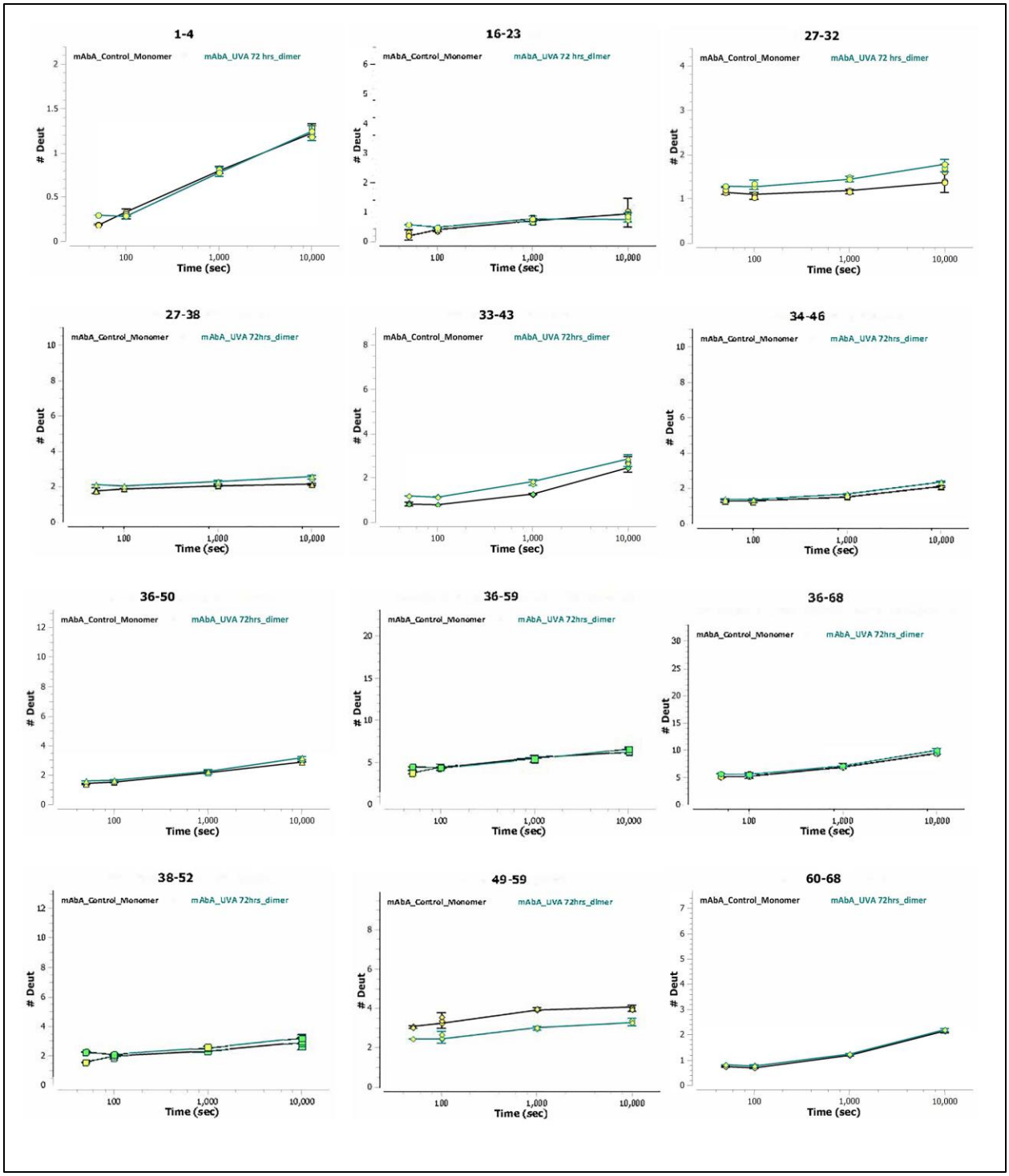

Fig. S7 Deuterium uptake curves for the segments from dimer fractionated from mAbA exposed to UVA light for 72 hours vs control monomer. Peptide segments containing oxidized Met residues were not readily found by HD-Examiner and hence are not reported. **(Heavy chain)**

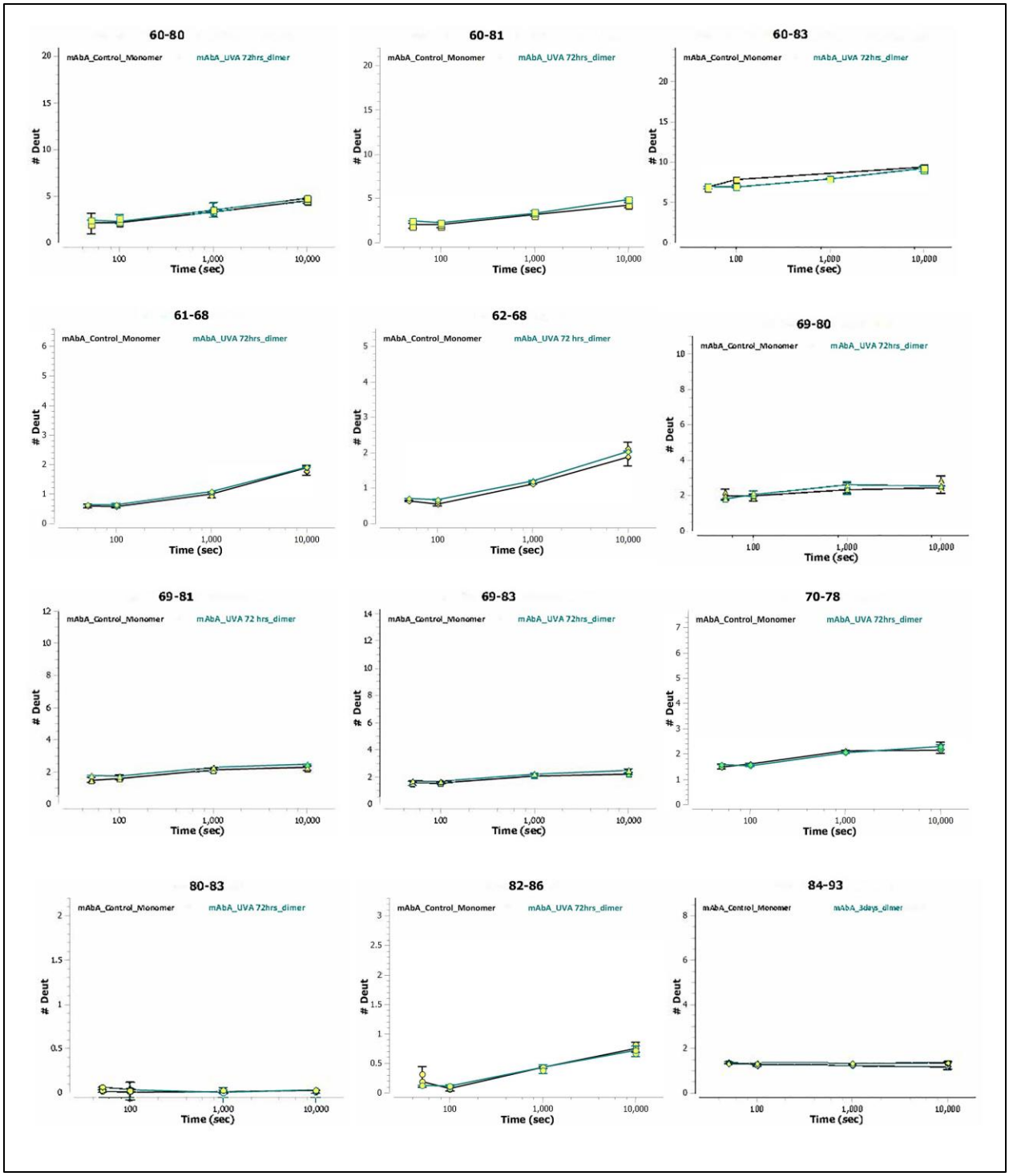

Fig. S7 Deuterium uptake curves for the segments from dimer fractionated from mAbA exposed to UVA light for 72 hours vs control monomer. Peptide segments containing oxidized Met residues were not readily found by HD-Examiner and hence are not reported. **(Heavy chain)**

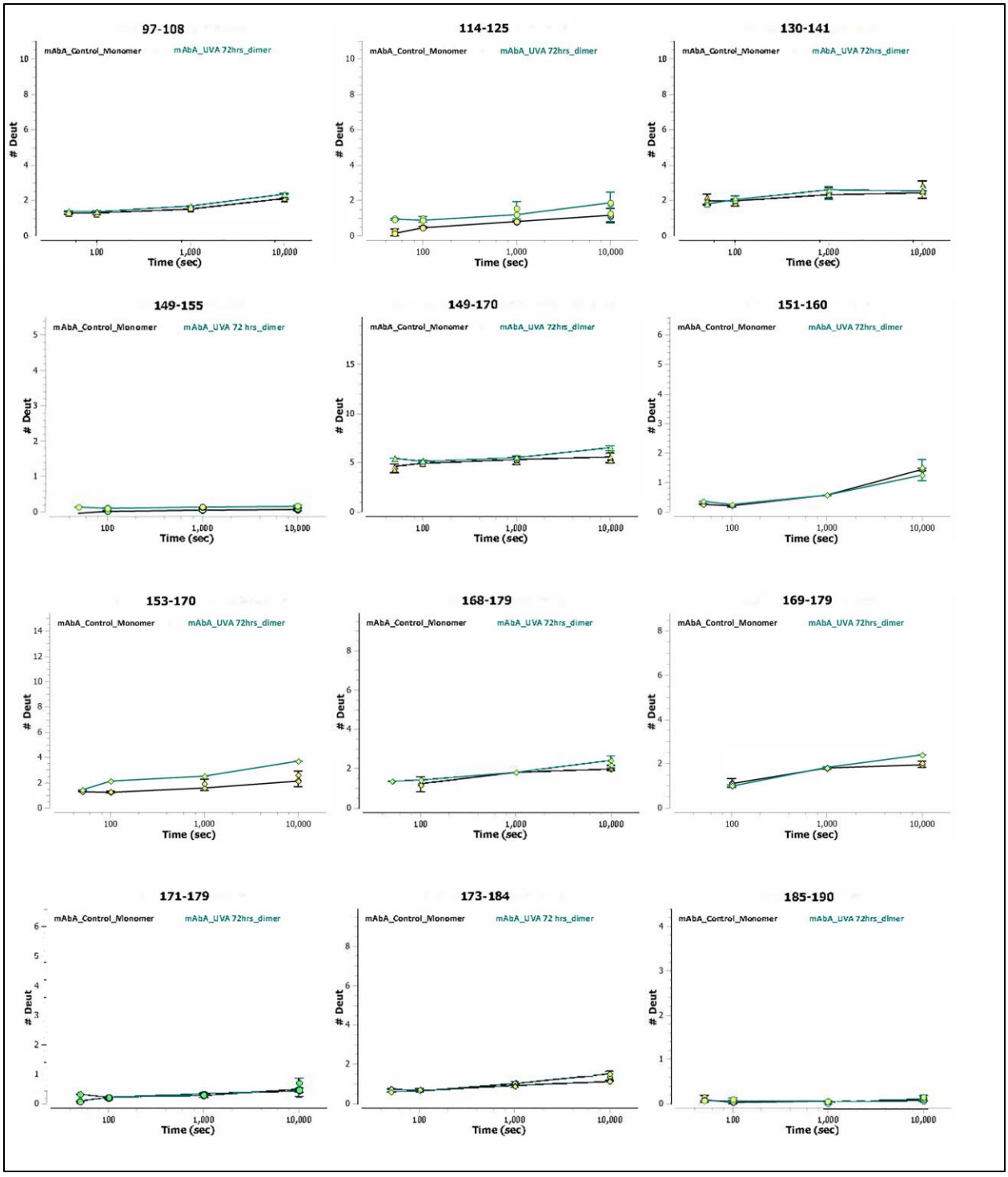

Fig. S7 Deuterium uptake curves for the segments from dimer fractionated from mAbA exposed to UVA light for 72 hours vs control monomer. Peptide segments containing oxidized Met residues were not readily found by HD-Examiner and hence are not reported. **(Heavy chain)**

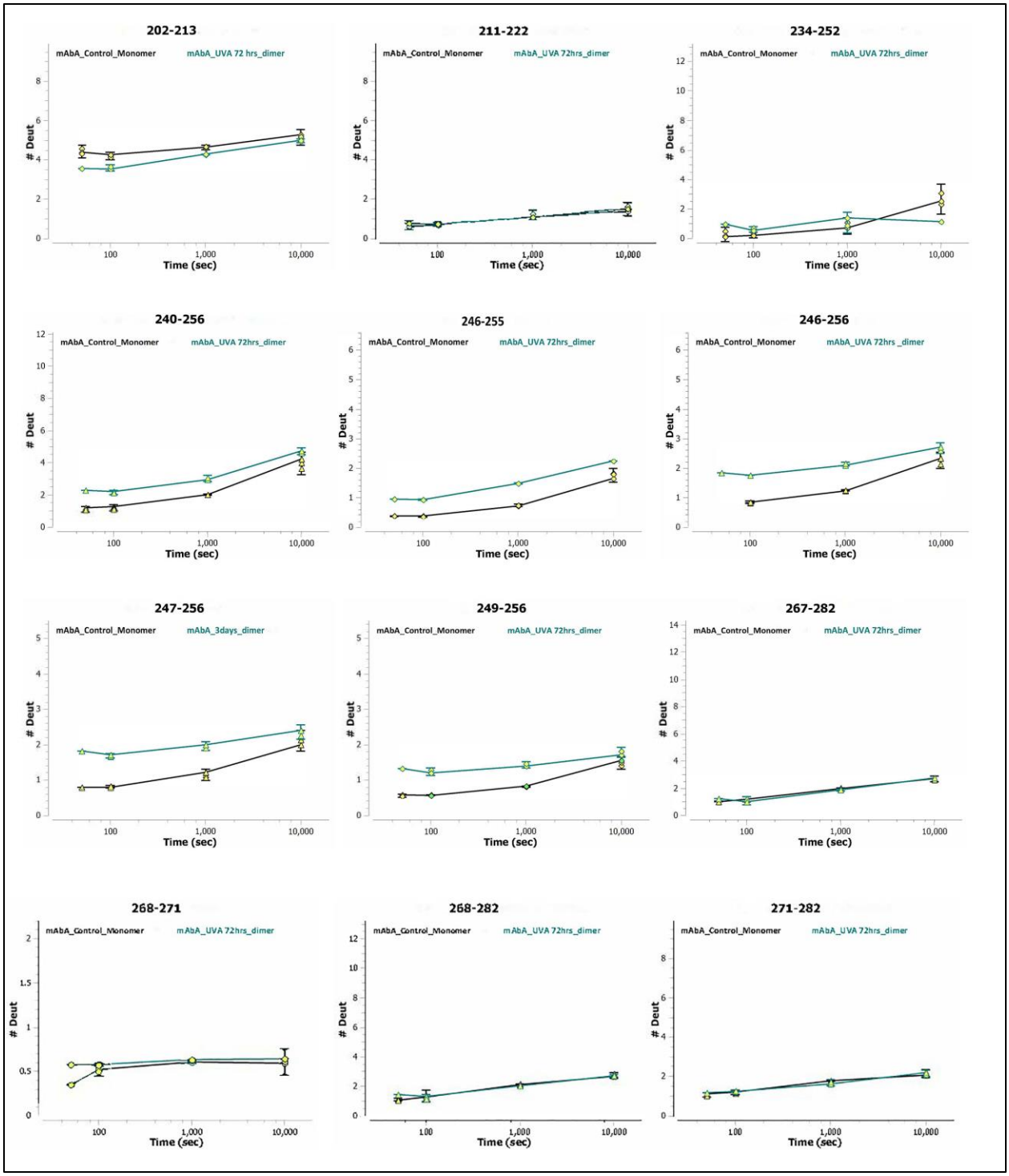

Fig. S7 Deuterium uptake curves for the segments from dimer fractionated from mAbA exposed to UVA light for 72 hours vs control monomer. Peptide segments containing oxidized Met residues were not readily found by HD-Examiner and hence are not reported. **(Heavy chain)**

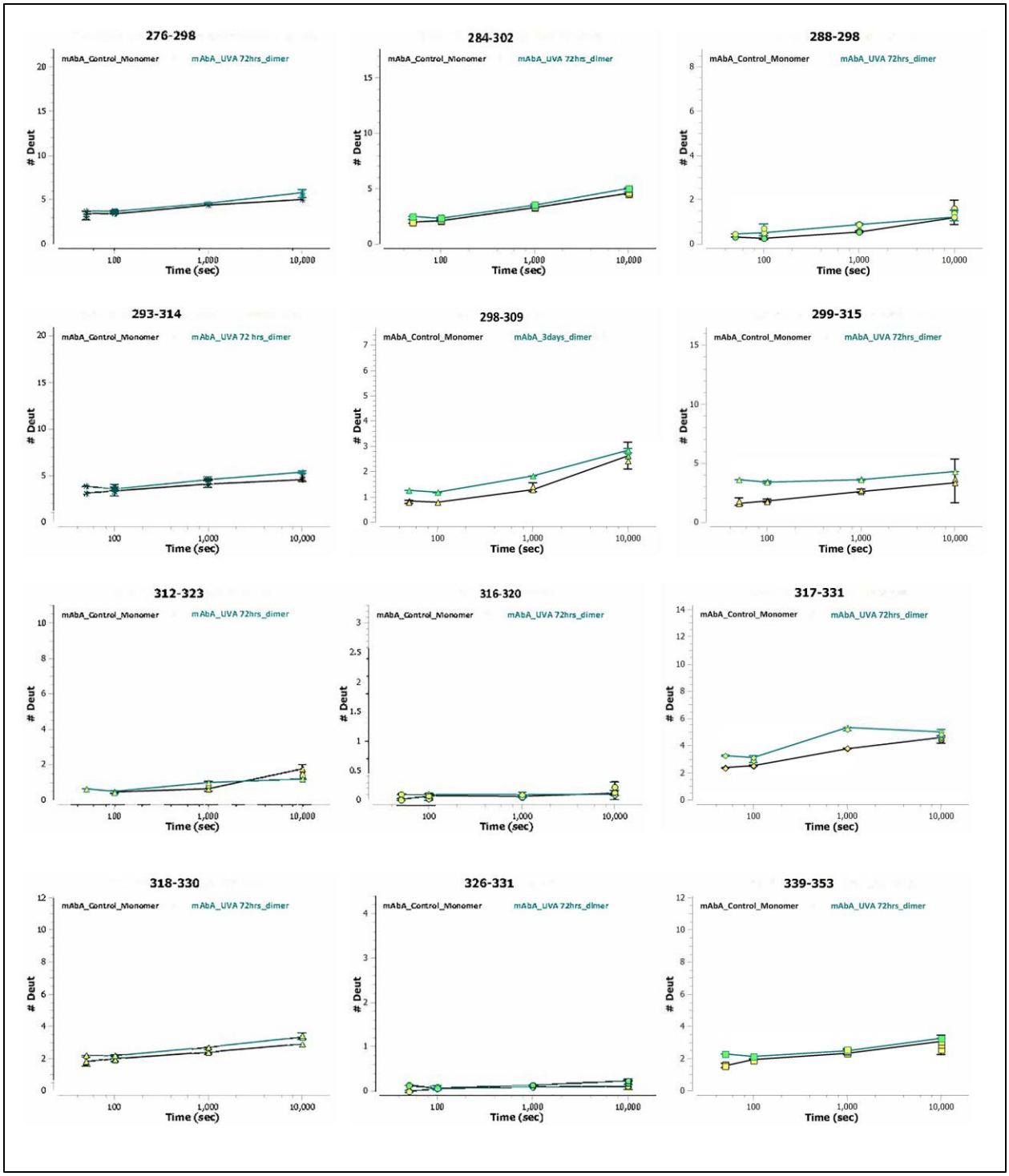

Fig. S7 Deuterium uptake curves for the segments from dimer fractionated from mAbA exposed to UVA light for 72 hours vs control monomer. Peptide segments containing oxidized Met residues were not readily found by HD-Examiner and hence are not reported. **(Heavy chain)**

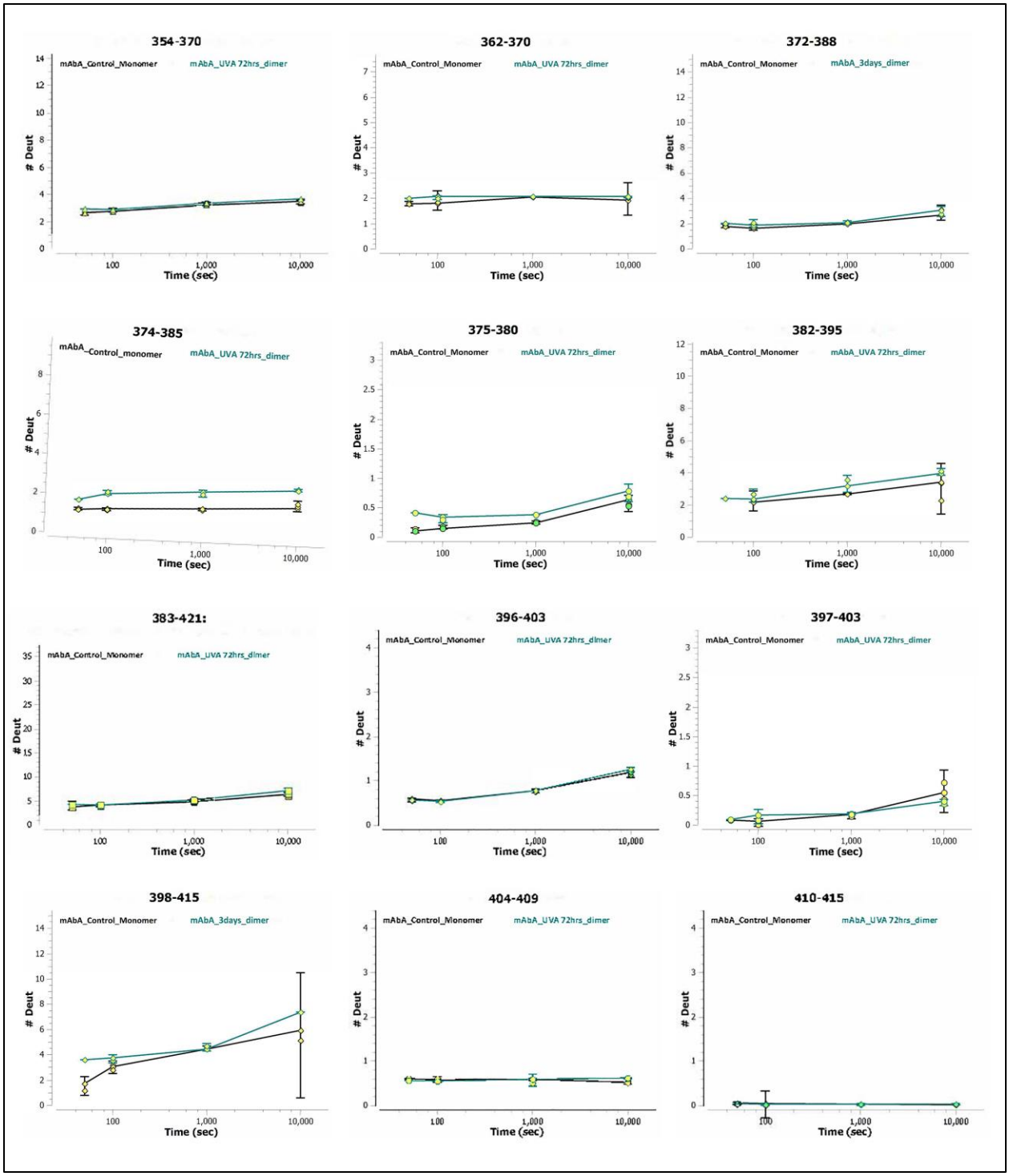

Fig. S7 Deuterium uptake curves for the segments from dimer fractionated from mAbA exposed to UVA light for 72 hours vs control monomer. Peptide segments containing oxidized Met residues were not readily found by HD-Examiner and hence are not reported. **(Heavy chain)**

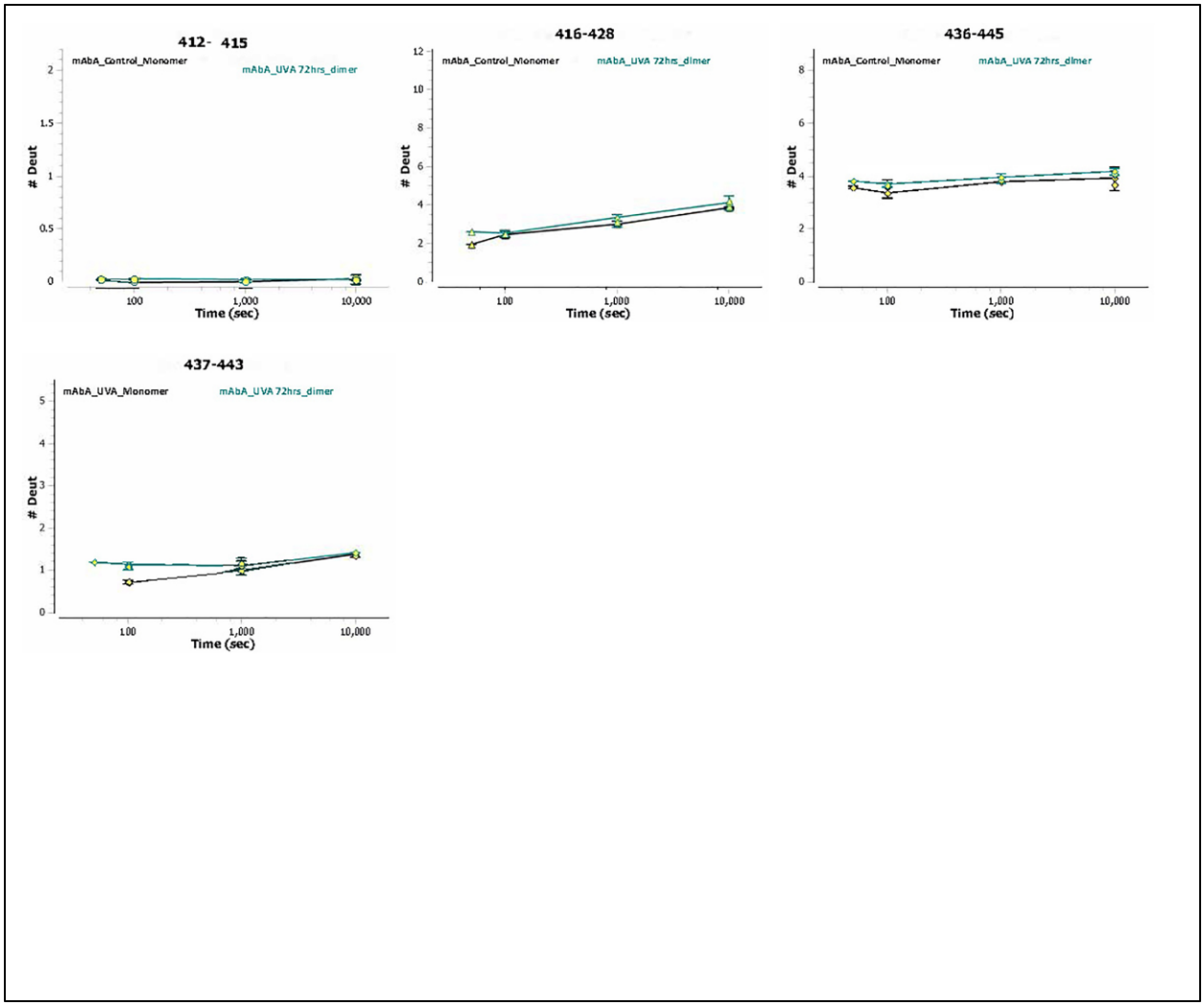

Fig. S7 Deuterium uptake curves for the segments from dimer fractionated from mAbA exposed to UVA light for 72 hours vs control monomer. Peptide segments containing oxidized Met residues were not readily found by HD-Examiner and hence are not reported. **(Heavy chain)**

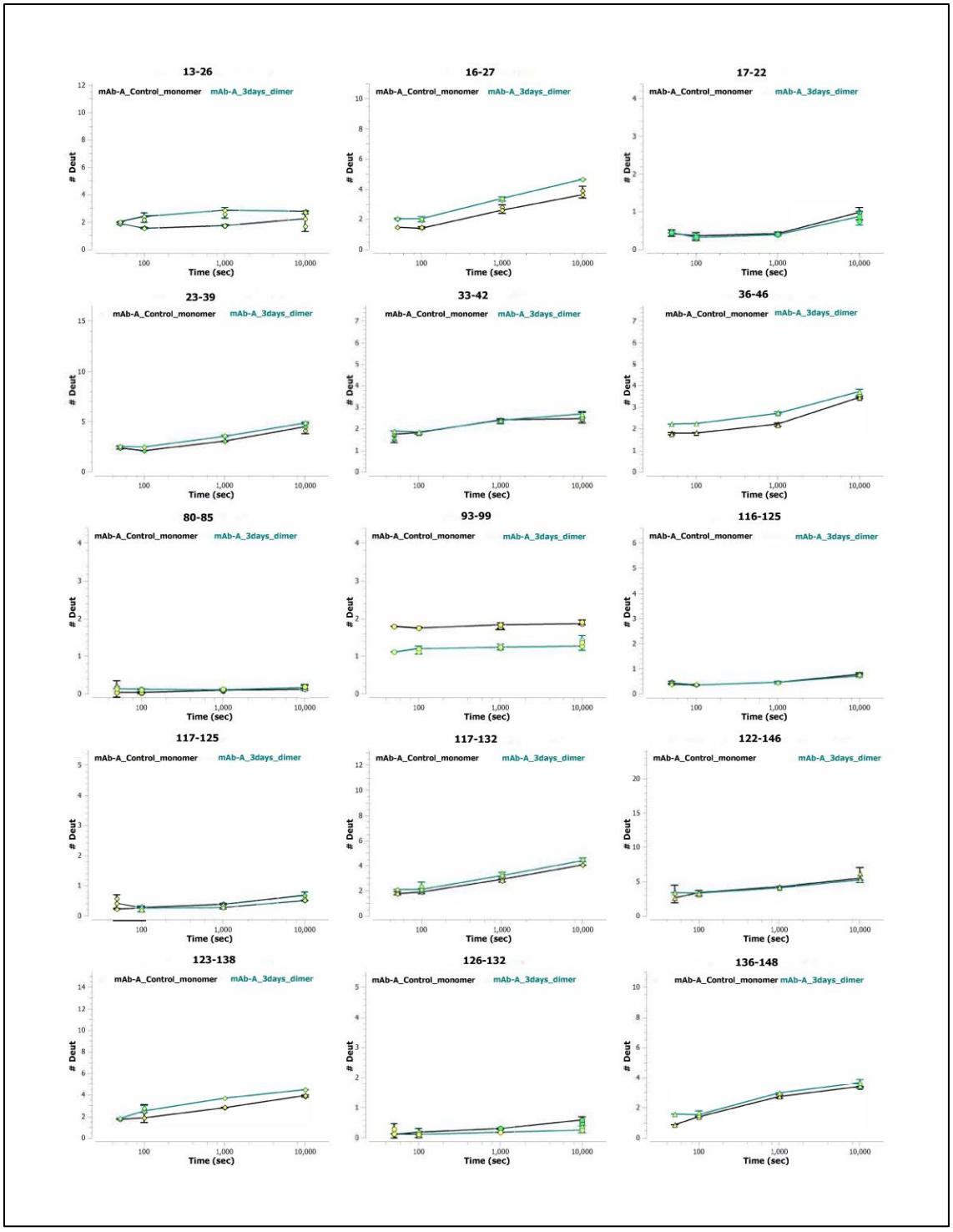

Fig. S7 Deuterium uptake curves for the segments from dimer fractionated from mAbA exposed to UVA light for 72 hours vs control monomer. Peptide segments containing oxidized Met residues were not readily found by HD-Examiner and hence are not reported. **(Light chain)**

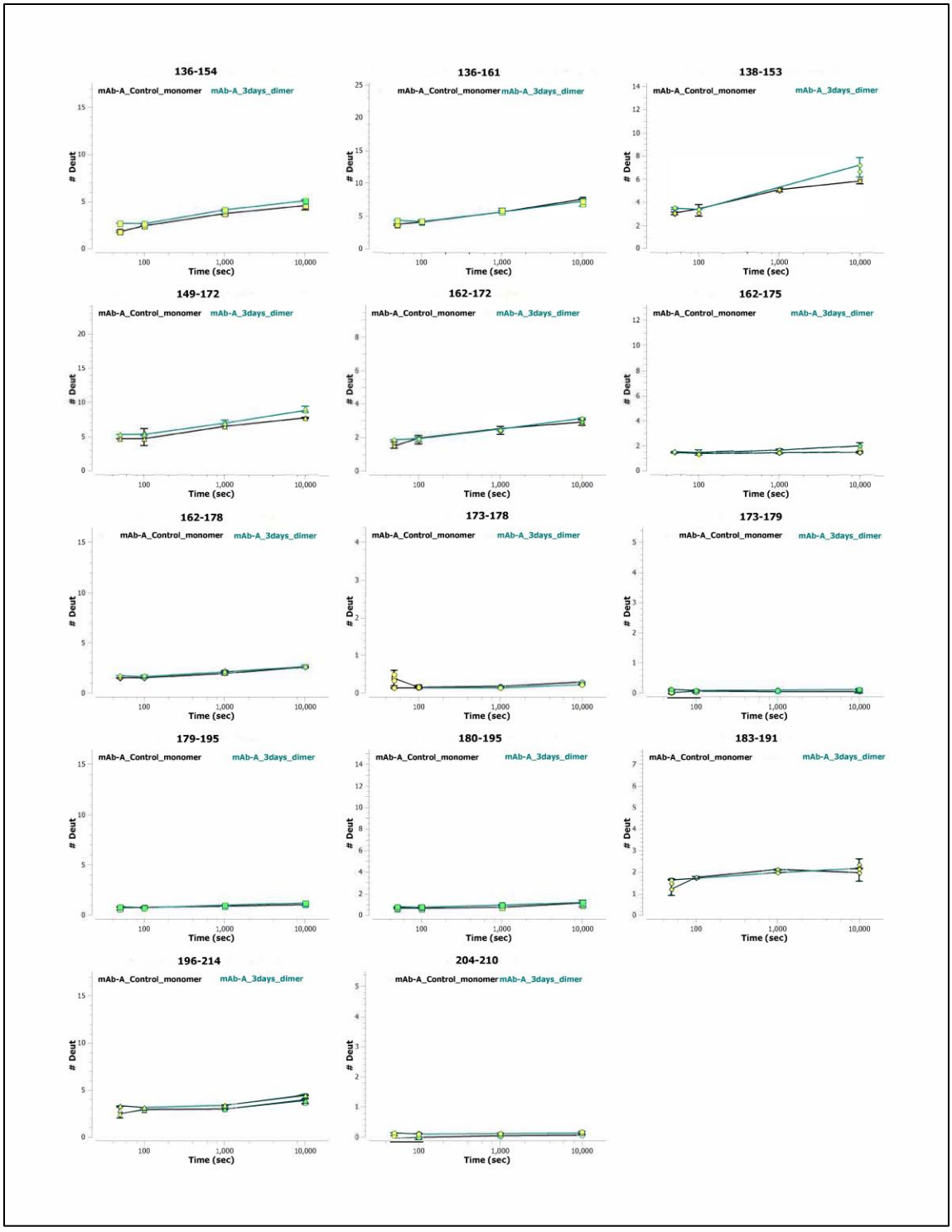

Fig. S7 Deuterium uptake curves for the segments from dimer fractionated from mAbA exposed to UVA light for 72 hours vs control monomer. Peptide segments containing oxidized Met residues were not readily found by HD-Examiner and hence are not reported. **(Light chain)**

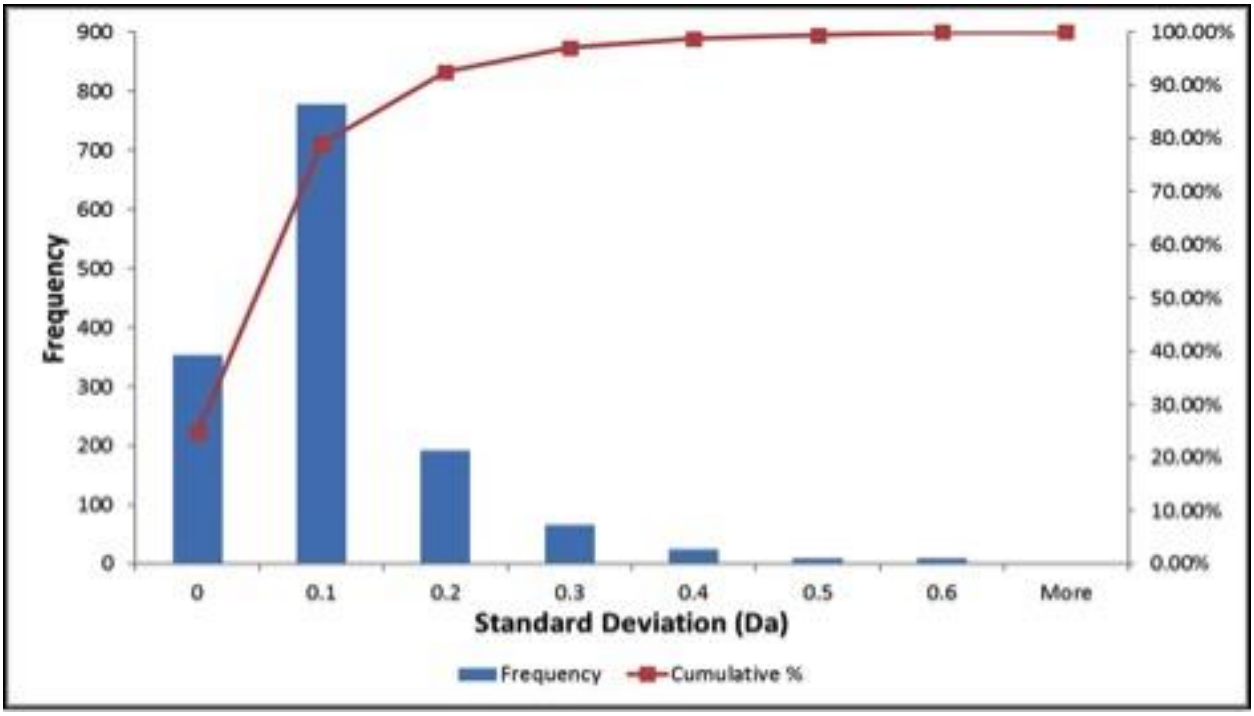

Fig. S8 Distribution of standard deviations for the mass increase of all peptides across all time points (N=1431). The 99th percentile for standard deviations was 0.59 Da.

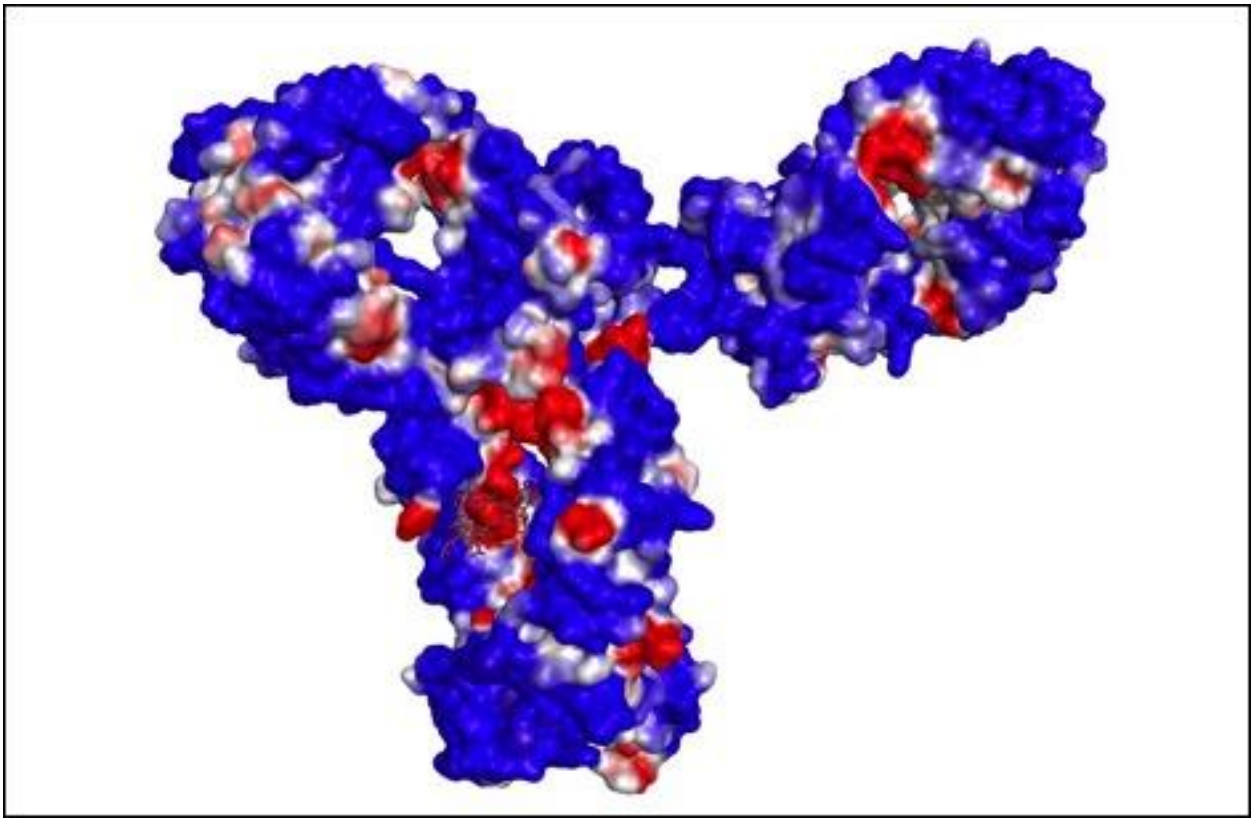

Fig. S9 Spatial aggregation propensity (SAP) for mAbA homology model. The SAP values at R = 5 Å are mapped onto the molecular surface of the mAbA homology model, where red regions represent hydrophobic and aggregation-prone regions and blue regions are hydrophilic and exposed regions, which are predicted to be less aggregation-prone regions.

Chapter 5. Investigating the photo degradation of rat growth hormone with extreme ultra-pressure liquid chromatography-mass spectrometry utilizing meter-long microcapillary columns.

5.1 Introduction

In the past three decades recombinant protein therapeutics have revolutionized the bearing of the modern medicine and commenced competent therapies for several diseases. Since 1982, when the first therapeutic protein- recombinant human insulin was introduced, the number of protein therapeutics in the global market have increased dramatically in number and their frequency of use.[1,2] Protein therapeutics constituted 17% of new drugs approved by the FDA in 2005, and increased to 32% by 2011. The Global Protein Therapeutics and Devices Market is expected to grow at a compound annual growth rate of around 8.6% over the next decade to reach approximately $315.90 billion by 2025.[3] The success of protein drugs over small-molecule drugs is attributed to several advantages such as 1) high specificity with low side effects, 2) well tolerated by the body, 3) clinical development and approval time can be shorter relative to small-molecule drugs and 4) their distinctive structure and functions permit for comprehensive patent protection.[1,2,4] Proteins are sensitive to various physical and chemical degradation pathways such as oxidation, deamidation, hydrolysis, aggregation, β-elimination, photochemical degradation, etc.[5-7] Photochemical damage could occur after proteins are exposed to light during manufacturing, purification, storage, and drug administration.[8]

In proteins, aromatic amino acids (Trp, Tyr, and Phe), and the disulfide bonds are more susceptible to photodegradation.[8] Upon absorption of light, aromatic amino acids generate an excited singlet state, which can undergo intersystem crossing to the first excited fluoresce, triplet state, or eject an electron into the solution, yielding a solvated electron and an aromatic radical cation.[8,9] The solvated electron can reduce the disulfide bond to yield a disulfide radical anion which, on further proton addition and cleavage, produces a thiol and thiyl radical.[9] Thiyl radicals can also be generated by the direct homolysis of disulfide bonds following exposure to UVC

light (λ = 254 nm). Eventually, thiyl radicals can recombine to native or scrambled disulfide bonds, disproportionate into thiol and thioaldehyde.[9-12] These initially formed sulfur-bearing residues have been shown to undergo a series of reactions ultimately leading to the formation of dithiohemiacetals, cyclic thioethers and cyclic vinylthioethers.[13] But, under aerobic conditions, thiyl radicals can react with oxygen to form thiyl peroxyl radicals, which eventually convert into sulfinic, sulfenic, or sulfonic acids.[10] The protein and peptide thiyl radicals can also participate in intramolecular hydrogen atom (H) abstraction reactions with adjacent side chain C-H or alpha carbon hydrogen (αC-H) bonds, generating intermediary carbon centered (C•) radicals. The C• may subsequently involve in cross-linking, fragmentation and oxidation pathways.[12-14] Specifically with αC-H bonds, such reversible H-atom transfer can induce epimerization.[15]

Proteins are large complex molecules, often consisting of heterogeneous mixtures. A comparison between small-molecule and protein drugs makes it clear as to why comprehensive analysis of proteins is challenging.[16-18] For example aspirin, which is considered as a small-molecule measures just 180 Da and has 21 atoms. In contrast, a typical monoclonal antibody measures 150,000 Da, contains ~ 500 amino acids comprising of ca. 20,000 atoms. The myriad of degradation products that can be formed in proteins further increases the complexity of their analysis.[17,18]

To reduce the complexity of these samples, analytical methods often rely on reversed phase liquid chromatography (RPLC) separations preceding the identification by mass spectrometry (MS).[19] The analytical work flow of proteins typically involves an enzymatic digestion step which generates a mixture of peptides.[17-19] The various photodegradation products previously described were identified by LC-MS analysis in model peptides and proteins such as insulin, and a monoclonal antibody. Even though LC-MS setup is extensively in any laboratory for

identification of various modifications, analytical scientists frequently encounter the problem of partial or complete co-elution which can cause incomplete profiling of degradation products. Complete resolution of the analytes can be achieved by development of more efficient LC techniques.

Peak capacity is the best measure of the performance of a gradient separation. Peak capacity is defined as the maximum number of components that can be resolved within a given separation window.[20] This can be achieved by extending the gradient time, but the increase in peak capacity with increase in gradient time reaches plateau as the gradient becomes shallow. Alternate to extending gradient time is increasing the length of the column packed with small particles. In general, peak capacity is proportional to the square root of length of the column and inversely proportional to square root of diameter of the particles used for packing the column.[21,22] One limitation using long columns packed with small particles is the pressure (more than 10,000 psi) that is needed to maintain a given linear velocity, which restricted the use of long column packed with sub-2 µm particles. In collaboration with Jorgenson group at UNC Chapel Hill, Stobaugh group at The University of Kansas has built a capillary-based chromatography system with operational capability over the 35-40 Kpsi range which we term as extreme ultra-pressure liquid chromatographic (XUPLC) system.[23] In this study, we used XUPLC system to delineate the photodegradation of rat growth hormone (rGH) protein.

5.2 Experimental methods

5.2.1 Materials

Optima-grade water, Optima-grade 0.1% formic acid in water, Optima-grade 0.1% formic acid in acetonitrile, Optima-grade formic acid, and HPLC-grade acetonitrile were obtained from Fisher

Scientific (Fairlawn, NJ, USA). HPLC-grade acetone was obtained from Sigma-Aldrich (St. Louis, MO, USA).

5.2.2 Protein production

The plasmid for rGH was provided by GenScript (New Jersey, USA). This plasmid was given to KanPro Research Inc. for expression of rGH. The plasmid was transfected into BL21 (DE3), a type of E. coli cells, which is mainly used for expression of various proteins. In brief, the E. coli cells were cultured in 10 ml lysogeny broth (LB) culture media with the antibiotics (kanamycin and chloramphenicol) for around 12 hours. This 10 ml culture was added to 1 L LB media and was placed in a shaking incubator at 37° C and 200 rpm with the antibiotics (kanamycin and chloramphenicol), until optical density of the media reached a value of 0.6. Isopropyl β-D-1-thiogalactopyranoside (IPTG) (1 mM) was added to the LB media and incubation was continued for 4 hours. Cells were centrifuged at 4,000 rpm for 10 mins and the cell pellet was suspended in the lysis buffer (50 mM tris hydrochloride, 500 mM sodium chloride, pH 8). This mixture was then sonicated, until it was no longer viscous. Inclusion bodies of rGH were isolated by centrifuging at 19,500 rpm for 30 mins and were washed with water. These inclusion bodies were dissolved in the lysis buffer containing 6 M urea. The dissolved inclusion bodies were refolded by following proprietary procedures and dialyzed in a phosphate buffer saline (PBS) containing 88 mM mannitol.

5.2.3 Photoirradiation

The photoirradiation was carried out in a Rayonet photoreactor RPR-200 [Southern New England Ultra Violet Company (Branford, CT)] equipped with four 35 W low pressure mercury lamps (RPR-2537Å) at $\lambda = 254$ nm. Each sample (200 μL) contained 45 μM (1 mg/mL) rGH in

25 mM sodium phosphate buffer at pH 7.2. Samples were placed in quartz tubes, and saturated with Argon (Ar) prior to photoirradiation. Samples were irradiated for 30 mins.

5.2.4 Reduction, alkylation and digestion

For peptide mapping of the rat growth hormone (rGH), 200 µL of either the controls or the photo- irradiated samples were mixed with 100 µL of 50 mM ammonium bicarbonate buffer (pH 8.2), 25 µL of guanidine hydrochloride solution (6 M, in ammonium bicarbonate buffer, 50 mM, pH 8.2) and 50 µL dithiothreitol solution (25 mM) for the reduction of the disulfide bonds. The mixtures were incubated at 50 °C for 30 mins. The thiolate groups of the reduced cysteine residues were then alkylated by the addition of 50 µL of iodoacetamide (100 mM). After 1 hour incubation in the dark at 37 ^{o}C, the protein was precipitated with 500 µL of 0.5 M perchloric acid, and centrifuged at 14,000 g for 10 mins at 4 ^{o}C. The resulting pellet was washed twice with milliQ water. Thereafter, the pellet was reconstituted in 200 µL of ammonium bicarbonate buffer (50 mM, pH 8.2). The digestion was performed by the addition of 10 µg of trypsin/chymotrypsin with a ratio [protein]: [trypsin] = 20 to each sample. After overnight incubation at 37 ^{o}C, the peptides were purified using Amicon ultra-0.5 centrifugal devices, equipped with 10 kDa cut-off membranes in order to separate undigested protein and trypsin/chymotrypsin from the proteolytic peptides.

5.2.5 XUPLC using capillary columns

The XUPLC (Fig. 2) system was assembled around a nanoAcquity UPLC and Xevo G2 QTof mass spectrometer (Waters Corporation, Milford, MA) equipped with a nano electrospray interface (nESI). Detailed description on assembling the XUPLC system was described by Mozziconacci et al.[24] In brief, XUPLC system (Fig.2) consists of a series of valves (V1, V2, V3

and V4), a pneumatic amplified pump (Haskel pump), gradient storage loop (GSL), series of tees (T1, T2, T3 and T4), a capillary chromatography column, connectors and tubings.

The XUPLC requires loading the GSL with solvent program that performs various functions. Optima-grade water with 0.1% formic acid and Optima-grade water with 0.1% formic acid was used as Mobile phase A (A) and Mobile phase B (B), respectively. The solvent gradient program was operated in a last in first out format (LIFO). The operation of the XUPLC system can be divided into 9 stages, as shown in Table 1. The solvent gradient program in Table 1, results in flowing approximately 10 µL of 7% B through the capillary column before meeting a gradient with linear increase in % B from 7% - 45%. This was followed by a series of brief steps such as: a brief isocratic hold at 45% B for 0.1 mins, a rapid surge to 70% B, and a return to 7% B. The gradient loading was followed by sample loading. Through- out the gradient and sample loading steps V2, V3, V4 were always open and V1 was closed allowing the flow of the solvents into the GSL. After the sample loading step, data acquisition step was initiated by opening V1 and closing V2, V3 and V4, which enabled the Haskel pump to push the solvent and the sample in the GSL onto the capillary column for chromatographic separation and eventually into Xevo QTof for mass spectrometric analysis. The column was housed in a column-heating device maintained at 45 ^{o}C.

5.2.6 Ultra-Performance Liquid Chromatography utilizing a commercial column

Liquid chromatography-mass spectrometry (LC-MS) analyses of the peptide maps were performed on a nanoAcquity ultra performance liquid chromatography system (Waters Corporation, Milford, MA). One microliter of each sample was injected onto a Symmetry C18

Waters Trap Column (2G-V/MTrap, 180 µm x 20mm, 5 µm) connected to an analytical nanoAcquity ultra performance Waters column (CSH C18, 75 µm x 250 mm, 1.7 µm). Mobile phases consisted of water/acetonitrile/formic acid at a ratio of 99%, 1%, and 0.08% (v:v:v) for solvent A and a ratio of 1%, 99%, and 0.06% (v:v:v) for solvent B. The injected sample was first loaded onto a trapping column at 4 µL/min for 3 min with 97% of solvent A and 3% of solvent B. After 3 min, the peptides were directed toward the analytical column and were separated with a linear gradient (3%-35% of solvent B within 50 mins) delivered at a rate of 0.3 µL/min.

5.2.7 Nano electrospray Ionization Time-of-Flight MS and MS/MS Analysis

Mass spectrometry was performed on a Waters Xevo-G2 (Waters Corporation, Milford, MA) .The outlet of the RPLC column was connected to a qTOF Premier (Waters Corp) through a stainless steel LC-MS (Thermo Scientific) emitter (50 mm x 30 µm I.D x 150 µm O.D) and each emitter was inserted into a micro sleeve (180 µm I.D) to facilitate installation on to a nanospray emitter tip (Waters Corp). The system was operated in the positive mode with spray voltage (+2.7kV) applied on a nanoflow emitter. The desolvation gas flow and the desolvation temperature were set to 1000 L/h and 100 ^{o}C, respectively. The cone gas flow was set to 25 L/h and a source temperature of 100 ^{o}C. The capillary voltage and cone voltage were set to 2,700 and 45 V, respectively. The Xevo-G2 acquisition rate was set to 0.5 s with a 0.0 s interscan delay. The instrument was operated in the MS^{E} mode, with the first resolving quadrupole in a wide pass mode with the collision cell operating with different alternating energies. To acquire the non-fragmented MS spectrum, the collision cell was operated at 3 eV and the fragmented MS/MS ion spectra were acquired by ramping the collision cell energies from 18 to 45 eV.

The MS and MS/MS spectra obtained by the Q-TOF G2 were analyzed with MassLynx program V4.1 from Waters Corporation. Furthermore, the LC-MS/MS data was processed using Byonic Software. The rGH digests were searched against a database with the amino acid sequence of the protein using 10 ppm and 20 ppm mass tolerance parameters for precursor and fragment ions, respectively.

5.3 Results

Here we define two terms that are used throughout the next sections from this point forward. First, the term "control" refers to an rGH sample which was directly diluted from the stock solution. Second, "irradiated" sample refers to an rGH sample, which was exposed to UV light (λ = 254 nm).

5.3.1 XUPLC separation of control rGH digest

As noted previously, unloading of the contents in the GSL (solvent gradient + sample) as shown in Table 1 happened over the data acquisition (295 mins) step with a flow rate of 0.29 µL/min. Fig. 3 shows a typical chromatogram for a control rGH digest. Data analysis with the Byonic software program indicated ~ 92% protein coverage. The retention time (t_R) of the first identified peak was at 41 mins (Fig. 3), with all identified peptides listed in Table 2. The peaks eluting prior to this peptide (41 mins) were not identified and appeared to be late-eluting peaks from the previous injection. The retention time values were highly reproducible with RSD < 0.15 (n=3), except for some of the peptides. The first two peptides identified (Fig. 3 insert) which eluted at t_R 41.3 min and 45.4 min represent pre-irradiation Met oxidation (Met 124) products. In addition, another peptide with Met (Met 102) oxidation was identified at a t_R of 152.4 min.

5.3.2 UPLC separation of control rGH digest

A chromatogram resulting from the separation of a control rGH digest using the UPLC system is shown in Fig. 4. Data analysis with the Byonic software program indicated ~ 92% protein coverage. All the UPLC separations were conducted in the non-trapping mode, which facilitates a better comparison with the XUPLC separations. The elution of the first identified peak occurred at t_R = 32.33 min, with all identified peptides listed in Table 3. The retention time values were reproducible with RSD < 0.62 (n=3). Peptides with oxidized Met residues (pre-light exposure) co-eluted in a single peak (Fig. 4 insert).

5.3.3 XUPLC separation of irradiated rGH

To examine the utility of XUPLC in analyzing protein degradation and identification of degradation products, rGH was exposed to UV light (λ = 254 nm), followed by reduction, alkylation and enzymatic digestion. The peptides resulting from the enzymatic digestion of control and irradiated rGH were separated using the XUPLC setup, which resulted in the chromatograms shown in Fig. 5. Fig.5 displays some interesting features: some of the peaks in the irradiated sample decreased, with newly formed products appearing as new peaks (Fig.5 insert). Focusing on the peaks in the insert of Fig.5, degradation of peptide $F_{184}AESSCAF_{191}$, eluting at t_R = 142.35 min, resulted in the formation of two chromatographically resolved products eluting at t_R = 137.7 and 142.35 min. MS analysis revealed that the two chromatographically resolved products were isobaric (both the products has the same mass) in nature.

5.3.4 MS/MS analysis of photo degradation of products

The C-terminal region of rGH contains one intra-chain disulfide bond between Cys 181 and Cys 189. As disulfide bonds undergo photo degradation upon exposure to light (especially $\lambda = 254$ nm), thus it become of primary importance to identify the b and y ions, which allows us to discriminate between different photodegradation products. The MS/MS spectrum reported in Fig. 7 provides evidence for the degradation of $F_{184}AESSCAF_{191}$ to $F_{184}AESSC(-2)AF_{191}$. The ions $b3^+$, $b4^+$, and $b5^+$ indicate that a part of sequence is unmodified on light exposure, where m/z 522.21 corresponds to the singly charged ion of FAESS. Instead, the ions $y5^+$ and $y6^+$, despite their low intensity, provide the evidence that cysteine (Cys 189) degraded to form an ene-thiol, which was eventually alkylated with iodoacetamide. For example, comparison of $b6^+$, $b7^+$, $y5^+$, and $y6^+$ ions between Fig.7 (MS/MS of Cys 189-containing peptide after irradiation) vs Fig.8 (MS/MS of Cys 189-containing peptide before irradiation) where all these ions show a mass difference of 2 Da further confirm the degradation of Cys 189 to the ene-thiol.

5.4 Discussion

Complete identification of the degradation products of proteins is essential to elucidate the complex degradation pathways. To reduce the complexity of these samples, analytical methods depend on reverse phase liquid chromatography (RPLC) for the separation of various chemical entities before their identification using mass spectrometry (MS). RPLC-MS analysis has become a preferred analytical tool for the identification of protein and their variants, location of post-translational modifications (PTMs) and confirm protein sequences.[25] Although, RPLC-MS is widely used in multiple investigations, frequently this analysis faces the problem of partial or complete co-elution, which can lead to oversimplication and/or incorrect estimation of the

degradation products that are formed. This can be resolved by developing more efficient LC techniques that will allow introducing better resolved chemical entities into the MS and increase degradation product identification.[22-24] The efficiency of LC gradient separation can be extended by increasing the length of the column.[23] In this study, emphasis is placed on analyzing photoinduced degradation of rGH using XUPLC system and comparing the results obtained by XUPLC to those obtained by using UPLC system.

5.4.1 Comparison between XUPLC and UPLC separations of rGH digests

By comparing chromatograms in Fig. 3 and Fig. 4, we can conclude that there is an overall increase in resolution between the peaks during XUPLC separations compared to the UPLC separations. Of particular interest are inserts in Fig.3 and Fig.4 where early eluting Met oxidation products are identified. During XUPLC analysis the Met oxidation products [M(O)QELEDGSPR] elute as two chromatographically resolved peaks. Resolution of Met oxidation products into two separate peaks can be rationalized by the formation of new stereocenter of either R or S configuration during the oxidation process, leading to formation of diasteriomeric peptides.[26] When the same samples underwent UPLC analysis the Met oxidation products co-eluted. The increased overall resolution during XUPLC analysis (118 cm column was used) when compared to UPLC analysis (25 cm column was used) can be explained by the large in theoretical plate count that are resultant of increase in length of the column.

In addition, similar conclusions can be made on comparison of Fig. 5 and Fig. 6, where irradiated rGH digests subjected to XUPLC analysis exhibited greater efficiency in separating photodegradation products into two chromatographically separated peaks, whereas with the UPLC analysis both the products co-eluted. Based on the MS/MS analysis and established

chemistry of photo-induced chemical degradation knowledge, the products were identified to be resultant of degradation of disulfide linkages (Cys 181-Cys 189). Even though these products were isobaric with same MS/MS fragmentation, they eluted as two separate peaks which are assigned as diastereomerically related cis/trans isomers; nonetheless, with the current data it is not possible to decide specific assignments. The formation of cis/trans products can be explained through the reaction scheme presented in Fig.9. Intra-chain disulfide bonds in UV irradiated (λ = 254 nm) rGH undergo homolytic cleavage forming a pair of thiyl radicals. The pair of thiyl radicals formed undergoes a disproportionation leading to the formation of thioaldehyde and thiol products. The resulting thioaldehyde products are known to participate in tautomeric equilibria to form ene-thiols.[10-14]

5.5 Conclusions

An XUPLC system with pressure capabilities upto 35-40 Kpsi and connected with capillary columns ranging 118 cm with sub-2 µm particles was used for profiling photo-induced degradation of rGH. Comparison of XUPLC separations with UPLC separations which were achieved with columns ranging 25 cm showed significant increase in resolution. Analysis of photo-induced degradation of rGH using XUPLC system resolved isobaric cis/trans diasteriomeric products into two chromatographically resolved peaks, which were unresolved on subjecting to UPLC separations. Chromatographic systems employing long capillary columns which are operated under high pressure will be an indispensable tool for analysis of complex protein digests.

5.6 References

1) Leader B, Baca QJ, Golan DE. Protein therapeutics: a summary and pharmacological classification. Nat. Rev. 2008; 7(1): 21

2) Carter PJ. Introduction to current and future protein therapeutics: a protein engineering perspective. Exp. Cell. Res. 2011; 317(9): 1261-9

3)https://globenewswire.com/news-release/2017/01/26/911299/0/en/Protein-Therapeutics-Market-Analysis-and-Trends-Report-2016-Therapeutic-Proteins-Application-Function-Forecast-to-2025-for-the-315-9-Billion-Market.html.

4) Pavlou AK, Reichert JM. Recombinant protein therapeutics—success rates, market trends and values to 2010. Nat. Biotechnol. 2004; 22(12): 1513-9

5) Wang W. Instability, stabilization, and formulation of liquid protein pharmaceuticals. Int. J. Pharm. 1999; 185(2): 129-88

6) Manning MC, Chou DK, Murphy BM, Payne RW, Katayama DS. Stability of protein pharmaceuticals: an update. Pharm. Res. 2010; 27(4): 544-75.

7) Li S, Schöneich C, Borchardt RT. Chemical instability of protein pharmaceuticals: Mechanisms of oxidation and strategies for stabilization. Biotechnol. Bioeng. 1995; 48(5): 490-500.

8) Kerwin BA, Remmele RL. Protect from light: photodegradation and protein biologics. J. Pharm. Sci. 2007; 96(6): 1468-79.

9) Vanhooren A, Devreese B, Vanhee K, Van Beeumen J, Hanssens I. Photoexcitation of tryptophan groups induces reduction of two disulfide bonds in goat α-lactalbumin. Biochemistry. 2002; 41(36): 11035-43.

10) Mozziconacci O, Kerwin BA, Schöneich C. Photolysis of an intrachain peptide disulfide bond: primary and secondary processes, formation of H2S, and hydrogen transfer reactions. J. Phys. Chem. B. 2010; 114(10): 3668-88.

11) Mozziconacci O, Kerwin BA, Schöneich C. Reversible hydrogen transfer reactions of cysteine thiyl radicals in peptides: the conversion of cysteine into dehydroalanine and alanine, and of alanine into dehydroalanine. J. Phys. Chem. B. 2011; 115(42): 12287-305.

12) Mozziconacci O, Sharov V, Williams TD, Kerwin BA, Schöneich C. Peptide cysteine thiyl radicals abstract hydrogen atoms from surrounding amino acids: the photolysis of a cysteine containing model peptide. J. Phys. Chem. B. 2008; 112(30): 9250-7.

13) Mozziconacci O, Kerwin BA, Schöneich C. Exposure of a monoclonal antibody, IgG1, to UV-light leads to protein dithiohemiacetal and thioether cross-links: a role for thiyl radicals?. Chem. Res. Toxicol51. 2010; 23(8): 1310-2.

14) Zhou S, Mozziconacci O, Kerwin BA, Schöneich C. The photolysis of disulfide bonds in IgG1 and IgG2 leads to selective intramolecular hydrogen transfer reactions of cysteine Thiyl radicals, probed by covalent H/D exchange and RPLC-MS/MS analysis. Pharm Res. 2013; 30(5): 1291-9.

15) Mozziconacci O, Schöneich C. Sequence-specific formation of D-amino acids in a monoclonal antibody during light exposure. Mol. Pharm. 2014; 11(11): 4291-7.

16) Walsh G, Jefferis R. Post-translational modifications in the context of therapeutic proteins. Nat. Biotechnol. 2006; 24(10): 1241.

17) Kim YJ, Doyle ML. Structural mass spectrometry in protein therapeutics discovery. Anal. Chem. 2010; 82(17): 7083-9.

18) Chen G, Warrack BM, Goodenough AK, Wei H, Wang-Iverson DB, Tymiak AA. Characterization of protein therapeutics by mass spectrometry: recent developments and future directions. Drug discovery today. 2011; 16(1): 58-64.

19) Xie F, Smith RD, Shen Y. Advanced proteomic liquid chromatography. Journal of Chromatography A. 2012; 1261: 78-90.

20) Neue UD. Theory of peak capacity in gradient elution. Journal of Chromatography A. 2005; 1079(1): 153-61.

21) Patel KD, Jerkovich AD, Link JC, Jorgenson JW. In-depth characterization of slurry packed capillary columns with 1.0-μm nonporous particles using reversed-phase isocratic ultrahigh-pressure liquid chromatography. Analytical chemistry. 2004; 76(19): 5777-86.

22) Liu H, Finch JW, Lavallee MJ, Collamati RA, Benevides CC, Gebler JC. Effects of column length, particle size, gradient length and flow rate on peak capacity of nano-scale liquid chromatography for peptide separations. Journal of Chromatography A. 2007; 1147(1): 30-6.

23) Grinias KM, Godinho JM, Franklin EG, Stobaugh JT, Jorgenson JW. Development of a 45kpsi ultrahigh pressure liquid chromatography instrument for gradient separations of peptides using long microcapillary columns and sub-2μm particles. Journal of Chromatography A. 2016; 1469:60-7.

24) Mozziconacci O, Stobaugh JT, Bommana R, Woods J, Franklin E, Jorgenson JW, Forrest ML, Schöneich C, Stobaugh JF. Profiling the Photochemical-Induced Degradation of Rat Growth Hormone with Extreme Ultra-pressure Chromatography–Mass Spectrometry Utilizing Meter-Long Microcapillary Columns Packed with Sub-2-μm Particles. Chromatographia. 2017:1-20.

25) Shen Y, Hixson KK, Tolic N, Camp DG, Purvine SO, Moore RJ, Smith RD. Mass spectrometry analysis of proteome-wide proteolytic post-translational degradation of proteins. Analytical chemistry. 2008; 80(15): 5819-28.

26) Vogt W. Oxidation of methionyl residues in proteins: tools, targets, and reversal. Free Radical Biology and Medicine. 1995; 18(1): 1493-105.

Tables

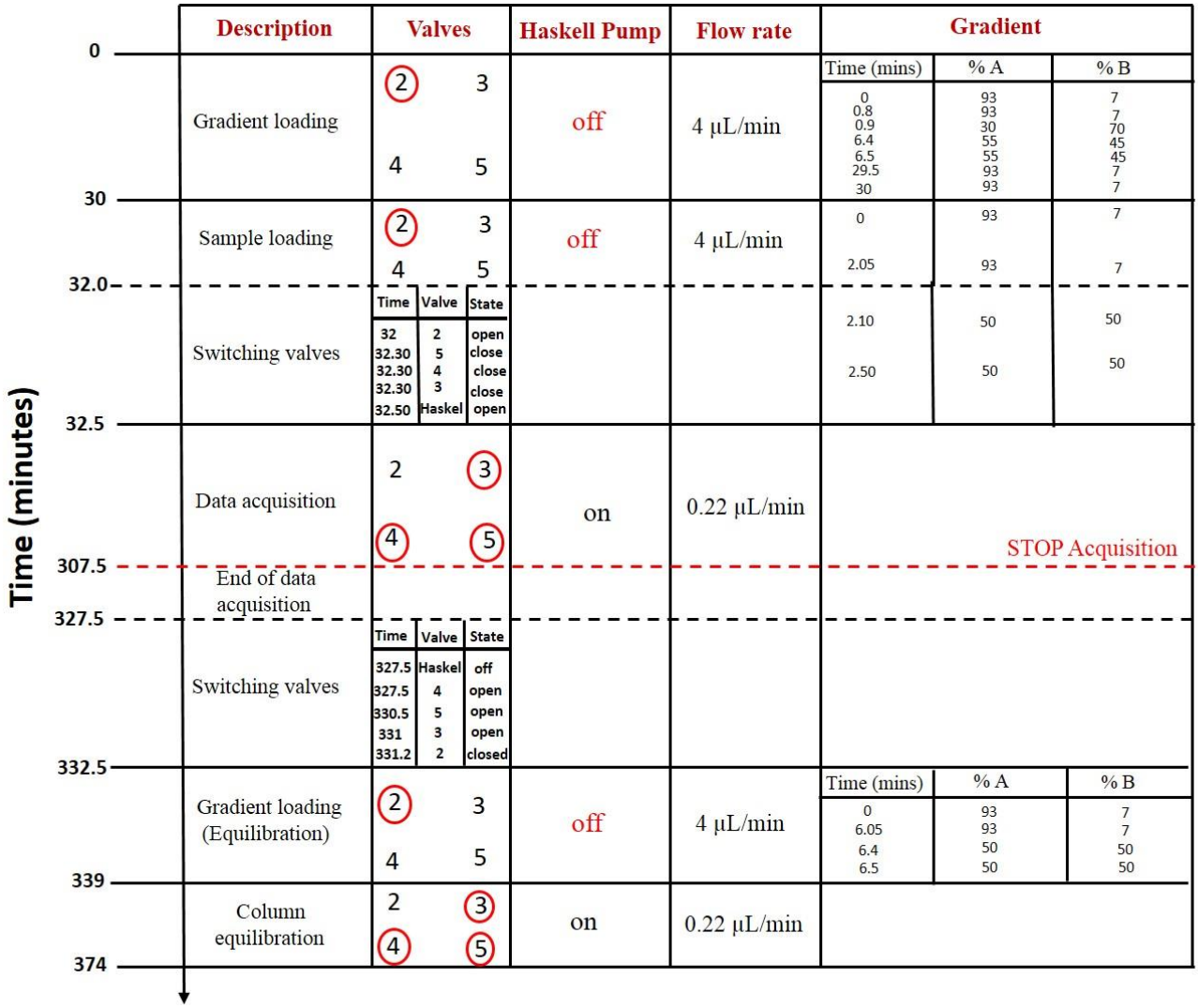

◯ Valves closed

Table 1. Detailed report of solvents loaded into the gradient storage loop together with a summary of the various aspects of solvent control.

#	Peptide	m/z	R.T (min)	S.D (min)	%RSD
1	M(O)QELEDGSPR	1117.52	41.27	0.112	0.11
2	M(O)QELEDGSPR	1117.52	45.39	0.107	0.11
3	FDANMR	753.33	53.59	0.181	0.337
4	AYIPEGQR	933.47	59	0.108	0.183
5	SETIPAPTGK	1000.53	65.39	0.061	0.093
6	QELEDGSPRI	1030.48	65.39	0.072	0.11
7	SDDALLK	648.69	66.14	0.127	0.192
8	IGQILK	671.8	66.14	0.115	0.173
9	MQELEDGSPR	1161.49	67.42	0.072	0.106
10	HQLAADTY	803.4	70.75	0.111	0.156
11	QTYDKF	801.87	70.84	0.075	0.105
12	AQHLHQLAADTY	1367.61	75.94	0.042	0.055
13	TNSLM	565.26	78.18	0.139	0.177
14	GLL	302.2	102.99	0.171	0.166
15	RFAESSCAF	1074.46	104.79	0.087	0.083
16	TDMELLR	877.44	125.65	0.11	0.087
17	GPVQF	547.28	125.65	0.135	0.107
18	CFSETIPAPTGK	1307.6	128.29	0.114	0.088
19	SIQNAQAAF	949.47	131.36	0.122	0.092
20	SSLF	453.51	138.84	0.167	0.12
21	SDDALL	633.31	139.75	0.168	0.12
22	FAESSCAF	918.344	142.35	0.123	0.086
23	IGQIL	543.35	144.48	0.164	0.113
24	TNSLM(O)F	728.33	152.39	0.197	0.11
25	IFTNSL	694.37	156.92	0.112	0.071
26	LIQSW	589.71	157.77	0.137	0.086
27	SLLL	445.58	176.3	0.246	0.139
28	YSIQNAQAAF	1188.56	180.8	0.174	0.096
29	TNSLMFGTSDR	1228.56	187.56	0.193	0.102
30	DLHKAETY	975.46	191.2	0.127	0.066
31	TDMELL	721.34	196.96	0.25	0.126
32	LGPVQF	660.37	198.36	0.193	0.097
33	SCF	413.37	198.78	0.302	0.151
34	FSLL	479.28	211.5	0.217	0.102
35	DLEEGIQAL	987.49	226.68	0.214	0.094
36	EEGIQAL	760.38	232.67	0.217	0.093
37	LIQSWL	759.44	232.67	0.217	0.093
38	MFPAMPL	806.39	258.63	0.261	0.1

Table 2. Control rGH digest eluted using XUPLC setup. Retention reproducibility was calculated using three independent injections of the digest. R.T represents retention time, m/z represents monoisotopic mass, S.D represents standard deviation, and % RSD represents relative standard deviation.

#	Peptide	m/z	RT (min)	SD (min)	% RSD
1	M(O)QELEDGSPR	1117.52	32.33	0.134	0.29
2	M(O)QELEDGSPR	1117.52	32.33	0.134	0.29
3	AYIPEGQR	933.47	35.2	0.195	0.553
4	FDANMR	753.33	35.2	0.169	0.48
5	SETIPAPTGK	1000.53	35.91	0.193	0.537
6	MQELEDGSPR	1161.49	35.91	0.197	0.548
7	HQLAADTY	918.4	35.91	0.191	0.531
8	AQHLHQLAADTY	1367.61	35.91	0.218	0.607
9	QELEDGSPRI	1030.48	35.91	0.179	0.498
10	SDDALLK	648.69	36.6	0.123	0.336
11	QTYDKF	801.87	37.2	0.231	0.62
12	IGQILK	671.8	38.01	0.198	0.507
13	RFAESSCAF	1074.46	41.42	0.181	0.436
14	TNSLM	565.26	42.2	0.186	0.44
15	CFSETIPAPTGK	1307.6	43.28	0.174	0.402
16	TDMELLR	877.44	45.51	0.157	0.344
17	SIQNAQAAF	949.47	46.49	0.141	0.303
18	FAESSCAF	918.344	47.68	0.122	0.255
19	GPVQF	547.28	47.68	0.124	0.26
20	GLL	302.2	47.68	0.174	0.364
21	SSLF	453.51	50.82	0.143	0.299
22	SDDALL	633.31	50.82	0.186	0.495
23	IGQIL	543.35	50.82	0.152	0.482
24	SLLL	445.58	50.82	0.252	0.394
25	TNSLM(O)F	728.33	51.23	0.237	0.41
26	LIQSW	646.35	51.23	0.247	0.262
27	IFTNSL	694.37	51.23	0.202	0.42
28	DLHKAETY	975.46	51.4	0.135	0.262
29	TNSLMFGTSDR	1228.56	52.31	0.22	0.42
30	YSIQNAQAAF	1112.56	52.31	0.246	0.47
31	LGPVQF	660.37	54.91	0.129	0.234
32	TDMELL	721.34	57.41	0.143	0.249
33	SCF	413.37	57.45	0.174	0.302
34	DLEEGIQAL	987.49	59.38	0.122	0.205
35	FSLL	479.28	60.39	0.18	0.298
36	EEGIQAL	760.38	61.34	0.181	0.295
37	LIQSWL	759.44	61.34	0.175	0.285
38	MFPAMPL	806.39	64.92	0.197	0.303

Table 3. Control rGH digest eluted using UPLC setup. Retention reproducibility was calculated using three independent injections of the digest. R.T represents retention time, m/z represents monoisotopic mass, S.D represents standard deviation, and % RSD represents relative standard deviation.

Figures

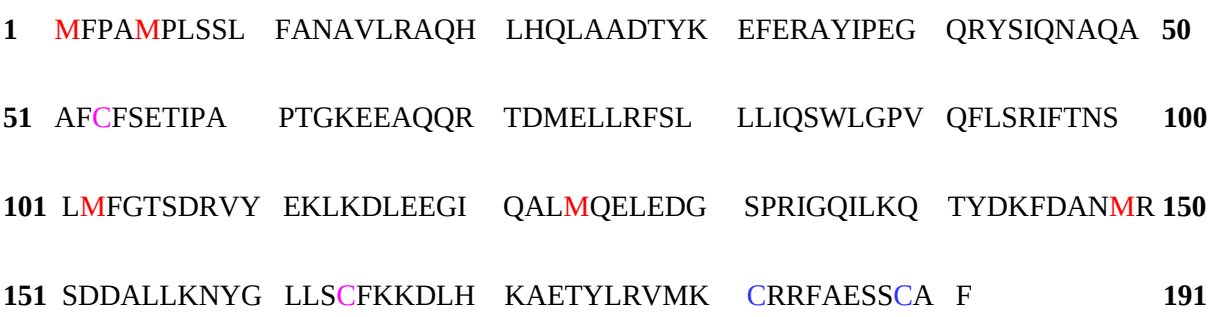

Figure 1. Sequence of rGH. Met residues are colored red and the two intra-chain disulfide linkages are colored in pink (Cys 53-Cys 164) and blue (Cys 181-Cys 189), respectively.

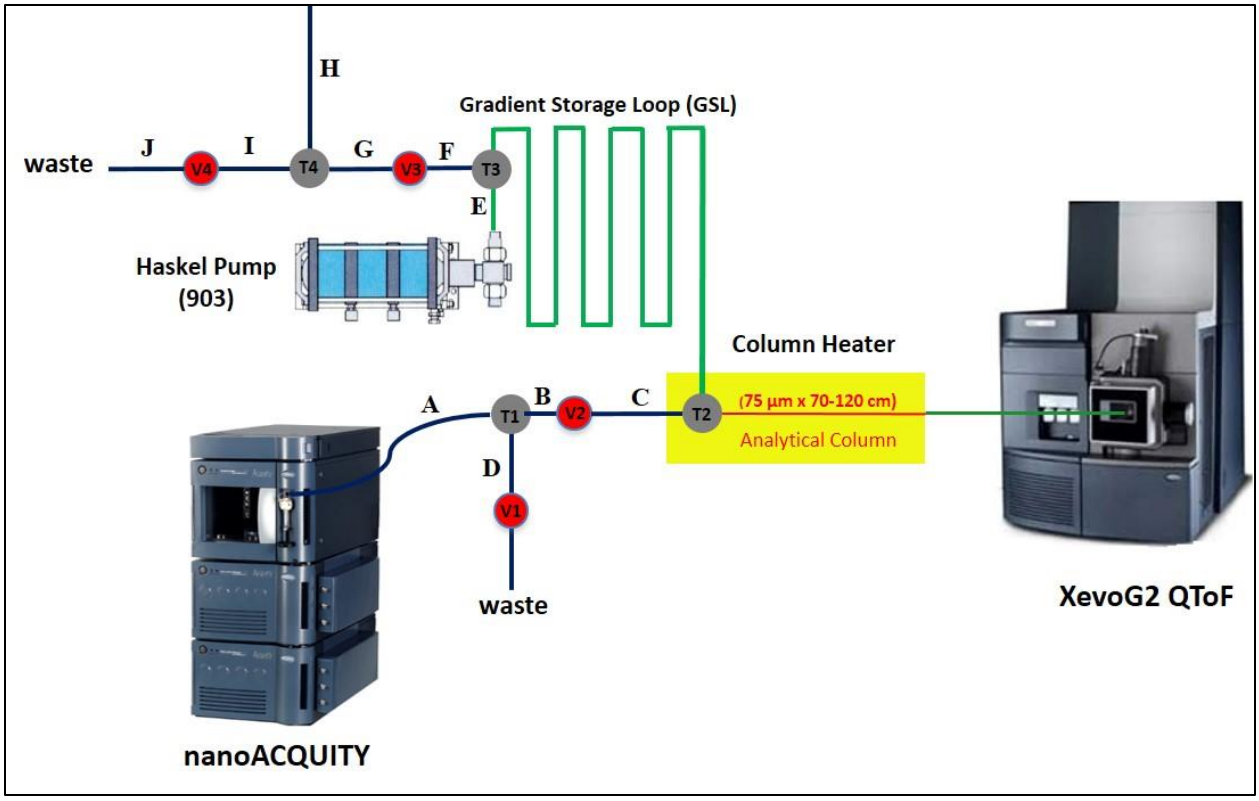

Figure 2. Schematic representation of the liquid flow path for the XUPLC add-on assembled around nanoAcquity UPLC and Xevo G2 ESI QTof MS. T1-T4 represent micro-volume connectors (tee), V1 represent 10 Kpsi air actuated on/off valves, V2-V4 represent 40 Kpsi air actuated on/off valves, A, B, E, F and H represent fused silica tubing, C-D represent Ni-clad fused silica tubing, G, I represent stainless steel tubing and J represent PTFE tubing.

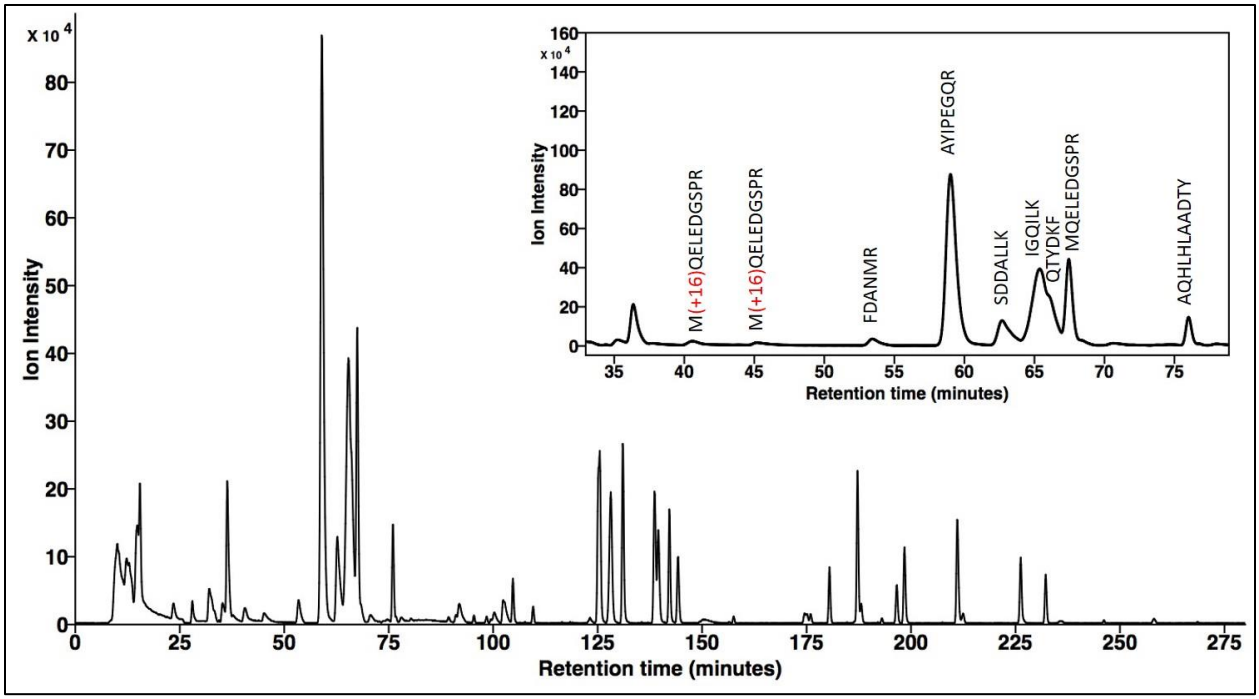

Figure 3. XUPLC separation of control rGH digest, with insert showing oxidation of Met residues

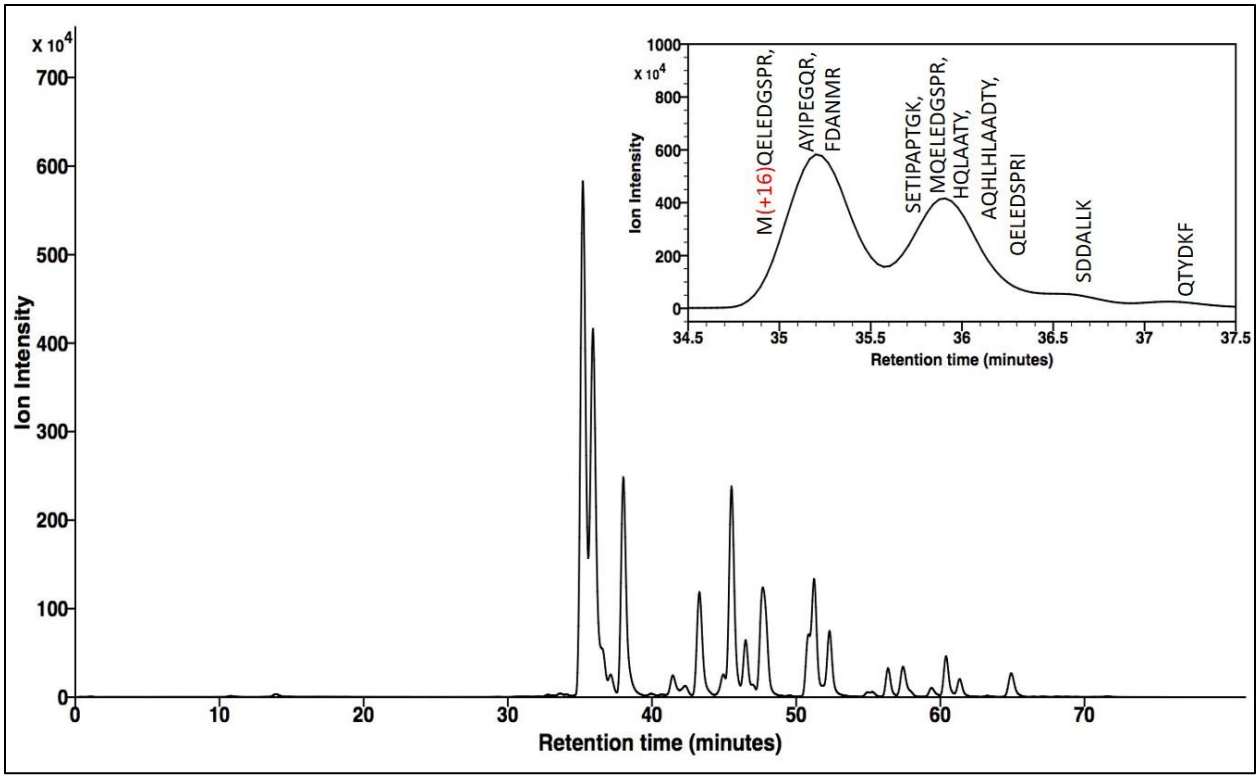

Figure 4. UPLC separation of control rGH digest, with insert showing oxidation of Met residues

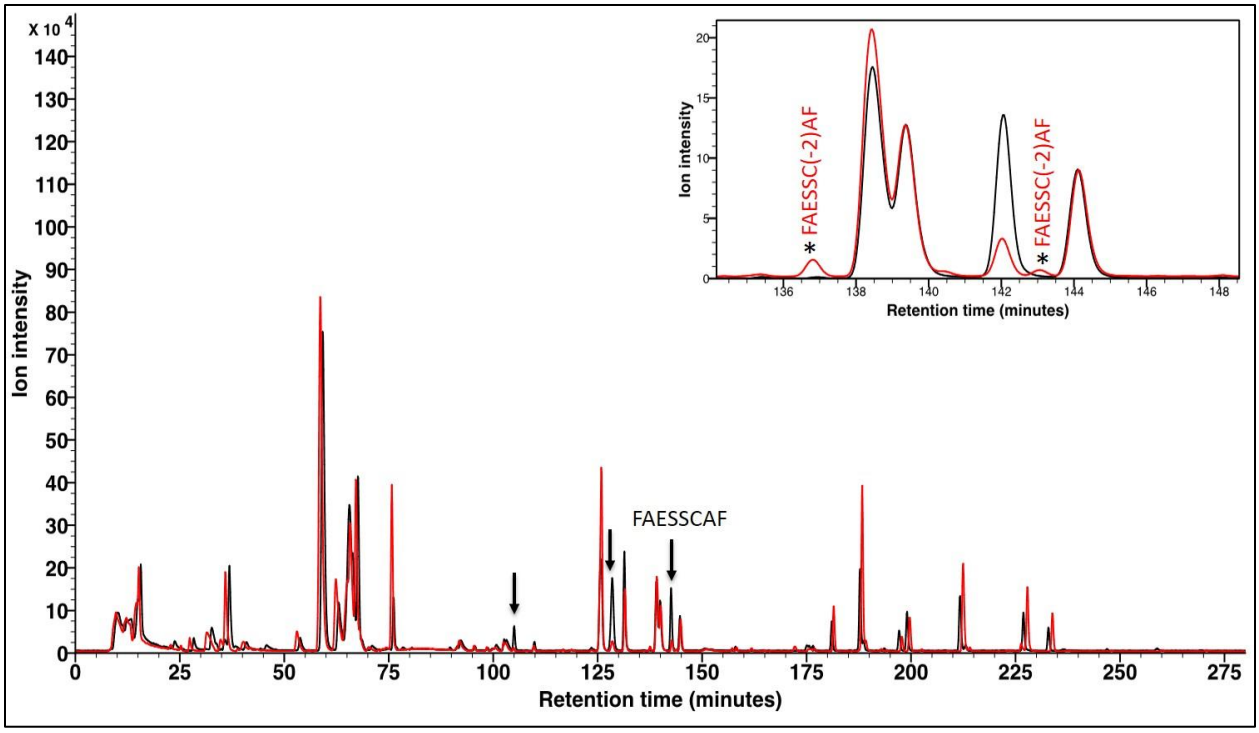

Figure 5. XUPLC separation of photo-induced (red) vs control rGH (black) digest, insert shows photodegradation products identified, which are isobaric (same mass). Arrows indicate tryptic peptides that exhibited decrease in intensity over time on exposure to 254 nm light.

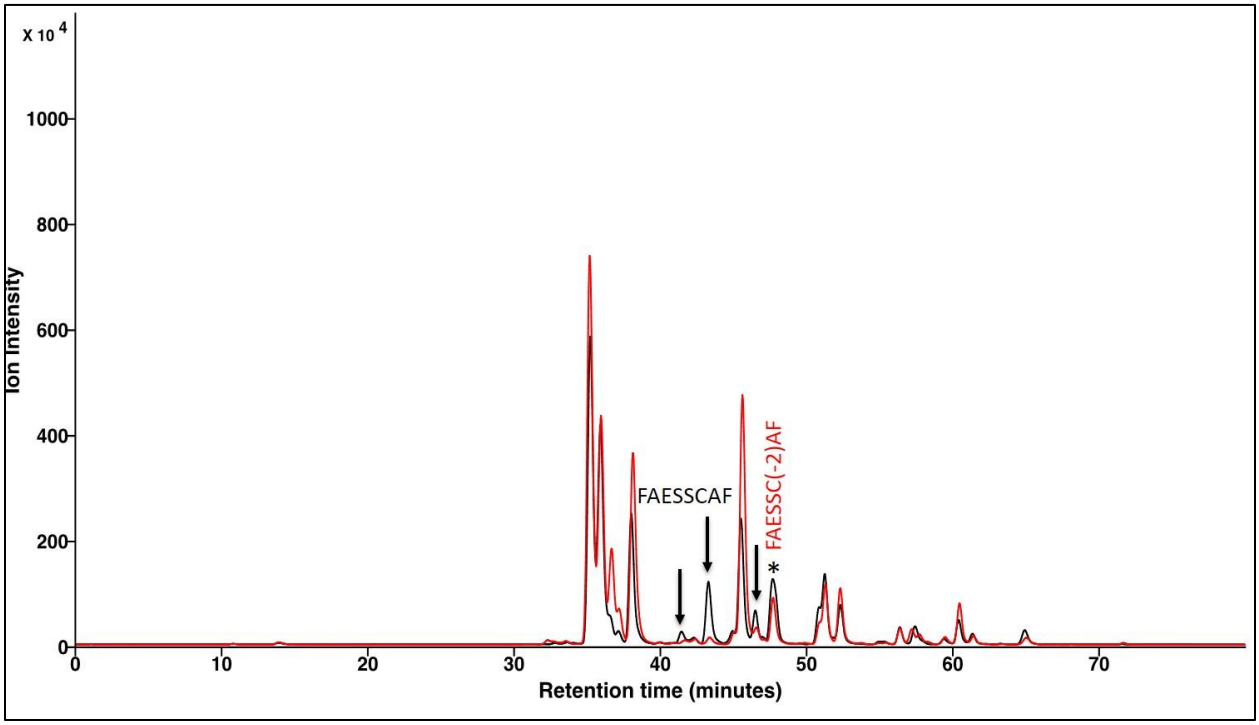

Figure 6. UPLC separation of photo-induced (red) vs control rGH (black) digest, insert shows photodegradation products identified. Arrows indicate tryptic peptides that exhibited decrease in intensity over time on exposure to 254 nm light.

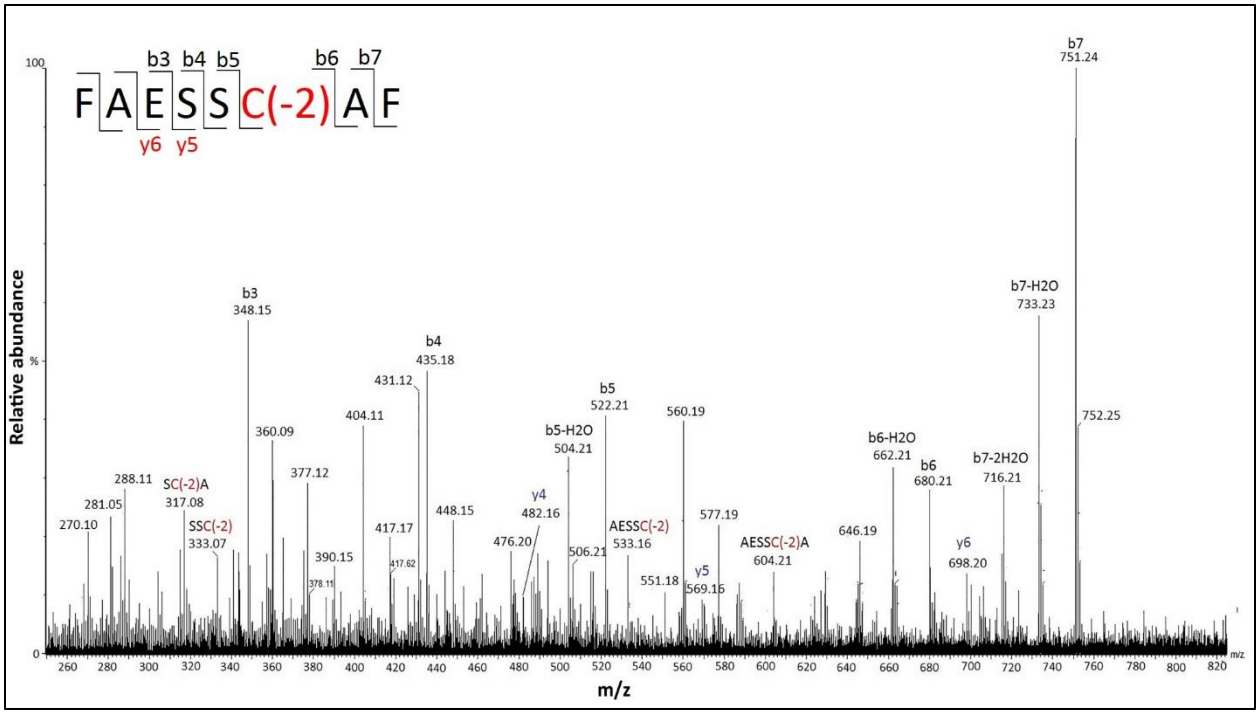

Figure 7. Collision-induced dissociation mass spectrum of the peptide FAESSC (-2) AF resulting from the digestion of rGH exposed to λ = 254 nm, which contains Cys 181 that underwent photo-induced degradation. Cys was alkylated with iodoacetamide.

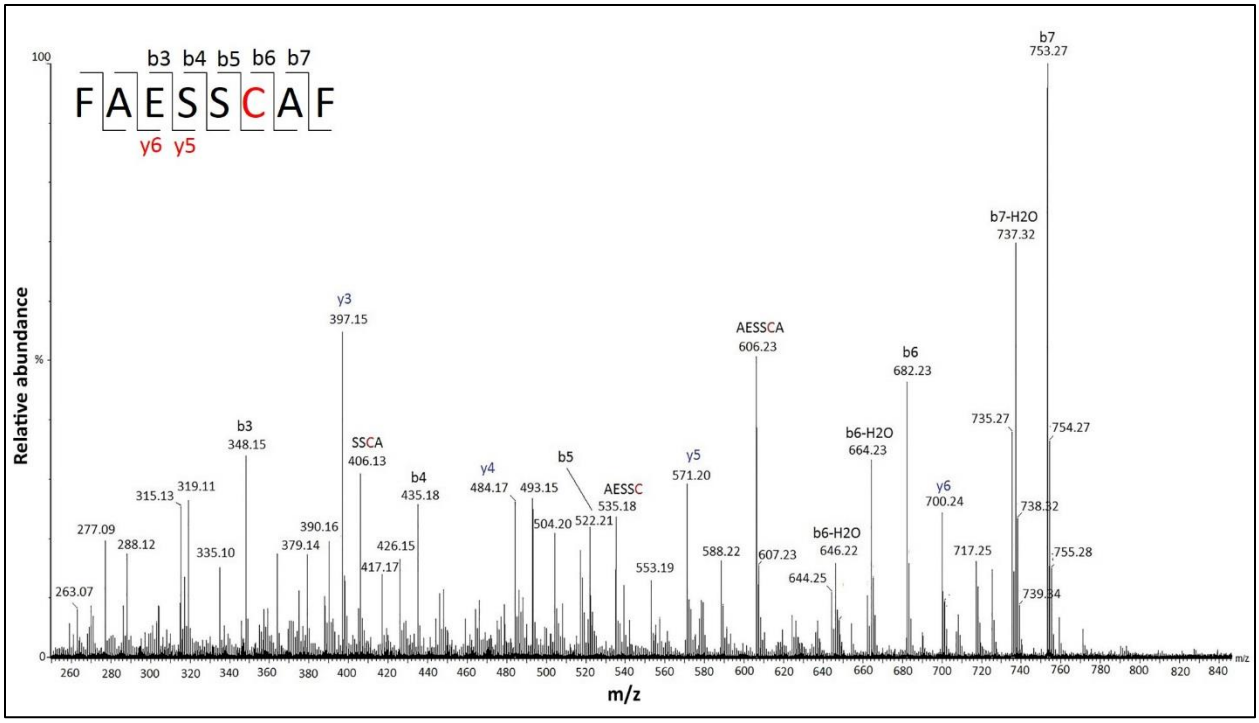

Figure 8. Collision-induced dissociation mass spectrum of the peptide FAESSCAF resulting from the digestion of control rGH that contains Cys 181, which is sensitive to photo-induced degradation. Cys was alkylated with iodoacetamide.

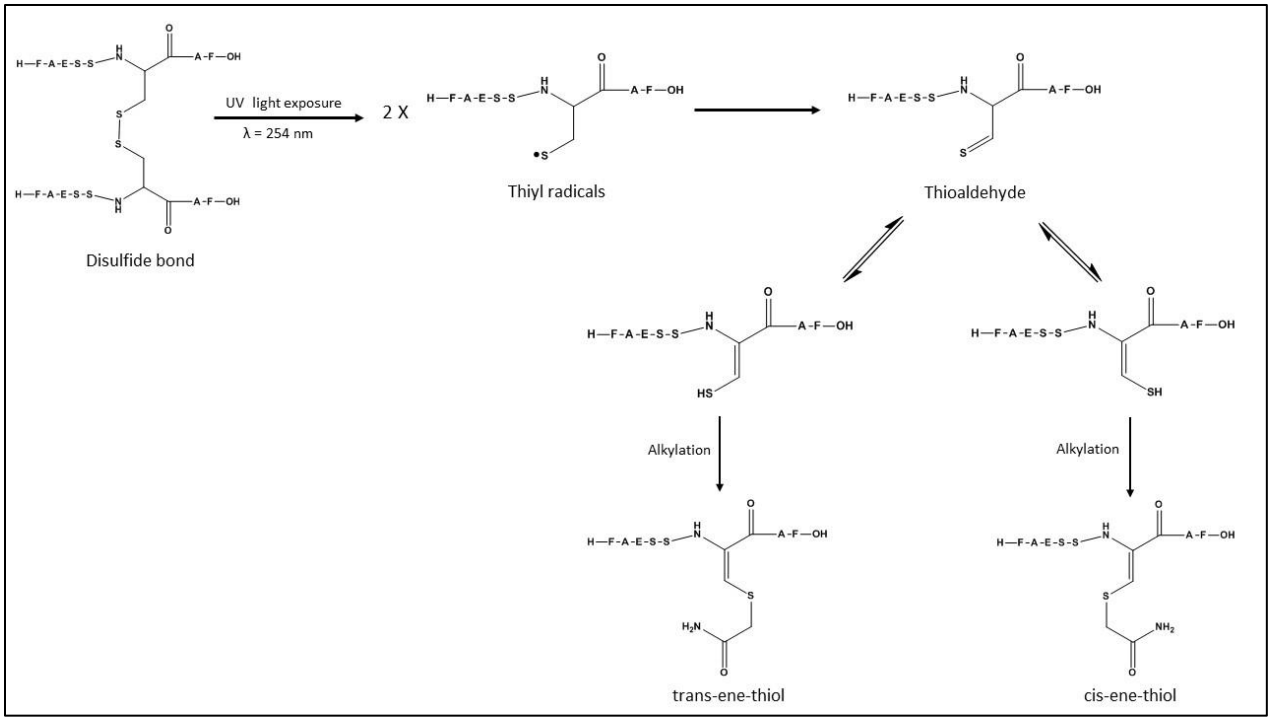

Figure 9. Mechanism showing the formation of rGH photodegradation products. Thioaldehyde and thiol products are formed from corresponding thiyl radicals generated due to photolysis of disulfide bonds. Tautomerization of thioaldehyde leads to cis/trans ene-thiols and alkylation with iodoacetamide to form cis/trans products detected by mass spectrometry.

Chapter 6. Conclusions and future directions

6.1 Summary and conclusions

The Protein therapeutics encounter various types of stress during production, processing, shipping and administration and hence are susceptible to a number of physical and chemical instability such as aggregation, oxidation, photodegradation, etc.[1-3] The aftermath of physical and chemical protein instability can include loss of potency and immunogenicity.[4,5] Previously, the immunogenicity of protein therapeutics was majorly associated with the formation of protein aggregates,[6-8] but in recent years there is an increase in evidence showing the role of chemical modifications in causing immunogenicity.[4,5] To fully understand the consequences of chemical degradation of protein therapeutics, the range and nature of chemical modifications formed should be characterized to the max. The comprehensive characterization of degradation products also requires development of novel methodologies to complement the existing analytical techniques. Therefore, the aim of this dissertation was to further investigate the mechanisms of chemical and physical degradation of proteins, which can assist in development of stable protein therapeutics.

Chapter 2 describes a rapid screening methodology to identify protein oxidation by monitoring Tyr and Phe oxidation. The oxidation of Tyr and Phe was first monitored by fluorogenic derivatization using fluorescence spectroscopy and complementary LC-MS analysis was done to identify the extent of methionine oxidation in oxidized proteins. The Fluorogenic derivatization technique was easily adapted to a 96-well plate, in which several protein formulations can be screened in a short time. Representatively for hGH, we showed that the formation of benzoxazole parallels the oxidation of Met to methionine sulfoxide which enables estimation of Met oxidation by just recording the fluorescence.

Chapter 3 illustrates the effect of various excipients (L-Arg, L-Leu, L-Met, glucose and sucrose) on the extent and site-specificity of D-amino acid formation in UV light exposed mAb formulations. The mAb-containing formulations were photo-irradiated at $\lambda = 254$ nm and $\lambda_{max} =$ 305 nm, followed by fractionation of aggregate and monomer fractions using size exclusion chromatography. Both aggregate and monomer fractions collected from all the formulations showed the formation of D-Glu and D-Val, whereas the formation of D-Ala was limited to the aggregate fraction collected from an L-Arg-containing formulation. Interestingly, quantitative analysis revealed higher yields of D-amino acids in the L-Arg-containing formulation. This can be rationalized by an increase in mAb flexibility in the C_H1 and C_H2 domains in the presence of L-Arg, which can increase the probability of D-amino acid formation. However, quantitative analysis failed to detect a clear trend of D-amino acid accumulation in aggregates, suggesting that the levels of D-amino acids generated under our experimental conditions do not generally lead to an enhanced potential for aggregate formation.

Chapter 4 compares the conformational stability, backbone flexibility, and aggregation propensity of monomer and dimer fractions of an IgG1 monoclonal antibody (mAb) generated upon UVA light exposure for upto 72 hours collected by preparative size-exclusion chromatography (SEC), compared to unstressed control. UVA light exposure induced covalent aggregation, fragmentation, and extensive oxidation of specific methionine residues (Met 257, Met 433, and Met 109) in both size fractions identified by reverse phase chromatography coupled to mass spectrometry. Compared to unstressed mAb, the monomer and dimer fractionated from 72 hours UVA light exposed mAb had decreases in thermal melting temperatures (T_{m1}) by 1.38 ^oC and 1.37 ^oC, respectively as measured by differential scanning calorimetry, minor changes in tertiary structure as measured by near UV-CD, and increased

monomer loss and aggregation on accelerated storage at 35 ^{o}C. Hydrogen/deuterium exchange mass spectrometry identified local segments with increased flexibility in C_H2 and C_H3 domains of both size fractions, and decreased flexibility in few segments of Fab and C_H1 domains in the dimer fraction. Segment 247-256 in heavy chain, an established aggregation hotspot in IgG1 mAbs had large increase in flexibility in both size fractions compared to unstressed mAb.

Chapter 5 outlines the use of a XUPLC system with pressure capabilities up to 38 Kpsi to improve the efficiency of one-dimensional separations using capillaries of 118 cm packed with sub-2 µm particles. A comparative analysis between XUPLC separations (using 118 cm length column) and commercial UPLC column (25 cm in length) revealed significant increase in resolution during the gradient separation. XUPLC analysis of photochemical degradation of rGH showed well-resolved isobaric cis/trans diastereomerically related ene-thiols, which co-eluted during UPLC analysis. Through this study we have demonstrated the capability of the XUPLC system in investigating complex chemical degradation problems.

6.2 Future directions

As a continuum, fluorogenic derivatization can be developed into a high-throughput technique where oxidative degradation can be quantified for multiple formulations. The consequences of chemical degradation can include loss of potency and immunogenicity.[4-7] Using this fluorogenic derivatization technique in pharmaceutical industries and pharmacies can limit the supply of degraded protein therapeutic to the patient.

Almost all the studies use the whole protein molecule to identify the immunogenic potential of degraded protein therapeutic which makes it difficult to deduce which immunogenicity of specific protein modification. Whereas, digestion of degraded protein into individual peptides

can help in identification of the immunogenic potential of a specific degradation products. This approach is currently being tested in our laboratory.

6.3 References

1) Manning MC, Patel K, Borchardt RT. Stability of protein pharmaceuticals. Pharm Res. 1989; 6(11): 903-18.
2) Manning MC, Chou DK, Murphy BM, Payne RW, Katayama DS. Stability of protein pharmaceuticals: an update. Pharm Res. 2010; 27(4): 544-75.
3) Kerwin BA, Remmele RL. Protect from light: photodegradation and protein biologics. J. Pharm. Sci. 2007; 96(6): 1468-79.
4) Torosantucci R, Sharov VS, van Beers M, Brinks V, Schöneich C, Jiskoot W. Identification of oxidation sites and covalent cross-links in metal catalyzed oxidized interferon beta-1a: potential implications for protein aggregation and immunogenicity. Mol. Pharm. 2013; 10(6): 2311-22.
5) Schöneich C. Novel chemical degradation pathways of proteins mediated by tryptophan oxidation: tryptophan side chain fragmentation. J. Pharm. Pharmacol. 2017.
6) Fradkin AH, Mozziconacci O, Schöneich C, Carpenter JF, Randolph TW. UV photodegradation of murine growth hormone: chemical analysis and immunogenicity consequences. Eur. J. Pharm. Biopharm. 2014; 87(2): 395-402.
7) Baker M, Reynolds HM, Lumicisi B, Bryson CJ. Immunogenicity of protein therapeutics: the key causes, consequences and challenges. Self/nonself. 2010; 1(4): 314-22.
8) Hermeling S, Crommelin DJ, Schellekens H, Jiskoot W. Structure-immunogenicity relationships of therapeutic proteins. Pharm. Res. 2004; 21(6): 897-903.